UNIVERSITY OF Southampton

University of Southampton Research Repository
ePrints Soton

Copyright © and Moral Rights for this thesis are retained by the author and/or other copyright owners. A copy can be downloaded for personal non-commercial research or study, without prior permission or charge. This thesis cannot be reproduced or quoted extensively from without first obtaining permission in writing from the copyright holder/s. The content must not be changed in any way or sold commercially in any format or medium without the formal permission of the copyright holders.

When referring to this work, full bibliographic details including the author, title, awarding institution and date of the thesis must be given e.g.

AUTHOR (year of submission) "Full thesis title", University of Southampton, name of the University School or Department, PhD Thesis, pagination

http://eprints.soton.ac.uk

UNIVERSITY OF SOUTHAMPTON

FACULTY OF PHYSICAL SCIENCES AND ENGINEERING

Electronics and Computer Science

Structure and Electrical Properties of Silica-based Polyethylene Nanocomposites

by

Kwan Yiew Lau

Thesis for the degree of Doctor of Philosophy

September 2013

UNIVERSITY OF SOUTHAMPTON

ABSTRACT

FACULTY OF PHYSICAL SCIENCES AND ENGINEERING

Electronics and Computer Science

Doctor of Philosophy

STRUCTURE AND ELECTRICAL PROPERTIES OF SILICA-BASED POLYETHYLENE NANOCOMPOSITES

by Kwan Yiew Lau

The topic of polymer nanocomposites remains an active area of research in the dielectrics community, due to the unique electrical properties that these materials could exhibit. To explain the behaviour of these materials, the importance of clarifying the interfaces between nanoparticles and polymer matrices has been emphasised. However, understanding of the interface in nanocomposites is unsatisfactory and, consequently, many experimental results remain unexplained. This thesis reports on an investigation into a polyethylene nanocomposite system that contains varying amounts of nanosilica that differ with respect to their surface chemistry. The addition of nanosilica, even with different surface chemistries, was found to enhance the nucleation density of polyethylene and perturb the spherulitic development. While less organised lamellar structures would be expected to lead to a lower breakdown strength, this does not appear to be the case for the material systems considered here under alternating current (AC) fields. In addition, nanosilica filled polyethylene was found to absorb significantly more water than unfilled polyethylene, with the consequence that both the permittivity and the loss tangent increase with increasing duration of water immersion. However, appropriate surface treatment of nanosilica reduces the water absorption effect and modifies the dielectric response of the nanocomposites compared with those containing an equivalent amount of untreated nanosilica. Although water absorption may not be a technologically desirable characteristic, the results indicate that water molecules can act as effective dielectric probes of interfacial factors. Meanwhile, the direct current (DC) breakdown strength reduces with the inclusion of increasing amount of nanosilica in the polyethylene, but surface treatment of nanosilica improves the DC breakdown strength with respect to equivalent nanocomposites containing untreated nanosilica. Results from space charge studies reveal increased space charge accumulation in the presence of the untreated nanosilica and, upon surface treatment of the nanosilica, the charge development was suppressed in comparison with nanocomposites containing an equivalent amount of untreated nanosilica. This observation suggests that space charge accumulation and DC failure are related in these systems and it would seem that control of surface chemistry is particularly critical in connection with the use of nanocomposites in DC applications. Finally, the mechanisms underpinning the concept of filler functionalisation in nanocomposites were investigated via the use of different aliphatic chain length silane coupling agents, and the results show that long silane chains enhance the DC breakdown strength of the resulting nanocomposites. The possible further enhancement in DC breakdown strength is also highlighted. Overall, this thesis demonstrates how a nanoparticle’s interface chemistry can affect both the structure and the electrical properties of the resulting nanocomposites, and serves as an important foundation towards the engineering of nanocomposites as the reliable electrical insulation materials of the future, through the understanding of the interface.

Contents

List of Figures

List of Tables

List of Appendices

Declaration of Authorship

I, Kwan Yiew Lau, declare that this thesis entitled:

"Structure and Electrical Properties of Silica-based Polyethylene Nanocomposites"

and the work presented in the thesis are both my own, and have been generated by me as the result of my own original research. I confirm that:

- this work was done wholly or mainly while in candidature for a research degree at this University;
- where any part of this thesis has previously been submitted for a degree or any other qualification at this University or any other institution, this has been clearly stated;
- where I have consulted the published work of others, this is always clearly attributed;
- where I have quoted from the work of others, the source is always given. With the exception of such quotations, this thesis is entirely my own work;
- I have acknowledged all main sources of help;
- where the thesis is based on work done by myself jointly with others, I have made clear exactly what was done by others and what I have contributed myself;
- parts of this work have been published as:
    1. Lau, K. Y., Vaughan, A. S., Chen, G., Hosier, I. L., Holt, A. F, and Ching, K. Y. On the space charge and DC breakdown behaviour of polyethylene/silica nanocomposites. *IEEE Transactions on Dielectrics and Electrical Insulation*, accepted for publication.
    2. Lau, K. Y., Vaughan, A. S., Chen, G., and Hosier, I. L., and Holt, A. F. Absorption current behaviour of polyethylene/silica nanocomposites. *Journal of Physics: Conference Series*, accepted for publication.
    3. Lau, K. Y., Vaughan, A. S., Chen, G., Hosier, I. L., and Holt, A. F. (2013). On the dielectric response of silica-based polyethylene nanocomposites. *Journal of Physics D: Applied Physics*, 45, 095303.

4. Lau, K. Y., Vaughan, A. S., Chen, G., and Hosier, I. L. (2013). Space charge dynamics in silica-based polyethylene nanocomposites. *Proceedings of the International Conference on Solid Dielectrics*, 30 June - 4 July. Bologna: IEEE, 880-883.
5. Lau, K. Y., Vaughan, A. S., Chen, G., Hosier, I. L., Holt, A. F. (2013). On nanosilica surface functionalisation using different aliphatic chain length silane coupling agents. *Proceedings of the International Conference on Solid Dielectrics*, 30 June - 4 July. Bologna: IEEE, 896-899.
6. Vaughan, A. S. (2013). Nano at nineteen. *Proceedings of the International Conference on Solid Dielectrics*, 30 June - 4 July. Bologna: IEEE, 706-709.
7. Lau, K. Y., Vaughan, A. S., Chen, G., and Hosier, I. L. (2012). Polyethylene nanodielectrics: The effect of nanosilica and its surface treatment on electrical breakdown strength. *Annual Report Conference on Electrical Insulation and Dielectric Phenomena*, 14-17 October. Montreal: IEEE, 21-24.
8. Lau, K. Y., Vaughan, A. S., Chen, G., and Hosier, I. L. (2012). Dielectric response of polyethylene nanocomposites: The effect of surface treatment and water absorption. *Annual Report Conference on Electrical Insulation and Dielectric Phenomena*, 14-17 October. Montreal: IEEE, 275-278.
9. Lau, K. Y., Vaughan, A. S., Chen, G., and Hosier, I. L. (2011). On the effect of nanosilica on a polyethylene system. *Journal of Physics: Conference Series*, 310, 012008.

Signed: ……

Date: ……

Acknowledgements

First of all, I would like to express my sincere and deepest thanks to my main supervisor, Professor Alun Vaughan for his expert guidance and encouragement. I am grateful for his insightful advice, understanding and patience in helping me for the completion of this thesis. I would also like to thank my secondary supervisor, Professor George Chen for his kind advice and continuous support to ensure the smoothness of my research.

Special thanks are dedicated to Dr. Ian Hosier for sharing the knowledge on materials processing and experimental techniques, and Dr. Christopher Green, Dr. Martin Reading, Dr. Ngoc Dao, Dr. Junwei Zhao, Dr. Qi Wang, Dr. Celia Yeung, Dr. Truc Nguyen, Dr. Matt Praeger and many of the Tony Davies High Voltage Laboratory members, including the Laboratory Operations Director, Professor Paul Lewin for providing their opinion, discussion and technical support when undertaking my experimental works. Not forgotten, to Professor Steve Swingler (the internal examiner for my first year viva and MPhil to PhD upgrade viva), and Professor Geoffrey Mitchell and Dr. Thomas Andritsch (the external and internal examiners for my PhD viva), thank you for your invaluable comments given during the vivas.

I would also like to thank Dr. Alex Holt from the School of Chemistry for her help and guidance provided in preparing the surface treated nanosilica and explaining the underlying chemistry. Ms. Kuan Yong Ching from the School of Engineering Sciences is also acknowledged for spending her precious time and effort together in characterising the nanocomposite samples using atomic force microscopy.

My sincere thanks to the Ministry of Higher Education, Malaysia and Universiti Teknologi Malaysia for providing generous financial support for me to undertake my PhD research at the University of Southampton, United Kingdom. Financial assistance from the University of Southampton for my research works and conference attendance is kindly acknowledged. Also, to my family and friends, thank you for your continuous and unconditional love and support.

Dear God, the journey of my PhD was not an easy one, but I put my faith in you. At times when I was flooded with endless problems, you made ways out of no way. I shall always remember that in my heart I plan my course, but you determine my steps. Thank you for the abundant blessings in my life.

Abbreviations and Symbols

AC	- Alternating current
AFM	- Atomic force microscopy
Al_2O_3	- Alumina
ASTM	- American Society for Testing and Materials
BPE	- Branched polyethylene
CH_3	- Methyl functional group
C_3H_7	- Propyl functional group
C_8H_{17}	- Octyl functional group
$C_{18}H_{37}$	- Octadecyl functional group
CO_2	- Carbon dioxide
COSHH	- Control of substances hazardous to health
C3-treated	- Trimethoxy(propyl)silane-treated
C8-treated	- Trimethoxy(octyl)silane-treated
C18-treated	- Trimethoxy(octadecyl)silane-treated
DC	- Direct current
DSC	- Differential scanning calorimetry
FTIR	- Fourier transform infrared
HDPE	- High density polyethylene
HVDC	- High voltage direct current
H_2O	- Water molecule
LDPE	- Low density polyethylene
LLDPE	- Linear low density polyethylene
LPE	- Linear polyethylene
MIRTGS	- Mid-infrared triglycine sulphate
MLE	- Maximum likelihood estimation
OH	- Hydroxyl functional group
PEA	- Pulsed electro-acoustic
POM	- Polarised optical microscopy
RMS	- Root mean square
SEM	- Scanning electron microscopy

SiH_3OH	- Silanol
SiO_2	- Silica
TEM	- Transmssion electron microscopy
THF	- Tetrahydrofuran
TiO_2	- Titania
XLPE	- Crosslinked polyethylene

A - Temperature dependent factor

b_0 - Thickness of one layer of folding chains

b_n - Constant representing the slope of the log-log current-time plot

C - Constant representing the influence of the transport term

d - Sample thickness

D - Dielectric flux density

exp - Exponential

E_i - Experimental breakdown strength

G - Growth rate of crystallising object

i - Progressive order of failed tests

I - Current

k - Boltzmann constant

K - Slope

K_3 - Three-dimensional crystallisation rate constant

K_{exp} - Experimental rate constant

K_g - Nucleation constant

log - Logarithmic

m - Total number of tests

M_d - Weight of a dry sample

M_w - Weight of a water absorbed sample

n - Avrami exponent

n_d - Dimensionality of crystal growth

n_n - Time dependence of nucleation

N - Number of nucleation sites per unit volume

$P(E_i)$ - Cumulative probability of failure at E_i

Q - Intercept

t - Time

t_c - Time at certain volume fraction of crystallinity

T_c - Crystallisation temperature

T_g - Glass transition temperature

t_i - Induction time

T_m - Melting temperature

T_{m1} - Lower peak melting temperature

T_{m2} - Upper peak melting temperature

t_p - Time at which slope change occurs

$tan\delta$ - Dielectric loss tangent

T_m^0 - Equilibrium melting temperature

V - Voltage

V_c - Volume fraction of crystallinity

$V_p(t)$ - Voltage pulse

V_∞ - Maximum crystallinity attained

α - Scale parameter

β - Shape parameter

δ - Phase difference

ε_o - Permittivity of vacuum

ε_s - Static, low frequency permittivity

ε_∞ - Permittivity at the high frequency limit

$\varepsilon_r^*(\omega)$ - Complex relative permittivity of polymer

$\varepsilon_r'(\omega)$ - Real part of the complex relative permittivity

$\varepsilon_r''(\omega)$ - Imaginary part of the complex relative permittivity

μ - Mobility of charge carriers

ω - Angular frequency

ω_f - Weight fraction of crystallisable material

χ - Crystallinity

σ - Gibbs specific surface energies of the growing nucleus

$\%\ Mass$ - Percentage increase in mass

% w/v - Percentage weight/volume

ΔH - Enthalpy of crystallisation or melting

ΔH_m - Enthalpy of the crystal melting

ΔH_o - Enthalpy corresponding to the melting of 100 % crystalline material

ΔT - Undercooling

$\Delta\sigma$ - The difference energy parameter

To my beloved family…

Chapter 1

Introduction

"There seems no limit to research, for as has been truly said, the more the sphere of knowledge grows, the larger becomes the surface of contact with the unknown."

- Sir William Cecil Dampier -

1.1 Polymer Nanocomposites

Polymer nanocomposites are defined as polymers within which nanometre-sized fillers are homogeneously dispersed at just a few weight percentage (wt%). Generally, a nanocomposite is speculated to consist of three main phases, namely, the matrix, the filler and the interaction zone (Lewis, 2004; Tanaka et al., 2005; Nelson, 2007). A simplified diagram illustrating a nanocomposite is shown in Figure 1.1. The matrix, also known as the base resin, can be a thermoplastic (e.g. polyethylene or polypropylene), a thermoset (e.g. epoxy resins or polyimides) or an elastomer (e.g. ethylene-vinyl acetate or silicone rubber). Meanwhile, the nanofillers can be of three distinct classes based on their dimensions. Nanoparticles such as montmorillonite clays are classified as one-dimensional nanoparticles due to their nanoscopic character in just one dimension. Two-dimensional nanoparticles such as carbon nanotubes exhibit nanoscopic character in two dimensions. Spherical particles such as silica (SiO_2), titania (TiO_2) and alumina (Al_2O_3) exhibit nanoscopic character in three dimensions and are therefore termed three-dimensional nanoparticles. The interaction zone, also known as the interface or the interphase, is determined by the interfacial area between the matrix and the fillers. Due to the size of nano-inclusions, large interfacial areas exist between the fillers and the matrix, which is considered to be one of the key roles leading to the unique properties of nanocomposites.

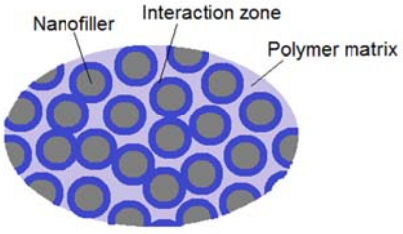

Figure 1.1: A simplified diagram illustrating a nanocomposite (drawing is not to scale)

1.2 Research Background and Motivation

The emergence of synthetic polymers has exerted a massive influence on the world of electrical insulation in that polymeric insulators now largely dominate the market. Although half a century has passed, today, polymeric insulators are still widely used as standard materials in many power delivery systems. No new materials have been introduced since the era of polymers. Most of the "new" materials, if available, are still largely based on polymers (e.g. microfilled polymers). While these materials enhance mechanical and thermal properties, they rarely improve, and in most case worsen, many electrical properties (e.g. breakdown strength). This results in design difficulties especially when dealing with increasing voltage levels.

In the early 1990s, polymer nanocomposites commercially emerged when the Toyota Motor Corporation successfully implemented nylon-6/clay nanocomposites as engineering plastics for timing belt covers in their cars (Usuki et al., 1993a; Usuki et al., 1993b; Hussain et al., 2006; Li et al., 2010a). This success initiated the use of polymer nanocomposites in automotive industries. For example, Mitsubishi introduced nylon-6/clay nanocomposites for engine covers on Gasoline Direct Injection engines while General Motor and Basell incorporated polyolefin/clay nanocomposites for application in a step assistant component for GMC Safari and Chevrolet Astro vans (Hussain et al., 2006; Bhattacharya et al., 2008). Later, research on polymer nanocomposites extended to various industries, including optics, electronics and food packaging. Some examples of such applications can be found in the publication by Bhattacharya et al. (2008).

Although research on polymer nanocomposites has sparked widespread attention across various industries since the early 1990s, their application was not emphasised in electrical insulating industries at that time. It was not until 1994 that Lewis (1994) inspired the future of such newly emerging materials into the world of electrical insulation by anticipating the potential property changes that would benefit electrical insulation due to the introduction of nanometre-sized inclusions. While polymer nanocomposites concern polymers within which nanometre-sized fillers are homogeneously dispersed at just a few weight percentage (wt%), the term "nanometric dielectrics" (Lewis, 1994) or "nanodielectrics" (Fréchette et al., 2004;

Psarras, 2008) was introduced into the dielectrics community to refer to nanocomposites of specific interest in connection with their dielectric characteristics. However, for the scope of electrical insulation research, the terms “nanocomposite” and “nanodielectric” are used interchangeably to refer to polymer/nanoparticle mixtures of dielectric interest.

In the late 20th century, early experimental studies of nanocomposites as dielectric materials (Henk et al., 1999; Henk et al., 2001) were published, but these studies did not attract significant attention in the dielectrics community. It was not until 2002 that researchers began to shift their attention to the potential deployment of such newly emerging materials, when the promising application of nanodielectrics as electrical insulating materials was experimentally demonstrated by Nelson et al. (2002). While conventional microfilled materials come with reduced dielectric strength due to bulk charge accumulation, Nelson et al. (2002) reported mitigated space charge accumulation and enhanced charge decay in nanofilled system compared with microcomposites, which could lead to improved dielectric strength.

Following Nelson’s studies (Nelson et al., 2002), numerous publications have emerged, exploring various combinations of polymers with different inorganic nanofillers. Electrical insulating properties such as partial discharge resistance, treeing progression, space charge formation and dielectric breakdown performance of nanocomposites have been compared with the unfilled and microfilled counterparts, and promising improvement in these properties has been reported with the addition of nanofillers (Yin et al., 2003; Zilg et al., 2003; Kozako et al., 2004; Nelson and Fothergill, 2004; Tanaka et al., 2004; Roy et al. 2005a; Roy et al., 2005b; Montanari et al., 2006; Green et al., 2008). The emerging trend of nanodielectrics research is shown in Figure 1.2, which shows how the number of publications has increased dramatically since 2002 (Nelson, 2010).

As previously mentioned, many current electrical insulation systems come with the compromise of reduced electrical performance, as a consequence of the need to address thermal, mechanical and economic requirements. For example, in order to produce mechanically strong insulation systems, microfillers are added to polymers to give a combination of properties that reflects both the filler and the polymer. The

incorporation of microfillers, despite improving mechanical properties such as tensile strength and elastic modulus, introduces more defects into the overall insulation system, thus reducing the dielectric breakdown strength of the material (Cao et al., 2004; Mayoux, 2000; Dakin, 1983). Interestingly, the use of polymer nanocomposites in electrical insulation is predicted to be capable of enhancing the dielectric performance of insulation systems. This is believed to be related to the much smaller size of the fillers, which subsequently leads to the presence of extensive interfacial areas. This is illustrated in Figure 1.3, in which Nelson (2007) correlated the radius of a particle to its surface area and the extent to which reductions in filler size result in substantial increases in specific surface area. In this regard, nanocomposites are expected to possess unique dielectric properties that reflect the resulting interphase regions (neither those of the polymers nor those of the nanofiller) rather than a simple binary combination of properties, as in conventional microcomposites. Such distinct property changes brought about by nanodielectrics have led to the suggestion that this could be a brand new class of materials that the dielectrics community has long been waiting for – dielectric materials with combined electrical, mechanical and thermal improvements.

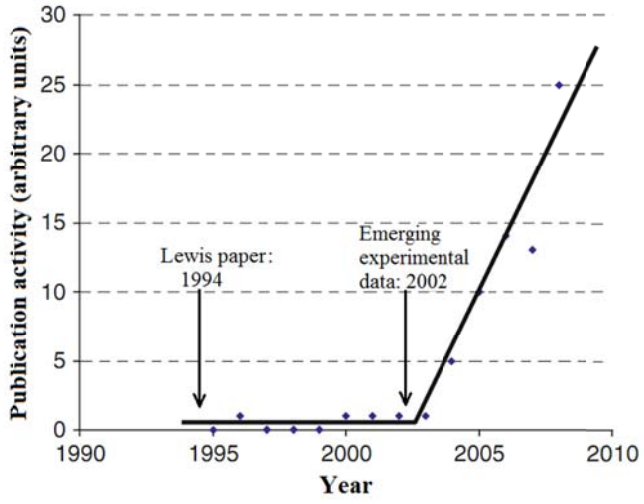

Figure 1.2: The number of publications in nanodielectrics (Nelson, 2010)

The concept of the interfacial area was also elaborated by Tanaka et al. (2004) and the improved properties of polymer nanocomposites were ascribed to the conversion of bulk polymer into interfacial polymer. In conventional composites, a large amount (usually more than 50 wt%) of microfillers is incorporated into the polymer. The mixture of polymer with microfillers results in significant changes in material

properties from those of the polymer itself. Meanwhile, nanocomposites consist of a very small quantity (usually less than 10 wt%) of nanofillers in the polymer. This is said to be capable of retaining the intrinsic polymer properties while exhibiting the unique interfacial properties, in which the nanofillers interact chemically and physically with polymer matrices and result in intermediate or mesoscopic properties that belong to neither the atomic nor the macroscopic frame.

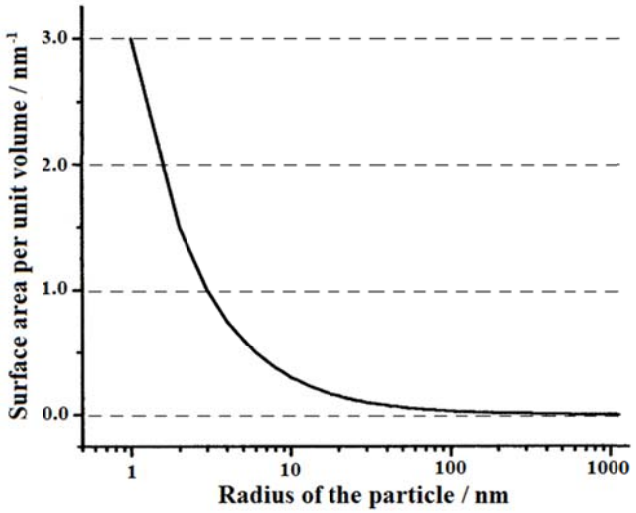

Figure 1.3: Surface-to-volume ratios of nanocomposites as a function of nanoparticle size (Nelson, 2007)

There are basically three main areas that can be contrasted when differentiating nanocomposites from conventional microcomposites. Firstly, the content of nanofillers is normally less than 10 wt%, while the content of microfillers can be 50 wt% or more, as previously mentioned. Secondly, for nanocomposites, the filler size falls in the nanometric range, and is usually less than 100 nm. For conventional fillers, the size is in the range of micrometres. The size difference means that neighbouring nanofillers are closely located to each other as compared with microfillers, when an equivalent amount of filler loading is considered. Lastly, nanofillers have much larger specific surface areas than conventional particulate-filled systems. These factors result in significant property differences between nanocomposites and microcomposites. A visual comparison between nanocomposites and microcomposites can be found in Figure 1.4.

To explain the behaviour of polymer nanocomposites that leads to distinct dielectric properties, a multi-layered core model, also simplified as the multi-core model, was

proposed by Tanaka et al. (2005). In the model, as shown in Figure 1.5, three layers, namely the bonded layer (the first layer), the bound layer (the second layer) and the loose layer (the third layer) were introduced, with the Gouy-Chapman diffuse layer overlapping all three. Through these layers, explanations for changes in properties such as permittivity, loss tangent, dielectric breakdown strength, partial discharge resistance, space charge and electroluminescence have been proposed (Tanaka, 2005). Although some of the property changes have been well-explained by the model, several contradictions nevertheless exist.

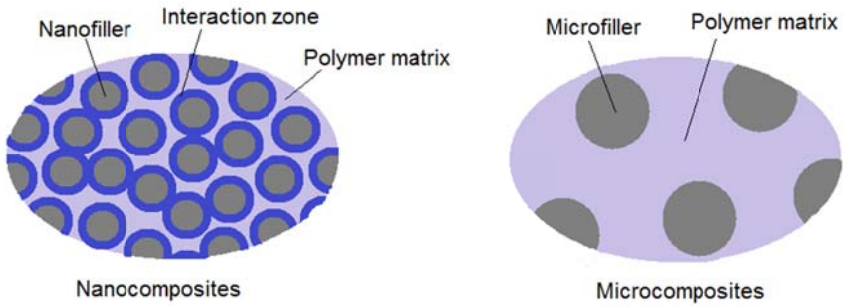

Figure 1.4: Visual comparison between nanocomposites and microcomposites, assuming an equivalent amount of filler loading (drawings are not to scale)

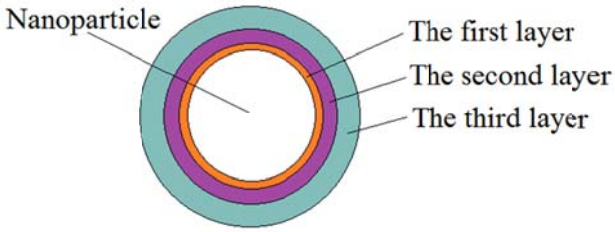

Figure 1.5: The multi-core model for polymer nanocomposites (Tanaka et al., 2005)

The importance of clarifying the interfaces between nanoparticles and polymer matrices has been emphasised by many researchers (Lewis, 2004; Tanaka et al., 2005; Nelson, 2007; Singha and Thomas, 2008; Andritsch, 2010; Li et al., 2010b; Raetzke and Kindersberger, 2010). However, it should be noted that such interfaces depend not only on the kind of nanoparticles and polymer matrices, but also on the surface conditions of the nanoparticles, the use of coupling agents and the incorporation of compatibilizers. As highlighted by Cao et al. (2004), understanding of the interface in nanodielectrics is unsatisfactory and exploration into issues such as the interaction between nanoparticles and the matrix, the interplay between nanoparticles and associated transport phenomena has to be emphasised. Unfortunately, this knowledge

gap still exists in today's nanodielectrics research and, consequently, many experimental results remain unexplained.

The difficulty in obtaining a complete picture of the material structure and composition due to nanostructuration constitutes a major obstacle to understanding the properties of nanocomposites. Many uncertainties arise and one can never understand the properties of nanocomposites at a macroscopic level while a complete understanding of nanostructuration at the nanometre level is absent. In some cases, restructuring of the polymer matrix (host material) was found due to the presence of nanofillers and the nanofillers' ability to interact with the polymer matrix. The use of various chemical processes further complicates the situation, since property changes are not only associated with the effect of nanoparticles alone. For example, optical properties depended on the compatibilization process (Ambid et al., 2006) while the space charge behaviour and dielectric loss depended on matrix and clay concentration respectively (Fuse et al., 2009). In these cases, it could be that chemical effects dominate nanosized effects. Such claims are yet to be verified and more experimental breakthroughs are certainly required.

While there have been numerous promising results supporting the dielectric enhancement brought about by nanostructuration in electrical insulation systems, it has not always been the case that nanodielectrics are favourable in electrical insulation systems (Fréchette et al., 2010). More importantly, the existence of contradictory results, even in systems that are apparently comparable, leads to further complications concerning the use of nanodielectrics (Tanaka et al., 2011). To date, observing improved or worsened electrical performance of nanodielectrics is not unusual, but explaining such observations represents a great challenge. In some cases, meagre improvements due to nanostructuration have raised questions concerning the worthiness of investing in nanodielectric systems.

Therefore, understanding of the mechanisms of nanodielectrics requires exploration into various factors, such as nanofiller/nanofiller interactions, nanofiller/matrix interactions and changes in matrix morphology, and these need to be considered at different dimensional levels, as depicted by Green and Vaughan (2008) in Figure 1.6. At the smallest dimensions, factors such as nanoparticle size and surface chemistry,

the properties of the matrix material and local interactions between the nanoparticle and the matrix material need to be considered. At intermediate dimensions, interactions of a nanoparticle with its neighbouring nanoparticles and with the matrix material, the matrix morphology, and charge formation and polarisation phenomena need to be considered. At larger dimensions, dispersion of nanoparticles becomes critical, and aggregation of nanoparticles may dominate the properties of nanodielectrics. Significantly, an in-depth understanding of the behaviour of nanodielectrics, especially on the underlying physics and chemistry governing changes in electrical properties, needs to be addressed; this will, inevitably, involve an emphasis on the interface – a key feature of nanodielectrics (this can also be inferred from Figure 1.6, where the presence of the interface is unavoidable at all dimensional levels).

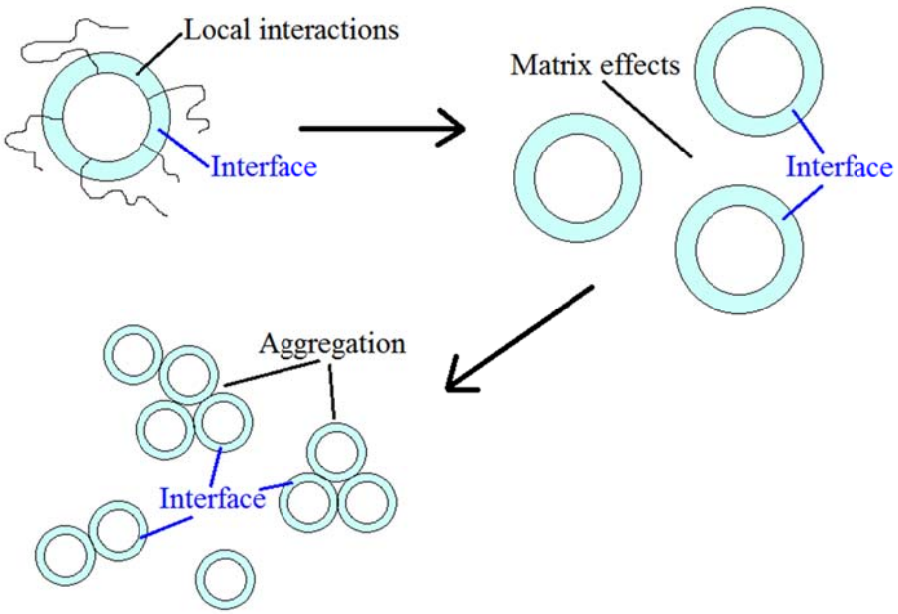

Figure 1.6: Schematic diagram indicating the range of different dimensional levels that need to be considered when attempting to characterise a nanocomposite. Nevertheless, the interface plays an important role even at different dimensional levels (Green and Vaughan, 2008)

1.3 Research Objectives and Scope

Research on nanodielectrics is still in its infancy. The current lack of fundamental understanding of nanodielectrics opens the way to further investigations, with the

hope of engineering them as the insulation materials of the future. Therefore, the main objectives and scope of this research are:

i) To formulate and characterise reproducible polymer nanocomposites for dielectric applications.

   Presently, research on nanocomposites focused on the use of a single polymer as the matrix material. While changes in electrical properties were found to be affected by the presence of nanofillers, the influence of the underlying morphological factor was difficult to identify. In this work, a polyethylene blend composed of 20 wt% of high density polyethylene (HDPE) in low density polyethylene (LDPE) was used as the base polymer. This allows the control of the underlying morphology through thermal treatment and enables structural changes to be readily detected. Meanwhile, nanosilica at varying loading levels was chosen as a nanofiller with a view to vary the surface chemistry of the nanofiller through the use of silane coupling agents so as better to understand the effect of interfacial chemistry.

ii) To investigate the effect of nanoparticles on electrical breakdown and space charge characteristics of polymer nanocomposites.

   Early experimental work on nanocomposites with regards to dielectric applications demonstrated that nanoparticles were favoured in improving the electrical breakdown performance. This was anticipated to be related to space charge development, in particular to direct current (DC) applications. This was, however, contradicted by several later findings that nanocomposites were, perhaps, not the panacea to electrical breakdown properties – reduced breakdown strength was reported in many nanocomposite systems. In this work, the influence of nanosilica (which varies in terms of surface chemistry) on a polyethylene blend were specifically studied further to understand the breakdown behaviour of the material systems, in both alternating current (AC) and DC applications. Space charge studies were also conducted to evaluate the effect of interfacial changes in nanocomposites on electrical properties, in particular, in an attempt to relate the space charge behaviour to the DC breakdown performance.

iii) To investigate the role of the interface in determining the unique dielectric properties of polymer nanocomposites.

In the current literature, various interface models have been proposed to explain the mechanisms governing changes in electrical properties of nanocomposites. In this work, detailed characterisations were carried out based upon nanocomposites containing untreated and treated nanosilica to understand the interfacial mechanisms associated with changes in electrical properties. Absorption current behaviour, which has not attracted significant attention, was considered to aid with data interpretation. Surface functionalisation of the nanofiller using different aliphatic chain length silane coupling agents was also performed, and the resulting nanocomposites were electrically tested – this helps to anticipate the possible improvement brought about by nanostructuration, in particular, in relation to the interfacial states.

1.4 Thesis Outline

This thesis is divided into ten chapters:

Chapter 1 contains the introduction, objectives and scope of this research while Chapter 2 provides details on the experimental parameters used throughout this research.

From Chapter 3 to Chapter 8, a comparison between two nanocomposite systems, i.e., one that contains an untreated nanosilica and the other that contains a treated nanosilica is made, with unfilled polyethylene as reference. This includes thermal analysis (Chapter 3), structural and morphological discussion (Chapter 4), dielectric response (Chapter 5), electrical breakdown behaviours (Chapter 6), space charge dynamics (Chapter 7) and absorption current measurements (Chapter 8).

In Chapter 9, the effect of silane chain length on the DC breakdown properties of the resulting nanocomposites is considered, and the possible enhancement in DC breakdown strength is highlighted.

Lastly, Chapter 10 concludes the current experimental findings and outlines possible future work.

Chapter 2

Materials and Experimental Techniques

"There is no such thing as a failed experiment, only experiments with unexpected outcomes."

- Richard Buckminster Fuller -

2.1 Introduction

Due to growing environmental concerns, the idea of polymer recycling has emerged, leading to the progressive replacement of thermosets by thermoplastics (Fréchette et al., 2010). This trend involves not only classical composites, but also the newly emerging polymer nanocomposites. The use of a polyolefin, such as polyethylene, as a base polymer, is therefore encouraged considering the ease with which they can be recycled. Here, a basic understanding of polyethylene is presented, before embarking on detailed discussions. Some of the reasons for polyethylene being favoured in electrical insulation applications include its low relative permittivity, low dielectric loss tangent and high dielectric strength.

Polyethylene is a thermoplastic polymer comprised exclusively of carbon and hydrogen. It is the polyolefin produced by polymerising the olefin ethylene. The chemical structure is a series of repeating $-CH_2-$ units as shown in Figure 2.1.

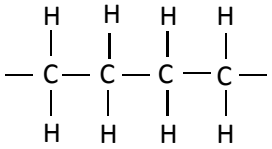

Figure 2.1: Polyethylene chain

Polyethylene is a semicrystalline polymer, i.e., it contains both crystalline and amorphous phases. Since the molecules adopt a closely packed all-trans configuration with the crystals and less perfect conformations within amorphous regions, increased crystallinity equates to a higher overall density. It is the crystalline regions that give polyethylene many good properties, such as toughness, high

modulus, and moisture and gas permeation resistance (Bernstein and Tarpey, 2003). For crystallinity to occur, the aligned chains must be able to approach each other closely and, consequently, chain branching influences the crystallisation process by interfering with the ability of the polyethylene chains to adopt a regular crystalline structure.

For this reason, polyethylene can be classified into different categories based on its density and branching. For example, low density polyethylene (LDPE) is defined by the density range of 0.910 to 0.940 g cm^{-3}. As shown in Figure 2.2, LDPE has a high degree of short and long chain branching. The branches cannot be packed into the crystal structure and therefore LDPE is less crystalline due to the side branches. LDPE is also regarded as a branched polyethylene (BPE).

Figure 2.2: Structure of low density polyethylene

Meanwhile, high density polyethylene (HDPE) is defined by a density greater than or equal to 0.941 g cm^{-3}. As illustrated in Figure 2.3, it has a low degree of branching and thus it is more crystalline, has higher density, has higher melting point, and is mechanically stronger when compared with LDPE. HDPE can also be regarded as linear polyethylene (LPE).

Figure 2.3: Structure of high density polyethylene

Although polyethylene possesses high potential for replacing currently available insulation materials, the use of LDPE and HDPE alone might not be advantageous. On the one hand, HDPE, although having a high dielectric breakdown strength, faces the downside of possessing a high mechanical modulus at room temperature. On the other hand, LDPE, although having reasonable breakdown strength, suffers from poor mechanical performance at high temperature. Therefore, the selection of a polyethylene blend composed of both LDPE and HDPE in an appropriate composition could be a good compromise, as reported elsewhere in the literature

(Hosier, 1996; Hosier et al., 1997). Moreover, the use of a suitable polyethylene blend enables structural changes to be readily detected.

The amorphous regions of a polymer are sites where foreign contaminants (e.g. impurities and ions) can reside. These regions are characterised by larger distances between the polymer chains compared to crystalline regions. In the case where a polymer is completely or almost completely amorphous, inorganic fillers are incorporated to provide the needed toughness. It should be noted that any additives or impurities will reside in the amorphous regions, not the crystalline regions (Bernstein and Tarpey, 2003).

When considering nanodielectrics, there are generally three types of nanofillers currently under development, namely one-, two- and three-dimensional nanoparticles. Out of those three types, nanoparticles with insulating properties are of primary interest for application in dielectric systems, and most of the one- and three-dimensional nanoparticles fall into this category. An example of a one-dimensional nanofiller is the layered silicate montmorillonite clay. This is nanoscopic in one dimension, while the other two dimensions of clay platelets can approach the micrometre range. However, the use of such nanoclays is very complicated, due to the exfoliated and intercalated structures that can form when incorporated into polymers. Such structures could affect the performance of nanocomposites and it is speculated that exfoliated nanoclay performs better than intercalated nanoclay. Furthermore, nanoclay is chemically incompatible with polyolefins (e.g. polyethylene and polypropylene) and compatibilizers such as maleic anhydride grafted polyethylene and maleic anhydride grafted polypropylene are required. This complexity brought about by layered silicate nanoparticles could lead to futher complication in understanding the behaviour of nanodielectrics. High dielectric losses have also been observed in such systems (Green, 2008).

Spherical nanoparticles are considered as three-dimensional nanoparticles possessing insulating properties. They are also commonly referred to as inorganic oxide nanoparticles. Silica nanoparticles belong to this group. Unlike layered silicate nanofillers, nanosilica can be rendered chemically compatible with polyolefins relatively easily. A common concern shared by all types of nanoparticles is the

homogenous dispersion of nanoparticles in polymers. Dispersing spherical nanoparticles in polymers is a challenging task but, generally, using this type of nanofiller is less complicated and less troublesome than layered silicate nanofillers.

2.2 Materials and Preparation

2.2.1 Materials

The polymers used in this research were the low density polyethylene (LDPE) grade LD100BW obtained from ExxonMobil Chemicals and the high density polyethylene (HDPE) grade Rigidex HD5813EA obtained from BP Chemicals. The nanofiller used was silicon dioxide (SiO_2) nanopowder (nanosilica) obtained from Sigma-Aldrich, with a quoted particle size range from 10 nm to 20 nm. The nanofiller is referred to as "untreated" nanosilica. For the purpose of nanosilica surface treatment, trimethoxy(propyl)silane, having purity of 97 %, was obtained from Sigma-Aldrich. The nanosilica subjected to surface treatment is referred to as "C3-treated" nanosilica.

2.2.2 Surface Treatment of Nanosilica

Surface treatment of the nanosilica was performed using the following anhydrous route (Holt et al., 2011). In a flask, 15 g of untreated nanosilica was suspended in 200 ml of dry tetrahydrofuran (THF), followed by the addition of 7 ml of trimethoxy(propyl)silane as the silane coupling agent. At room temperature, the mixture was sonicated for 10 min, followed by stirring on a sealed rotary evaporator at 180 rpm for 20 min and subsequently 80 rpm for 40 h. The resulting mixture was divided into flasks of equal weight prior to centrifugation at 3500 rpm for 10 min and decanting of the supernatant. Fresh, dry THF was then added to each container, which was vigorously shaken until the nanosilica was again suspended in the solvent. The washing process was repeated three times with THF and two times with dry ether to remove the residuals. The resulting solid was washed from the containers into a round bottom flask. All solvent was removed on a rotary evaporator before drying the white solid for 24 h under high vacuum.

2.2.3 Preparation of Materials

The materials of interest were prepared using a solution blending method. To begin with, the desired amount of nanosilica was added into the xylene and sonicated for 1 h to create a suspension. This was followed by the incorporation of polymer. The desired amount of polymer was weighed and added into the xylene/nanosilica suspension to give a 5 % w/v (polymer/xylene) concentration. For example, a polyethylene blend containing 80 wt% of LDPE and 20 wt% of HDPE was composed of 8 g of LDPE and 2 g of HDPE in 200 ml of xylene. In order to comply with COSHH regulations, a refluxing apparatus was used to prepare the material, so that none of the solvent was lost through evaporation. The task was carried out in a fume cupboard to avoid further exposure to solvent vapour.

The polymer and xylene/nanosilica suspension were mixed inside a round bottomed flask attached to a water filled condenser, which was heated by a stirrer mantle (Electrothermal Model EMA0500CEB). Within the stirrer mantle, the polymer/xylene/nanosilica mixture was heated to the boiling point of xylene, i.e., about 140 ºC, and stirred simultaneously by using a magnetic stirrer bar. The heat was turned off after 15 min of boiling, by which time, all the polymer pellets had dissolved and none of the pellets were visible. Meanwhile, methanol with a volume greater than that of the xylene (e.g. 300 ml of methanol for 200 ml of xylene) was prepared in a Pyrex beaker.

The hot polymer/xylene/nanosilica mixture was poured into the methanol quickly with vigorous stirring, resulting in immediate precipitation of the nanocomposite as a gel. The precipitated gel containing the entrained nanoparticles was filtered, dried and melt pressed at 150 ºC, followed by vacuum drying at 100 ºC for 1 h. All the prepared materials were finally examined using differential scanning calorimetry to ensure uniformity of the base material. Further material preparation steps were undertaken, based on the requirement of the experimental tests. For comparison purposes, unfilled polyethylene was prepared in the same way as the nanocomposites.

Since residual solvent or impurities may affect the electrical properties, care was taken to dry all materials thoroughly. FTIR spectra obtained from samples processed

as above showed no evidence of absorption peaks relevant to solvents or impurities; this will be discussed in Chapter 4. Also, dielectric spectroscopy studies, which will be discussed in Chapter 5, clearly showed that polar molecules can be readily detected in this way; none were found in the as-prepared samples. Finally, previous work has compared the electrical response of polymers processed directly from the melt and the same polymer after solution processing as conducted here: no differences were found. As such, it is concluded that the samples considered here do not contain significant residual solvent or impurities.

2.3 Experimental Techniques

2.3.1 Differential Scanning Calorimetry

The thermal behaviour of the materials was characterised using differential scanning calorimetry (DSC). A Perkin Elmer DSC 7 with Perkin Elmer Pyris software was used for this purpose. For each measurement, a sample of about 5 mg in weight was used, placed in a sealed aluminium pan. The experiment was performed in a nitrogen atmosphere. The equipment was allowed to warm up for 1 hour prior to calibration and measurement. High purity indium, having a known melting temperature of 156.6 ºC and melting enthalpy of 28.45 J g^{-1}, was used for calibration purposes. Generally, a scan rate of 10 ºC min^{-1} was used to determine the melting behaviour of the material, unless otherwise mentioned. It should be noted that the calibration values vary for different temperature scan rates. Therefore, calibration has to be performed distinctly for each temperature scan rate. Overall, an accuracy of ± 1 ºC in temperature and ± 3 % in enthalpy is estimated based upon repeated measurements from a similar set of test samples.

Avrami analysis was performed by DSC. The procedures involved are summarised in Figure 2.4. For the case of isothermal crystallisation, the calibration values for 1 ºC min^{-1}, 5 ºC min^{-1} and 10 ºC min^{-1} were taken into account before extrapolation was done to determine the calibration value for 0 ºC min^{-1}, which was required for the offset of the crystallisation temperature in the DSC. An example of a DSC isothermal crystallisation trace as a function of time is shown in Figure 2.5.

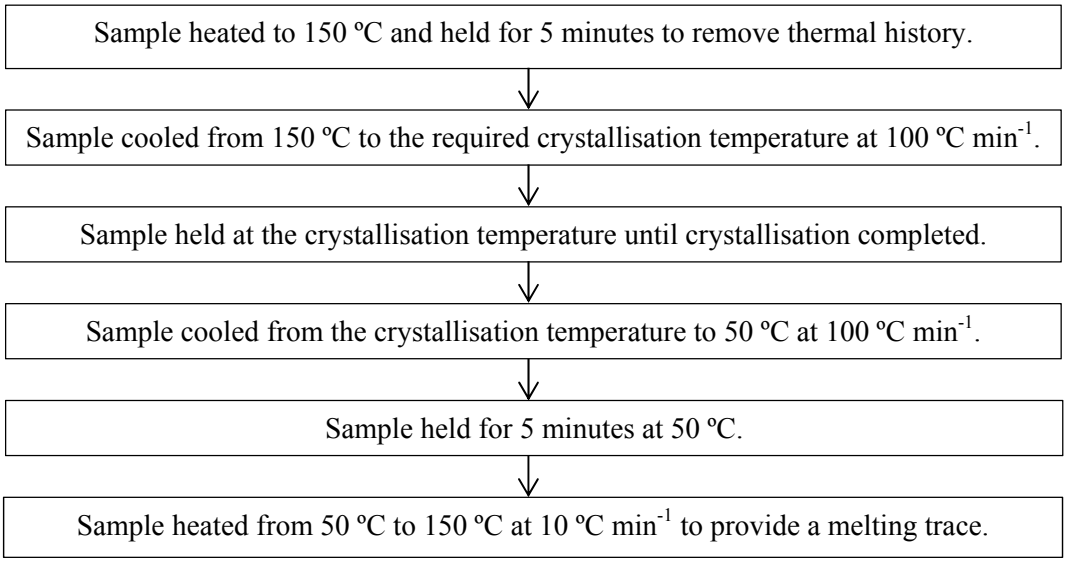

Figure 2.4: DSC procedures for Avrami analysis

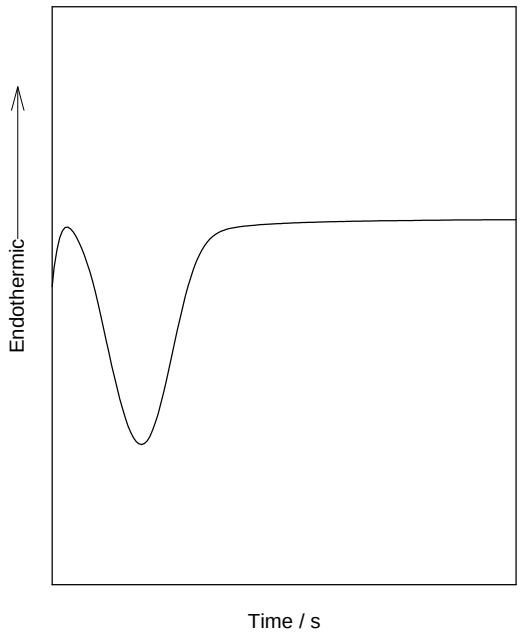

Figure 2.5: DSC isothermal crystallisation trace as a function of time

2.3.2 Fourier Transform Infrared Spectroscopy

Fourier transform infrared (FTIR) spectroscopy was used to obtain chemical information pertaining to appropriate samples. A Perkin Elmer Spectrum GX spectrometer with a standard mid-infrared triglycine sulphate (MIRTGS) detector was used for this purpose. The data for each spectrum were collected from 400 cm^{-1}

to 4000 cm^{-1} over 8 scans at 4 cm^{-1} resolution. The sample used was ~85 μm in thickness.

FTIR microspectroscopy was used to characterise samples of silica nanopowder by collecting spectral data. A Perkin Elmer Spectrum GX spectrometer with an infrared microscope was used for this purpose. The data for each spectrum were collected from 700 cm^{-1} to 4000 cm^{-1} over 32 scans at 4 cm^{-1} resolution.

2.3.3 Polarised Optical Microscopy

To prepare samples for polarised optical microscopy (POM), the material prepared using the solution blending method was cut into a small piece and placed between two microscope slides. It was left on a hot plate to melt at 150 ºC for 5 min. Pressure was then gently applied to the sample to avoid any unnecessary stress being transferred to the polymer. The sample was then isothermally crystallised using a Linkam THM600 hot stage after being melted at 150 ºC for 5 minutes.

2.3.4 Scanning Electron Microscopy

Samples for scanning electron microscopy (SEM) were prepared using a standard permanganic etching technique (Olley and Bassett, 1982). Internal surfaces were first exposed through microtomy using an RMC MT7 cryo-ultramicrotome. The sample was then etched for 4 hours in a permanganic reagent composed of a 1 % w/v solution of potassium permanganate in an acid mixture composed of 5 parts concentrated sulphuric acid, 2 parts phosphoric acid and 1 part water. After etching, the reagent was quenched using 1 part hydrogen peroxide in 4 parts dilute sulphuric acid. Samples were finally rinsed in distilled water followed by acetone. Etched samples were mounted onto standard aluminium SEM stubs and gold coated. Gold coating of samples was required in order to create a grounding path for the beam electrons during SEM.

A JEOL Model JSM-5910 was used for SEM analysis. A voltage of 15 kV and a working distance of 11 mm were used. For the purpose of gold coating, an Emitech

K550X coating unit was used with an Edwards E2M2 high-vacuum pump. Coating was carried out at 25 mA for 3 min.

2.3.5 Atomic Force Microscopy

Samples for atomic force microscopy (AFM) were prepared in the same way as the samples prepared for SEM, but without gold coating.

AFM experiments were carried out using an MFP-3D^{TM} (Asylum Research) instrument equipped with an MFP head and MFP scanner. The images were captured in alternating current (AC) mode. Real time scanning was performed in air at room temperature with a scan rate of 0.5 Hz. A silicon cantilever type OMCL-AC200TS-R3 (nominal spring constant 9 N m^{-1}, Olympus) with a tetrahedral tip (nominal radius 7 nm) was used. The images were recorded and analysed using the AFM software Igor Pro version 6.22A.

2.3.6 Dielectric Spectroscopy

Samples for dielectric spectroscopy testing were prepared using a Graseby Specac 25.011 hydraulic press. The desired material was cut into small pellets or thin sheets. To prepare a sample disk, the desired amount of the material was placed centrally between two aluminium foils within a suitable mould ring. At a temperature of 150 ºC, the pellets/sheets were preheated for 3 min prior to a load of 3 ton being applied (the load was increased slowly from 0 to 3 ton). The pressed disk was then left to relax for 5 min before being removed from the mould.

To obtain an isothermally crystallised sample, the disk was isothermally crystallised in an oil bath (Grant Model W28) from the melt at 115 ºC for 1 h, followed by quenching into water. The thickness of the prepared samples was ~420 μm. If a quenched sample was required, the disk was quenched directly into water from the melt. Both sides of the sample were gold coated to ensure good electrical contact between the sample and the electrodes. An Emitech K550X sputter coater was used

for this purpose and a coating current of 25 mA and coating time of 3 min were used such that the surface resistance was about 10 Ω, which gave a high signal-to-noise ratio.

Dielectric spectroscopy is used to measure the dielectric properties of an insulating material as a function of frequency. It is based on the interaction of an external field with the electric dipoles within the sample, often expressed as permittivity. The dielectric response was measured using a Solartron 1296 dielectric interface together with a Schlumberger SI 1260 impedance/phase gain analyser and a Solartron 12962A sample holder with a 20 mm diameter electrode. In order to collect the data, an AC voltage of 1 V was applied and the frequency was swept from 0.1 Hz to 0.1 MHz at 8 points per decade. 10 cycle integrations per point was found sufficient for de-noising. The real relative permittivity and dielectric loss tangent of each sample were calculated; at least two samples were tested to ensure reproducibility of the test data and an overall accuracy of ± 5 % is estimated based upon repeated measurements from a similar set of test samples.

Prior to dielectric spectroscopy testing, the samples were dried in a vacuum oven at 60 ºC until no significant weight change could be observed. In order to investigate the effect of water absorption, the samples were immersed in 40 ml of distilled water and placed in a sealed chamber for different time intervals. The samples were then carefully dried with a tissue before being weighed and subjected to dielectric spectroscopy testing. The sample weights (typically 0.23 g to 0.27 g) were monitored by a 5 digit balance (Sartorius MC210P) to an accuracy of ± 0.00005 g. Since the measurement uncertainty is ± 0.00005 g, this provides an uncertainty of about 0.02 %.

2.3.7 Electrical Breakdown Test

2.3.7.1 AC Breakdown Test

Samples for AC breakdown testing were prepared in the same way as for the samples prepared for dielectric spectroscopy testing. However, the thickness of the samples used was changed to ~85 μm and the samples were not subjected to gold coating.

AC breakdown testing was conducted based upon the general consideration laid down in the ASTM Standard D149-87 (Dissado and Fothergill, 1992; Fournier and Lamarre, 1992; Ku and Liepins, 1987). Figure 2.6 shows the main components used in the test equipment. Components surrounded by the dashed line were used at high voltage and were therefore enclosed in an interlocked safety cage. In the test cell, the test sample was placed between two opposing 6.3 mm diameter steel ball-bearing electrodes immersed in Dow Corning 200/20cs silicone fluid to prevent surface flashover. The upper electrode was connected to the high voltage supply while the lower electrode was grounded. A 50 g load was applied to the upper electrode (total mass of upper electrode, 56 g) in order to expel any fluid from the electrode and sample, which would affect the breakdown data.

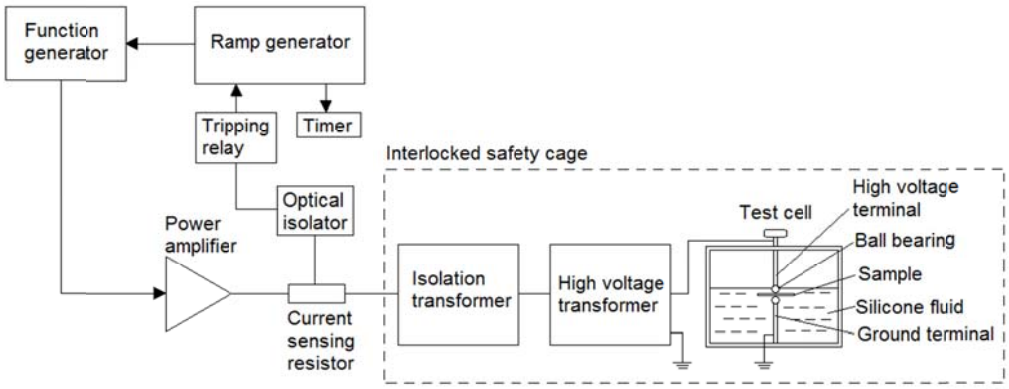

Figure 2.6: AC breakdown test configuration

A warm up time of 1 h was required before the calibration of the equipment was performed. An AC voltage of 50 Hz was generated from the function generator, the amplitude of which was controlled by a ramp generator to give a ramp rate of 50 $V_{(RMS)}$ s^{-1}. This signal was fed to the power amplifier and then to the transformers, which could generate up to 30 kV. The voltage was applied until the sample failed. When the sample failed, a voltage was generated across the current sensing resistor and detected by the tripping relay through the optical isolator, which prevents unwanted feedback. The relay then cut-off the signal to the power amplifier and the circuit remained tripped until the relay was manually reset. It should be noted that the maximum acceptable output voltage of the system was about 18 kV.

On each sample, only 5 breakdown tests were conducted to avoid the problem of electrical flashover caused by adjacent breakdown holes. A total of 20 breakdown

tests were performed on each type of material, with the ball-bearing electrodes being changed after 10 tests in order to avoid pitting of the electrodes, which would affect the breakdown data (Hosier, 1996). The voltage obtained from the test was divided by the sample thickness at the breakdown point in order to obtain the breakdown field. The resulting breakdown data were statistically analysed assuming two-parameter Weibull statistics.

2.3.7.2 DC Breakdown Test

Samples for DC breakdown testing were prepared using a large hydraulic press. This is due to the need for specimens of a larger diameter which could not be fulfilled by the Graseby Specac 25.011 hydraulic press. The larger diameter was required to ensure that the separation distance between each breakdown point was large enough to avoid the possibility of electrical flashover caused by adjacent breakdown holes due to the higher DC breakdown voltage (more than 2 times higher than the AC breakdown voltage).

A moulding temperature of 150 ºC was used. The pellets/sheets were preheated for 2 min prior to a load of 3 ton being applied. The pressed disk was then left to relax for 2 min before being removed from the mould. The disk was finally subjected to quenching or isothermal crystallisation at 115 ºC. The size of the prepared samples was ~85 μm in thickness.

The test setup used for DC breakdown testing is comparable to the AC breakdown system described above and, therefore, a detailed explanation is not warranted here. Generally, the test was conducted between two opposing 6.3 mm diameter steel ball-bearing electrodes immersed in Dow Corning 200/20cs silicone fluid to prevent surface flashover. A warm up time of 1 h was required before the calibration of the equipment was performed. A DC ramp voltage increasing at 100 $V_{(DC)}$ s^{-1} was applied until the sample failed. It should be noted that the maximum acceptable voltage of the system was about 75 kV. As with AC breakdown testing, a total of 20 breakdown tests were performed on each material. The resulting dielectric

breakdown data were again statistically analysed assuming a two-parameter Weibull distribution.

2.3.8 Pulsed Electro-acoustic Test

Disk samples for pulsed electro-acoustic (PEA) testing were prepared in the same way as described above, but the thickness of the samples was ~200 μm. Figure 2.7 shows the experimental PEA setup. Generally, the test system consists of a high voltage electrode (top electrode), ground electrode (bottom electrode), piezoelectric transducer, amplifiers and oscilloscope. An acoustic absorber (not shown in the figure for simplicity) is used to absorb the acoustic wave. The test sample was inserted between the top and bottom electrodes and silicone oil was used to ensure good acoustic coupling between the sample and the electrodes. In order to protect the circuit from damage due to high currents, a resistor was connected in series with the DC power supply and a capacitor was connected to the pulse power supply.

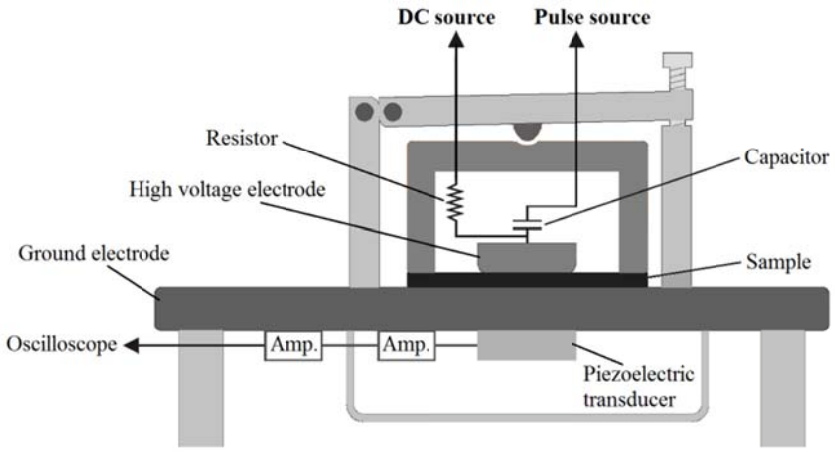

Figure 2.7: Pulsed electro-acoustic test setup

In PEA, a pulse voltage of 600 V with a pulse width of 5 ns was applied to the sample to generate an acoustic wave. Calibration was conducted at 10 kV mm^{-1} with a short period of voltage application time to minimise any possible space charge effects. Space charge accumulation testing was then conducted at the desired DC field of 25 kV mm^{-1} or 40 kV mm^{-1} for the required period at room temperature. The sample was then short-circuited upon the removal of the external voltage and the charge decay process was monitored. The resulting data were analysed using the

calibration trace and a deconvolution technique was applied to restore the original signal. LabVIEW software was used for the purpose of data analysis.

2.3.9 Absorption Current Measurements

Samples for absorption current measurements were prepared in the same way as those for dielectric spectroscopy. However, the thickness of the samples used was changed to ~200 μm. Both sides of the sample were gold coated with a coating current of 25 mA and a coating time of 3 min to ensure gold electrical contact between the electrodes and the sample.

Absorption current measurements were performed by using a Keithley 6487 picoammeter / voltage source and a sample holder with two opposing 20 mm diameter electrodes. A DC field of 25 kV mm^{-1} or 40 kV mm^{-1} was applied and the resulting current was recorded as a function of time. Prior to measurement, each sample was grounded at 60 ºC in vacuum for at least 72 h so that excess charge would dissipate.

Chapter 3

Thermal Analysis

"Science is perhaps the only human activity in which errors are systematically criticised and, in time, corrected."

- Karl Popper -

3.1 Introduction

According to Callister (2007), there are three important thermal phenomena that should be considered when dealing with polymeric insulation materials, namely crystallisation, melting and the glass transition. Since the base materials utilised in nanocomposites are mainly based on polymers, such phenomena should therefore receive adequate attention when dealing with nanocomposites.

Crystallisation is a process by which, upon cooling, nuclei (crystalline), an ordered solid phase, is produced from a liquid melt, wherein small regions of the tangled and random molecular conformations become ordered and aligned in the manner of chain-folded layers, as shown in Figure 3.1. It should be noted that the folded surfaces are non-crystalline. Therefore, in polyethylene, as well as in any other polymer, the achievement of complete crystallisation (100 % crystallinity) is not possible. The temperature at which crystallisation occurs is termed the crystallisation temperature, T_c . Polymers that are crystallised from the melt are usually semicrystalline and form a spherulitic structure. The spherulite is roughly spherical in shape, as illustrated in Figure 3.2.

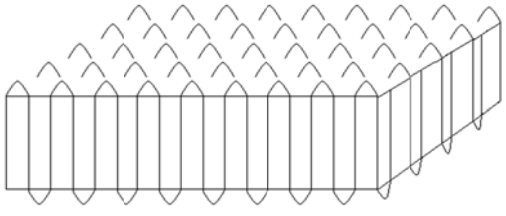

Figure 3.1: The chain-folded structure for a plate-shape polymer crystallite (lamellae)

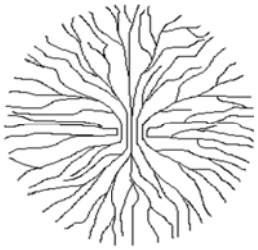

Figure 3.2: Spherulite structure

Melting is the reverse process of crystallisation, and occurs when the polymer is heated above its melting temperature. It is a transformation of a solid material having an ordered structure of aligned molecular chains into a viscous liquid, in which the structure is highly random. The temperature at which melting occurs is termed the melting temperature, T_m.

The glass transition, on the other hand, occurs in amorphous or non-crystallisable polymers (or amorphous regions within a semicrystalline system) such that, when cooled from the liquid melt, become rigid solids yet retain the disordered molecular structure that is characteristic of the liquid state. Upon cooling, the glass transition corresponds to the gradual transformation from a liquid to a rubbery material, and finally to a rigid solid. The temperature at which the polymer experiences the transition from rubbery to rigid state is termed the glass transition temperature, T_g. This sequence of events occurs in the reverse order when a rigid glass at a temperature below its glass transition temperature is heated.

For semicrystalline polymers, crystalline regions will experience melting and crystallisation, while non-crystalline regions pass through the glass transition. In other words, T_m and T_c are the properties of the crystalline phase while T_g is the property of the amorphous phase in semicrystalline materials. The thickness of the chain folded-lamellae will depend on the crystallisation temperature. The thicker the lamellae, the higher the melting temperature. An increase in lamellar thickness may be induced by annealing just below the melting temperature. A diagram illustrating the melting, crystallisation and glass transition temperatures for a semicrystalline material is shown in Figure 3.3. It should be noted that there is a discontinuous change in specific volume at T_m.

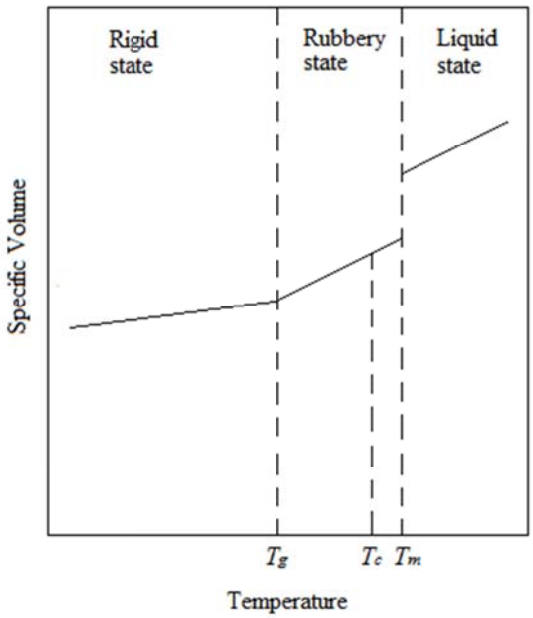

Figure 3.3: Melting, crystallisation and glass transition temperatures for a semicrystalline polymer

3.2 Avrami Theory

The Avrami equation (Avrami, 1939; Avrami, 1940; Avrami, 1941) can be used to describe the crystallisation kinetics of any material and describes the time evolution of the overall crystallinity (Gedde, 1995). In the simplest derivation of the Avrami equation, it is assumed that crystallisation starts simultaneously at different locations and propagates outwards from the nucleation sites; the nuclei are formed and start to grow at zero time and the growth occurs at a constant rate in all directions. In a slightly more complex case, the nuclei are formed at a constant rate both in space and time, as illustrated in Figure 3.4.

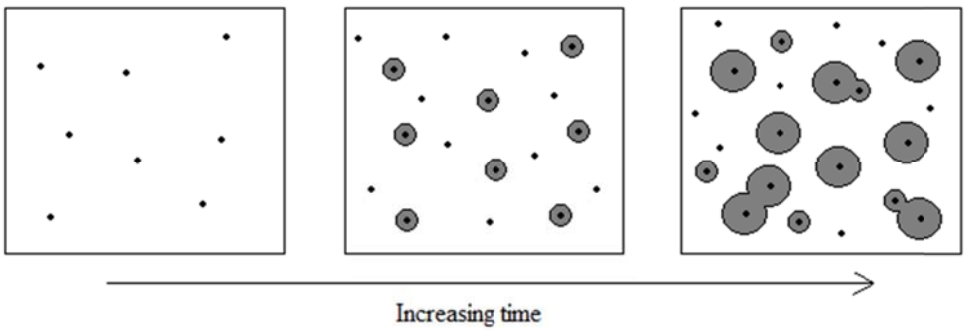

Figure 3.4: Nuclei growth based on Avrami model

The extent of crystallisation is often seen to follow a characteristic S-shape, in which the crystallisation rate is slow at the beginning and the end but rapid in between, as shown in Figure 3.5. The initial slow rate is attributed to the low crystallisation activity around the nuclei. The rapid crystallisation rate in between is attributed to primary crystallisation, which is characterised by the radial growth of nuclei into particles (e.g. spherulites) combined with the continuous generation of nuclei. Near the end of crystallisation, secondary crystallisation takes place, in which few nuclei are formed and the particles begin to impinge on one another, causing their growth to stop.

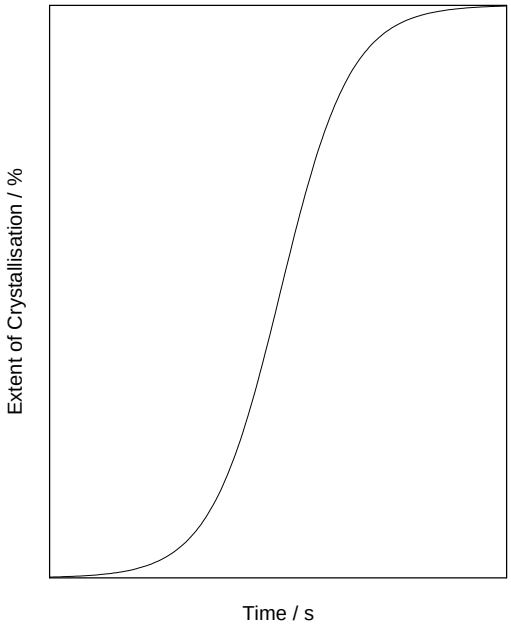

Figure 3.5: Extent of crystallisation under isothermal condition

Crystallisation based on different nucleation and growth mechanisms can generally be described using the following Avrami equation:

$$1 - \frac{V_c}{V_\infty} = \exp(-K_{exp} t_c^n) \tag{3.1}$$

where V_c is the volume fraction of crystallinity, V_∞ is the maximum crystallinity attained, t_c is the time elapsed after the onset of crystallisation, K_{exp} is the experimental rate constant or overall crystallisation rate constant containing contributions from both nucleation and growth and n is the Avrami exponent or dimensionality of the growth.

Theoretically, there are two cases of nucleation to be considered, namely athermal nucleation and thermal nucleation. For athermal nucleation (instantaneous nucleation), all nuclei are simultaneously formed and start to grow at an induction time, t_i, i.e., $t_c = 0$. For thermal nucleation (sporadic nucleation), the nuclei are formed at a constant rate both in space and time. Practically, the nucleation is seldom either completely athermal or completely thermal, and a mixture of the two is common. This will have an effect on the interpretation of the Avrami exponent, n.

It should be noted that the Avrami index, n, is composed of two terms:

$$n = n_d + n_n \tag{3.2}$$

where n_d represents the dimensionality of crystal growth, with values such as 1, 2 or 3 corresponding to one-, two- or three-dimensional entities that are formed, while n_n represents the time dependence of the nucleation, with values such as 0 or 1, which correspond to ideal athermal nucleation or thermal nucleation, respectively. For example, for a polymer that crystallises in a spherulitic morphology (three-dimensional), ideal athermal nucleation should exhibit an Avrami index of 3 while ideal thermal nucleation should exhibit an Avrami index of 4.

3.3 Results and Discussion

3.3.1 Isothermal Crystallisation Behaviour

The crystallisation behaviour of polyethylene nanocomposites was investigated using DSC and analysed using the Avrami method. For a polymer, Avrami theory would provide a good fit of the experimental data at least up to approximately 50 % relative crystallinity (Lorenzo et al., 2007). Later, the impingement of spherulites starts to occur, so marking the end of primary crystallisation. Meanwhile, the determination of the relative crystallinity at 0 % is affected by the onset of crystallisation. Consequently, the percentage crystallinity of the material as a function of time was obtained in the range 5 % to 50 % in 5 % increments using the Perkin Elmer Pyris software. Rearranging Equation 3.1, the following equation was obtained:

$$\chi = 1 - \exp[-K_{exp}(t - t_i)^n] \quad (3.3)$$

where χ represents the crystallinity fraction at time t while t_i represents the induction time, with other parameters remaining unchanged. The obtained experimental values of χ and t were then fitted to Equation 3.3 using a non-linear approach to estimate the K_{exp}, t_i and n.

Figure 3.6 shows non-linear Avrami plots of the development of crystallinity as a function of time for the unfilled polyethylene, nanocomposites containing 5 wt% of untreated nanosilica and nanocomposites containing 5 wt % of C3-treated nanosilica, isothermally crystallised at different temperatures. Generally, from all the figures, the time required for complete crystallisation varies with temperature. Specifically, for all the investigated polyethylene systems, there is a noticeable trend where the higher the crystallisation temperature, the longer the crystallisation process takes. Such observations fall well within the theory of crystallisation and are attributed to the temperature dependence of nucleation and growth rates.

At a fixed crystallisation temperature, all the nanocomposites experienced faster crystallisation when compared with the unfilled polyethylene, as illustrated in Figure 3.7. This could be mainly attributed to the presence of nanosilica that acts as nucleating sites for the formation of spherulites, as opposed to the unfilled polyethylene, which contains sparse nucleating sites. Comparable observations have also been reported by Tian et al. (2006) in an investigation into poly(ethylene terephthalate)/silica nanocomposites. It is noteworthy that with the presence of nanosilica as nucleating sites, the separation distance between the spherulites in the nanocomposites would be reduced, causing the spherulite impingement to happen more rapidly when compared with the unfilled polyethylene. With regard to this, crystallisation in nanocomposites may be dominated by the nucleation sites per unit volume, N, as opposed to the unfilled polyethylene, which seems to be dominated by the crystal growth rate, G.

Assuming three-dimensional crystal growth, Kowalewski and Galeski (1986) suggested that the effective three-dimensional crystallisation rate constant, K_3, can be determined from the experimentally measured K_{exp} using the following equation:

$$K_3 = \frac{4}{3}\pi N G^3 \cong (K_{exp})^{\frac{3}{n}} \tag{3.4}$$

where N is the number of nucleation sites per unit volume and G is the growth rate of the crystallising objects.

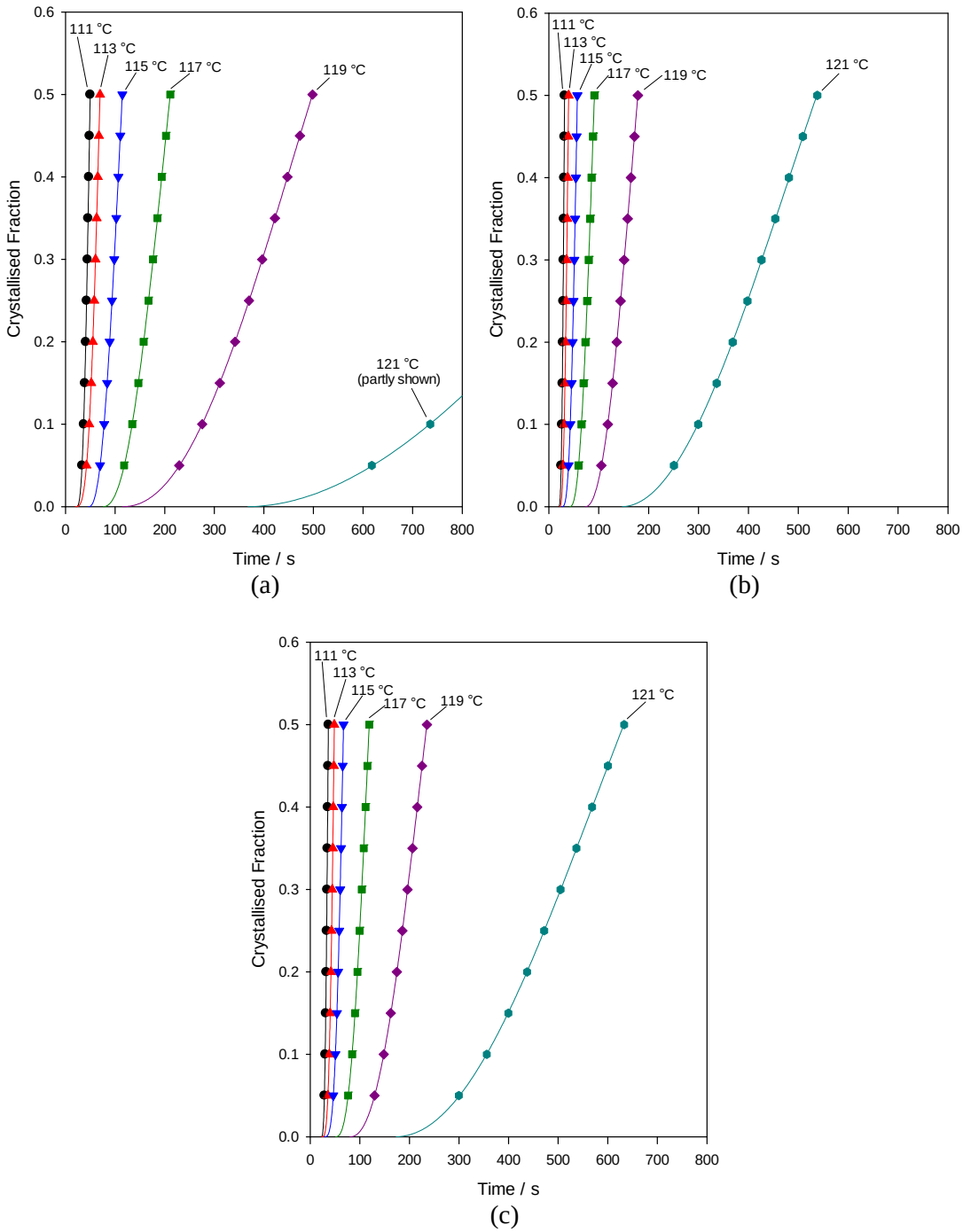

Figure 3.6: Non-linear Avrami fitting to the development of crystallinity for (a) unfilled polyethylene, (b) nanocomposites containing 5 wt% of untreated nanosilica, (c) nanocomposites containing 5 wt% of treated nanosilica, at different isothermal crystallisation temperatures

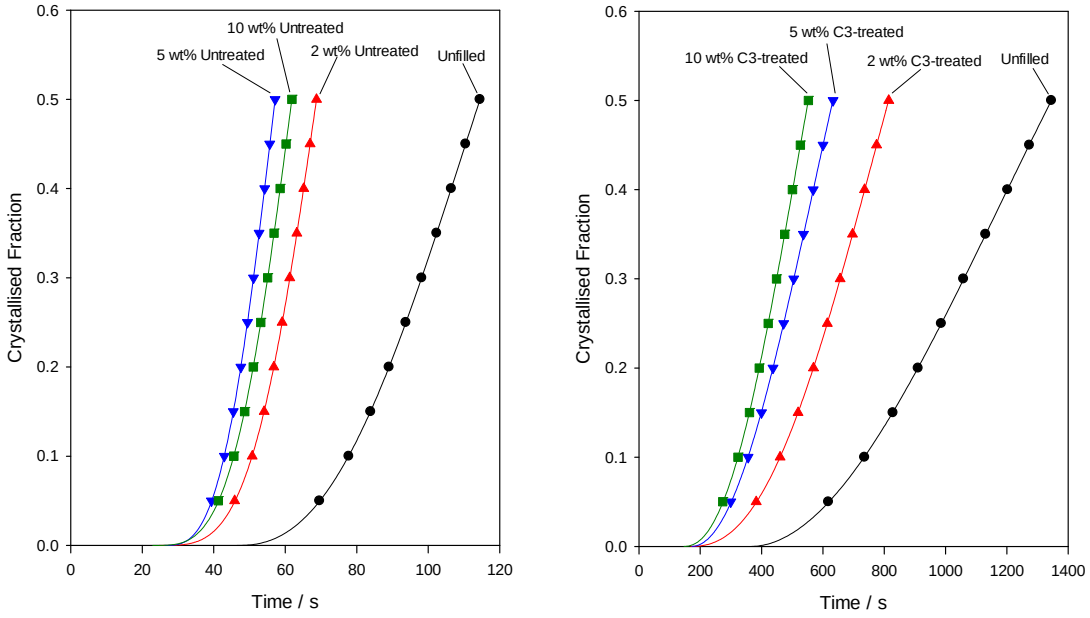

Figure 3.7: Comparison of the development of crystallinity between unfilled polyethylene and (a) nanocomposites containing untreated nanosilica crystallised isothermally at 115 ºC, (b) nanocomposites containing treated nanosilica crystallised at 121 ºC

Vaughan et al. (2006) proposed that heterogeneous nucleation is closely related to the local interactions that occur between the crystallising polymer and the substrate, in which nucleation is expected to be enhanced if the polymer and the substrate interact strongly and vice versa. Consequently, N will reflect the local molecular interactions between the filler and the polymer. However, in order to determine the absolute number of nuclei from the equation, G must be known and this is often not directly measurable for the case of nanofilled material. Therefore, the results that are presented are not in terms of absolute nucleation densities but rather, in terms of the crystallisation rate constant, K_3. This removes the need to assume that crystal growth occurs in the same way for the unfilled and filled systems.

The Avrami parameters, n, K_{exp} and K_3 generated for each of the material systems at different crystallisation temperatures are shown in Table 3.1. In these cases, it is assumed that variations in the Avrami exponent, n, are caused by factors such as secondary crystallisation and mixed nucleation modes, rather than being a genuine reflection of non-three dimensional development (Kowalewski and Galeski, 1986). The determination of the K_3 parameter was conducted based on Equation 3.4, in

which three-dimensional crystal growth was assumed in all the investigated polyethylene systems.

Table 3.1: Avrami parameters for different materials

Sample	T_c / °C	n	K_{exp} / s^{-1}	K_3 / s^{-3}
Unfilled	111	2.956 ± 0.031	$3.66\times10^{-5} \pm 0.46\times10^{-5}$	3.14×10^{-5}
	113	3.271 ± 0.076	$1.98\times10^{-6} \pm 0.70\times10^{-6}$	5.88×10^{-6}
	115	2.420 ± 0.016	$2.55\times10^{-5} \pm 0.20\times10^{-5}$	2.02×10^{-6}
	117	2.248 ± 0.018	$1.12\times10^{-5} \pm 0.11\times10^{-5}$	2.47×10^{-7}
	119	2.170 ± 0.013	$1.72\times10^{-6} \pm 0.15\times10^{-6}$	1.07×10^{-8}
	121	1.927 ± 0.017	$1.20\times10^{-6} \pm 0.15\times10^{-6}$	6.06×10^{-10}
2 wt% Untreated	111	2.488 ± 0.063	$1.26\times10^{-3} \pm 0.26\times10^{-3}$	3.19×10^{-4}
	113	3.378 ± 0.036	$1.30\times10^{-5} \pm 0.18\times10^{-5}$	4.58×10^{-5}
	115	3.606 ± 0.073	$8.02\times10^{-7} \pm 0.27\times10^{-7}$	8.48×10^{-6}
	117	2.784 ± 0.034	$4.64\times10^{-6} \pm 0.78\times10^{-6}$	1.79×10^{-6}
	119	2.376 ± 0.021	$3.49\times10^{-6} \pm 0.42\times10^{-6}$	1.29×10^{-7}
	121	1.922 ± 0.015	$6.13\times10^{-6} \pm 0.63\times10^{-6}$	7.31×10^{-9}
	122	1.898 ± 0.045	$1.86\times10^{-6} \pm 0.62\times10^{-6}$	8.78×10^{-10}
2 wt% C3-treated	111	2.754 ± 0.060	$4.00\times10^{-4} \pm 0.87\times10^{-4}$	1.99×10^{-4}
	113	3.316 ± 0.052	$1.23\times10^{-5} \pm 0.26\times10^{-5}$	3.61×10^{-5}
	115	3.297 ± 0.064	$2.79\times10^{-6} \pm 0.81\times10^{-6}$	8.83×10^{-6}
	117	2.769 ± 0.017	$3.33\times10^{-6} \pm 0.30\times10^{-6}$	1.16×10^{-6}
	119	2.395 ± 0.017	$2.40\times10^{-6} \pm 0.24\times10^{-6}$	9.13×10^{-8}
	121	2.375 ± 0.023	$1.46\times10^{-7} \pm 0.24\times10^{-7}$	2.32×10^{-9}
5 wt% Untreated	111	3.000 ± 0.115	$4.18\times10^{-4} \pm 1.53\times10^{-4}$	4.18×10^{-4}
	113	2.861 ± 0.051	$1.68\times10^{-4} \pm 0.31\times10^{-4}$	1.10×10^{-4}
	115	3.067 ± 0.046	$1.85\times10^{-5} \pm 0.36\times10^{-5}$	2.35×10^{-5}
	117	2.555 ± 0.017	$3.20\times10^{-5} \pm 0.25\times10^{-5}$	5.28×10^{-6}
	119	2.209 ± 0.028	$2.37\times10^{-5} \pm 0.35\times10^{-5}$	5.23×10^{-7}
	121	2.001 ± 0.036	$4.50\times10^{-6} \pm 1.07\times10^{-6}$	9.63×10^{-9}
	122	1.805 ± 0.036	$5.01\times10^{-6} \pm 1.27\times10^{-6}$	1.55×10^{-9}
5 wt% C3-treated	111	3.206 ± 0.056	$1.00\times10^{-4}\pm 0.25\times10^{-4}$	1.81×10^{-4}
	113	3.737 ± 0.084	$3.72\times10^{-6} \pm 1.27\times10^{-6}$	4.38×10^{-5}
	115	3.444 ± 0.035	$2.31\times10^{-6} \pm 0.36\times10^{-6}$	1.23×10^{-5}
	117	2.667 ± 0.016	$8.93\times10^{-6} \pm 0.71\times10^{-6}$	2.09×10^{-6}
	119	2.297 ± 0.012	$6.42\times10^{-6} \pm 0.43\times10^{-6}$	1.65×10^{-7}
	121	2.059 ± 0.027	$2.27\times10^{-6} \pm 0.41\times10^{-6}$	5.98×10^{-9}
10 wt% Untreated	111	2.846 ± 0.063	$4.38\times10^{-4} \pm 0.91\times10^{-4}$	2.88×10^{-4}
	113	3.316 ± 0.067	$2.08\times10^{-5} \pm 0.54\times10^{-5}$	5.81×10^{-5}
	115	3.494 ± 0.063	$1.92\times10^{-6} \pm 0.54\times10^{-6}$	1.23×10^{-5}
	117	2.690 ± 0.024	$1.20\times10^{-5} \pm 0.13\times10^{-5}$	3.25×10^{-6}
	119	2.273 ± 0.023	$1.10\times10^{-5} \pm 0.14\times10^{-5}$	2.85×10^{-7}
	121	1.805 ± 0.021	$1.34\times10^{-5} \pm 0.19\times10^{-5}$	7.99×10^{-9}
	122	1.982 ± 0.027	$1.27\times10^{-6} \pm 0.25\times10^{-6}$	1.19×10^{-9}
10 wt% C3-treated	111	3.342 ± 0.146	$8.60\times10^{-5} \pm 4.34\times10^{-5}$	2.24×10^{-4}
	113	3.588 ± 0.072	$6.27\times10^{-6} \pm 1.81\times10^{-6}$	4.47×10^{-5}
	115	3.434 ± 0.042	$2.55\times10^{-6} \pm 0.47\times10^{-6}$	1.30×10^{-5}
	117	2.693 ± 0.014	$9.50\times10^{-6} \pm 0.65\times10^{-6}$	2.54×10^{-6}
	119	2.256 ± 0.011	$1.02\times10^{-5} \pm 0.06\times10^{-5}$	2.30×10^{-7}
	121	2.270 ± 0.029	$8.27\times10^{-7} \pm 1.59\times10^{-7}$	9.15×10^{-9}

Figure 3.8 contains plots of crystallisation rate constant, K_3, as a function of crystallisation temperature, T_c, for unfilled polyethylene and nanocomposites containing untreated and C3-treated nanosilica at 2 wt%, 5 wt% and 10 wt% loadings. From this, it is apparent that nanosilica has a marked impact on the crystallisation kinetics of the polyethylene. At any given temperature, the unfilled polyethylene shows the lowest K_3 values when compared with the nanocomposites. With the addition of nanosilica, the K_3 values obtained from the nanocomposites were typically about one order of magnitude greater than that of the equivalent unfilled polyethylene (see the fitted lines). From Equation 3.4, it is evident that changes in K_3 could result from changes in either nucleation density or crystal growth rate.

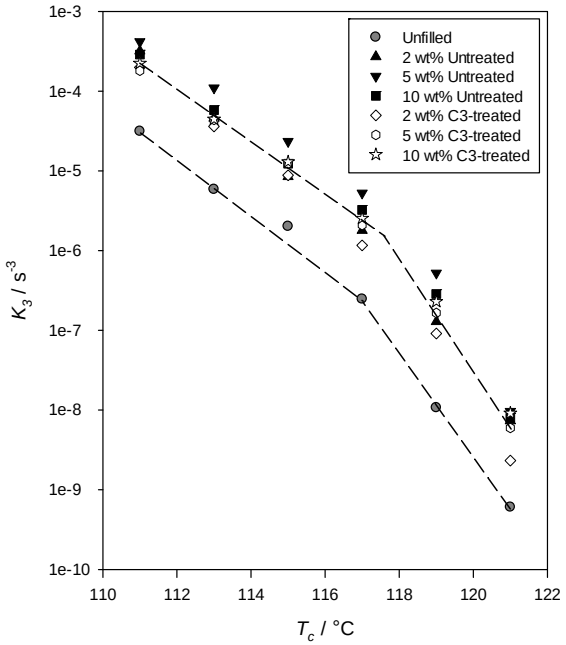

Figure 3.8: Plot showing the effect of nanosilica on the K_3 parameter of random polyethylene-based systems. The fitted lines compare the K_3 parameter of the unfilled polyethylene and the nanocomposites

Figure 3.9 compares the K_3 values obtained from nanocomposites containing untreated nanosilica and C3-treated nanosilica at representative crystallisation temperatures of 113 ºC and 119 ºC. Considering first the systems containing the untreated nanosilica, the addition of 2 wt% nanofiller increases the K_3 value by about one order of magnitude compared with the unfilled polyethylene; increasing the nanosilica content to 5 wt% results in a yet higher K_3 value. However, a further increase in untreated nanosilica content to 10 wt% causes the K_3 value to decrease. Although the reduced K_3 value for this nanocomposite could be due to experimental

uncertainty, repetition showed the effect to be reproducible. Consequently, this effect is suggested to be an indicative of nanosilica aggregation, which reduces the nanosilica's effectiveness as a nucleating agent.

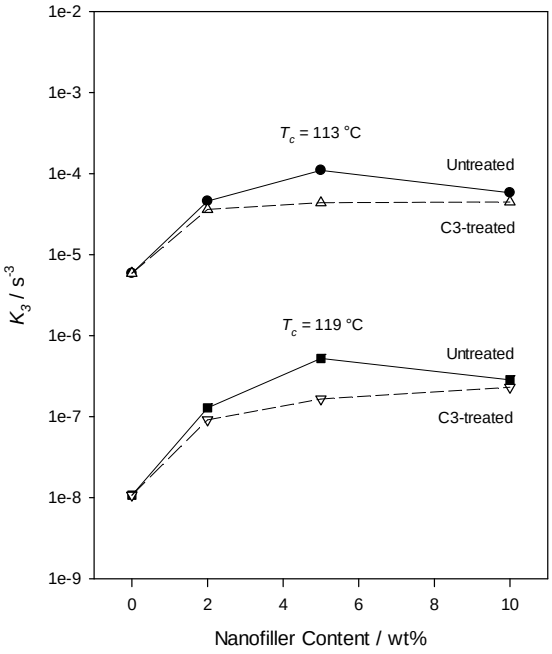

Figure 3.9: Plot showing the effect of nanosilica surface chemistry and nanosilica content on K_3 at representative crystallisation temperatures of 113 ºC and 119 ºC. The filled symbols represent nanocomposites containing untreated nanosilica while the open symbols represent nanocomposites containing C3-treated nanosilica. The straight lines represent the K_3 variation of the untreated system while the dashed lines represent K_3 variation of the C3-treated system

Comparing the filled and open symbols in Figure 3.9, two features are immediately evident. First, K_3 increases monotonically with loading level for the C3-treated nanosilica; there is no evidence of a reduction in nucleating ability at higher nanofiller loadings, suggesting that aggregation has been reduced by surface treatment. Second, it is evident that, at all loading levels, K_3 is lower in the C3-treated case, compared with a nanocomposite containing an equivalent amount of untreated nanosilica. That is, chemical treatment has modified the surface interactions between the polymer and the silica in such a way as to reduce its effectiveness as a nucleating agent. According to the theory of Muchová and Lednický (1996), heterogeneous nucleation is closely related to the energy barrier associated with the transport of molecular chain segments from the polymer melt onto the substrate surface. That is, the local interactions between the polymer and the substrate; if the polymer and the substrate interact strongly, enhanced nucleation

would be expected. In this case, the increased nucleating capacity of the untreated nanosilica compared with its C3-treated equivalent is surprising and suggests that simplistic concepts such as polar, non-polar, hydrophilic and hydrophobic are insufficient when considering the precise factors that determine the compatibility between a filler and a polymer. Indeed, many studies of true epitaxial, pseudo-epitaxial and graphoepitaxial effects (Fenwick et al., 1996; Greso and Phillips, 1994; Kopp et al., 1994) in polymers have been conducted, which focus on structural rather than chemical factors.

The properties of nanocomposites are closely related to the distribution of nanoparticles within the system, which in turn, is determined by a combination of features related to nanoparticle/matrix and nanoparticle/nanoparticle interactions. Considering the first of these, the propensity to form a stable dispersion of nanoparticles within a matrix can be considered in terms of the Gibbs free energy of the system and, as such, will depend on the change in entropy and enthalpy on distributing the nanoparticles into the matrix. Mathematically, this has much in common with the problem of dissolution, as described by Flory (1953), where polymer molecules are successively added to a lattice and the change in the Gibbs free energy is evaluated in terms of the configurational entropy of the assembly and the change in enthalpy associated with the breaking and formation of solvent/solvent, polymer/polymer and polymer solvent bonds. Here, the analogy would involve the same approach, but where nanoparticles are introduced into a lattice initially occupied by polymer molecules. In which case, the stability of the final system would be expected to be largely independent of changes in entropy and dominated by enthalpic effects. However, analysis of the nucleation kinetics suggests that both nanosilica systems interact strongly with the matrix polymer; indeed, the nucleating efficiency suggests that the energy barrier at the melt/substrate interface (Muchová and Lednický, 1996) is less in the case of the untreated nanosilica. Certainly, there is no evidence from this work that the C3-treated nanosilica is more thermodynamically compatible with the polyethylene matrix. In which case, returning to Flory's concepts (Flory, 1953), if matrix/matrix and matrix/nanofiller interactions are comparable for nanocomposites containing both untreated and C3-treated nanosilica, any variations in structure or properties should be related to variations in nanofiller/nanofiller interactions. In the case of the systems considered here, the

effect of surface treatment is ascribed to a combination of reduced hydrogen bonding between nanoparticles and enhanced steric stabilisation (Lopez et al., 2011) in the case of the C3-treated system.

3.3.2 Subsequent Melting Behaviour

Figure 3.10 compares the DSC melting traces for unfilled polyethylene and nanocomposites at various isothermal crystallisation temperatures. It is noteworthy that there are at least two major melting peaks that can be seen in the DSC melting traces since the base polymer used is a polyethylene blend composed of 80 wt% of LDPE and 20 wt% of HDPE. The upper melting peak is relatively sharp and corresponds to an HDPE-rich phase that results from isothermal crystallisation. The lower melting peak corresponds to the LDPE-rich phase, which is only able to crystallise upon cooling in the DSC. At lower crystallisation temperatures, a clear intermediate feature occurs between the peaks, which is indicative of extensive isothermal co-crystallisation of the low molar mass fractions in the HDPE and the more linear fractions of the LDPE. Such observations are not unusual and have been reported elsewhere in the literature (Hosier et al., 2010; Hosier et al., 2000; Hosier et al., 1997).

It should be noted that the melting traces were generally the same for all investigated nanocomposites and thus only the melting traces for nanocomposites containing 5 wt% of untreated nanosilica and 5 wt% of C3-treated nanosilica are shown in Figure 3.10. Considering Figure 3.10, the melting behaviour was generally the same for unfilled polyethylene and nanocomposites containing untreated and C3-treated nanosilica throughout the crystallisation temperature range investigated. The only minor consequence of the addition of nanosilica is upon crystallisation at 111 ºC, where the HDPE-rich phase of the unfilled polyethylene exhibits a pronounced double peak (as indicated by the arrow) in contrast to the more singular peak observed for all the nanocomposites. This feature was reproducible and the observed double peak could be attributed to reorganisation during the course of the DSC scan, as reported elsewhere in the literature (Green et al., 2008).

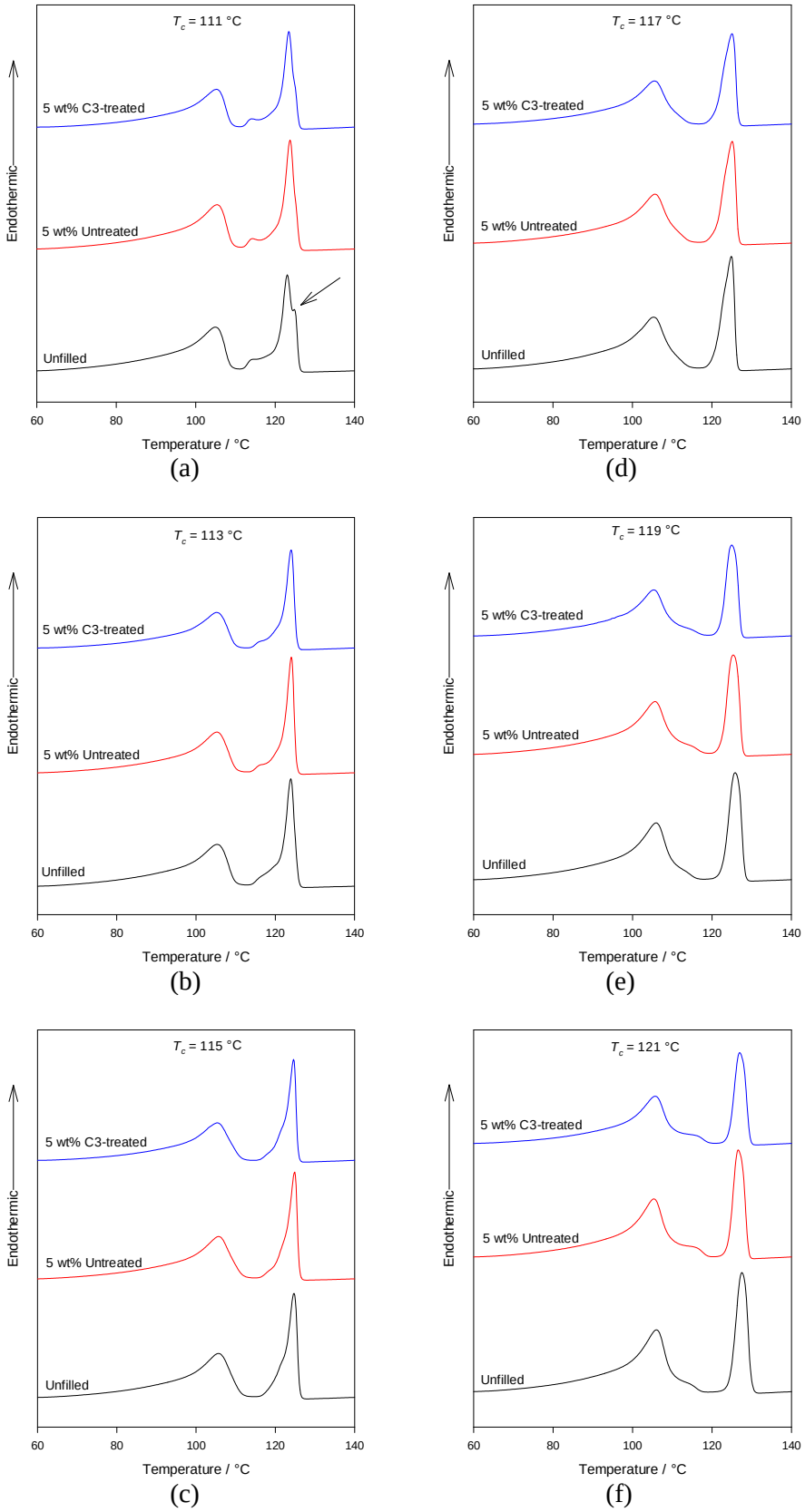

Figure 3.10: DSC melting traces comparing unfilled polyethylene and nanocomposites containing untreated and C3-treated nanosilica upon isothermal crystallisation at (a) 111 ºC, (b) 113 ºC, (c) 115 ºC, (d) 117 ºC, (e) 119 ºC, (f) 121 ºC

Table 3.2 provides peak melting temperatures data obtained for all the investigated polyethylene systems. It is noteworthy that the lower peak melting temperature is denoted as T_{m1} while the upper peak melting temperature is denoted as T_{m2}. The lower peak melting temperatures did not vary with increasing isothermal crystallisation temperatures. Meanwhile, the upper peak melting temperature increases as the isothermal crystallisation temperature increases. However, the upper peak melting temperature for the investigated polyethylene systems did not change based on different types and amounts of nanosilica at fixed crystallisation temperatures, where the slight variation seen is simply within experimental errors. The equivalent melting temperatures seen in the nanocomposites and unfilled polyethylene indicates that, for any given crystallisation temperature, the thickness of the lamellae is similar in all the investigated materials, irrespective of the type of filler or composition of the system.

Table 3.2: Lower and upper peak melting temperatures data obtained from DSC

	T_c = 111 ºC		**T_c = 113 ºC**		**T_c = 115 ºC**	
Sample	**T_{m1} / ºC**	**T_{m2} / ºC**	**T_{m1} / ºC**	**T_{m2} / ºC**	**T_{m1} / ºC**	**T_{m2} / ºC**
Unfilled	105.1	123.1	105.4	123.9	105.7	124.7
2 wt% Untreated	105.6	123.7	105.9	124.6	105.4	124.9
2 wt% C3-treated	105.6	123.9	105.6	124.3	105.6	124.6
5 wt% Untreated	105.4	123.7	105.4	124.1	105.7	124.9
5 wt% C3-treated	105.4	123.4	105.4	123.9	105.6	124.6
10 wt% Untreated	105.6	123.9	105.7	124.4	105.9	124.9
10 wt% C3-treated	104.9	123.6	105.6	124.3	105.6	124.6

	T_c = 117 ºC		**T_c = 119 ºC**		**T_c = 121 ºC**	
Sample	**T_{m1} / ºC**	**T_{m2} / ºC**	**T_{m1} / ºC**	**T_{m2} / ºC**	**T_{m1} / ºC**	**T_{m2} / ºC**
Unfilled	105.4	124.9	106.1	125.9	106.2	127.5
2 wt% Untreated	105.7	125.1	105.9	125.7	106.0	127.3
2 wt% C3-treated	105.6	124.9	106.1	125.6	105.6	126.8
5 wt% Untreated	105.7	125.1	105.7	125.4	105.5	126.7
5 wt% C3-treated	105.8	125.1	105.4	124.9	105.8	126.9
10 wt% Untreated	105.7	125.2	105.9	125.6	105.3	126.5
10 wt% C3-treated	105.6	124.9	106.1	125.4	105.8	126.9

3.3.3 Equilibrium Melting Temperature

Further analysis was performed using the above data to estimate the equilibrium melting temperature, T_m^0, of the investigated polyethylene systems. Since surface treatment of nanosilica did not generate notable effects towards the melting behaviour of the final nanocomposites, only the unfilled polymer and the nanocomposites containing untreated nanosilica were considered. Figure 3.11 shows melting point data plotted according to the conventional Hoffman-Weeks approach (Hoffman and Weeks, 1962) and, in this case, the temperature of the melting peak that corresponds to the isothermal HDPE-rich phase, T_{m2}, has been plotted against T_c. Commonly, a linear extrapolation to $T_m = T_c$ provides an estimate of T_m^0 and adopting this approach here leads to values for T_m^0 of ~137 ºC and ~134 ºC to ~135 ºC for the unfilled polyethylene and the nanocomposite respectively. This difference is within the uncertainty in the extrapolation and, consequently, it can be concluded that the nanocomposites and unfilled polyethylene appear equivalent in this respect. From the published literature (Wunderlich and Czornyj, 1977; Christ, 2007), the commonly accepted value of T_m^0 for polyethylene is about 142 ºC. The low T_m^0 values of 134 ºC to 137 ºC found in this study are therefore anomalous and require further discussion.

A similar observation has previously been reported by Gherbaz (2008), who proposed that data obtained at lower crystallisation temperatures should be treated separately from those obtained at higher crystallisation temperatures in order to generate a more meaningful plot of T_m^0; nevertheless, such an approach still leads to an unreasonable value for T_m^0. Secondly, although the experimental implementation of Hoffman-Weeks approach is straightforward, it was not developed to provide the best estimate of T_m^0, but to explain the observed increase in the melting temperature with crystallisation temperature (Hoffman and Miller, 1997). As such, accurate values of T_m^0 should not, in general, be expected. Furthermore, Marand et al. (1998) found that the use of a linear Hoffman-Weeks extrapolation procedure can lead to an underestimation of T_m^0; nevertheless, linear extrapolations have not previously led to large errors in the case of polyethylene, suggesting that the approach is reasonable for this polymer. However, this fails to recognize the blended nature of the system

considered here, which may lead to effects not previously identified in studies of single component materials.

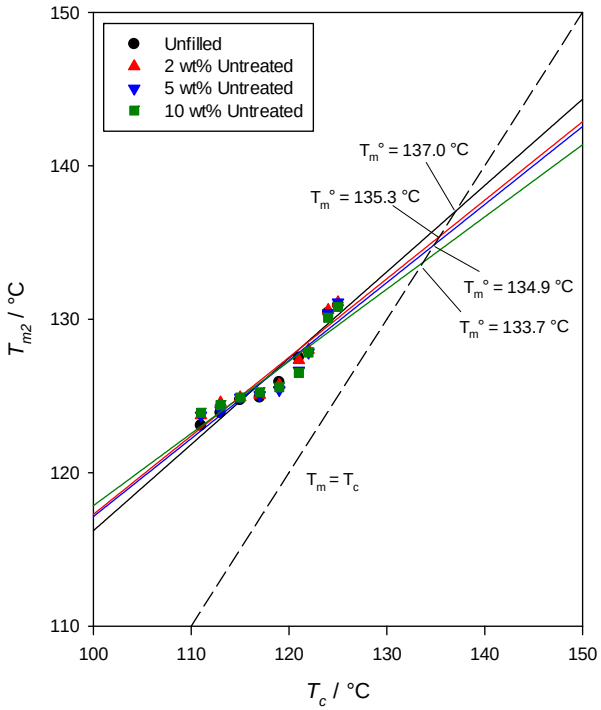

Figure 3.11: Plot of T_{m2} against T_c for unfilled polyethylene and nanocomposites containing 2 wt%, 5 wt% and 10 wt% of untreated nanosilica. The intercept shows an estimate of T_m^0 for each material

Examination of the raw data shown in Figure 3.11 demonstrates clearly that T_m does not increase in a linear manner with T_c, as suggested by Nishi and Wang (1975):

$$T_m^0 - T_m = \emptyset(T_m^0 - T_c) \tag{3.5}$$

where $\emptyset$ is the stability parameter that depends on the crystal thickness, and assumes values between 0 and 1; $\emptyset = 0$ implies $T_m = T_m^0$ for all T_c whereas $\emptyset = 1$ implies $T_m = T_c$. The crystals are most stable at $\emptyset = 0$ and inherently unstable at $\emptyset = 1$. The parameter $\emptyset$ can be replaced by $1/\gamma$, where γ is the thickening factor of the crystal (Groeninckx et al., 2002). Rather, the data can be divided into two subsets that correspond to temperature regimes of T_c < ~118 ºC and T_c > ~118 ºC. Specifically, in the lower temperature range, the rate of increase of T_m with T_c is very much less than would be anticipated, based upon T_m^0 = 142 ºC. Since lamellar thickness affects the melting point of the polymer crystal, expressed in a form of the Gibbs-Thomson equation:

$$T_m = T_m^0\left(1 - \frac{2\sigma_e}{l_e \Delta H_f}\right) \tag{3.6}$$

where l_e is the lamellar thickness (longitudinal dimensions of the crystal), ΔH_f is the melting enthalpy of the perfect crystal and σ_e is the surface free energy of the end faces at which chains fold, the above observation suggests that, at intermediate temperatures, the lamellar thickness is suppressed in the systems considered here. The explanation for this phenomenon is evident in the DSC traces shown in Figure 3.10, which reveal a number of features at temperatures intermediate between the two dominant exotherms specified by T_{m1} and T_{m2}. Consider, first, the samples crystallised at 111 ºC to 115 ºC; all of these reveal clear evidence of intermediate features that lie above the isothermal crystallisation temperature and which manifest themselves as a low temperature shoulder on the upper peak. That is, co-crystallisation of the HDPE and the more linear fractions of the LDPE occurred during the isothermal crystallisation phase, with the consequence that subsequent isothermal thickening will have been restricted by branches, which will be located at lamellar surfaces and, thereby limit the attainable crystal thickness. Conversely, the samples crystallised at 119 ºC and above reveal no evidence of a comparable shoulder on the upper melting peak but, rather, contain a high temperature shoulder on the quenched peak. For these materials, the effect described above becomes increasingly unimportant as T_c is increased, so explaining the rapid increase of T_m with T_c in this temperature regime.

From the above explanations, the use of Hoffman-Weeks theory in estimating the T_m^0 is not satisfactory for the materials considered here; the commonly accepted T_m^0 of 142 ºC was therefore used throughout this work.

3.3.4 Induction Time

The crystallisation induction time of the nanocomposites and the unfilled polyethylene was further explored using the theory of Muchová and Lednický (1995; 1996), which relates the crystallisation induction time to the thermodynamics of nucleation. In the case of heterogeneous nucleation (see Figure 3.12), induction time

can be expressed as a sum of the time necessary for the formation of the first layer on the foreign material surface (usually filler surfaces) and the time period in which further layers are formed until the growth of the critical nucleus is completed. For sufficiently high temperatures of crystallisation, the time of the formation of the first layer can be neglected in comparison with the time in which remaining layers are formed. In this case, the equation for the induction time can be simplified into a logarithmic form as:

$$\ln\left(t_i \Delta T\right) = \ln\left(\frac{C \Delta\sigma T_m^0}{\Delta H_m b_0}\right) + \left(\frac{4\sigma_{bl}\sigma_{ab} b_0 T_m^0}{k \Delta H_m}\right)\left(\frac{1}{T_c \Delta T}\right) \tag{3.7}$$

where σ_{bl} and σ_{ab} are Gibbs specific surface energies of the growing nucleus, $\Delta\sigma$ is the difference energy parameter which characterises the surface energy of the material initiating the nucleation, ΔH_m is the enthalpy of the crystal melting, ΔT is undercooling ($\Delta T = T_m^0 - T_c$), b_0 is the thickness of one layer of folding chains (given by the thickness of the polymer chains), C is the constant representing the influence of the transport term and k is the Boltzmann constant.

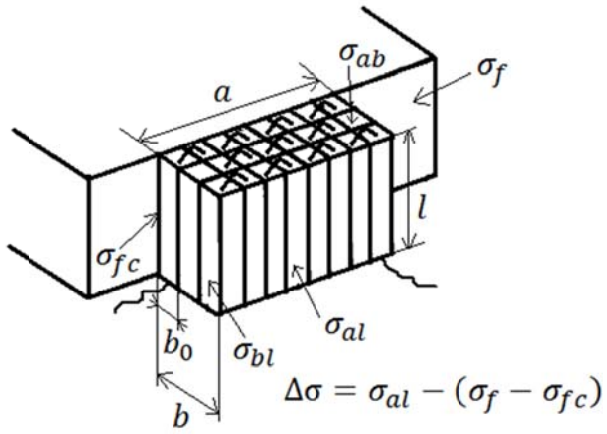

Figure 3.12: Growth of a heterogeneous crystallisation nucleus. a, b, l nucleus dimensions, b_0 thickness of one stacking layer, σ_{al}, σ_{bl}, σ_{ab} specific surface energies of the nucleus growing from the melt, σ_f specific surface energy of the foreign substance in polymer melt, σ_{fc} specific Gibbs energy of the foreign substance-crystal interface (Muchová and Lednický, 1996)

From Equation 3.7, the dependence of $\ln\left(t_i \Delta T\right)$ on $1/T_c \Delta T$ is a straight line with slope, K, and intercept, Q, on the axis of $\ln\left(t_i \Delta T\right)$, where:

$$K = \frac{4\sigma_{bl}\sigma_{ab}b_0 T_m^0}{k\Delta H_m} \tag{3.8}$$

$$Q = \ln\left(\frac{C\Delta\sigma T_m^0}{\Delta H_m b_0}\right) \tag{3.9}$$

The quantities K and Q can be acquired from experimental measurement of the induction time dependence on crystallisation temperature. In the case here, the analysis procedure was undertaken and plots of $\ln(t_i\Delta T)$ against $10^4/T_c\Delta T$ are shown in Figure 3.13; the analysed values are listed in Table 3.3.

First consider Figure 3.13a (plots for unfilled polyethylene and nanocomposites containing untreated nanosilica), the slope, K, appears similar in each sample when taking into account the experimental uncertainties (see the data in Table 3.3). These systems can be considered to exhibit a non-epitaxial nucleation process, in which the quantities σ_{bl}, σ_{ab}, b_0, ΔH_m and T_m^0 must be constant (Muchová and Lednický, 1995). In this case, the intercept, Q, should provide information about the difference energy parameter, $\Delta\sigma$; the value of Q for nanocomposites containing the untreated nanosilica appears to be higher than that of the unfilled polyethylene. However, the uncertainties are such that there is the possibility of overlapping of the Q values (see Table 3.3) and, consequently, the precise effect of nucleation efficiency is difficult to deduce clearly from these data.

Now consider Figure 3.13b (plots for unfilled polyethylene and nanocomposites containing C3-treated nanosilica), where the situation becomes more complex. Both the slope, K, and the intercept, Q, were found to be different for nanocomposites containing the C3-treated nanosilica in comparison with both the unfilled polyethylene and nanocomposites containing the untreated nanosilica. Although the thermodynamics of nucleation can be related to the crystallisation induction time using the theory of Muchová and Lednický (1995; 1996), the application of this theory to the data derived in this study does not lead to any additional insights. Indeed, it is difficult to see how changes in the nucleating substrate could lead to any significant changes in the parameters that make up K in equation 3.8. Also, this K

parameter is identical to the so-called nucleation constant, K_g, for Regime I in the Lauritzen-Hoffman theory of crystal growth (Hoffman et al., 1976).

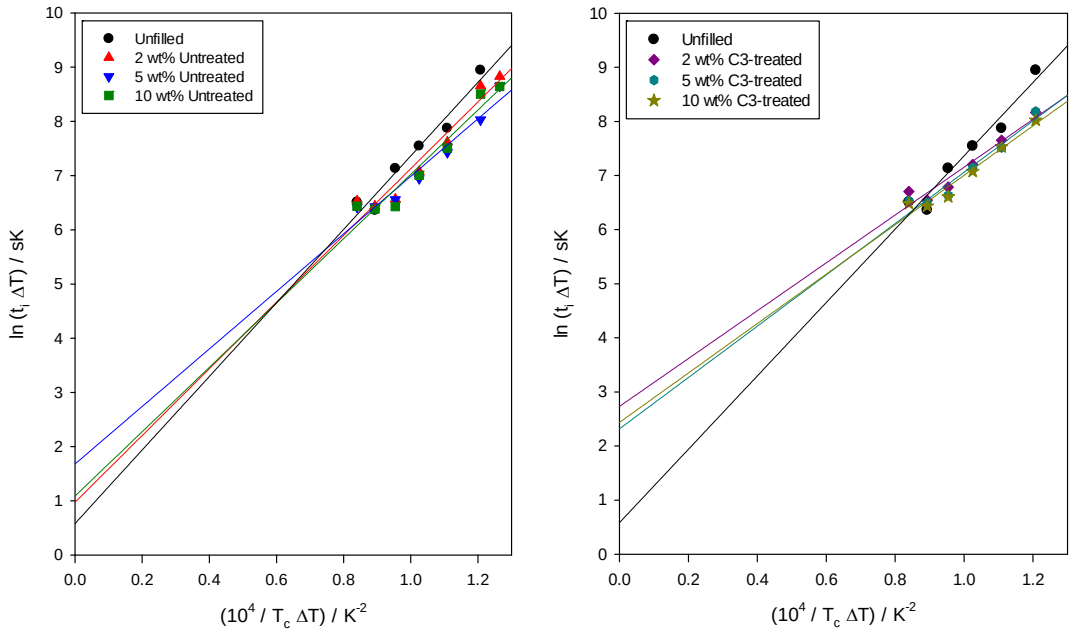

(a) (b)

Figure 3.13: Analysis of crystallisation induction times for nanocomposites containing (a) untreated nanosilica, (b) C3-treated nanosilica, with unfilled polyethylene as reference

Table 3.3: Data for slope, K and intercept, Q

Sample	Slope, K	Intercept, Q
Unfilled	6.7814 ± 0.7606	0.5823 ± 0.7703
2 wt% Untreated	6.1526 ± 0.6962	0.9757 ± 0.7327
5 wt% Untreated	5.3060 ± 0.5527	1.6801 ± 0.5816
10 wt% Untreated	5.9341 ± 0.6796	1.0888 ± 0.7152
2 wt% C3-treated	4.4225 ± 0.5792	2.7317 ± 0.5802
5 wt% C3-treated	4.7443 ± 0.5683	2.3166 ± 0.5755
10 wt% C3-treated	4.5681 ± 0.4953	2.4355 ± 0.5015

3.3.5 Thermodynamics of Crystallisation and Melting

In the previous analysis, enhancement of nucleation was suggested due to the nanostructuration of the polyethylene. However, the level of crystallinity present will depend upon the thermal history and molecular composition of the material. Therefore, the thermodynamics of crystallisation and melting provide invaluable insights into the crystallinity level of the materials. The enthalpies of crystallisation

and melting were therefore determined as a function of crystallisation temperature for each material and then converted into the percentage of HDPE present in each blend that was involved in each phase transition (Mandelkern, 1992). In short, the percent crystallinity, χ, was calculated by dividing the heat of fusion normalised by weight with the enthalpy of 100 % crystalline material, taken as 293 J g^{-1} for polyethylene (Wei et al., 2004), using the following equation (Panaitescu et al., 2011):

$$\chi = \frac{\Delta H}{\omega_f \Delta H_o} \times 100 \tag{3.10}$$

where ΔH is the crystallisation or melting enthalpy, ΔH_o is the value of enthalpy corresponding to the melting of a 100 % crystalline material and ω_f is the weight fraction of the crystallisable material.

Table 3.4 and Table 3.5 show the data for enthalpy and crystallinity at various crystallisation temperatures based on crystallisation and melting data, respectively. The crystallinity of the materials at various crystallisation temperatures based on crystallisation and melting data are summarised in Figure 3.14. Generally, reducing the crystallisation temperature increases the crystallised fraction of the material due to the increased crystallisation and melting enthalpies as a result of increased co-crystallisation between the low molar mass fractions of the HDPE and the more linear fractions of the LDPE. It is also noteworthy that the crystallinity obtained from melting data is higher than that obtained from crystallisation data as a result of annealing effects that occur during the DSC melting scan.

At a fixed crystallisation temperature, all the nanocomposites did not present significant differences in the percentage of crystallinity as compared with the unfilled polyethylene when taking into account the random experimental uncertainties. The unchanged crystallinity of nanosilica filled polyethylene was also reported by other researchers (Calebrese et al., 2011) at loadings below 15 wt%, while only slight changes were observed with varying nanosilica surface chemistry (Huang et al., 2010), if there at all. It is therefore reasonable to conclude that the incorporation of nanosilica, with either untreated or C3-treated surfaces, into polyethylene does not

Table 3.4: Enthalpy and crystallinity at various crystallisation temperatures based on crystallisation data

	T_c = 111 ºC		T_c = 113 ºC		T_c = 115 ºC	
Sample	ΔH / J g^{-1}	χ / %	ΔH / J g^{-1}	χ / %	ΔH / J g^{-1}	χ / %
Unfilled	34.7	59.2	33.5	57.1	25.2	43.0
2 wt% Untreated	34.5	60.1	32.4	56.4	28.3	49.3
2 wt% C3-treated	29.0	50.4	30.9	53.7	27.9	48.7
5 wt% Untreated	30.2	54.2	27.4	49.1	25.0	44.8
5 wt% C3-treated	30.6	54.9	29.3	52.6	26.7	47.9
10 wt% Untreated	31.9	60.4	30.2	57.3	26.5	50.3
10 wt% C3-treated	29.0	54.9	28.9	54.8	25.7	48.7

	T_c = 117 ºC		T_c = 119 ºC		T_c = 121 ºC	
Sample	ΔH / J g^{-1}	χ / %	ΔH / J g^{-1}	χ / %	ΔH / J g^{-1}	χ / %
Unfilled	23.2	39.6	22.6	38.5	21.9	37.4
2 wt% Untreated	25.0	43.6	23.4	40.7	19.3	33.6
2 wt% C3-treated	25.8	44.9	24.1	42.0	18.6	32.4
5 wt% Untreated	22.1	39.7	20.3	36.4	20.7	37.1
5 wt% C3-treated	23.3	41.9	22.4	40.3	22.7	40.8
10 wt% Untreated	22.7	43.1	19.9	37.6	17.9	34.0
10 wt% C3-treated	22.2	42.1	21.0	39.8	19.2	36.4

Table 3.5: Enthalpy and crystallinity at various crystallisation temperatures based on melting data

	T_c = 111 ºC		T_c = 113 ºC		T_c = 115 ºC	
Sample	ΔH / J g^{-1}	χ / %	ΔH / J g^{-1}	χ / %	ΔH / J g^{-1}	χ / %
Unfilled	38.9	66.3	36.8	62.9	34.3	58.5
2 wt% Untreated	37.7	65.7	36.0	62.7	33.8	58.9
2 wt% C3-treated	38.4	66.9	36.3	63.2	34.5	60.1
5 wt% Untreated	37.2	66.9	34.8	62.5	32.2	57.8
5 wt% C3-treated	37.0	66.5	35.0	62.9	33.2	59.6
10 wt% Untreated	34.6	65.5	32.3	61.3	30.8	58.4
10 wt% C3-treated	34.4	65.3	32.8	62.3	31.4	59.6

	T_c = 117 ºC		T_c = 119 ºC		T_c = 121 ºC	
Sample	ΔH / J g^{-1}	χ / %	ΔH / J g^{-1}	χ / %	ΔH / J g^{-1}	χ / %
Unfilled	31.9	54.5	31.3	53.4	30.8	52.6
2 wt% Untreated	31.2	54.4	27.8	48.4	26.9	46.8
2 wt% C3-treated	32.2	56.0	29.0	50.6	27.0	47.0
5 wt% Untreated	30.5	54.8	27.8	49.8	26.7	48.0
5 wt% C3-treated	31.0	55.7	27.8	49.9	26.8	48.1
10 wt% Untreated	28.6	54.3	25.9	49.2	25.0	47.4
10 wt% C3-treated	29.1	55.1	26.2	49.7	25.4	48.2

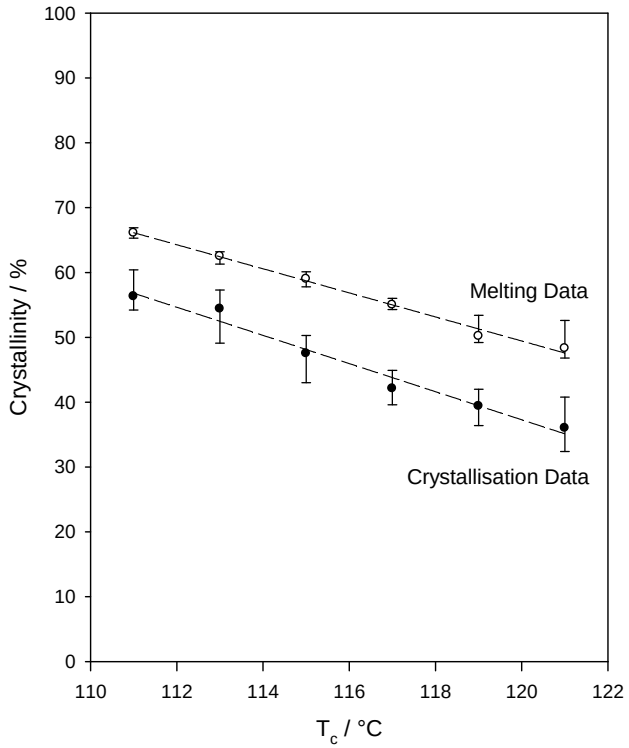

Figure 3.14: Crystallinity as a function of crystallisation temperature. The crystallinity at a certain crystallisation temperature was determined from the mean value of the data presented in Table 3.4 and Table 3.5. The upper and lower boundaries were obtained from the data variations shown in Table 3.4 and Table 3.5. A line is fitted on the melting data and the crystallisation data, respectively to show that reducing the crystallisation temperature increases the crystallised fraction of the material

exert a significant effect on the final crystallinity of the polymer, despite the nanosilicas acted as nucleating agent.

3.4 Summary

From thermal analysis, the addition of both the untreated and C3-treated nanosilica into polyethylene enhances the nucleation density; the nanosilica provides nucleation sites from which spherulites grow. This is evinced by the faster crystallisation process based on non-linear Avrami analysis and higher values of crystallisation rate constant, K_3, for the nanocomposites when compared with the unfilled polyethylene. Nucleation effects were stronger in the case of nanocomposites based upon the untreated nanofiller, despite the fact that simplistic concepts might suggest that surfaces containing propyl moieties would be more compatible with polyethylene than polar surfaces dominated by hydroxyl groups. This leads to the suggestion that

polymer/nanofiller interactions should be considered in terms of both chemical and structural factors.

Meanwhile, the inclusion of nanosilica, either untreated or C3-treated, did not exert an appreciable influence on the melting traces of polyethylene; the peak melting temperatures are similar when subjected to the same isothermal crystallisation condition. This indicates that the thickness of lamellae is similar in all the investigated polyethylene systems. An investigation into the thermodynamics of crystallisation and melting indicates that both types of nanosilica used (untreated and C3-treated) did not significantly influenced the final crystallinity of the polyethylene. In short, while the presence of nanosilica does affect nucleation, otherwise, it does not affect the crystallisation process.

Chapter 4

Structural and Morphological Characterisation

"The most exciting phrase to hear in science, the one that heralds new discoveries, is not 'Eureka!' (I found it!), but 'That's funny...'"

- Isaac Asimov -

4.1 Introduction

Previous understanding of nanodielectrics assumed that the addition of nanoparticles resulted in an interaction zone between the polymer and the fillers without altering the morphology of the polymer. Conversely, some researchers (Ma et al., 2003; Ma et al., 2005a) reported that the incorporation of nanoparticles into a polymer disturbed the morphology of the polymer, where the incorporation of nanoparticles affected the internal arrangement of spherulites (also known as internal spherulite disorder), resulting in morphological changes and subsequently modified the dielectric behaviour. For example, the intra-spherulitic regions were believed to have higher breakdown strength than that of the inter-spherulitic regions (Ma et al., 2003). However, the observation was not universal since the process changes entirely with changing surface chemistry.

In the research work carried out by Green and Vaughan (2008), the addition of clay nanofillers seemed to interfere with the structural evolution of polyethylene by promoting nucleation but inhibiting subsequent crystal growth suppressing crystallinity and resulting in morphological changes. Such observations suggested that morphological changes indeed occur in nanodielectrics. In a study by Tanaka (2005), orientation of polymer chains in polyamide 6/montmorillonite nanocomposites was found and it was said to be caused by the simultaneous existence of large and tiny spherulites that were formed in the polyamide 6 and around nanofillers as nuclei respectively.

Polarised optical microscopy (POM) is a simple technique that can be used to observe the crystalline morphology of a material. It involves the illumination of the sample with polarised light. Generally, two polarising filters are used, one termed the polariser, the other the analyser. The polariser is positioned in the illumination path beneath the sample, while the analyser is placed above the objective lenses and can be moved in and out of the light path as required. When both the polariser and the analyser are inserted into the optical path at an orientation perpendicular to each other (crossed polars), no light passes through the system in the absence of birefringence (also known as double refraction). It should be noted that birefringence is the decomposition of a ray of light into two rays which propagate at different rates and consequently a phase difference is introduced between the two rays. In the presence of a birefringent material, the polarised light interacts strongly with the material and generates contrast, in which plane polarised light enters the material while elliptically polarised light leaves the material. Only light parallel to the plane of the polarisation of the analyser will be transmitted while the rest will be absorbed. This generally results in image contrast in the presence of crystalline entities (e.g. spherulites).

Scanning electron microscopy (SEM), on the other hand, allows the morphological observation of a material at much higher resolution than that of POM. SEM is a type of electron microscope that can have an obvious advantage over an optical microscope in that the wavelength of the electrons can be made much shorter than that of visible light. Resolution is theoretically limited by the wavelength of the radiation used and, in the case of an electron is related to its energy and therefore the chosen accelerating voltage. At a typical operating voltage of an SEM, high resolution images of a sample surface can be produced, revealing details less than 1 nm in size.

In conventional SEM, a narrow beam of high energy electrons is produced by thermionic emission from an electron gun fitted with a tungsten filament cathode. The emitted electrons are accelerated through a potential difference before impinging upon the sample. Interactions between the electron and the sample produce a variety of signals including the secondary electrons that provide information about the

sample's morphology. The detector signal is further amplified electronically and fed to a monitor screen, which is scanned synchronously with the electron beam.

An alternative surface imaging technique that can be used is atomic force microscopy (AFM). AFM is a very high resolution type of scanning probe microscopy with a demonstrated resolution on the order of fractions of a nanometre. It is one of the foremost tools for imaging, measuring and manipulating matter at the nanoscale. AFM consists of a cantilever with a sharp tip (probe) at its end that is used to scan the sample surface. When the tip is brought into the proximity of a sample surface, forces between the tip and the surface lead to the deflection of the cantilever. The deflection is detected by means of a laser beam, which is reflected from the back side of the cantilever onto a position-sensitive detector and thus allows the construction of an image of the studied surface.

AFM has several advantages over SEM. Firstly, AFM can provide higher resolution than SEM and can even provide a three-dimensional surface profile as opposed to the two-dimensional images of SEM. The high resolution of AFM is comparable in resolution to transmission electron microscope (TEM). In addition, samples viewed by AFM do not require any special treatment (e.g. gold coating) that could irreversibly change or damage the sample. Moreover, samples subjected to AFM do not typically suffer from charging artefacts in the final image. Despite all the advantages over SEM, the use of AFM suffers from the downside of having relatively small image size, which might not represent the overall morphology. This is providentially replenished by the use of SEM, where larger scan areas can be obtained.

Meanwhile, Fourier transform infrared (FTIR) spectroscopy can be used to obtain an infrared spectrum of a solid, liquid or gas. FTIR is useful for identifying types of chemical bonds (functional groups). In FTIR, spectral data are simultaneously collected over a wide spectral range. Since the wavelength of light absorbed corresponds specifically to chemical bonds, the types of chemical bonds in a specimen can be identified by interpreting the infrared absorption spectrum. For most common materials, the spectrum of an unknown can be identified by comparison with spectral libraries of known compounds.

4.2 Results and Discussion

4.2.1 Fourier Transform Infrared Spectroscopy

The mechanisms involved in the exchange of functional groups on the surface of nanosilica during surface treatment using trimethoxy(propyl)silane are complex and can be interpreted in several ways. For the sake of brevity, surface treatment process for the nanosilica can be illustrated as in Figure 4.1. The methoxy groups of the silane coupling agent hydrolyse to hydroxyl (OH) groups (silanol) that can condense with hydroxyl groups on the nanosilica surface to form Si-O-Si bonds, leaving the surface of the C3-treated nanosilica to carry the propyl (C_3H_7) functional groups. The effectiveness of the surface treatment process was determined by combustion analysis (MEDAC Ltd., 2011), where the analysis demonstrated the elemental fraction of C and H on the untreated nanosilica were less than 0.10 % and 0.91 %, respectively, which then increased to 0.46 % and 1.09 %, respectively upon surface treatment, indicative of the presence of propyl groups.

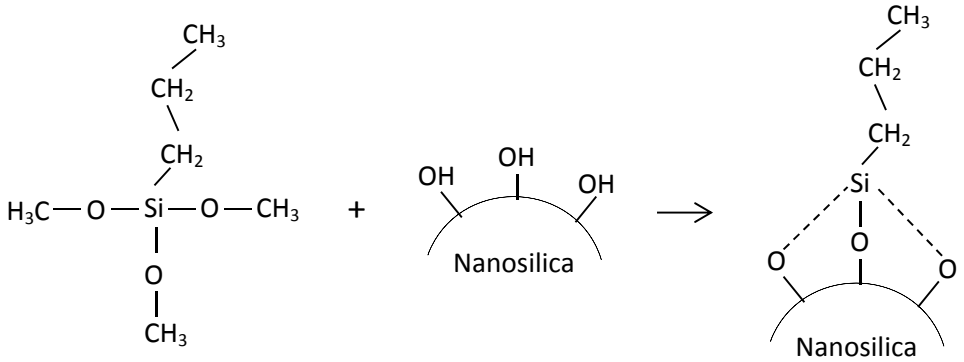

Figure 4.1: Schematic of the reactions taking place between the original nanosilica and the trimethoxy(propyl)silane coupling agent (drawings are not to scale)

The chemical structures of the investigated material systems were analysed using FTIR spectroscopy. Figure 4.2 shows the FTIR spectra of the investigated material systems. The characteristic absorption bands for the unfilled polyethylene are 2840-2928 cm^{-1}, 1465 cm^{-1} and 720 cm^{-1}, which are typical of polyethylene (Gulmine et al., 2002; Lai et al., 2011; Wu and Liao, 2003). The opaque spectral interval for 2840-2928 cm^{-1} is associated with the stretching of CH_2, while the absorption band at 1465 cm^{-1} and 720 cm^{-1} are assigned to bending deformation and rocking deformation, respectively.

With the addition of nanosilica into polyethylene, there are three additional characteristic absorption bands that could be observed, mainly at 1088 cm^{-1}, 800 cm^{-1} and 465 cm^{-1}, respectively. Similar observations have also been reported by other researchers (Cheng et al., 2011; Daoud et al., 2006; Lai et al., 2011; Stefanescu et al., 2010; Wu and Liao, 2003), where the bands are indicative of Si-O-Si bonds. As the nanosilica concentration increase, the absorption bands become stronger.

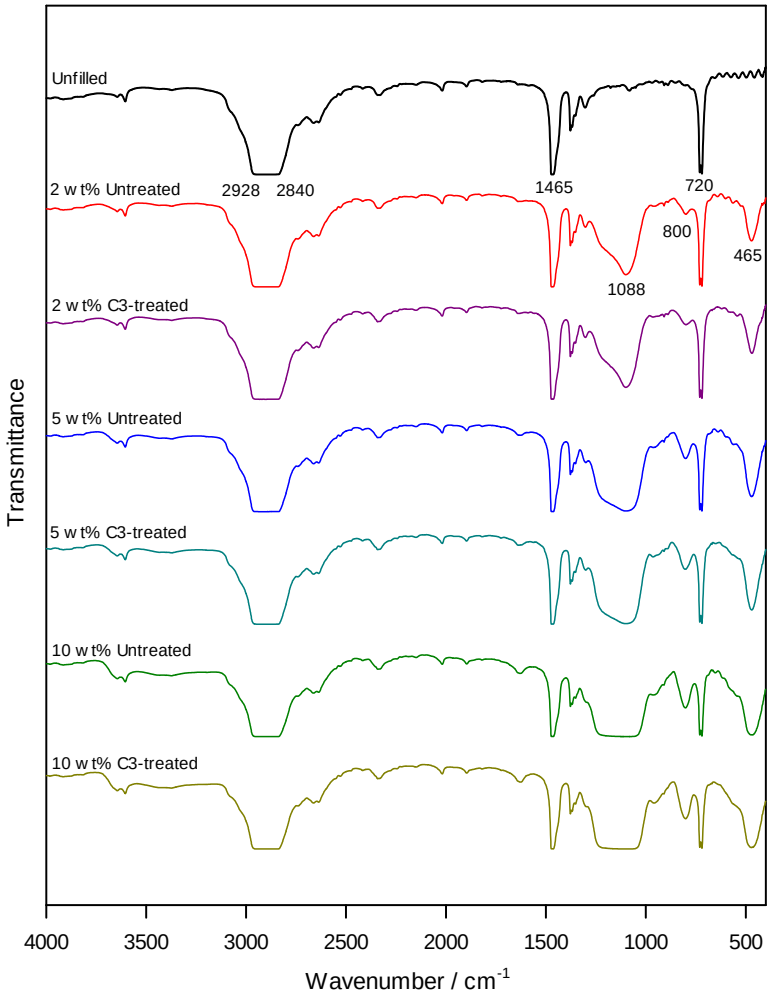

Figure 4.2: FTIR spectra comparing unfilled polyethylene with nanocomposites containing untreated and C3-treated nanosilica, crystallised isothermally at 115 ºC

Although FTIR was performed to assess interfacial interactions, it is rather difficult to justify the specific effects of the untreated and C3-treated nanosilica due to the non-specific interaction between the C3-treated nanosilica and polyethylene. According to Chen et al. (2004), new peaks at 2921 cm^{-1} and 2849 cm^{-1} can be found in the FTIR spectrum of methacryloxy(propyl)trimethoxysilane treated nanosilica when compared with the FTIR spectrum of untreated nanosilica. Unfortunately, comparable peaks cannot be observed in the nanocomposite samples investigated

here due to the fact that the polyethylene itself exhibits an opaque spectral interval of 2840-2928 cm^{-1}. Later, discussion on morphology and dielectric properties, however, are able to justify the effect of C3-treated nanosilica within the polyethylene. Nevertheless, the absence of an absorption band at 1720 cm^{-1} in all samples indicates that no oxidation occurred during sample preparation, as highlighted by Ma et al. (2005b).

To further confirm the effect of nanosilica surface treatment, the untreated and C3-treated silica nanopowders were characterised using FTIR microspectroscopy. Figure 4.3 shows FTIR spectra obtained from the untreated and C3-treated silica nanopowder. The characteristic absorption bands at 1088 cm^{-1} and 800 cm^{-1} are indicative of Si-O-Si bonds, as also found in the nanocomposites. A broad band at 3400 cm^{-1} is attributed to the surface hydroxyl groups and associated water molecules on the surface of the nanosilica (Parvinzadeh et al., 2010). Upon surface treatment of nanosilica, the intensity at 3400 cm^{-1} was reduced, suggesting that the surface hydroxyl groups have been replaced by propyl groups. The peak at 2350 cm^{-1} is associated with carbon dioxide (CO_2) from the atmosphere (Gulmine et al., 2002), and is an experimental artefact that results from the FTIR microscope used to acquire these data in air.

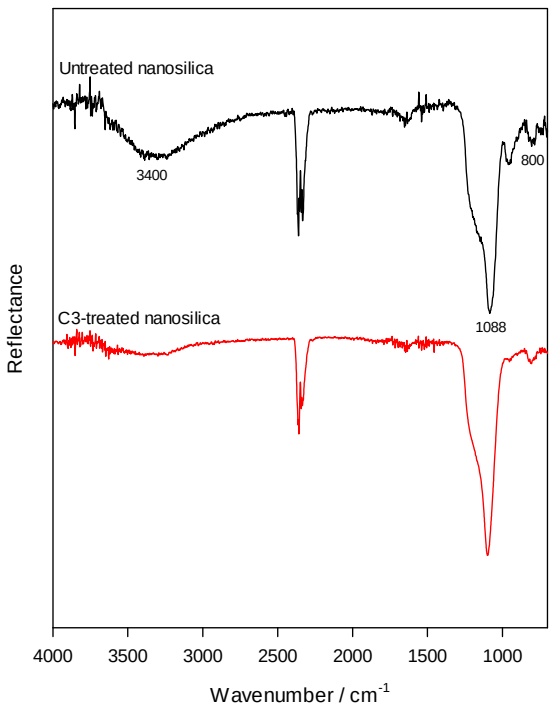

Figure 4.3: FTIR spectra comparing untreated and C3-treated silica nanopowder

4.2.2 Polarised Optical Microscopy

POM was used to determine the effect of isothermal crystallisation on the investigated material systems. Generally, this technique would not be able to reveal the dispersion of nanofiller in the polymer, but it facilitates visualisation of the morphological changes at larger scales. The polarised optical micrographs were recorded every second in order to follow the growth of spherulites. It is noteworthy that the crystallisation is dominated by the HDPE component.

Figure 4.4 shows the evolution of spherulites comparing unfilled polyethylene, nanocomposites containing 2 wt% of untreated nanosilica and nanocomposites containing 2 wt% of C3-treated nanosilica, crystallised at 115 ºC. In Figure 4.4, it was assumed that $t = 0$ s is the time where the material started to crystallise, based on visual inspection. It can be seen that for unfilled polyethylene (see Figure 4.4a), a number of spherulites had developed at $t = 10$ s, roughly spherical in shape. The spherulites continued to develop at $t = 20$ s, resulting in larger size of the spherulites, while new spherulites continued to emerge. At $t = 70$ s, impingement of spherulites became prevalent.

In the presence of nanosilica, the morphology of the crystallised systems was perturbed. This is evident in Figure 4.4b and Figure 4.4c, which shows nanocomposites containing 2 wt% of untreated nanosilica and nanocomposites containing 2 wt% of C3-treated nanosilica, respectively. From these POM micrographs, addition of both the untreated and C3-treated nanosilica resulted in similar morphologies. At $t = 10$ s, a large number of small-sized spherulites had emerged, and spherulitic development seems to have stopped at $t = 30$ s. When comparing the unfilled polyethylene and the nanocomposites, it is apparent that the size of the spherulites observed in the nanocomposites was not comparable to that observed in the equivalent unfilled polyethylene; the number of spherulites had increased significantly.

Among the nanocomposites containing 2 wt%, 5 wt% and 10 wt% of untreated nanosilica, the addition of 2 wt% of untreated nanosilica seems to result in larger size of spherulites in the final morphology; no clear distinction can be made between

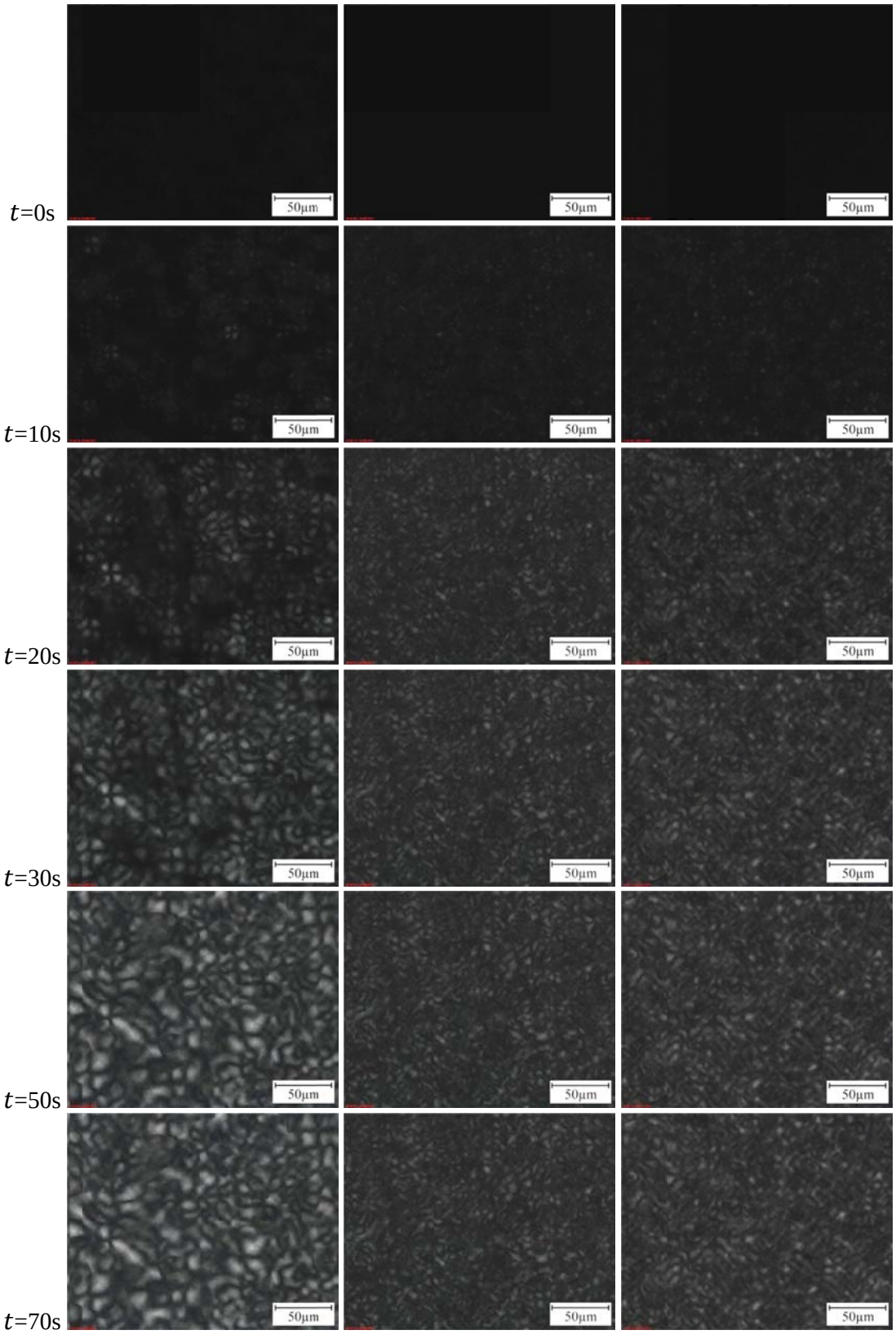

Figure 4.4: Polarised optical micrographs showing the evolution of spherulites for (a) unfilled polyethylene, (b) nanocomposites containing 2 wt% of untreated nanosilica, (c) nanocomposites containing 2 wt% of C3-treated nanosilica, crystallised isothermally at 115 ºC

nanocomposites containing 5 wt% and 10 wt% of untreated nanosilica. This is also true for the case of nanocomposites containing C3-treated nanosilica. Examples of the final morphological structures of the unfilled polyethylene and nanocomposites containing 2 wt%, 5 wt% and 10 wt% of untreated nanosilica crystallised at 117 ºC are shown in Figure 4.5.

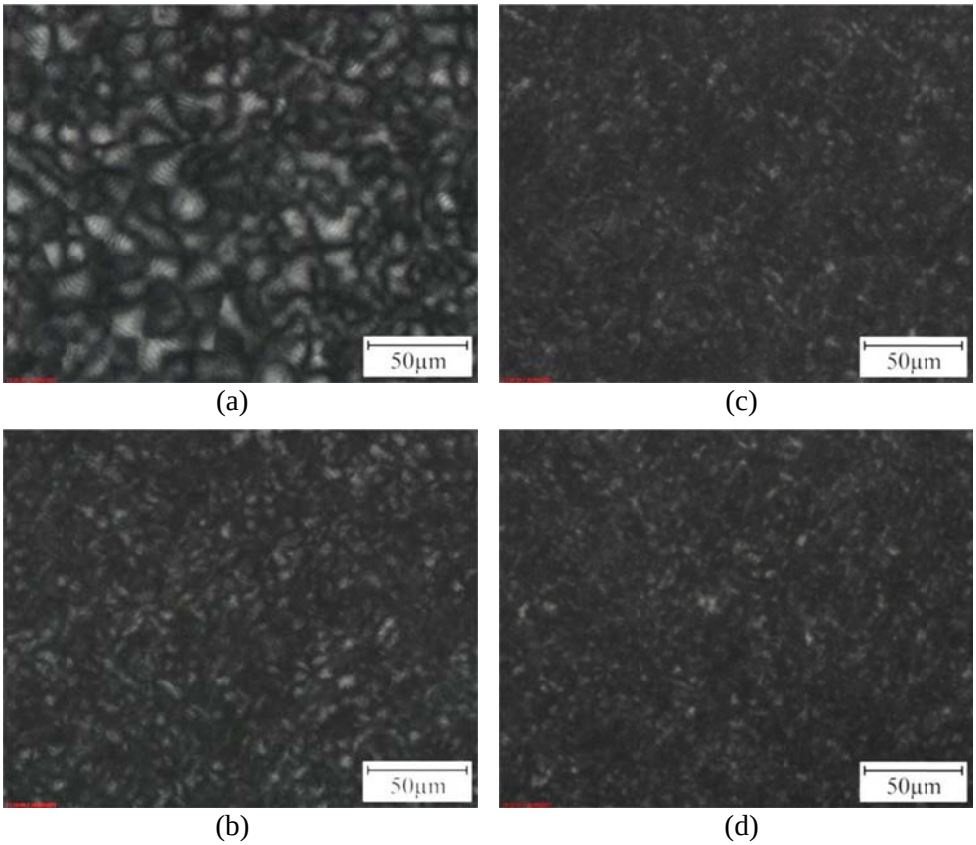

(a) (c)

(b) (d)

Figure 4.5: Spherulites observed through polarised optical microscopy for (a) unfilled polyethylene and nanocomposites containing (b) 2 wt%, (c) 5 wt%, (d) 10 wt% of untreated nanosilica, crystallised isothermally at 117 ºC

The morphological effect reported here is in line with previous thermal analysis, where inclusion of nanosilica resulted in faster crystallisation, as deduced from the increased number of spherulites observed from Figure 4.4 and Figure 4.5. This, as previously considered, is the effect of enhanced nucleation brought about by the incorporation of nanosilica that serves as nucleation sites, whereupon, spherulite impingement limits the development of spherulites in the nanocomposites so resulting in smaller spherulite size, when compared with the unfilled polyethylene. The increased number but smaller size of spherulites in the nanocomposites containing 5 wt% and 10 wt% of nanosilica, as compared with that containing 2 wt%

of nanosilica, indicates yet faster crystallisation but further suppressed spherulitic development.

4.2.3 Scanning Electron Microscopy

The use of POM allows the observation of gross morphological changes between the unfilled and nanofilled materials that were isothermally crystallised. However, the dispersion of nanosilica could not be observed through POM. Therefore, SEM has to be used in order to determine the dispersion of nanosilica in the polyethylene. The use of SEM also allows detailed investigation of the morphology of the materials at higher resolutions, which is limited by the use of POM.

From Figure 4.6, isothermal crystallisation of unfilled polyethylene at 115 ºC yielded open banded spherulitic structures. These are composed of extensive isothermal lamellae (HDPE-rich phase) that are separated from each other by regions of quenched matrix (LDPE-rich phase), and the texture appears to be space filling. Meanwhile, Figure 4.7 shows the morphology of unfilled polyethylene quenched directly into water, where HDPE and LDPE crystallise quickly on quenching to give characteristic banded spherulites separated by featureless regions. Such morphological structures are not atypical and are similar to those reported elsewhere in the literature (Hosier et al., 2010; Hosier et al., 2000; Hosier et al., 1997).

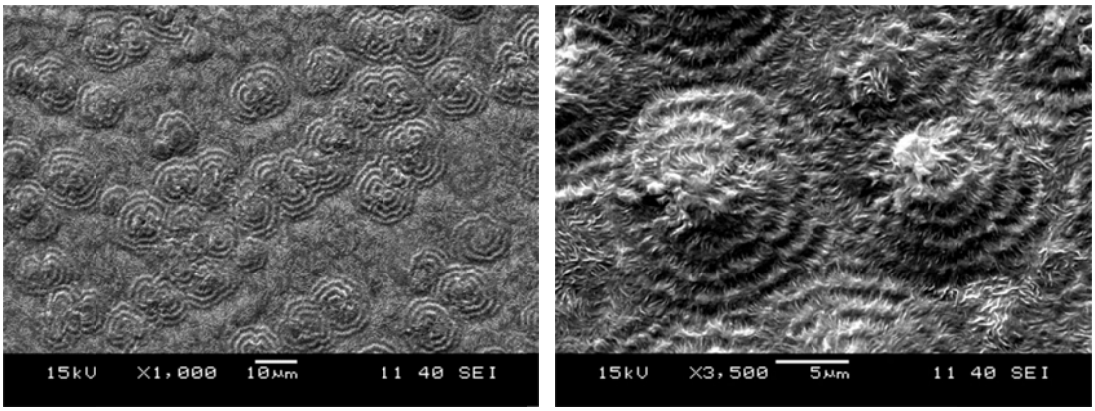

(a) (b)

Figure 4.6: SEM micrographs for unfilled polyethylene crystallised isothermally at 115 ºC under (a) low magnification, (b) high magnification

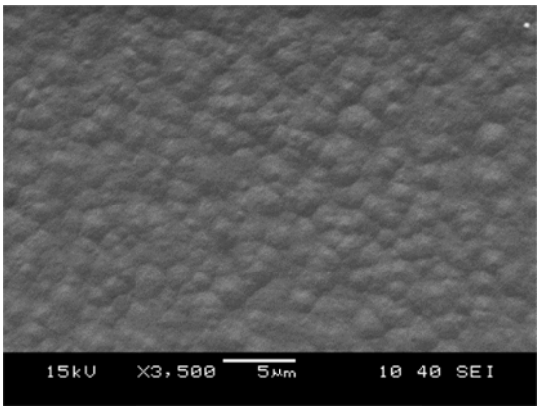

Figure 4.7: SEM micrographs for unfilled polyethylene quenched directly into water

Figure 4.8 shows representative SEM micrographs of the nanocomposites containing untreated and C3-treated nanosilica. By comparing Figure 4.8 with Figure 4.6b, the morphology of the nanocomposites and unfilled polyethylene are evidently different. Perturbed spherulitic development can be observed in both types of nanocomposite systems (i.e., with untreated and C3-treated nanosilica). At 2 wt% of nanosilica loading, banded spherulites can still be observed (see Figure 4.8a and Figure 4.8d), but the size of the spherulites in the nanofilled polyethylene is not comparable to that of the unfilled polyethylene. This is presumably due to the effect of nucleation caused by the inclusion of the nanofiller within polyethylene, as previously explained in connection with the thermal analysis and POM results.

As the nucleation increases, more spherulites develop, which results in earlier spherulite impingement that limits further growth. When the amount of nanosilica is increased to 5 wt%, the effect of spherulite banding becomes less pronounced, and the texture of the spherulites appears perturbed (see Figure 4.8b and Figure 4.8e). Although faint banding is still visible, it is much less pronounced than in the unfilled polyethylene. The addition of 10 wt% of nanosilica into polyethylene causes the growth of spherulites to be largely suppressed, resulting in highly disordered systems (see Figure 4.8c and Figure 4.8f). Again, such an observation is in line with thermal analysis and POM characterisation and is supported by literature findings (Huang et al., 2010).

In terms of nanoparticle dispersion, it is evident from Figure 4.8 that the nanosilica particles span a wide size range (from nanometre to micrometre), but that they are generally well distributed throughout the polyethylene. Here, agglomeration of

nanosilica could not be completely avoided; it is well known that nanoparticles commonly appear as agglomerates rather than as isolated particles in such systems (Nelson and Fothergill, 2004; Tanaka et al., 2011). With increasing amounts of nanosilica, aggregation of nanosilica becomes more apparent.

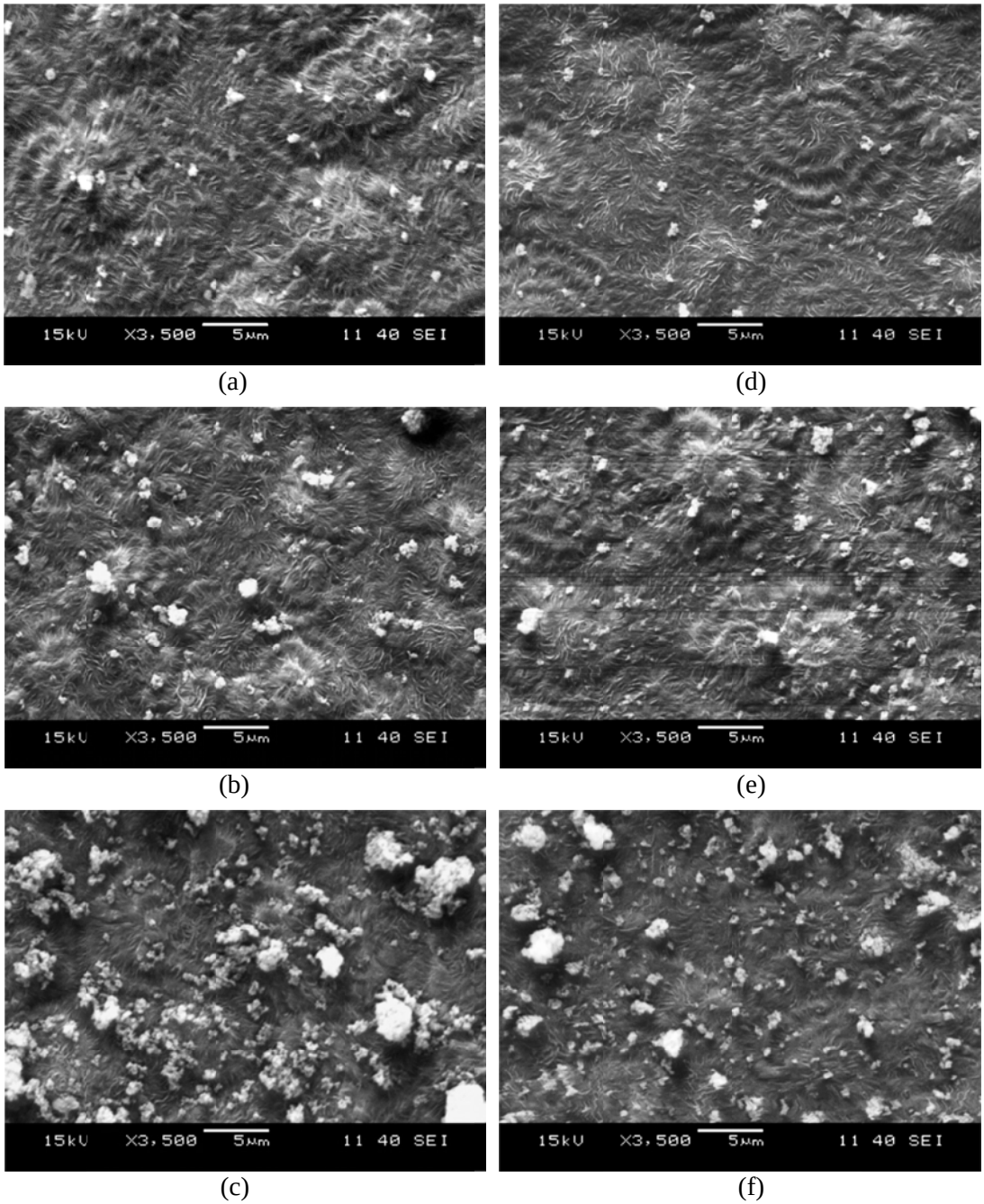

Figure 4.8: Dispersion state of (a) 2 wt%, (b) 5 wt%, (c) 10 wt% of untreated nanosilica and (d) 2 wt%, (e) 5 wt%, (f) 10 wt% of C3-treated nanosilica in polyethylene crystallised isothermally at 115 ºC

At 10 wt% of nanosilica loading, the nanosilica particles tend to form clusters and the clustering effect could be up to about ten micrometres in size. Agglomeration of

nanosilica can also be explained in terms of van der Waals forces between the nanoparticles (Huang et al., 2008). At low nanosilica loading levels, the attractive van der Waals forces between the nanoparticles are relatively weak due to the long particle-to-particle distance. The particle-to-particle distance decreases with increasing amount of nanoparticles such that the effect of attractive forces between the nanoparticles becomes more significant. This subsequently results in more and more agglomeration of nanoparticles.

Considering the effect of surface treatment on the dispersion of nanosilica, the SEM micrographs shown in Figure 4.8d, Figure 4.8e and Figure 4.8f appear equivalent to those in Figure 4.8a, Figure 4.8b and Figure 4.8c, respectively, although perhaps, the distribution of particle sizes appears displaced somewhat to smaller dimensions upon surface treatment. This is particularly evident at 10 wt% of C3-treated nanosilica loading, where the clustering effect of nanosilica is significantly less than that of the equivalent untreated nanosilica loading. This is probably attributed to the substitution of hydroxyl groups with propyl groups and the subsequent removal of molecularly adsorbed water on the surface of the nanosilica. Similar observations have also been reported by other researchers (Huang et al., 2010), where it was proposed that surface treatment not only decreases the surface free energy of nanoparticles but also prevents the formation of hydrogen bonds between the nanoparticles and subsequently reduces agglomeration.

4.2.4 Atomic Force Microscopy

While the use of a crystallised polyethylene blend enables structural changes to be readily detected, this system comes with the compromise of having a complex lamellar texture, i.e., the lamellar texture of the matrix prevents the complete particle size distribution from being imaged using SEM. AFM was therefore used in an attempt to look for nanometre-sized distributions.

Figure 4.9 shows AFM topography images obtained from unfilled polyethylene, while Figure 4.10 compares AFM topography images obtained from nanocomposites containing 5 wt% of untreated nanosilica and 5 wt% of C3-treated nanosilica.

Generally, the AFM images are in line with the SEM micrographs shown in Figure 4.6 and Figure 4.8. For unfilled polyethylene, banded spherulitic structures can be observed. Meanwhile, for nanocomposites, the particle distribution can be clearly observed through the height and amplitude images shown. From the phase images, it can be deduced that the white regions are indicative of nanosilica, not seen in the phase image of unfilled polyethylene.

Comparison of the nanocomposites containing untreated and C3-treated nanosilica supports the assertion that the nanocomposites containing C3-treated nanosilica contained more smaller-sized particles than the nanocomposites containing untreated nanosilica. This is in line with the SEM micrographs shown in Figure 4.8b and Figure 4.8e, where the increased number of smaller-sized particles means less particle agglomeration following surface treatment. Again, the size of the spherulites in the nanocomposites is smaller than in the unfilled polyethylene, as previously found from SEM and POM images. It is noteworthy that the image artefacts, which appear as streaks in Figure 4.10, could be related to the presence of sharp features and edges on the sample surface (Eaton and West, 2010). Since no comparable features exist in images of the unfilled polyethylene, it is likely that these are related to the presence of nanosilica, which causes locations with different surface roughness or protrusions.

Figure 4.11 and Figure 4.12 show high magnification AFM images of the unfilled polyethylene and the nanocomposites, respectively. Lamellae can be clearly observed in the unfilled polyethylene, where the brighter regions (see Figure 4.11a) are regions of the banded spherulitic features. From Figure 4.12, there are more fine-sized distributions in the nanocomposite containing the C3-treated nanosilica than in the nanocomposite containing the untreated nanosilica; particle agglomeration is more apparent in the absence of surface treatment. These features can be clearly observed in the three-dimensional AFM height images shown in Figure 4.13, where the presence of nanosilica is indicated by the protrusions. From these AFM images, although nanometre-sized distributions remained difficult to image due to the presence of the underlying lamellar texture, agglomerates down to ~100 nm in size can be resolved. Nevertheless, in the grade of the nanosilica used here, agglomeration could not be completely eliminated through the use of the silane

coupling agent; commercially available nanoparticulate systems commonly take the form of agglomerates of primary particles, which are difficult to break apart and affect the ability of the coupling agent to penetrate into the agglomerated structures (Kontou and Niaounakis, 2006).

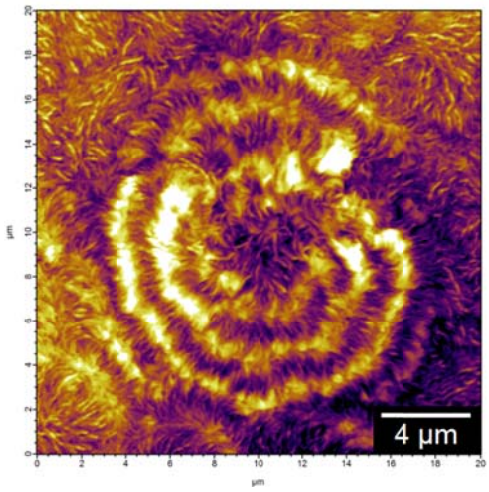

(a)

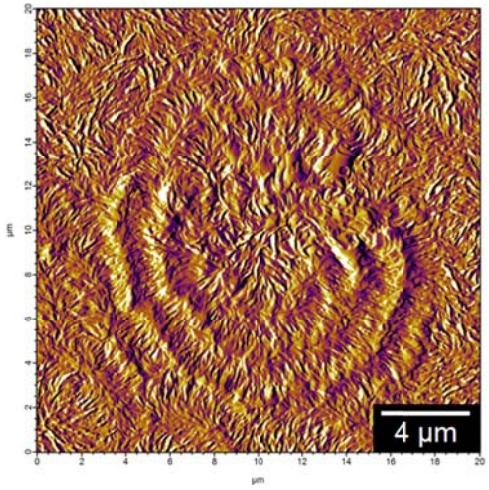

(b)

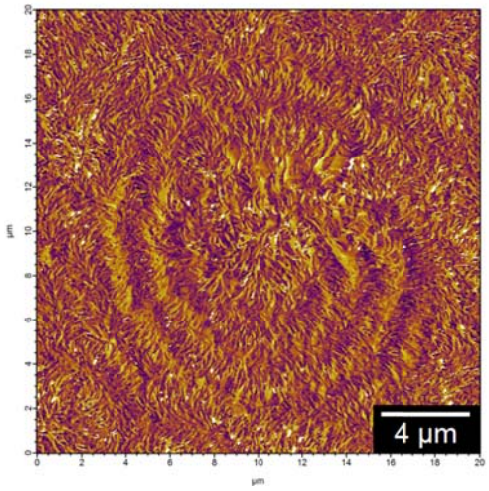

(c)

Figure 4.9: AFM (a) height, (b) amplitude, (c) phase images for unfilled polyethylene crystallised isothermally at 115 ºC

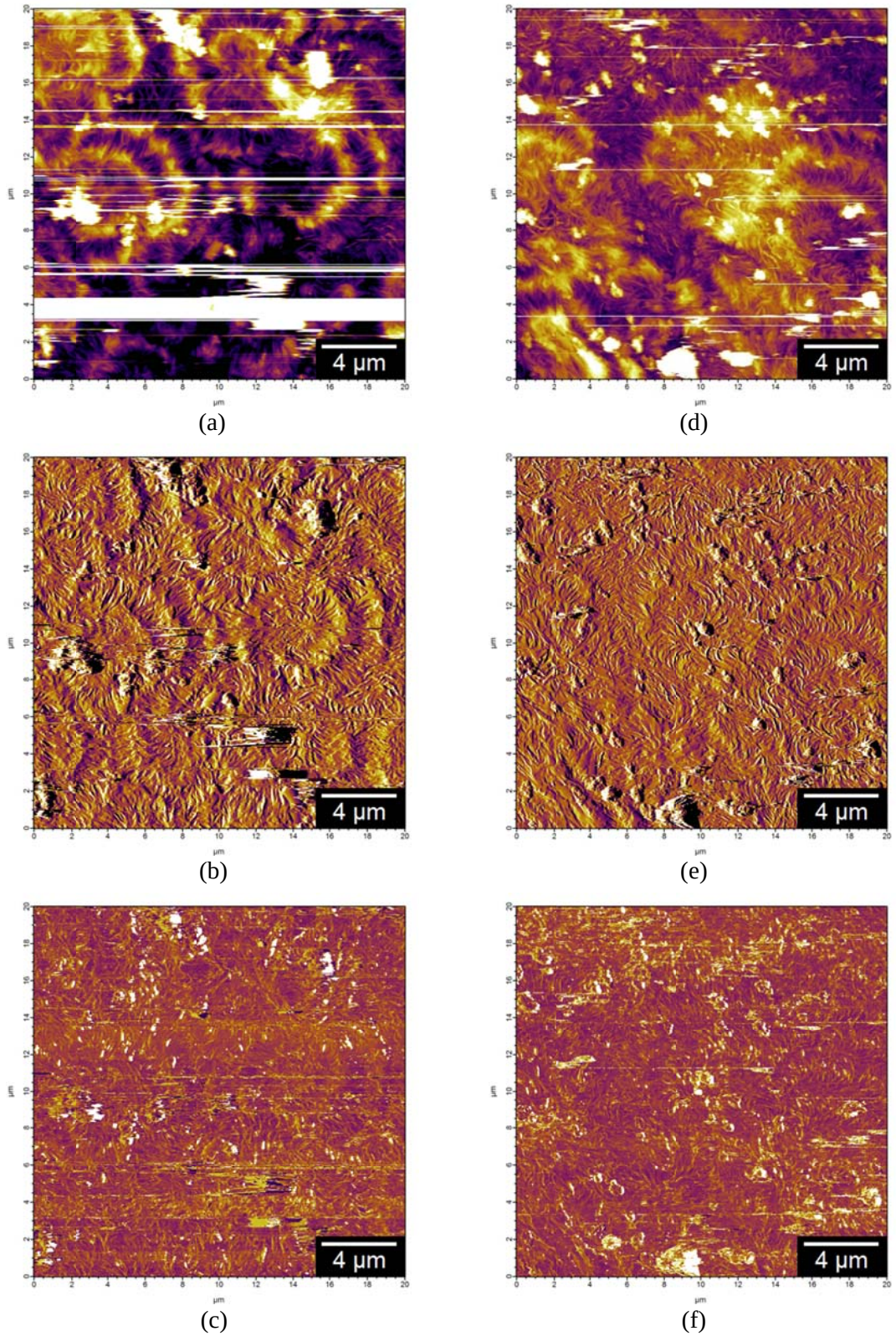

(a) (d)

(b) (e)

(c) (f)

Figure 4.10: AFM (a) height, (b) amplitude, (c) phase images for nanocomposites containing 5 wt% of untreated nanosilica, and AFM (d) height, (e) amplitude, (f) phase images for nanocomposites containing 5 wt% of C3-treated nanosilica, crystallised isothermally at 115 ºC

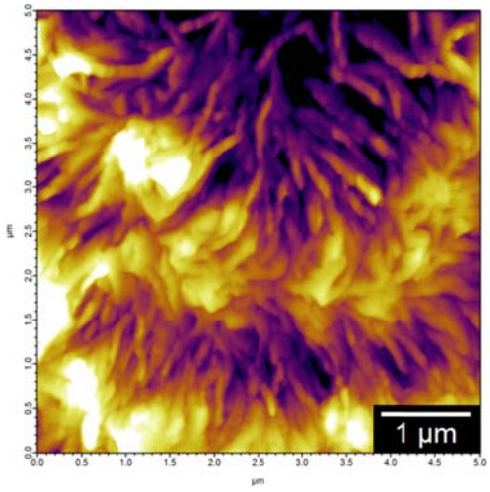

(a)

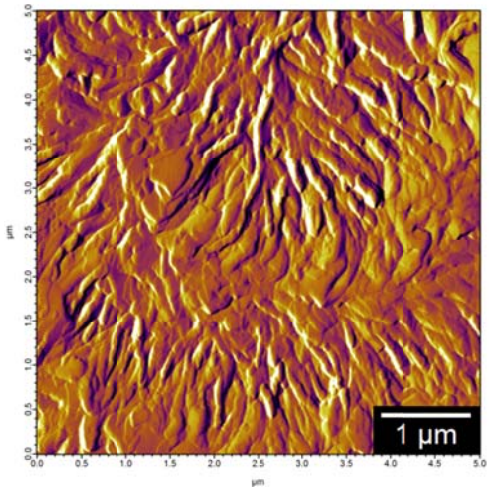

(b)

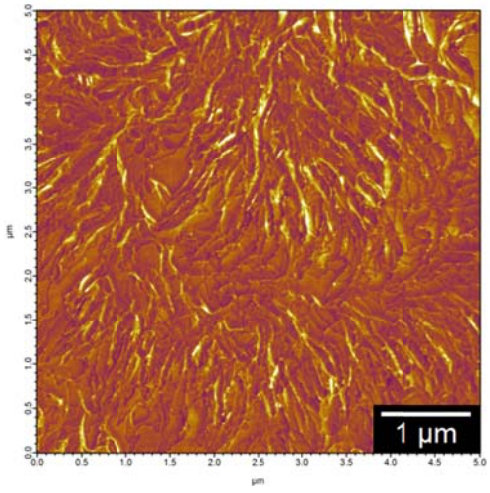

(c)

Figure 4.11: AFM (a) height, (b) amplitude, (c) phase images for unfilled polyethylene at higher magnification, crystallised isothermally at 115 ºC

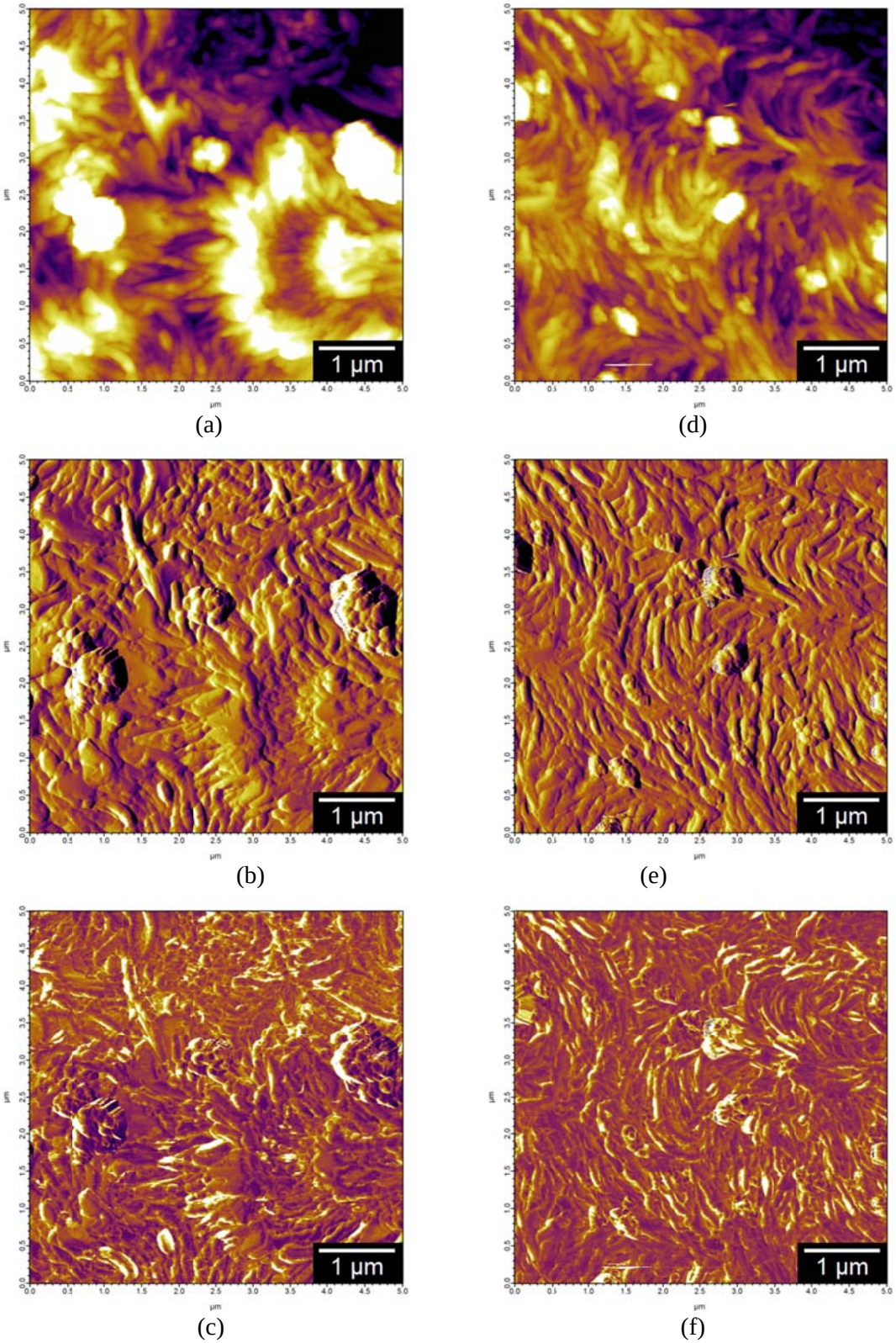

(a) (d)

(b) (e)

(c) (f)

Figure 4.12: AFM (a) height, (b) amplitude, (c) phase images for nanocomposites containing 5 wt% of untreated nanosilica, and AFM (d) height, (e) amplitude, (f) phase images for nanocomposites containing 5 wt% of C3-treated nanosilica at higher magnification, crystallised isothermally at 115 ºC

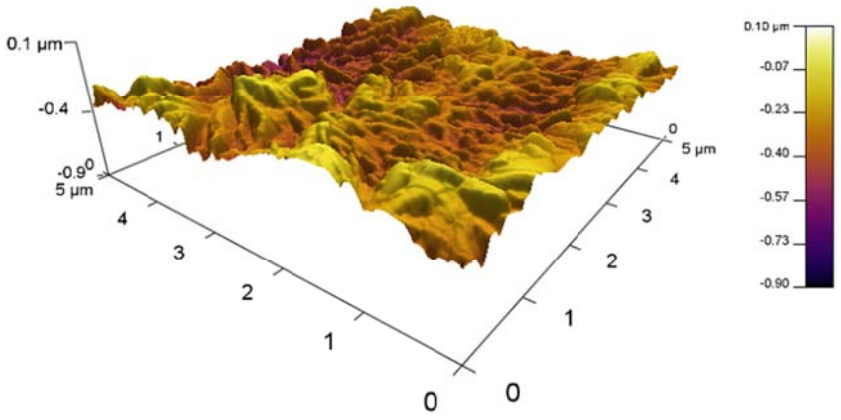

(a)

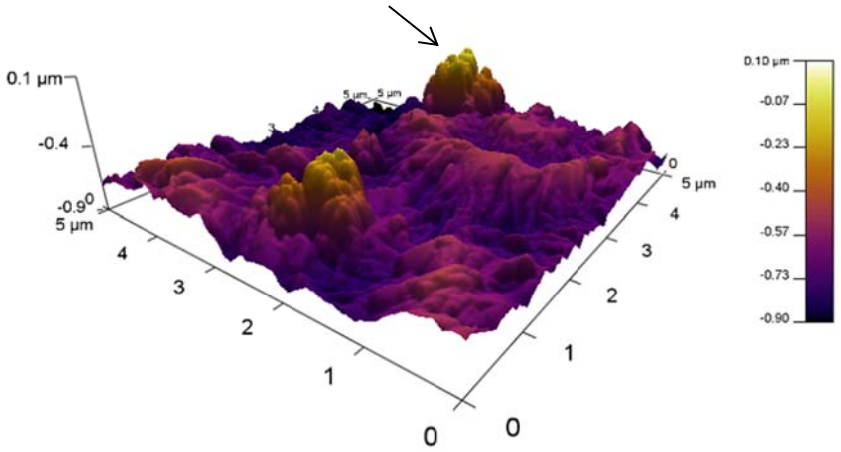

(b)

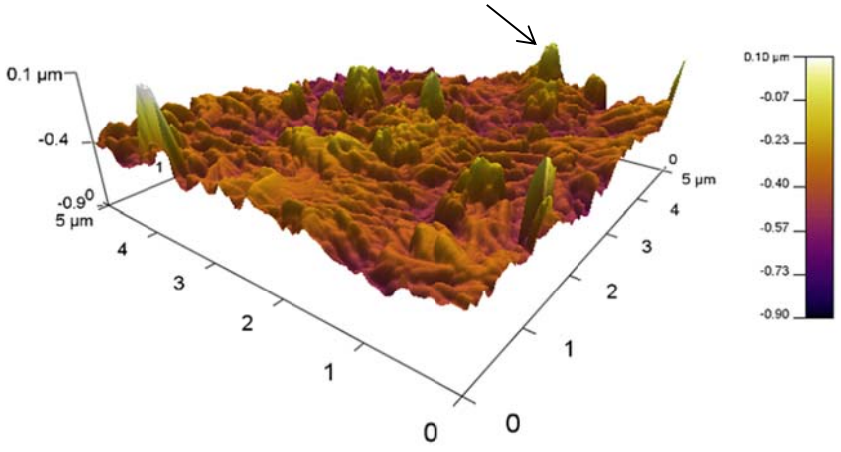

(c)

Figure 4.13: Three-dimensional AFM height images for (a) unfilled polyethylene, (b) nanocomposites containing 5 wt% of untreated nanosilica, (c) nanocomposites containing 5 wt% of C3-treated nanosilica (arrow indicates protrusion), crystallised isothermally at 115 ºC

4.3 Summary

FTIR spectroscopy indicates the presence of Si-O-Si bonds following the introduction of nanosilica into polyethylene. As the amount of nanosilica increases, the relevant absorption bands increase in strength. Meanwhile, the effect of nanosilica surface treatment was assessed using FTIR microspectroscopy, and the reduction of intensity at 3400 cm^{-1} suggests that surface hydroxyl groups of the nanosilica have been replaced by propyl groups of the silane coupling agent.

From POM observation, the size of the spherulites observed in the nanocomposites was not comparable to that observed in the equivalent unfilled polyethylene, and the number of spherulites had increased significantly. Therefore, nanostructuration appears to perturb spherulitic development with an increased number of spherulites but suppressed spherulitic development. This is further confirmed by SEM characterisation, where the effect of spherulite banding become less and less pronounced with increasing amounts of nanosilica, which finally led to a highly disordered texture at 10 wt% of nanosilica. In Chapter 3, it was deduced that the addition of nanosilica caused enhanced nucleation density, as evinced by the increase in K_3 parameter for all the investigated nanocomposites in comparison with unfilled polyethylene. The images obtained from POM and SEM therefore confirm the nucleation effect of nanosilica on polyethylene.

The particle size of untreated nanosilica was found to span a wide range (from nanometre to micrometre). Increasing the amount of untreated nanosilica causes more aggregation of nanosilica. The SEM images of nanocomposites containing C3-treated nanosilica appear equivalent to nanocomposites containing untreated nanosilica, although perhaps, the distribution of particle sizes appears displaced somewhat to smaller dimensions. This assertion was further confirmed through the AFM topography images; agglomerates down to ~100 nm in size could be resolved using the AFM.

Chapter 5

Dielectric Response

"If we knew what it was we were doing, it would not be called research, would it?"

- Albert Einstein -

5.1 Introduction

When a dielectric material is subjected to an external electric field, a dielectric displacement will occur within the material, leading to polarisation of the material. The most common polarisation mechanisms are electronic polarisation, atomic polarisation and orientational polarisation: i) electronic polarisation is effective in every atom or molecule as the centre of charge of the electrons surrounding the positive atomic cores will be displaced by the action of the electric field, thus creating a dipole moment; ii) atomic polarisation occurs when an applied electric field distorts the arrangement of atomic nuclei in a molecule or lattice, and it happens at a lower frequency than electronic polarisation due to the larger mass of the atom when compared to the electron; iii) orientational polarisation, also known as dipolar polarisation, occurs in materials containing molecules with permanent dipole moments (e.g. water) where, under the influence of an electric field, the dipoles will be aligned to some extent thus inducing polarisation of the material.

From the possible polarisation mechanisms, orientation of molecular dipoles is a relatively slow process in comparison with electronic transitions or molecular vibrations (Blythe and Bloor, 2005). If orientational polarisation is measured immediately after an electric field is applied, the observed instantaneous relative permittivity will be low since no time is allowed for the orientation of dipoles. However, if a sufficient time is allowed after the application of an electric field, maximum orientational polarisation could be achieved, and this would correspond to the highest observable relative permittivity; this is called the static relative permittivity.

Consider an example where a dielectric material is subjected to an AC electric field, E having an amplitude, E_o, and an angular frequency, ω:

$$E = E_o \cos(\omega t) \tag{5.1}$$

This will produce polarisation and, at sufficiently high frequencies, orientation of dipoles, also known as dielectric displacement, D will lag behind the applied field, resulting in a phase difference, δ:

$$D = D_o \cos(\omega t - \delta) \tag{5.2}$$

where D_o is the corresponding displacement. The dielectric displacement can also be written as:

$$D = D_1 \cos(\omega t) + D_2 \sin(\omega t) \tag{5.3}$$

where

$$D_1 = D_o \cos(\delta) \tag{5.4}$$

$$D_2 = D_o \sin(\delta) \tag{5.5}$$

Since D_o is proportional to E_o and D_o/E_o is a function of ω, two terms of relative permittivity, i.e., $\varepsilon_r'(\omega)$ and $\varepsilon_r''(\omega)$ can be introduced:

$$\varepsilon_r'(\omega) = \frac{D_1}{\varepsilon_o E_o} \tag{5.6}$$

$$\varepsilon_r''(\omega) = \frac{D_2}{\varepsilon_o E_o} \tag{5.7}$$

where ε_o is the permittivity of vacuum. The complex relative permittivity can be written as:

$$\varepsilon_r^*(\omega) = \varepsilon_r'(\omega) - j\varepsilon_r''(\omega) \tag{5.8}$$

where $\varepsilon_r'(\omega)$ is the real part of the complex relative permittivity, also known as the lossless permittivity, and $\varepsilon_r''(\omega)$ is the imaginary part of the complex relative permittivity, which is caused by bound charge and dipole relaxation phenomena that result in an energy loss.

The dielectric loss tangent, $tan\delta$, also known as the ratio of energy loss, can be expressed as:

$$tan\delta = \frac{\varepsilon_r''(\omega)}{\varepsilon_r'(\omega)} \tag{5.9}$$

It is noteworthy that the build-up of polarisation following the sudden application of an electric field takes a finite time interval before the polarisation reaches the static relative permittivity from the instantaneous relative permittivity. This phenomenon is described by the general term dielectric relaxation. Specifically, the single dielectric relaxation response of an ideal, non-interacting population of dipoles to an AC electric field is termed the Debye relaxation, which is expressed as:

$$\varepsilon_r^*(\omega) = \varepsilon_\infty + \frac{\varepsilon_s - \varepsilon_\infty}{1 + j\omega\tau} \tag{5.10}$$

where ε_∞ is the permittivity at the high frequency limit, ε_s is the static, low frequency permittivity and τ is the characteristic relaxation time of the medium.

When considering the dielectric response of a multi-phase system such as a composite, interfacial polarisation needs to be taken into account. A related effect is Maxwell-Wagner-Sillars polarisation, where charge carriers blocked at inner dielectric boundary layers or external electrodes lead to a separation of charges. The charges may be separated by a considerable distance and therefore make contributions to the dielectric loss tangent that are orders of magnitude larger than the response due to molecular fluctuations.

5.2 Results and Discussion

5.2.1 The Effect of Nanosilica on Dielectric Response

Figure 5.1 shows the real relative permittivity and dielectric loss as a function of frequency for samples containing different types and amounts of nanosilica. For unfilled polyethylene, there will always be some impurities present, such as oxidised functional groups on the polyethylene chain as a consequence of a small degree of oxidative degradation upon material processing. Such oxidised regions will respond more readily to electric field due to their more polar nature (Bernstein, 2003). However, the increase in relative permittivity is low as the amount of polar functionality is very small, and the real relative permittivity remains constant (~2.3) throughout the measured frequency range.

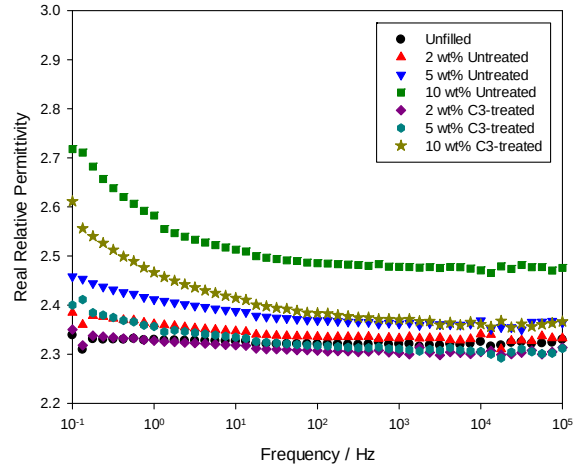

(a)

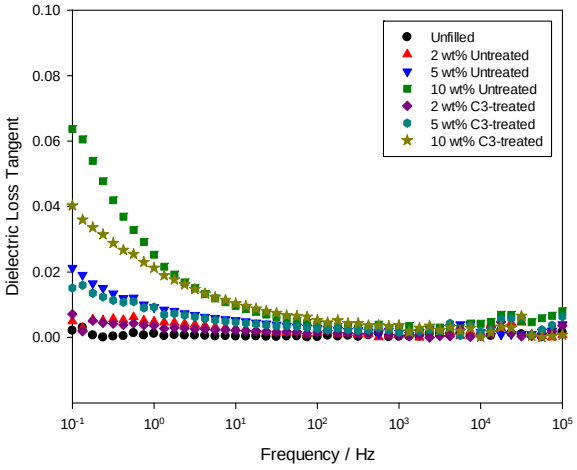

(b)

Figure 5.1: (a) Real relative permittivity, (b) dielectric loss tangent of various polyethylene systems crystallised isothermally at 115 ºC upon vacuum drying at 60 ºC

For nanocomposites containing both untreated and C3-treated nanosilica, their real relative permittivity and dielectric loss are dependent both on the frequency and nanosilica loading level. First consider the case of untreated nanosilica, where the permittivity (see Figure 5.1a) of the nanocomposites exhibits different behaviour in the low frequency range with just as little as 2 wt% of untreated nanosilica loading. As the amount of untreated nanosilica increases, an apparent increase in permittivity can be observed. The same trend was observed for the case of C3-treated nanosilica.

In Figure 5.1b, the higher dielectric loss of the nanocomposites observed in the low frequency range is possibly associated with Maxwell-Wagner-Sillars interfacial polarisation, where the frequency dependent contributions to dielectric response may come from charge build-up at the interfaces of nanocomposites; as the amount of nanofiller increases, the total effective area of the interfaces increases, resulting in a significant increase of interfacial polarisation (Huang et al., 2007; Huang et al., 2008).

Comparing the dielectric response of nanocomposites containing untreated and C3-treated nanosilica reveals that the permittivity and loss of samples containing C3-treated nanosilica yield lower values than that of their respective untreated nanosilica counterparts. These differences are believed to be attributed to the interfacial region between the polyethylene and the nanosilica (Todd and Shi, 2003), or more specifically, the surface state of the nanosilica; the surface of the untreated nanosilica is mainly characterised by hydroxyl (OH) functional groups while the surface of the C3-treated nanosilica is mainly characterised by propyl (C_3H_7) functional groups (see Figure 4.1).

The increased permittivity and loss can therefore be attributed to the response of the hydroxyl groups and associated species attached to the surface of the untreated nanosilica, since hydroxyl groups and any bound water should be more sensitive towards the electric field. As the amount of nanosilica increases, the number of hydroxyl groups increases, resulting in a higher permittivity and increased loss. Meanwhile, propyl (C_3H_7) functional groups on the surface of the C3-treated nanosilica generally do not respond to the applied electric field due to their non-polar nature. Nevertheless, there will still be some residual hydroxyl groups on the surface

of the C3-treated nanosilica due to incomplete surface functionalisation. Consequently, the permittivity and loss of the nanocomposites containing C3-treated nanosilica are lower than that of the respective nanocomposites containing untreated nanosilica.

From the above discussion, it is likely that the dielectric response of the nanocomposites would be affected by the presence of water. Water (H_2O) is a polar molecule and the oxygen attached to it is highly prone to hydrogen bonding with hydroxyl groups on the surface of nanosilica. Since water itself has a relatively high permittivity, i.e., ~80, the presence of water, even in very small amounts, could considerably affect the overall permittivity and the dielectric loss of the system. Water could therefore serve as an effective medium to explore mechanisms pertaining to interfacial region in nanocomposites.

5.2.2 The Effect of Water Absorption on Dielectric Response

In practical applications, the presence of absorbed water in insulation materials is unavoidable and could have a negative impact on dielectric properties. Despite attempts to remove water through sample drying, it is rather difficult to judge how dry is considered to be thoroughly dried (Reed, 2010; Tanaka et al., 2011).

The effect of water absorption in nanocomposites is still far from fully understood. Zou et al. (2008) highlighted that epoxy nanocomposites absorb significantly more water than unfilled epoxy when exposed to humid environmental conditions. The extra water was found to be located around the surface of the nanoparticles, resulting in the existence of water shells surrounding the nanoparticles. Conversely, filler particles that have surfaces that are functionalised to be hydrophobic reduce considerably the amount of absorbed water in nanocomposites under the same conditions of humidity.

Fabiani et al. (2010) investigated the effect of nanoparticle drying procedures on the water content of the final nanocomposites. In this experimental work, one batch of nanoparticles was exposed to a non-dry environment, while the other batch of

nanoparticles was dried at 80 ºC under vacuum. The experimental results showed an increase of permittivity and loss in the samples containing nanoparticles exposed to the non-dry environment in contrast to the samples containing dried nanoparticles.

To date, published literature on the effect of water absorption, especially in connection with the dielectric properties of nanocomposites, is relatively scarce. Polyethylene nanocomposites, for example, have not drawn significant attention with respect to water absorption. Although polyethylene itself is hydrophobic, the addition of a nanofiller could significantly alter the water absorption behaviour of the resulting nanocomposites. It is suggested that this phenomenon is due to the presence of the nanofiller/polymer interface, which acts as a preferred location for the aggregation of water molecules (Kinloch et al., 2000).

To investigate further the effect of water absorption on the polyethylene systems, the samples were immersed in distilled water for different time intervals and the percentage increase in mass for each sample was calculated based on the following equation:

$$\% \, Mass = \left| \frac{M_w - M_d}{M_d} \right| \times 100\% \tag{5.10}$$

where M_w is the weight of a water absorbed sample and M_d is the weight of a dry sample.

Figure 5.2 shows water uptake data obtained from each sample, from which it is evident that water absorption in unfilled polyethylene is negligible. Dielectric spectroscopy data (see Figure 5.3) also indicate that both permittivity and loss tangent of the unfilled polyethylene do not change upon exposure to water; the dielectric response is generally the same up to 30 days of water immersion, indicating the strongly hydrophobic nature of the polymer (Steeman et al., 1991).

For nanocomposites containing both types of nanosilica, significant quantities of water are absorbed by all systems (see Figure 5.2). The amount of absorbed water increases with increasing nanosilica content and is reduced considerably for the

samples containing the C3-treated nanosilica (see Figure 5.2b), compared with samples containing an equivalent loading level of untreated nanosilica (see Figure 5.2a). For example, after 30 days of water immersion, nanocomposites containing 10 wt% of C3-treated nanosilica contain ~0.75 % by mass of water, compared to ~1.69 % for nanocomposites containing 10 wt% of the untreated nanosilica.

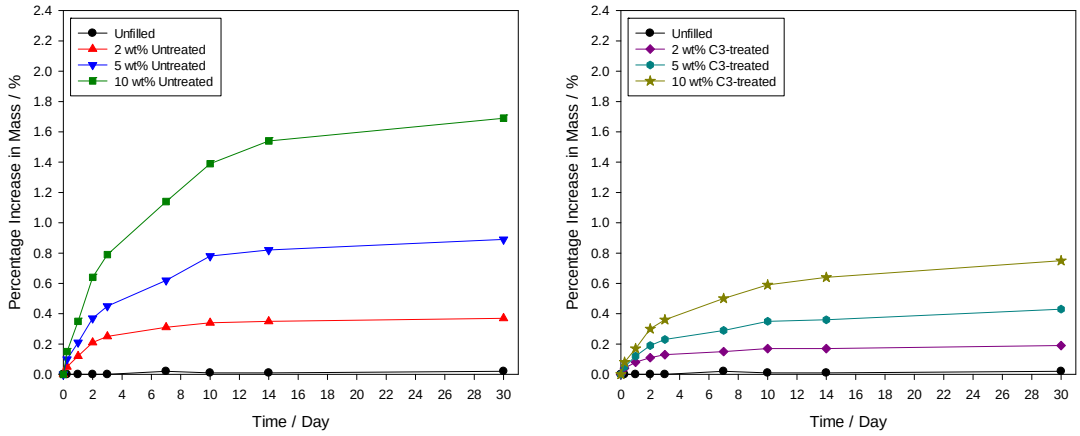

(a) (b)

Figure 5.2: Water uptake capability of nanocomposites crystallised isothermally at 115 ºC containing (a) untreated nanosilica, (b) C3-treated nanosilica, with unfilled polyethylene as reference

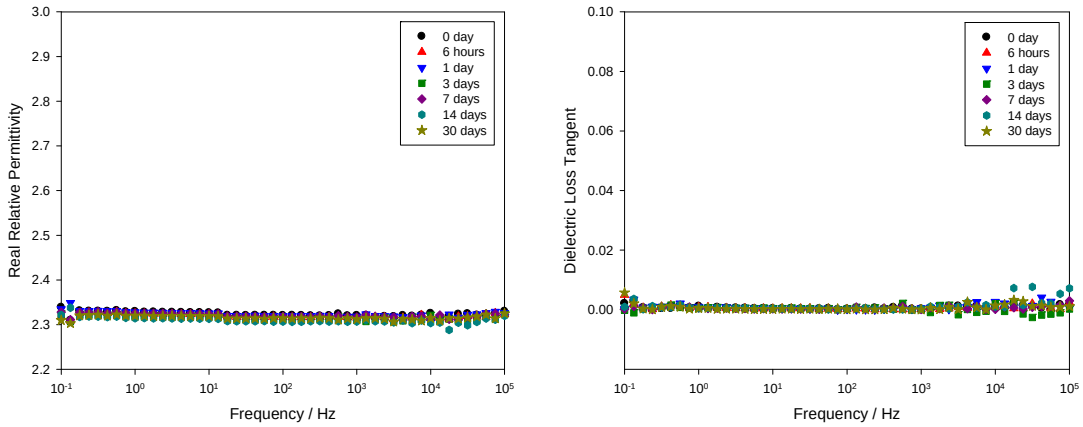

(a) (b)

Figure 5.3: (a) Real relative permittivity, (b) dielectric loss tangent of unfilled polyethylene crystallised isothermally at 115 ºC upon water immersion

From the data shown in Figure 5.4, it is evident that the equilibrium water content increases approximately linearly with filler loading level; although it is not possible reliably to evaluate the absolute interfacial areas in these systems, this observation and the reduction in absolute water content that results from surface treatment suggests that water uptake is indeed associated with nanoparticle interfaces. This proportionality is also significant in view of the agglomeration effects discussed in

Chapter 4 – clearly, the systems containing 10 wt% of nanosilica contain larger agglomerates than the systems containing just 2 wt%. If this aggregation were materially to influence the effective interfacial area, then this should manifest itself in a deviation from linearity between equilibrium water uptake and nanofiller loading level. However, the uncertainties in the data are such that any deviations are within experimental uncertainties and therefore, either the agglomeration shown in Figure 4.8 is insufficient materially to affect the nanofiller/polymer interfacial area, or else, water molecules are still able to penetrate the agglomerated nanosilica structures. Replotting the data using logarithmic axes (see Figure 5.5) reveals a power law relationship between water uptake and time and suggests that, initially, the behaviour is intermediate between Fickian and Case II (Alfrey et al., 1966).

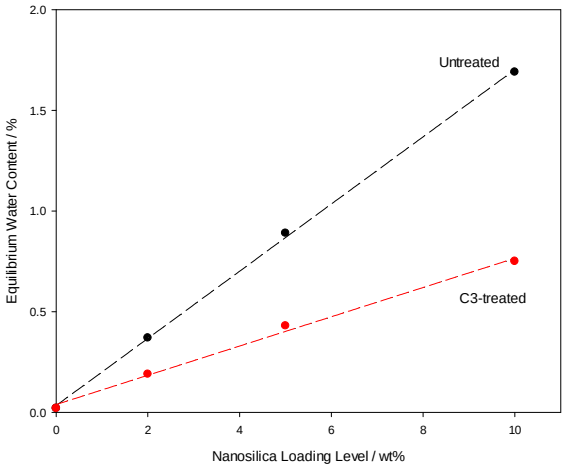

Figure 5.4: Plots of equilibrium water uptake against nanofiller loading level. The lines are fitted to show an approximately linear increase of equilibrium water content with the nanofiller loading level

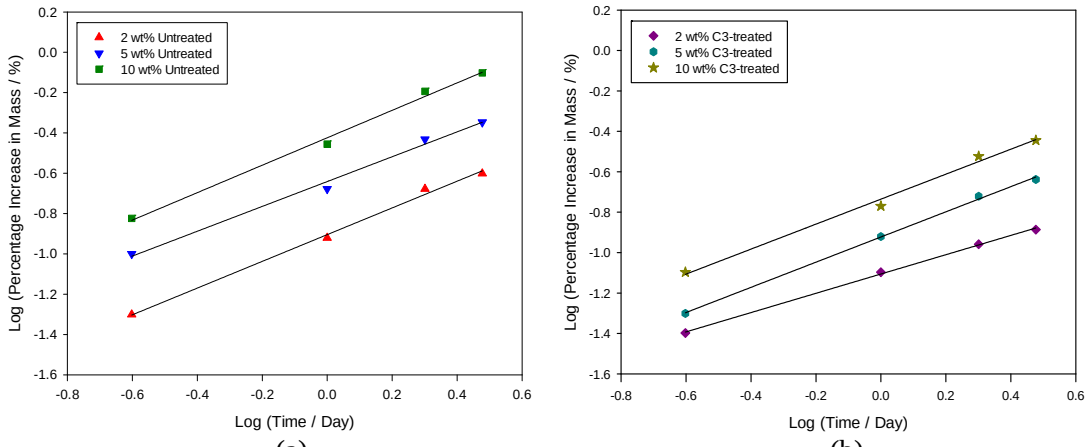

(a) (b)

Figure 5.5: Logarithmic plots of percentage increase in mass against water immersion duration (up to 3 days) for nanocomposites containing (a) untreated nanosilica, (b) C3-treated nanosilica. The fitted lines are based on power law relationship

Figure 5.6 shows plots of permittivity and loss tangent against frequency for nanocomposites containing 2 wt%, 5 wt% and 10 wt% of untreated nanosilica after different periods of water immersion. For the case of 2 wt% of untreated nanosilica, the permittivity of the nanocomposite sample does not vary significantly across the frequency range studied, prior to water immersion (see Figure 5.6a, plot for 0 day). In the low frequency range, the slightly higher dielectric loss of the sample (see Figure 5.6d, plot for 0 day) is possibly associated with Maxwell-Wagner-Sillars (MWS) interfacial polarisation, as previously discussed. With increased water absorption, the permittivity increases and the loss peak shifts to higher frequencies.

Investigating the dielectric response of nanocomposites containing varying amounts of untreated nanosilica reveals that all materials exhibit common elements (see Figure 5.6b, Figure 5.6c, Figure 5.6e and Figure 5.6f). Again, the permittivity increases with increased water absorption. For discussing the loss behaviour of these systems, it is convenient to consider this in terms of three frequency dispersion regions, although, in reality, the loss peaks will move progressively to higher frequencies as water absorption increases: the low-frequency dispersion region (10^{-1} Hz to 10^{0} Hz); the intermediate-frequency dispersion region (10^{0} Hz to 10^{3} Hz); the high-frequency dispersion region (10^{3} Hz to 10^{5} Hz). The loss processes associated with the lowest frequencies (below the measurement range for 5 wt% and 10 wt% of untreated nanosilica loading) move to higher frequencies on exposure to water and combine to form a broad loss peak with increased intensity. For nanocomposites containing 10 wt% of untreated nanosilica, 14 days of water immersion induces pronounced double loss peaks at two different frequencies, one at ~600 Hz and the other at ~20 kHz (arrowed in Figure 5.4f). It is noteworthy that the vertical scale of the graphs of both real relative permittivity and dielectric loss tangent shown in Figure 5.6 vary with nanofiller loading level, to give a better illustration of the dielectric processes.

The dielectric response of nanocomposites is strongly influenced by interfacial relaxation processes, which are affected by both the character of the interface between the matrix and the filler and dipolar relaxations related to the presence of water molecules. Therefore, the broad loss peak may have been caused by two effects (Steeman et al., 1991). Firstly, as the content of nanoparticles increases, it is

more difficult to achieve good dispersion of nanoparticles throughout the sample and agglomeration increases. This results in structurally different interfacial regions, which cause the width of the loss peak to increase with increasing nanoparticle loading, as also suggested by Zhang and Stevens (2008). Secondly, different states of water bonding could exist due to different interfaces, which would also contribute to the observed broad loss peaks.

When considering the effect of surface treatment of the nanosilica, the dielectric response of the nanocomposites containing C3-treated nanosilica appears to be different from that of the nanocomposites containing untreated nanosilica. This is illustrated in Figure 5.7. In all three cases (2 wt%, 5 wt% and 10 wt% of C3-treated nanosilica loading), a distinct low-frequency loss peak is evident after 3 days of water immersion. This loss peak then shifts slightly to higher frequencies with further exposure to water; in these materials the dispersion is confined to the low frequency region, in contrast to the behaviour reported above for the nanocomposites containing untreated nanosilica. The dielectric loss behaviour of the nanocomposites containing varying amount of C3-treated nanosilica is generally comparable, albeit that the strength of the relaxation increases with filler loading level.

In addition, the broad loss peaks in the nanocomposites containing C3-treated nanosilica are narrower than those in the nanocomposites containing an equivalent amount of untreated nanosilica (compare Figure 5.7d, Figure 5.7e and Figure 5.7f with Figure 5.6d, Figure 5.6e and Figure 5.6f, respectively). This may indicate, firstly, that the dispersion of nanosilica throughout the sample has improved and, secondly, that the water absorption mechanism has changed. Also, the increase in permittivity is less when compared with nanocomposites containing an equivalent amount of untreated nanosilica (compare Figure 5.7a, Figure 5.7b and Figure 5.7c with Figure 5.6a, Figure 5.6b and Figure 5.6c, respectively). For example, the real part of the permittivity at 0.1 Hz for nanocomposites containing 10 wt% of C3-treated nanosilica saturated at ~4.1, compared with ~6.7 in the case of nanocomposites containing 10 wt% of untreated nanosilica.

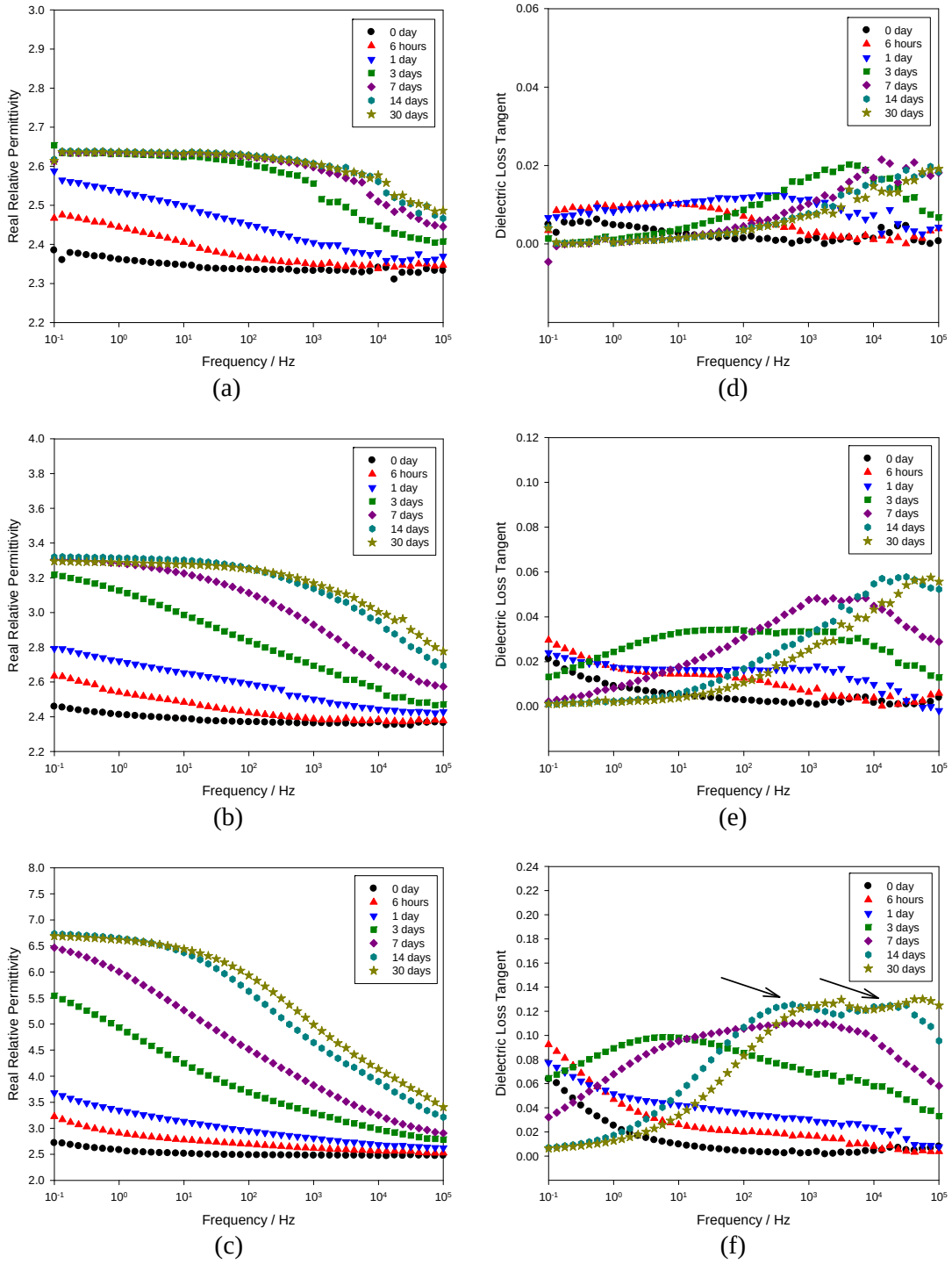

Figure 5.6: Real relative permittivity of nanocomposites crystallised isothermally at 115 ºC containing (a) 2 wt%, (b) 5 wt%, (c) 10 wt% of untreated nanosilica and dielectric loss tangent of nanocomposites crystallised isothermally at 115 ºC containing (d) 2 wt%, (e) 5 wt%, (f) 10 wt% of untreated nanosilica upon water immersion at different time intervals (Note the scaling difference)

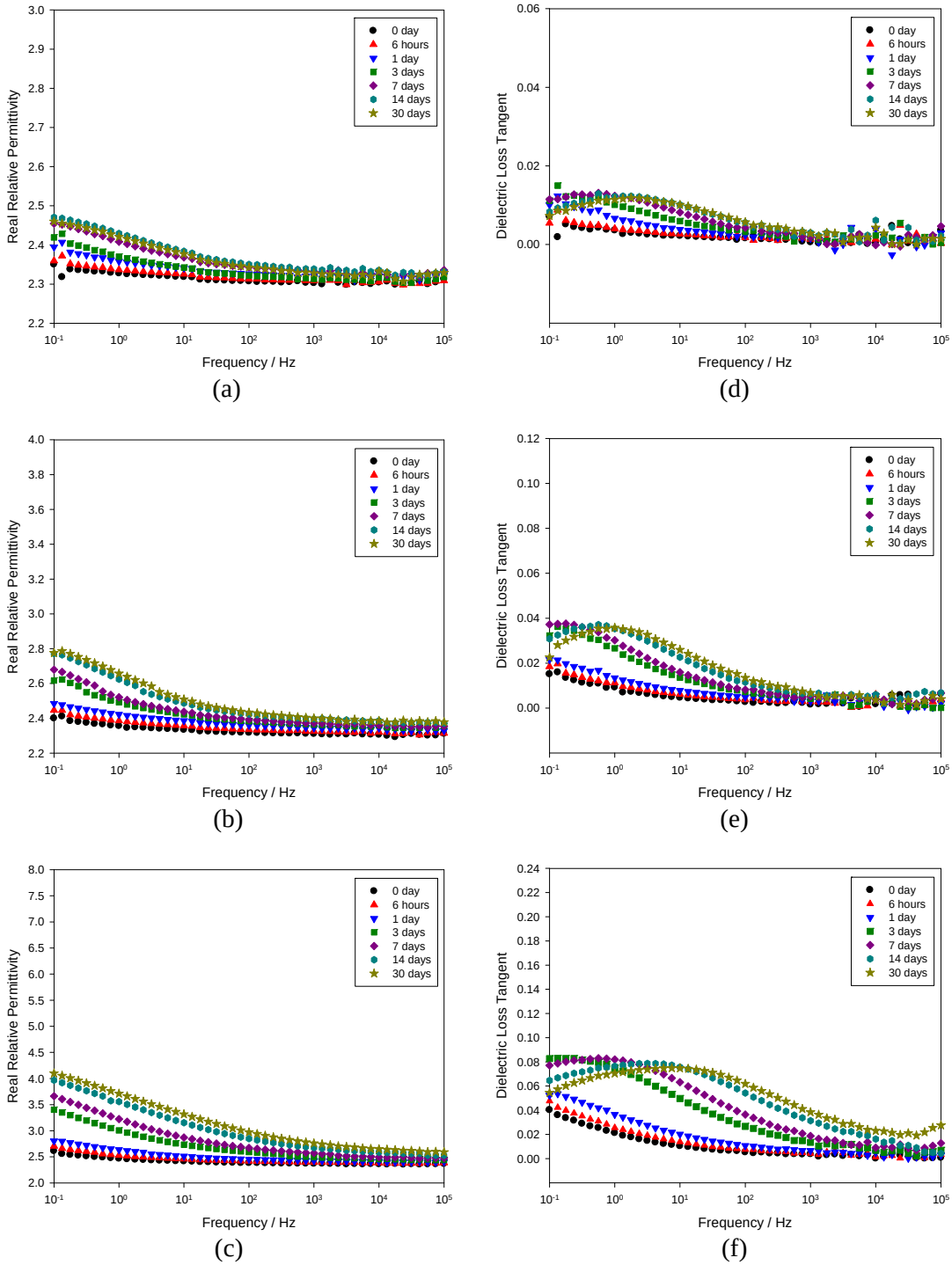

Figure 5.7: Real relative permittivity of nanocomposites crystallised isothermally at 115 ºC containing (a) 2 wt%, (b) 5 wt%, (c) 10 wt% of C3-treated nanosilica and dielectric loss tangent of nanocomposites crystallised isothermally at 115 ºC containing (d) 2 wt%, (e) 5 wt%, (f) 10 wt% of C3-treated nanosilica upon water immersion at different time intervals (Note the scaling difference)

5.2.3 Discussion

The above experimental work on water absorption reveals dielectric processes that are in qualitative agreement with the interlayer model proposed by Steeman and Maurer (1990), which describes the influence of a conductive interlayer (water adsorbed at the filler-matrix interface) on the dielectric behaviour of a composite (glass-bead filled polyethylene) as a function of volume fraction and interlayer properties. The model assumes that the permittivity of the matrix and the filler are frequency independent and that neither component is electrically conducting; the water interlayer is assigned a specific frequency independent conductivity. This results in the associated relaxation process being displaced to higher frequencies with increasing interlayer volume fraction (or increasing interlayer conductivity), as seen experimentally here. Although a detailed discussion of the interlayer model is not warranted here, the concepts help, in this case, to reveal the possible water absorption mechanisms that could occur at interfaces in nanocomposites containing nanosilica with different surface chemistries. More importantly, the presence of different frequency dispersion states suggests that different states of water (or different layer thickness of water) may exist within the nanocomposites. An attempt was therefore made to deduce the possible water absorption processes that could occur at interfaces in nanocomposites containing nanosilica with different surface chemistries.

For nanocomposites containing untreated nanosilica, water can readily be adsorbed onto the surface of the nanosilica, creating the primary volume fraction of water. These molecules are tightly bound to the surface, presumably, through hydrogen bonding with hydroxyl groups on the untreated nanosilica. These tightly bound molecules explain the high dielectric loss in the low frequency region. With increasing water absorption, more water molecules reside at the interface, resulting in the formation of a secondary, less tightly bound water layer. With a higher content of inorganic particles, a greater overall amount of water can be contained in the interfacial regions (Zou et al., 2008). This is believed to cause the loss peaks observed in the intermediate frequency region. A tertiary volume fraction of water is believed to be an extension of the loosely bound water which is suggested to result in the observed loss peak shifting to higher frequencies. Meanwhile, the increase in

permittivity is closely related to the dielectric loss processes. With increased water absorption, more water molecules exist in the nanocomposite sample. Consequently, more polar dipoles (i.e., hydroxyl groups) from the water can readily respond to the applied field, resulting in higher permittivity.

For nanocomposites containing C3-treated nanosilica, since the surface of the nanosilica has been rendered more hydrophobic, it will contain mainly propyl groups. Nevertheless, some hydroxyl groups will still exist, due to incomplete surface functionalisation, as previously described. These hydroxyl groups facilitate water adsorption at the surface of the C3-treated nanosilica, but in a quantity much smaller than that of the untreated nanosilica. This creates the tightly bound water on the surface of the C3-treated nanosilica, which is evident from the increased dielectric loss within the low frequency region. With increased duration of water exposure, more water molecules come to reside in the interfacial regions. However, less loosely bound water can be accommodated upon surface treatment, resulting in only a slight increase of permittivity and slight shift of loss peak towards the intermediate frequency region. It is therefore reasonable to deduce that surface treatment of nanosilica causes a change in the water diffusion processes (and also the layer thickness or aggregation state of water) in the nanocomposites, and it is suggested that this is mainly attributable to changes in the interface between the filler and the matrix.

The proposed water shell model corresponds with observations by other researchers (Hui et al., 2010), where it was reported that loss peaks at frequencies of 10 kHz and 10 Hz found in 5 wt% of nanosilica filled XLPE are probably due to the dielectric response of bound water; the Debye relaxation of free water should be observed at frequency of about 10 GHz. Hui et al. (2010) assumed in general only one type of bound water, while in this case, it is proposed that at least three types of bound water exist. Nevertheless, the observed dispersion peaks fall within a similar range.

It is noteworthy that the broad loss peak may reflect a range of interface and aggregation states, which subsequently affect the water diffusion process via interfaces (Steeman and Maurer, 1990). As the content of nanoparticles increases, it is more difficult to achieve good dispersion of nanoparticles throughout the sample

and more agglomerations exist. This results in different interfacial regions, which causes the width (and also the magnitude) of the dielectric loss peaks to increase with increasing nanoparticle loading.

5.3 Summary

For unfilled polyethylene, the permittivity and loss remained constant throughout the investigated frequency range. For nanocomposites containing both untreated and C3-treated nanosilica, the permittivity and loss are dependent both on the frequency and nanosilica loading level. However, such effects are less pronounced in samples containing C3-treated nanosilica in comparison with samples containing an equivalent amount of untreated nanosilica. This is attributable to a change in surface chemistry of the nanofiller; the surface of the untreated nanosilica is mainly characterised by hydroxyl functional groups while the surface of the C3-treated nanosilica is mainly characterised by propyl functional groups. Consequently, surface treatment of nanosilica has a profound impact on the water absorption and dielectric response of the nanocomposites. The results presented indicate that nanosilica filled polyethylene absorbs significantly more water than unfilled polyethylene, with the consequence that both the permittivity and loss tangent increase with increasing duration of water immersion. However, appropriate surface treatment of nanosilica reduces the water absorption effect and modifies the dielectric response of the nanocomposites compared with those containing untreated nanosilica. Since the influence of water appears quite different in the nanocomposites following nanosilica surface treatment, it is reasonable to deduce that the interfacial structure of nanocomposites containing untreated nanosilica is different from that of the nanocomposites containing C3-treated nanosilica. While water absorption may not be a technologically desirable characteristic, these results suggest that water molecules can act as effective dielectric probes of interfacial factors.

Chapter 6

Electrical Breakdown Strength

"Research is to see what everybody else has seen, and to think what nobody else has thought."

- Albert Szent-Gyoergi -

6.1 Introduction

Electrical breakdown strength, also known as dielectric breakdown strength, is a topic of great academic and technological interest. The dielectric strength of an insulation material is defined as the limiting voltage stress beyond which the insulation can no longer maintain its integrity. In other words, it reflects the ability of an insulation material to resist decomposition under voltage stress. The applied voltage causes the insulation to fail, where a discharge occurs through the insulation and causes the insulation to rupture. The dielectric strength is usually expressed as a voltage per unit thickness, such as kV mm^{-1}.

A theoretical concept that has been discussed in the literature is the intrinsic strength. It is defined by the characteristics of the material itself in its pure and defect-free state. In practice, this can never be achieved experimentally, since it is impossible to obtain defect-free samples. However, it is noteworthy that there is less chance for a critical defect to exist in a thinner sample. Furthermore, there exist many external factors that affect the measured dielectric strength of an insulation material. In this regard, many theories associated with breakdown mechanisms have been proposed, which may include thermal, electrical and mechanical as well as chemical parameters (Kuffel et al., 2000; Bernstein, 2003) but, in practice, it is difficult to determine the exact underlying mechanisms that lead to breakdown.

In laboratory scale analysis, there exists a wide variety of different testing methods and electrode geometries to assess the breakdown performance of polymers, and the value of breakdown strength is relevant only if the manner of testing is known. There

are generally two types of testing methods commonly used, i.e., the constant-stress test, in which the time-to-breakdown is measured at a constant electric field, and progressive-stress test, in which the electrical field magnitude at breakdown is measured when the applied electrical stress is a function of time. Nevertheless, the progressive-stress test is preferable because the variation in the measured results is found to be less than that of the equivalent constant-stress test (Dissado et al., 1984). Furthermore, in the constant-stress test over an extended period of time, critical control of electric field is required as small variations in field can give rise to significant variation in the time to breakdown. Therefore, the progressive-stress test is popular with the advantage that all samples can be forced to fail within a reasonably short time (Stone et al., 1979).

In terms of electrode geometry, the needle plate arrangement remains popular due to its ease of implementation. Unfortunately, this geometry can lead to voiding problems when the needle is inserted. In addition, electric field enhancement at the tip of the needle, which induces high localised stress, could lead to premature failure of the sample. In this case, the dielectric strength measured would be related more to the manner in which the test was performed than the properties of the insulation itself. Alternatively, a plate-plate geometry can be used, but electric field enhancement at the edge of the electrodes may lead to flashover at the edges of the sample (Miller, 1993). To avoid such problem, an electrode arrangement that approximate the plate-plate geometry, such as two ball-bearings, can be used, provided that the radius of curvature of the ball-bearing is much greater than the thickness of the sample. With this, flashover at the edges of the sample can be reduced since the electrodes at the edges are at a greater distance away from the sample when compared to the plate-plate geometry. Such a geometry provides a uniform stress gradient and enhances the opportunity to obtain meaningful data, although the existence of a triple point may be problematical.

Generally, the breakdown performance of a solid insulation system can be described using two-parameter Weibull distribution analysis. The Weibull probability distribution (Weibull, 1951), also known as the extreme-value distribution, is commonly used to analyse the data for time-to-breakdown from constant-stress voltage endurance tests or breakdown voltage of field from progressive-stress tests

on solid electrical insulation systems (The Institute of Electrical and Electronics Engineers, 1987). The two-parameter Weibull cumulative distribution function for the population fraction below E_i is:

$$P(E_i) = 1 - \exp\left[-\left(\frac{E_i}{\alpha}\right)^{\beta}\right] \tag{6.1}$$

where $P(E_i)$ is the cumulative probability of failure at E_i, E_i is the experimental breakdown strength, α is the scale parameter and β is the shape parameter. The probability of failure, $P(E_i)$ is zero at $E_i = 0$. The probability of failure rises continuously as E increases, and finally approaches certainty, that is, $P(E_i) = 1$. The scale parameter, α represents the breakdown strength at the cumulative failure probability of 63.2 %. The units of α are the same as E_i. The shape parameter, β represents a measure of the spread of the breakdown data. The larger the β, the smaller is the range of the experimental breakdown strength values.

To plot the Weibull distribution on a probability graph paper, one axis of the graph should be in a non-linear cumulative probability of failure scale, while the other axis should indicate the breakdown strength. The axes are scaled so that plotted data from the two-parameter Weibull distribution tend to follow a straight line. When the data are plotted, the data are ordered from the smallest to the largest, and a cumulative probability of failure, $P(E_i)$ has to be assigned to each point. A best straight line is fitted through such points using the Maximum Likelihood Estimation (MLE) technique, that gives better estimates for α and β. ReliaSoft Weibull 7++ software was used for this analysis in this study and breakdown data were plotted between the two-sided 90 % confidence bounds that give a graphical representation of the spread in the data.

The cumulative probability of failure, $P(E_i)$ was approximated using the median rank method:

$$P(E_i) = \frac{i - 0.3}{m + 0.4} \tag{6.2}$$

where i is the progressive order of failed tests and m is the total number of tests. This method has been proven to be an excellent approximation of cumulative failure probability and is more consistent with the accepted computational use of the MLE technique (Fothergill, 1990). Other methods, such as the mean rank method, where:

$$P(E_i) = \frac{i}{m+1} \tag{6.3}$$

and symmetrical cumulative distribution function method, where:

$$P(E_i) = \frac{i - 0.5}{m} \tag{6.4}$$

can also be used, but they introduce significant systematic errors into graphical estimates of the distribution's parameter and are not consistent with the use of the MLE technique. An example of a Weibull plot is shown in Figure 6.1.

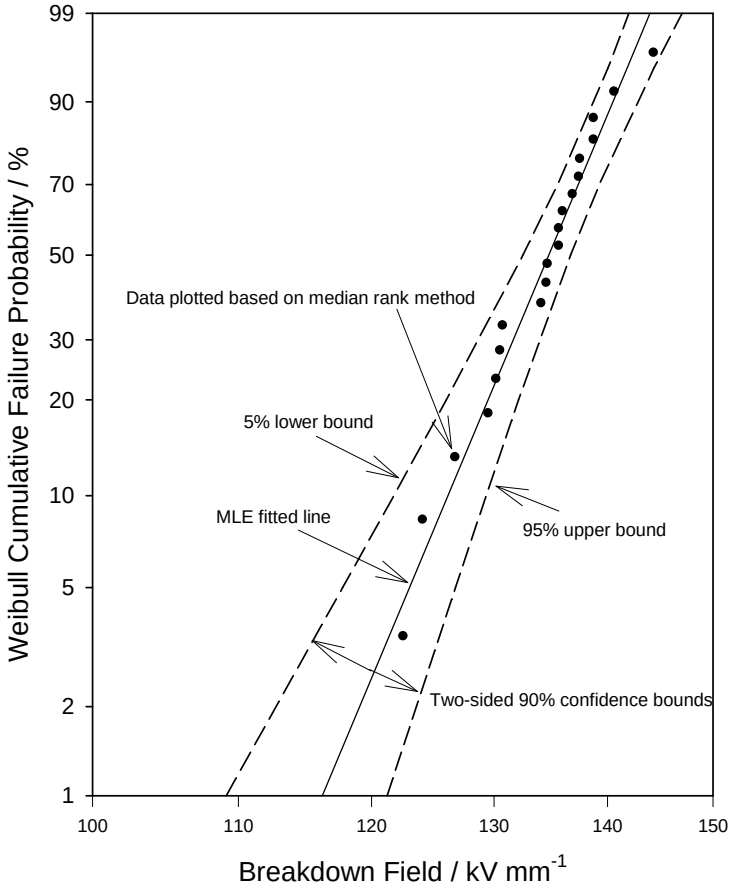

Figure 6.1: Weibull plot of MLE fitted line and two-sided 90 % confidence bounds

One of the most attractive property changes associated with nanocomposites is the potential enhancement of dielectric breakdown strength brought about by nanostructuration. This is because the desired mechanical and thermal properties of conventional microcomposite systems were often achieved at the cost of reduced electrical strength. For example, microsilica-filled polyethylene exhibited reduced breakdown strength when compared with unfilled polyethylene (Nelson, 2007). Interestingly, the breakdown strength of nanocomposites is generally better than that of microcomposites (Li et al., 2010b; Nelson, 2007), and can be even better than that of the base polymer (Sarathi et al., 2007).

Due to the promising features of nanodielectrics, various nanocomposite systems have been investigated with respect to breakdown strength, such as polyethylene/silica nanocomposites (Roy et al., 2005b; Nelson, 2007), epoxy/titania nanocomposites (Nelson, 2007), polyimide/silica nanocomposites (Cao et al., 2004), polyethylene/clay nanocomposites (Green, 2008) and polypropylene/layered silicate nanocomposites (Montanari et al., 2004). Positive experimental results on breakdown strength of nanocomposites bring an opportunity where it might be possible to develop this new class of nanocomposite materials, such that they possess dielectric strength that is higher or at least commensurate with the base polymer, thus resulting in combined electrical, mechanical and thermal improvements over conventional microcomposites.

However, contradictory results do exist for the breakdown strength of nanocomposites. For example, the experimental work of Huang et al. (2009) revealed that the breakdown performance of polyethylene/aluminium nanocomposites was not as good as the base polymer, even though surface-treated nanoparticles and a compatibilizer were introduced. This shows that the incorporation of nanoparticles does not always improve the breakdown strength and that there might be subtle unidentified factors that jeopardise the breakdown performance due to nano-inclusions.

Danikas and Tanaka (2009) reported on the relationship between dielectric breakdown strength and treeing mechanisms and found that increased breakdown strength is strongly related to tree retardant effects. Nanoparticles were said to act as

barriers to prevent electrical treeing, ideally, through optimal dispersion of nanofillers. A zig-zag tree path was seen where the tree path avoided nanoparticles and thus, indirectly, slowed down the tree growth (Danikas and Tanaka, 2009; Imai et al., 2004) and subsequently resulted in improved breakdown performance.

The role of interfaces has been assumed to be the pivotal reason for the improved breakdown strength of nanodielectrics (Roy et al., 2005b) and consequently in an attempt to improve the interaction between the nanofiller and the matrix, various chemical compatibilizers have been used. In addition, the use of surfactants to modify the surface of nanoparticles has also been employed. However, the use of such additional chemicals raises a controversial question as to whether the unique dielectric properties are really caused by the interaction zone alone. Here, the effect of interaction might have been over-emphasised, while other contributing factors (e.g. the use of compatibilizers, surfactants, type of nanoparticles) were neglected, as highlighted in a recent paper published by an international collective of scientists (Fréchette et al., 2010). While the contributing interfacial effect of nanoparticles is to be emphasised, other influencing factors should not be neglected. Furthermore, the breakdown characteristics of nanodielectrics under an AC field could be different from under DC. More research is therefore required to understand breakdown mechanisms in nanodielectrics.

6.2 Results and Discussion

6.2.1 AC Breakdown Testing

Figure 6.2 compares Weibull plots of AC breakdown strength for unfilled polyethylene and nanocomposites containing 2 wt%, 5 wt% and 10 wt% of untreated nanosilica, isothermally crystallised at 115 ^{o}C. With the addition of 2 wt% of untreated nanosilica, the AC breakdown strength was the same as the unfilled polyethylene. This indicates that 2 wt% of untreated nanosilica is a very low amount and does not alter the breakdown strength of the system when compared with unfilled polyethylene. The addition of 5 wt% of untreated nanosilica into polyethylene, on the other hand, slightly reduced the AC breakdown strength of the

material. However, considering the uncertainty in Weibull analysis, this slight reduction is negligible; the breakdown strength is still commensurate with that of the unfilled polyethylene. Conversely, when the amount of untreated nanosilica was increased to 10 wt%, there was a significant reduction in the AC breakdown strength, in that the value was found to be 31 kV mm^{-1} lower than that of the unfilled polyethylene.

To confirm the AC breakdown behaviour of polyethylene with the addition of untreated nanosilica, another batch of material systems was investigated, where comparable material systems were subjected to quenching into water directly from the melt. Figure 6.3 shows the effect of untreated nanosilica content on the AC breakdown strength of the quenched polyethylene systems. Unsurprisingly, the AC breakdown strength of nanocomposites containing 2 wt% and 5 wt% of untreated nanosilica is commensurate with the AC breakdown strength of unfilled polyethylene subjected to quenching, whereas the AC breakdown strength of polyethylene with 10 wt% of untreated nanosilica is significantly reduced compared with unfilled polyethylene. The AC breakdown trend shown here is therefore in agreement with that shown in the isothermally crystallised polyethylene systems.

Upon surface treatment of nanosilica, the AC breakdown strength of the resulting nanocomposites that contained 2 wt%, 5 wt% and 10 wt% of C3-treated nanosilica exhibited slightly higher AC breakdown strength when compared with the unfilled polyethylene. This is illustrated in Figure 6.4. In these cases, all the samples were subjected to isothermal crystallisation at 115 °C. However, such a marginal increase of AC breakdown strength gained by surface treatment is within Weibull uncertainty bounds. This is confirmed by the Weibull plots comparing the AC breakdown strength of the equivalent sets of material systems subjected to quenching into water (see Figure 6.5). Therefore, surface treatment of nanosilica did not yield meaningful improvement towards the AC breakdown strength of the nanocomposites when compared with the unfilled polyethylene.

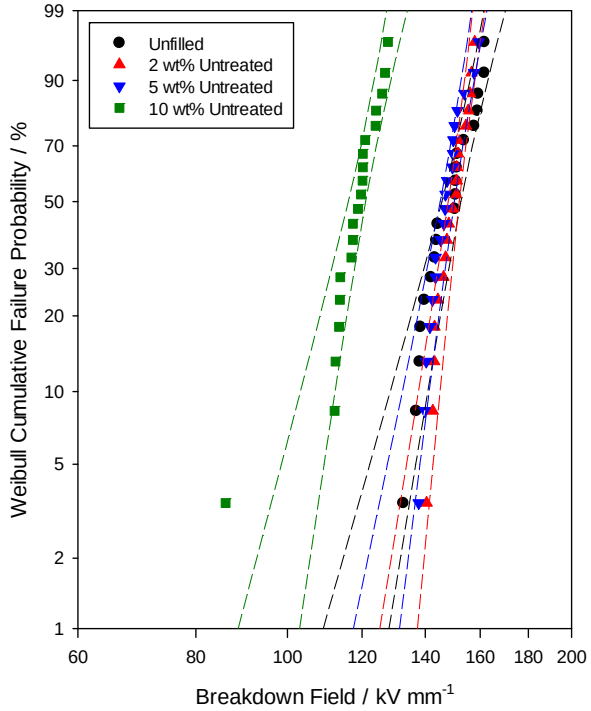

Sample	α / kV mm^{-1}	β
Unfilled	152 ± 3	19 ± 6
2 wt% Untreated	152 ± 2	33 ± 10
5 wt% Untreated	150 ± 2	26 ± 7
10 wt% Untreated	121 ± 2	21 ± 7

Figure 6.2: Weibull plots comparing the AC breakdown strength of unfilled polyethylene and nanocomposites containing 2 wt%, 5 wt% and 10 wt% of untreated nanosilica, crystallised isothermally at 115 ºC

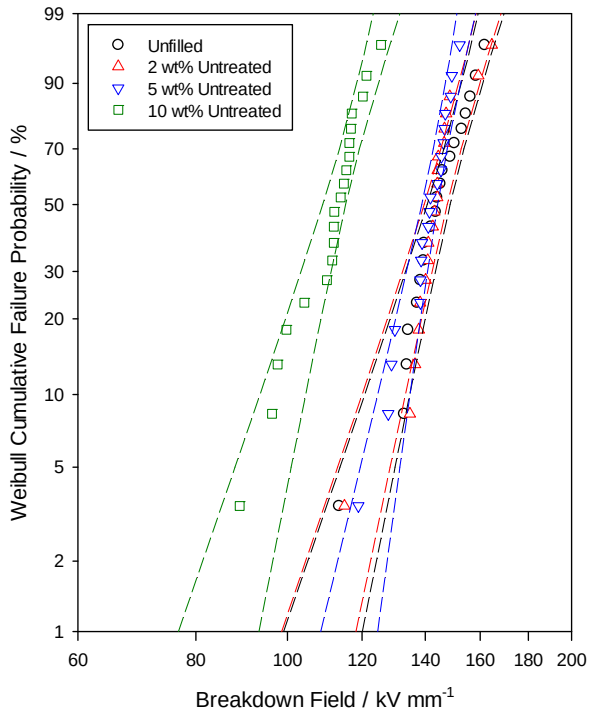

Sample	α / kV mm^{-1}	β
Unfilled	148 ± 4	16 ± 5
2 wt% Untreated	147 ± 4	16 ± 4
5 wt% Untreated	144 ± 3	23 ± 7
10 wt% Untreated	115 ± 3	16 ± 5

Figure 6.3: Additional (with samples subjected to quenching) Weibull plots comparing the AC breakdown strength of unfilled polyethylene and nanocomposites containing 2 wt%, 5 wt% and 10 wt% of untreated nanosilica

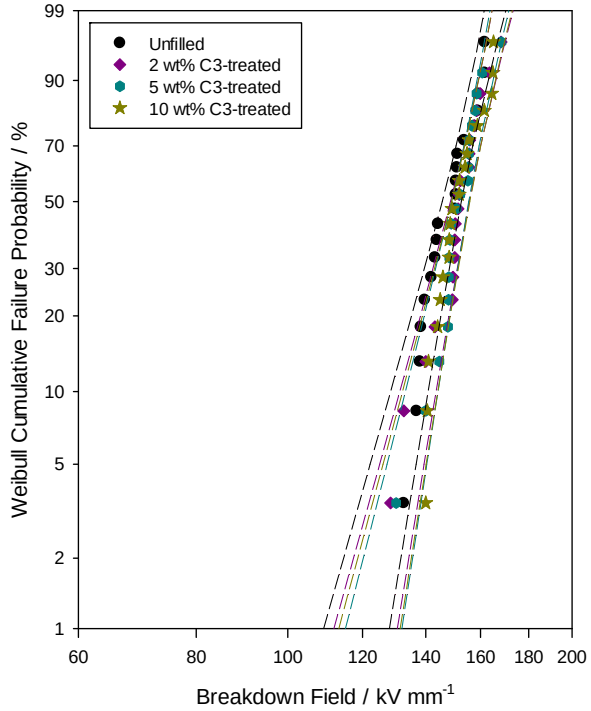

Sample	α / kV mm^{-1}	β
Unfilled	152 ± 3	19 ± 6
2 wt% C3-treated	155 ± 4	20 ± 6
5 wt% C3-treated	155 ± 3	21 ± 6
10 wt% C3-treated	156 ± 4	20 ± 6

Figure 6.4: Weibull plots comparing the AC breakdown strength of unfilled polyethylene and nanocomposites containing 2 wt%, 5 wt% and 10 wt% of C3-treated nanosilica, crystallised isothermally at 115 ºC

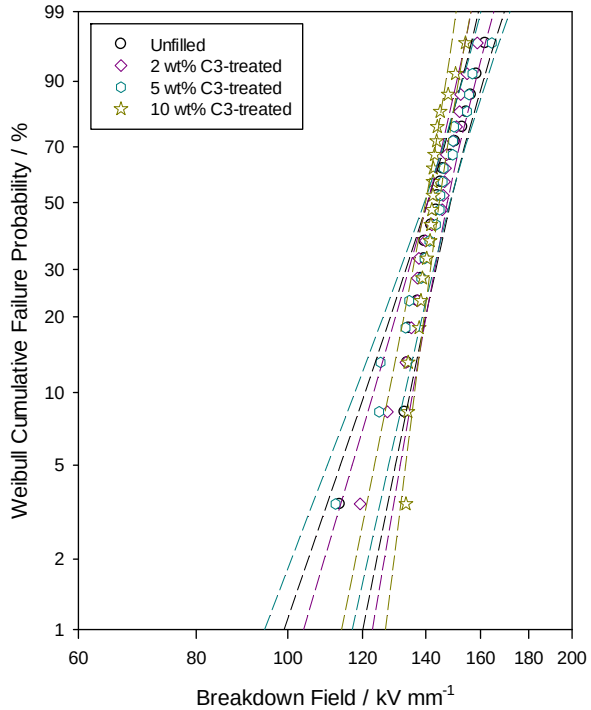

Sample	α / kV mm^{-1}	β
Unfilled	148 ± 4	16 ± 5
2 wt% C3-treated	147 ± 3	19 ± 5
5 wt% C3-treated	148 ± 4	14 ± 5
10 wt% C3-treated	144 ± 3	27 ± 7

Figure 6.5: Additional (with samples subjected to quenching) Weibull plots comparing the AC breakdown strength of unfilled polyethylene and nanocomposites containing 2 wt%, 5 wt% and 10 wt% of C3-treated nanosilica

6.2.2 DC Breakdown Testing

As previously highlighted, the effect of the nanofiller could be different when subjected to AC and DC applied fields. For example, an investigation by Bamji et al. (2005) into polypropylene/organoclay nanocomposites showed that although having the same AC and DC breakdown trend, the nanofiller had a less pronounced effect on AC breakdown compared to DC breakdown. While polypropylene possessed a higher breakdown strength with organoclay addition, the increase in AC breakdown strength is marginal, which could imply that the nanofiller does little for AC breakdown strength improvement, and this is in sharp contrast to the observed dramatic increase in DC breakdown strength.

The previous section demonstrated that, on AC breakdown testing, nanosilica does not have a significant effect on the AC breakdown properties in general. But would nanosilica alter the DC breakdown behaviour of polyethylene? The answer can be deduced from Figure 6.6. Clearly, the DC breakdown trend is completely different from that of the previously discussed AC breakdown trend; the DC breakdown strength of polyethylene is found to be sensitive to the amount of untreated nanosilica used.

For unfilled polyethylene, the DC breakdown strength is as high as 480 kV mm^{-1}. The addition of 2 wt% of untreated nanosilica reduces the DC breakdown strength to 278 kV mm^{-1}. Further reductions in DC breakdown strength were seen as the amount of untreated nanosilica increases, and could be up to 307 kV mm^{-1} lower than that of the unfilled polyethylene at 10 wt% of untreated nanosilica loading. Despite the reduced DC breakdown strengths, the shape parameters improved for all the investigated nanocomposite samples.

For nanocomposites containing C3-treated nanosilica, the DC breakdown strength is higher that of the nanocomposite containing untreated nanosilica counterparts, as illustrated in Figure 6.7. At 2 wt%, 5 wt% and 10 wt% of C3-treated nanosilica loading, the respective breakdown values are 58 kV mm^{-1}, 55 kV mm^{-1}, 21 kV mm^{-1} higher than that of the comparable amount of untreated nanosilica loading. Despite this, the breakdown strength is still lower than that of the unfilled polyethylene.

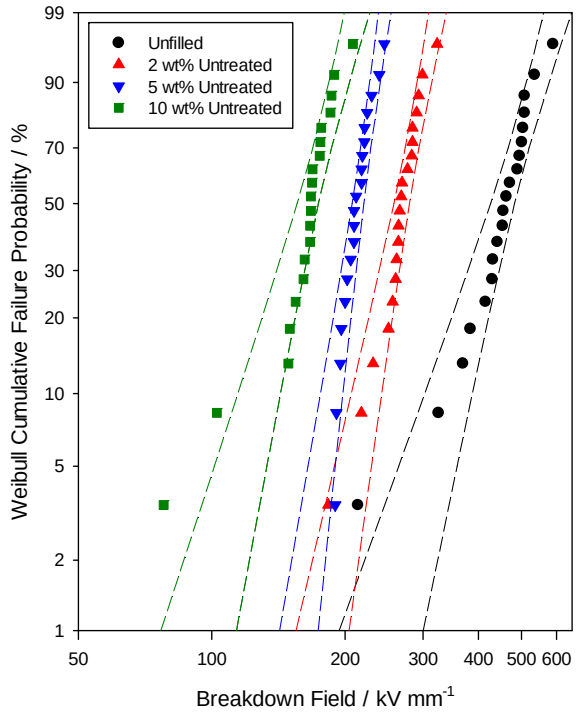

Sample	α / kV mm^{-1}	β
Unfilled	480 ± 28	7 ± 2
2 wt% Untreated	278 ± 11	11 ± 3
5 wt% Untreated	220 ± 6	15 ± 4
10 wt% Untreated	173 ± 9	8 ± 2

Figure 6.6: Weibull plots comparing the DC breakdown strength of the unfilled polyethylene and nanocomposites containing untreated nanosilica, crystallised isothermally at 115 ºC

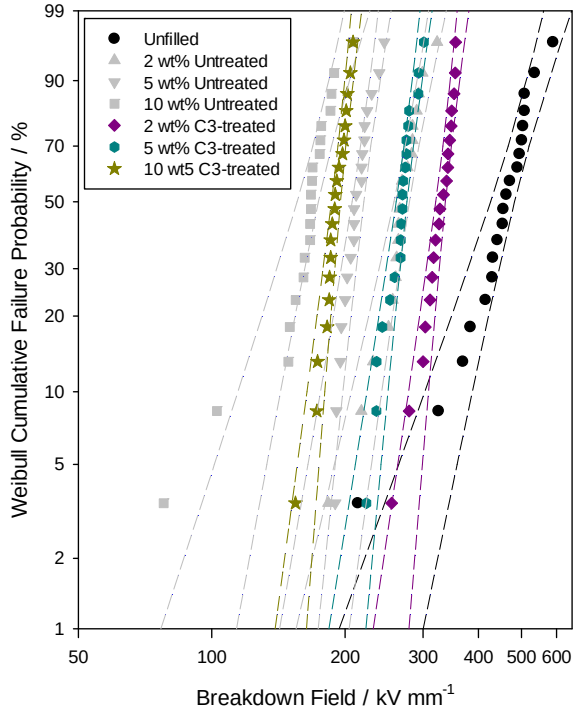

Sample	α / kV mm^{-1}	β
Unfilled	480 ± 28	7 ± 2
2 wt% C3-treated	336 ± 8	18 ± 5
2 wt% Untreated	278 ± 11	11 ± 3
5 wt% C3-treated	275 ± 7	16 ± 5
5 wt% Untreated	220 ± 6	15 ± 4
10 wt% C3-treated	194 ± 9	19 ± 6
10 wt% Untreated	173 ± 9	8 ± 2

Figure 6.7: Weibull plots showing the effect of surface treatment of nanosilica on the DC breakdown strength of the resulting nanocomposites, crystallised isothermally at 115 ºC (nanocomposites containing untreated nanosilica are re-shown as grey coloured background)

6.2.3 Discussion

The addition of untreated and C3-treated nanosilica into polyethylene does not alter the AC breakdown strength of the resulting nanocomposites in comparison with unfilled polyethylene. This is in line with the recent experimental findings by other researchers (Iyer et al., 2011; Tanaka et al., 2011). Huang et al. (2010) also reported that the AC breakdown strength of nanosilica-filled LLDPE is only marginally lower than that of the neat LLDPE, indicating that nanosilica does not exert a significant effect on the AC breakdown strength.

The unaltered AC breakdown strength of the nanocomposites in comparison with the unfilled polyethylene can probably be attributed to the unchanged crystallinity of the samples as reported in Chapter 3. Since it is well known that the degree of crystallinity can affect the breakdown strength of polymers (Ieda, 1980; Ku and Liepins, 1987; Kolesov, 1980), similar level of crystallinity observed in all samples means that the AC breakdown strength is expected to be similar. However, the decrease of AC breakdown strength upon inclusion of 10 wt% of untreated nanosilica cannot be linked to crystallinity effects. This leads to a second possibility – the effect of spherulitic morphology, which could affect the breakdown strength irrespective of molecular composition (Hosier et al., 2000; Hosier et al., 1997).

With an increasing amount of untreated nanosilica, the banded spherulitic textures of polyethylene appeared to be largely suppressed, especially at a loading level of 10 wt% of untreated nanosilica (see Figure 4.8). Less organised lamellar arrangements could lead to a lower breakdown strength and this could be the case here. However, when examining the AC breakdown behaviour of samples subjected to direct quenching into water, where the formation of a well-developed lamellar structure is suppressed, the drop in strength for 10 wt% of untreated nanosilica inclusion was still noticeable. Moreover, when examining the morphology of nanocomposites containing 10 wt% of C3-treated nanosilica, severely disrupted spherulitic morphology was observed as well, but such morphology can still lead to a similar AC breakdown strength when compared with unfilled polyethylene. The influence of spherulitic morphology on the AC breakdown strength of the nanocomposites is therefore ruled out in these cases.

The aforementioned crystallinity level and spherulitic morphology could be secondary reasons in explaining the AC breakdown characteristics. The primary reason is, however, probably attributable to the aggregation state of the nanoparticles. From SEM micrographs, many severe aggregates of nanosilica were found in nanocomposites containing 10 wt% of untreated nanosilica. Such aggregates can act as electrical defects that amplify the electric field intensity around the interfaces between the filler and the matrix and subsequently reduce the breakdown strength (Huang et al., 2009). Consequently, it is likely that agglomeration effect dominates any effect of the nanosized particles.

Here, the saturation effect of nanofiller is seen at about 5 wt% of untreated nanosilica loading, where any amount exceeding that limit results in a detrimental effect on the AC breakdown strength of the nanocomposite systems. With nanosilica surface treatment, the sizes of aggregates in the sample containing 10 wt% of C3-treated nanosilica is reduced compared with the nanocomposite containing the untreated nanosilica counterpart. This could be the reason for the improved AC breakdown strength of the former system. This implies that surface treatment did indeed help to improve the AC breakdown strength, albeit that the strength is still no better than that of the unfilled polyethylene.

It is therefore reasonable to conclude that severe agglomeration of nanoparticles can cause the AC breakdown strength to reduce significantly. However, if the nanosilica is well distributed throughout the sample, the AC breakdown strength is comparable with that of the unfilled polyethylene. Although the addition of nanosilica only shows a moderate effect on the AC breakdown strength of the final nanocomposites, it is encouraging. Furthermore, this modest positive effect is in sharp contrast with the use of a microsized filler which, in many cases, reduces the breakdown strength significantly.

Unlike AC breakdown strength, where particle agglomeration seems to be the main factor in reducing the breakdown strength, the reason for the reduced DC breakdown strength of polyethylene on the addition of nanosilica is more difficult to ascertain as it could be influenced by several factors. Nevertheless, the simplest explanation in the case of reduced DC breakdown strength of nanocomposites can also be attributed

to particle agglomeration. However, agglomeration of nanosilica has much more pronounced effect on the DC breakdown strength rather than the AC breakdown strength of nanocomposites – the DC breakdown strength reduces as the amount of aggregates in polyethylene increases, which is evidenced from the SEM micrographs shown in Chapter 4.

Upon surface treatment of nanosilica, the distribution of particle sizes appears displaced somewhat to smaller dimensions, as previously explained, where the clustering effect of nanosilica is less than that of the equivalent loading of untreated nanosilica. As such, the DC breakdown strength of nanocomposites containing C3-treated nanosilica is improved compared with an equivalent loading of untreated nanosilica in polyethylene. This implies that the effect of surface treatment is more pronounced in DC breakdown testing rather than AC breakdown testing but, sadly, such positive effects do not cause higher DC breakdown values when compared with the unfilled polyethylene.

While the degree of crystallinity may not be significant in controlling the DC breakdown behaviour, it is noteworthy that the morphology could also play a significant role in the DC breakdown strength determination. Through the SEM micrographs presented in Chapter 4, it can be clearly seen that the spherulitic morphology became less and less pronounced with increasing amounts of nanosilica. This could explain the reduced DC breakdown strength with increasing amount of nanosilica. However, such morphological changes are not adequate in explaining the improvement in the DC breakdown values upon surface treatment of nanosilica as compared with equivalent loading of untreated nanosilica in polyethylene.

Another possible explanation for the reduced DC breakdown strength is that the incorporation of nanosilica introduces defects that could enhance charge concentration and thus lead to electrical breakdown. In other words, the reduction of DC breakdown strength is possibly related to space charge accumulation in the materials (Khalil et al., 1990; Ma et al., 2005b). Since space charge effects are more pronounced under DC rather than AC conditions, it can be expected that DC breakdown strength can be significantly affected by the inclusion of nanosilica. The poor dispersion of nanosilica and incompatible interfaces between nanosilica and

polyethylene can introduce more defects and free volume into the nanocomposites, resulting in a higher degree of space charge development and, consequently, a lower DC breakdown strength. The effect of space charge will be further discussed in Chapter 7.

The mechanistic origins of changes in the breakdown performance of nanodielectrics have been actively investigated, in an attempt to obtain a complete picture of breakdown processes in these systems. According to Bamji et al. (2005), in a polypropylene/clay nanocomposite system, the DC breakdown strength was found to be higher than that of the unfilled system. Such effects could be due to the trapped charges at the interfaces thus reducing the probability of breakdown. However, in the comparison between 2 wt% and 4 wt% nanofilled system, slightly lowered breakdown strength was found in the 4 wt% nanofilled system. Such an observation was related to the reduction of spherulite size and density caused by nucleation and poorer dispersion of nanoparticles.

While the above explanation does provide some insights into the possible factors that can influence the DC breakdown behaviour of the investigated nanocomposites, it should be emphasised that the exact mechanisms that govern DC breakdown behaviour are complex. Nevertheless, the use of nanofiller in polymer does seem promising, since, although the incorporation of nanosilica into polyethylene reduces the DC breakdown strength, the improvement of DC breakdown strength brought about by nanosilica surface treatment underlines the potential of appropriately engineering such dielectric materials. The possible improvement of DC breakdown strength will be revisited in Chapter 9.

6.3 Summary

The addition of nanosilica into polyethylene does not have a notable effect on AC breakdown testing. This applies to both the untreated and C3-treated nanofillers, where the AC breakdown strength is commensurate with that of the unfilled polyethylene. However, severe clustering effects can cause the AC breakdown strength to be reduced significantly, as seen in samples containing 10 wt% of

untreated nanosilica. Although the addition of nanosilica only exerts a modest effect on the AC breakdown strength of the final nanocomposites, the results are encouraging. Furthermore, this modest positive effect is in sharp contrast with the use of microsized fillers which, in many cases, reduces the breakdown strength significantly.

In DC breakdown testing, increasing the amount of untreated nanosilica further reduces the DC breakdown strength of the polyethylene. Surface treatment of nanosilica increases the DC breakdown strength relative to samples containing an equivalent amount of untreated nanosilica. There could be several explanations for the observed DC breakdown behaviour – the particle size distribution, the morphology and the existence of electrical defects that promote space charge development. Nevertheless, the exact mechanisms that govern the DC breakdown behaviour are complex. Although the incorporation of nanosilica into polyethylene reduces the DC breakdown strength, the use of surface treated nanosilica underlines the potential of appropriately engineering such dielectric materials with improved DC breakdown strength.

Chapter 7

Space Charge Dynamics

"Attempt the end and never stand to doubt. Nothing's so hard, but search will find it out."

- Robert Herrick -

7.1 Introduction

Space charge formation occurs when the rate of charge accumulation is different from the rate of charge removal, which arises due to moving charges or trapped charges upon the application of an electric field. This could be caused by electrons or ions depending upon the mechanism of charge transfer. The presence of space charge modifies the electric field, enhancing the local internal field within the dielectric material as a function of time, which introduces non-linearities that influence the dielectric behaviour and lead to faster degradation and premature failure of the material. The mechanism of space charge formation is therefore considered as one of the most influencing factors in determining the overall dielectric properties of a polymeric insulation system (Ieda, 1977; Mizutani, 1994).

Generally, there are three main processes that cause the formation of space charge, as described by Lewiner (1986) in Figure 7.1. In the first case, the dipoles are oriented in a homogenous material and the associated space charge occurs as two peaks near the electrodes. In the second case, the electric field causes migration of ions, where the negative charges migrate to the positive electrodes while the positive charges migrate to the negative electrodes. Since the mobility of the charge is not equal, a global negative space charge develops near the positive electrode while a global positive space charge develops near the negative electrode. This form of space charge is termed heteropolar charges (heterocharges). In the third case, charge injected at the electrodes generates a space charge when the mobility of charges is low, resulting in the accumulation of charges near each electrodes that is of the same polarity. Such space charge is termed homopolar charges (homocharges).

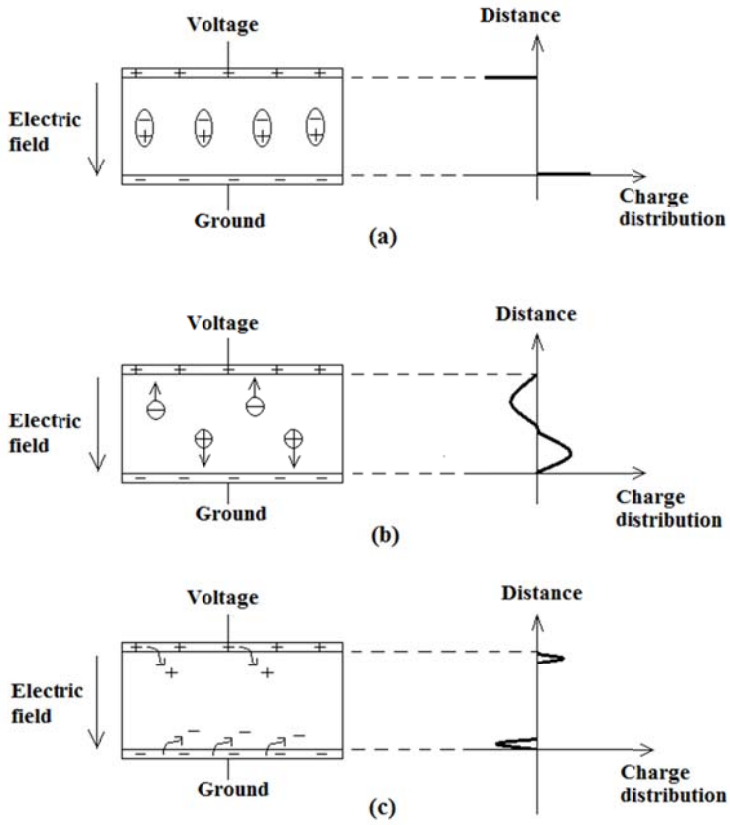

Figure 7.1: Development of charge distribution in a dielectric material subjected to an electric field (a) dipole orientation, (b) ion migration, (c) charge injection at the interfaces (Lewiner, 1986)

Many techniques have been developed to measure the space charge distribution in a dielectric material. One of the most commonly used techniques is the pulsed electro-acoustic technique, first developed by Takada and Sakai (1983) and subsequently refined by many researchers. The pulsed electro-acoustic technique is based on the principle that, when an electrical pulse is applied to a dielectric containing stored charges, acoustic pulses are generated by displacement of each locally charged region. The basic principle of the pulsed electro-acoustic technique is shown schematically in Figure 7.2 (Xu, 2009).

When a voltage pulse is applied to a sample, charges stored in the sample move under the influence of the Coulomb force. The stored charge causes the generation of an acoustic pulse, for example, from the high voltage electrode (Electrode A) through the ground electrode (Electrode B) to the piezoelectric transducer. The transducer detects the acoustic signal and transforms it into an electrical signal. The amplitude obtained is determined by the wave profile as a function of time and is proportional to the local charge density. The signal is amplified and fed to an

oscilloscope for further analysis. It should be noted that an acoustic absorber is required to absorb the acoustic wave in order to prevent the reflection of acoustic waves, which would cause interference and distortion to the signal.

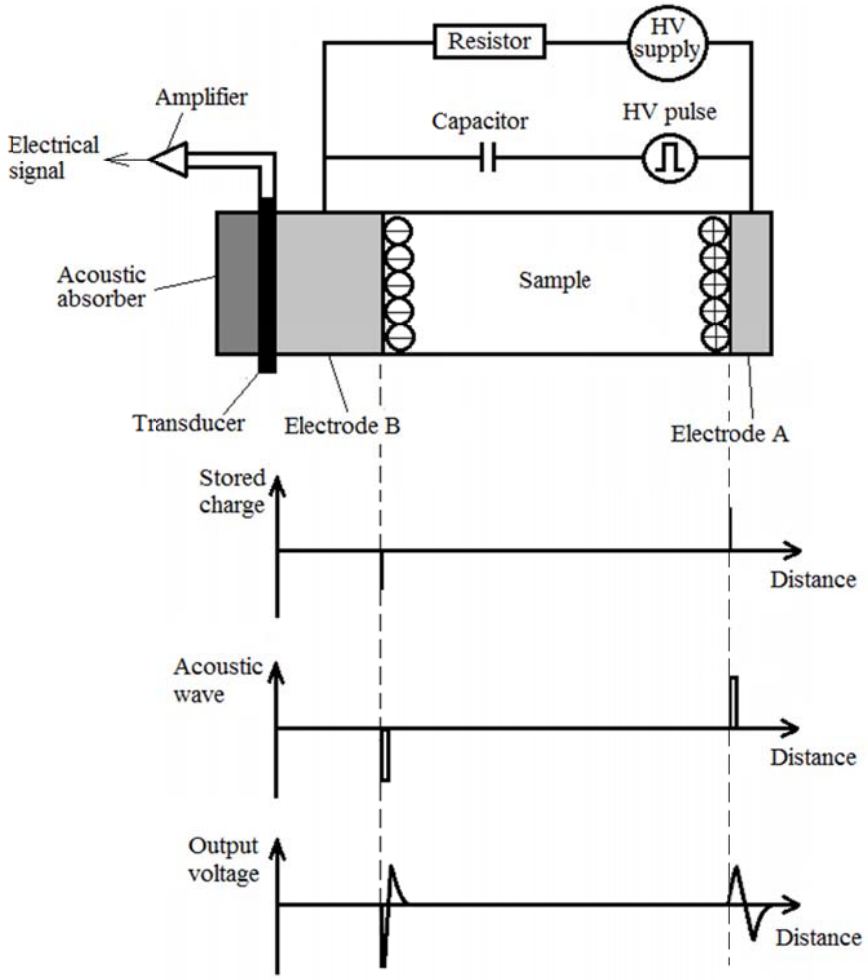

Figure 7.2: Basic principle of pulsed electro-acoustic technique (Xu, 2009)

Bulk charge accumulation has been a problematic issue in conventional microcomposite systems, where it leads to a significant reduction in dielectric breakdown strength, especially in connection with direct current (DC) applications. Conversely, mitigated space charge accumulation was found upon the incorporation of nanometre-sized fillers in early experimental work on nanocomposites in connection with their dielectric properties (Nelson et al., 2002). Rapid charge decay was also found in nanocomposites when compared with microcomposites. Such observations have led to the idea that carefully designed nanocomposites could exhibit improved dielectric breakdown performance, thus enabling the utilisation of

higher voltages especially in high voltage direct current (HVDC) transmission applications.

Bearing such a concept in mind, research into the DC space charge behaviour of nanocomposites has been emphasised. In 2003, Yin et al. (2003) performed an investigation into the effect of space charge on LDPE/TiO_2 nanocomposites prepared by a solution blending approach. Using the pulsed electro-acoustic method, mitigated space charge accumulation and faster space charge decay rates were found with increasing amounts of nano-titania. Unfortunately, no detailed explanation was given of the space charge behaviour due to nano-inclusions.

Space charge effects are a direct outcome of trapping, de-trapping and transport of charges in insulating polymers and, consequently, space charge varies with trap density, trap depth distribution and charge carrier mobility. In the case of filled polymers, particulate fillers often directly contribute to changes in the space charge distribution by actively responding to the electric field and interacting with the polymer molecules. For example, Ma et al. (2005b) reported that heterocharge developed near the electrodes in unfilled LDPE samples while homocharge developed near the electrodes in nanofilled samples. Upon surface treatment of the nanoparticles, heterocharge was observed near the electrodes, but in much smaller quantities than in the unfilled LDPE samples and had no prominent change with time.

Studies of space charge have indicated that nanocomposites usually exhibit lowered and redistributed space charge when compared with microfilled composites (Smith et al., 2008). The magnitude of the internal charge is much less for nanocomposites and the dynamics of charge decay are much faster for nanocomposites (Tanaka, 2005). Montanari et al. (2006) investigated nanosilicate-filled polypropylene and ethylene-vinylacetate nanocomposites and found a new relaxation process, which they thought to be related to charge trapping at interfaces between the nanofillers and the polymer. Besides that, Tanaka et al. (2004) observed that the space charge inception threshold shifted to lower values for both polypropylene and ethylene-vinylacetate nanocomposites. A shorter decay constant was also recorded, which means that the charge was dissipated more quickly in nanocomposites.

Nelson (2007) deduced that lower and redistributed space charge is due to the presence of homopolar charge adjacent to the electrode, which is contrary to the heteropolar charge seen in microcomposites. The existence of homopolar charge was also reported by Montanari et al. (2006) and Tanaka et al. (2011). In view of these modified space charge characteristics, nanocomposites are considered to be attractive materials for use in high voltage direct current (HVDC) applications (Aoyama et al., 2006; Gochowaki et al., 2008).

While suppressed space charge development in nanocomposites can be explained through the introduction of a shallow trap band (Nelson et al., 2002; Tanaka et al., 2004) at interfaces and the resulting increase in charge carrier mobility, the presence of deep traps has also been suggested in certain nanocomposites (Tanaka et al., 2004). With the presence of deep traps, space charge accumulation could be worsened. According to Chen et al. (2007), a thorough understanding of the interaction between nanoparticles and their matrix could be achieved by studying the space charge dynamics of polymer nanocomposites. It is expected that space charge behaviour is affected by the nature of the filler and the matrix and the properties of the interface, which are related to the dispersion of the fillers, and filler/filler and filler/matrix interactions. Therefore, space charge measurement should be very informative in understanding of polymer nanocomposites, as it is sensitive to charges formed at interfaces.

From the dielectric spectroscopy data presented in Chapter 5, the nanocomposites exhibit higher values in the low frequency range. One reason for this could be Maxwell-Wagner-Sillars interfacial polarisation caused by space charge accumulation at the interfaces between the polymer and the filler. This has outlined the importance of examining the space charge behaviour of the nanocomposites, albeit such investigation will only show net charge distribution. Moreover, the variation in DC breakdown strength with comparison of the nanocomposites is markedly different to the variation in AC breakdown strength, as shown in Chapter 6. Examination of the space charge behaviour could help understand such behaviour, especially since the development of space charge is considered to be more detrimental in DC rather than in AC.

7.2 Results and Discussion

7.2.1 Measurements for Unfilled Polyethylene

For reference purpose, Figure 7.3 shows the space charge behaviour of an unfilled polyethylene sample stressed at a DC field of 25 kV mm^{-1}. Although a very small amount of homocharge development is evident near the cathode, such space charge development is minimal. Indeed, the charge decay process shows that very small quantities of homocharge actually developed near both electrodes. The homocharge near the anode could not be clearly observed during charging due to the presence of the associated large peak at the anode caused by the applied field.

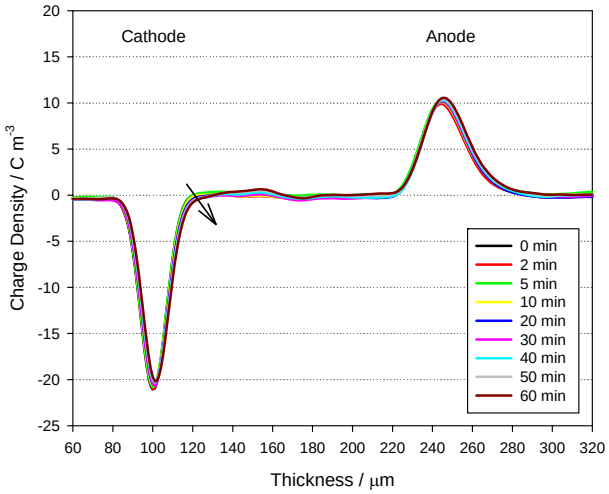

Figure 7.3: Space charge behaviour of unfilled polyethylene crystallised isothermally at 115 ºC stressed at 25 kV mm^{-1} (arrow indicates increasing time)

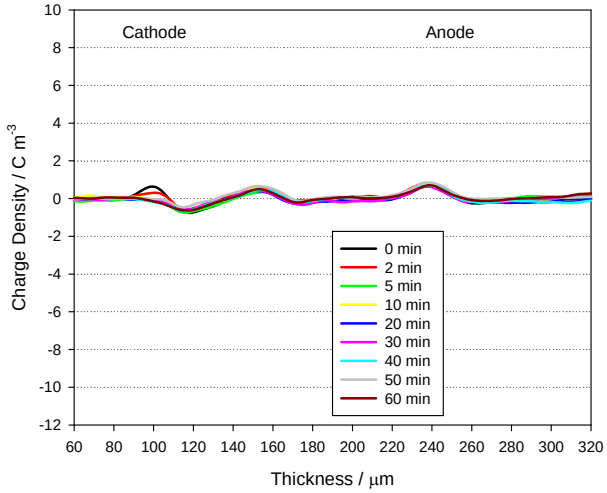

Figure 7.4: Charge decay of unfilled polyethylene crystallised isothermally at 115 ºC upon removal of 25 kV mm^{-1} applied field

To confirm the space charge behaviour of the unfilled polyethylene sample, a higher DC field was employed. Figure 7.5 shows the space charge distribution of an unfilled polyethylene sample stressed at a 40 kV mm^{-1} DC field. Homocharge development was found near the cathode, similar to the observations previously made upon voltage stressing at 25 kV mm^{-1}. In addition, an increase in homocharge can now be clearly seen near the anode. The charge decay process shown in Figure 7.6 is in line with the previous observation for the case of 25 kV mm^{-1} voltage stressing (see Figure 7.4), but with higher charge density throughout the measured period. It is noteworthy that the oscillation in the space charge signal is an artefact associated with the calibration process, and is particularly noticeable during the charge decay process.

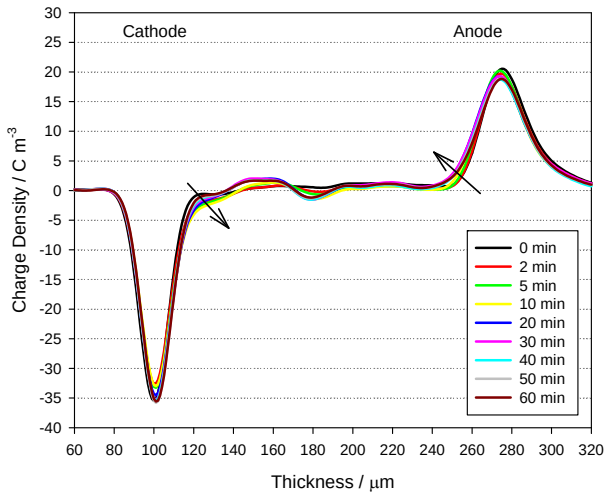

Figure 7.5: Space charge behaviour of unfilled polyethylene crystallised isothermally at 115 ºC stressed at 40 kV mm^{-1} (arrow indicates increasing time)

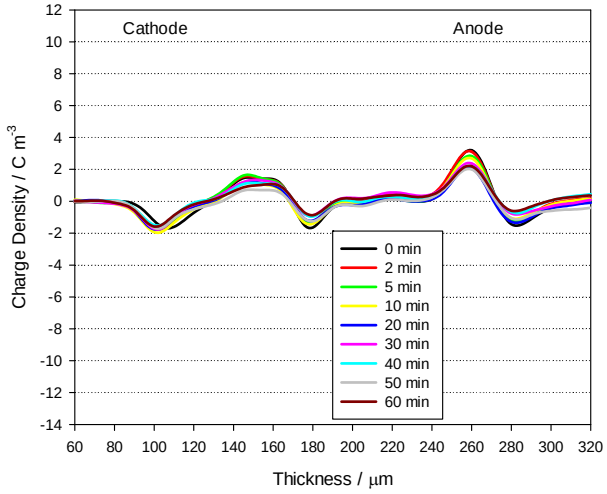

Figure 7.6: Charge decay of unfilled polyethylene crystallised isothermally at 115 ºC upon removal of 40 kV mm^{-1} applied field

7.2.2 Measurements for Nanocomposites Containing Untreated Nanosilica

Figure 7.7 shows the development of space charge in a nanocomposite sample containing 2 wt%, 5 wt% and 10 wt% of untreated nanosilica stressed at a 25 kV mm^{-1} DC field. First, consider Figure 7.7a, where the development of homocharge can be clearly seen near both electrodes with as little as 2 wt% of untreated nanosilica. Increasing the nanofiller loading level to 5 wt% and 10 wt% results in the accumulation of increased quantities of homocharge near both electrodes (see Figures 7.7b and 7.7c). Evidently, the space charge behaviour becomes very different from that of the unfilled polyethylene at higher loadings of untreated nanosilica. Nevertheless, the space charge dynamics in all these nanocomposites reveal a similar pattern as a function of time; the homocharge near the cathode and anode increases in magnitude with time and moves towards the sample bulk.

For nanocomposite samples containing untreated nanosilica, development of space charge near both electrodes became more pronounced when subjected to a higher field of 40 kV mm^{-1} (see Figure 7.8) in comparison with an equivalent sample subjected to 25 kV mm^{-1}. For example, at a loading level of 5 wt% of untreated nanosilica, homocharge development near the cathode reached about -13 C m^{-3} at an applied field of 40 kV mm^{-1} (see Figure 7.8b) after 60 min, in contrast to the -7 C m^{-3} seen at 25 kV mm^{-1} (see Figure 7.7b) after the same time. Adjacent to the anode, the charge density was also higher for the case of the 40 kV mm^{-1} applied field. Nevertheless, the development of space charge at both voltage levels reveals a similar trend in terms of the role of the nanofiller, albeit that transport of charge towards the bulk appears to be suppressed as the nanofiller loading level increases.

Figure 7.9 compares the short-circuited space charge behaviour of the nanocomposites containing untreated nanosilica upon the removal of the 25 kV mm^{-1} and 40 kV mm^{-1} applied fields. The homocharge decays progressively once the applied field has been removed, and this effect is particularly noticeable at the higher field. As previously mentioned, the oscillation shown in the figures is an artefact from space charge measurements and this effect is not reproducible.

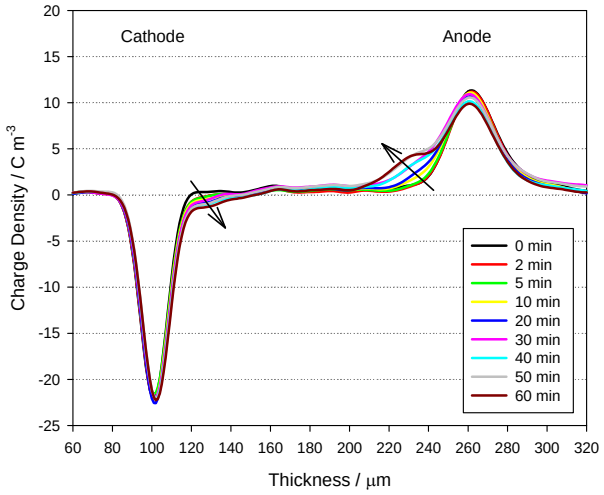

(a)

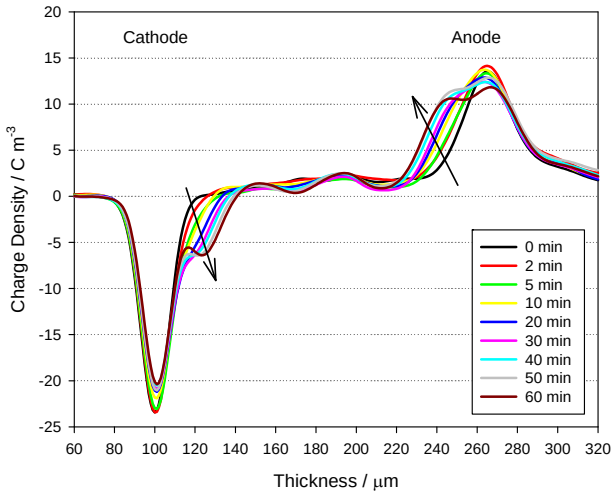

(b)

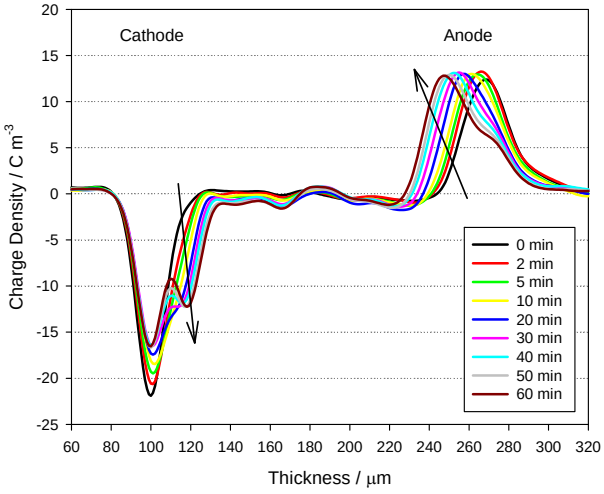

(c)

Figure 7.7: Space charge behaviour of nanocomposites crystallised isothermally at 115 ºC containing (a) 2 wt%, (b) 5 wt%, (c) 10 wt% of untreated nanosilica stressed at 25 kV mm^{-1} (arrow indicates increasing time)

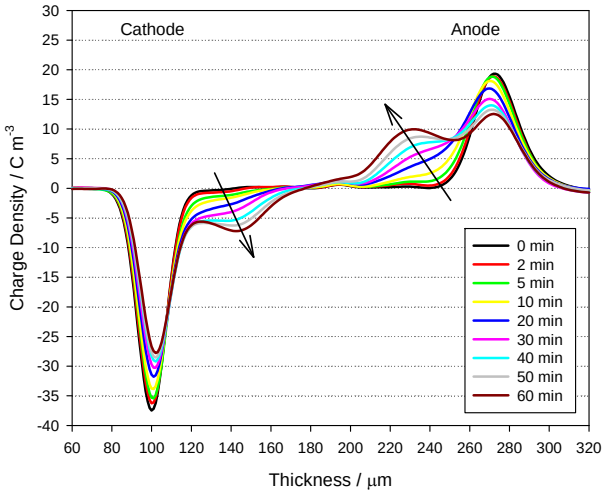

(a)

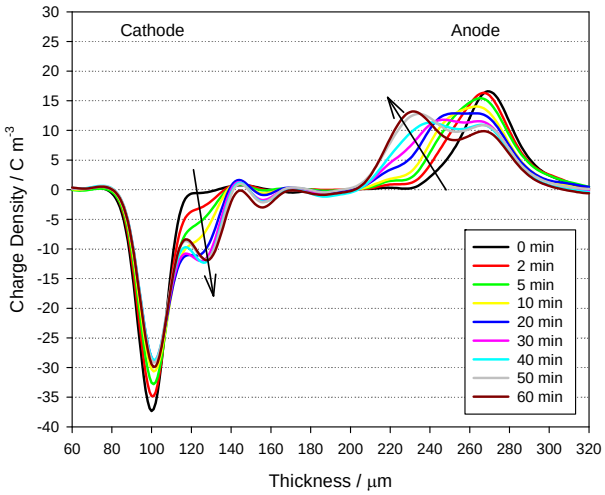

(b)

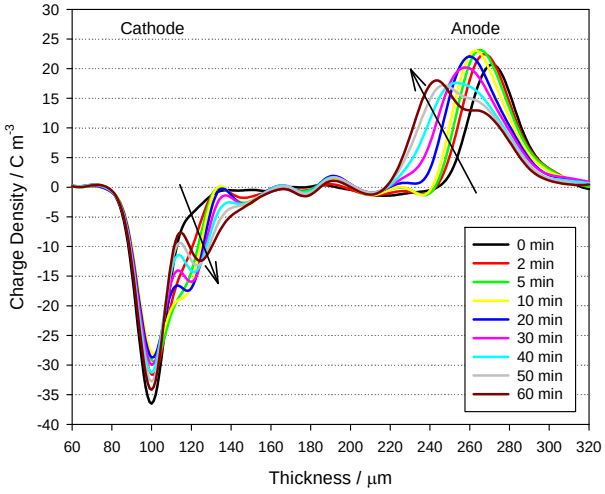

(c)

Figure 7.8: Space charge behaviour of nanocomposites crystallised isothermally at 115 ºC containing (a) 2 wt%, (b) 5 wt%, (c) 10 wt% of untreated nanosilica stressed at 40 kV mm^{-1} (arrow indicates increasing time)

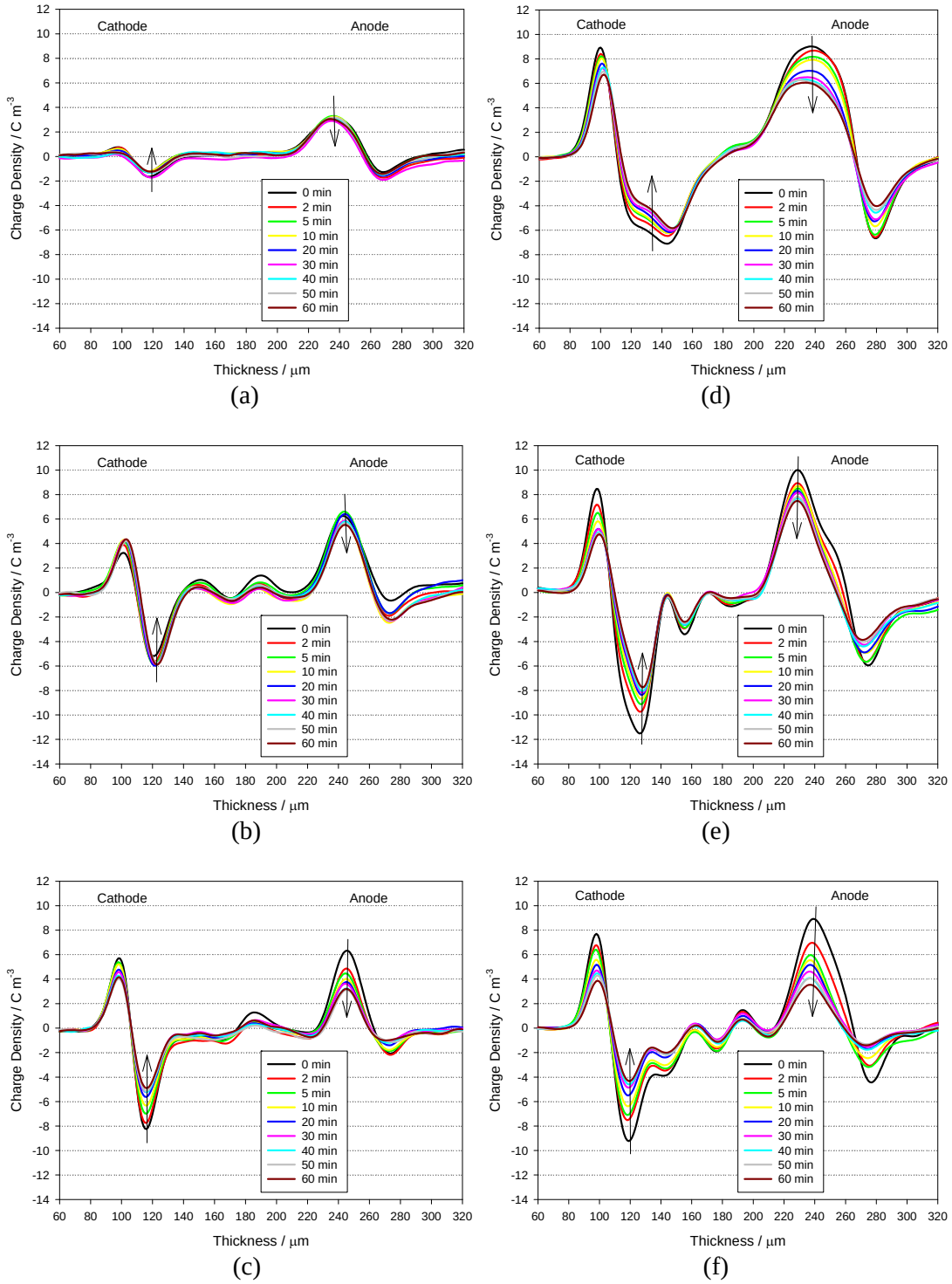

Figure 7.9: Charge decay of nanocomposites crystallised isothermally at 115 ºC containing (a) 2 wt%, (b) 5 wt%, (c) 10 wt% of untreated nanosilica upon the removal of 25 kV mm^{-1} electric field and (d) 2 wt%, (e) 5 wt%, (f) 10 wt% of untreated nanosilica upon the removal of 40 kV mm^{-1} electric field (arrow indicates increasing time)

7.2.3 Measurements for Nanocomposites Containing C3-treated Nanosilica

Figure 7.10 shows space charge development in nanocomposite samples containing C3-treated nanosilica at an applied DC field of 25 kV mm^{-1}. From this, it is evident that upon surface treatment of the nanosilica, the magnitude of the space charge is dramatically reduced and becomes similar to that exhibited by the unfilled polyethylene; homocharge development near both electrodes is very small and can be neglected for the case of nanocomposites containing 2 wt% of C3-treated nanosilica. Increasing the amount of C3-treated nanosilica again results in the density of space charge at both electrodes increasing, but the effect is much less pronounced than in the untreated case.

For the case of C3-treated nanosilica, the development of space charge at an applied field of 40 kV mm^{-1} differs greatly from that found at 25 kV mm^{-1}. Homocharge development can be clearly seen in all nanocomposite samples containing 2 wt%, 5 wt% and 10 wt% of C3-treated nanosilica (see Figure 7.11). While it is difficult to compare the effect of varying the amount of C3-treated nanosilica on the space charge at 25 kV mm^{-1} (see Figure 7.10), clear distinction of the amount of homocharge development near both electrodes can be made under the applied field of 40 kV mm^{-1}. The amount of charge increased with increasing nanosilica loading. That is, the charge injection appears to be enhanced at higher DC fields although, as in Figure 7.8, the extent to which charge moves into the bulk appears to decrease as the filler loading level increases. Nevertheless, the accumulation of space charge at 40 kV mm^{-1} is, again, less than that in the nanocomposites containing an equivalent amount of the untreated nanofiller.

Figure 7.12 compares the short-circuited space charge behaviour of the nanocomposite samples containing C3-treated nanosilica upon the removal of the 25 kV mm^{-1} and 40 kV mm^{-1} applied fields. Again, the space charge decays progressively and this effect is particularly noticeable at the higher field. Nevertheless, the amount of space charge accumulated at the beginning of the charge decay process in the C3-treated systems is less than that of the untreated systems (see Figure 7.10) at an equivalent nanosilica loading level.

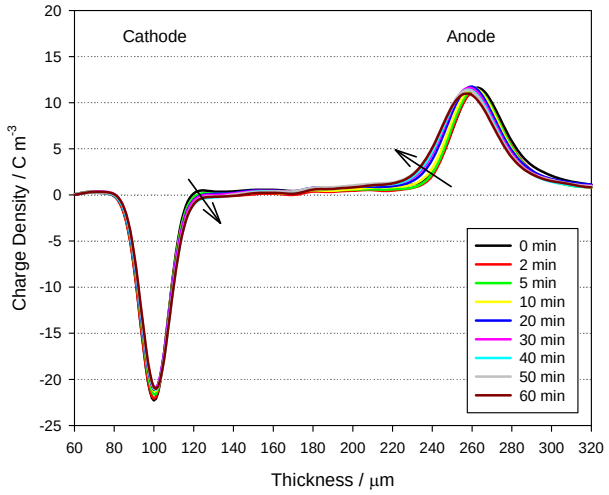

(a)

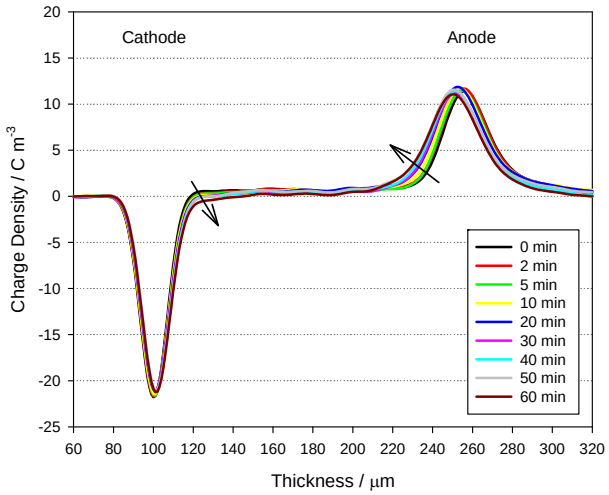

(b)

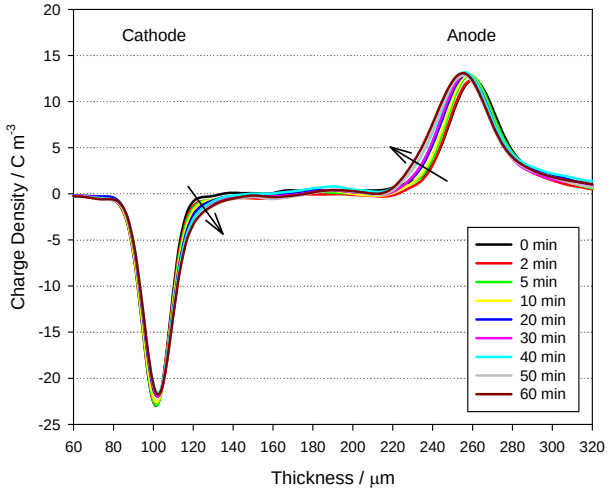

(c)

Figure 7.10: Space charge behaviour of nanocomposites crystallised isothermally at 115 ºC containing (a) 2 wt%, (b) 5 wt%, (c) 10 wt% of C3-treated nanosilica stressed at 25 kV mm^{-1} (arrow indicates increasing time)

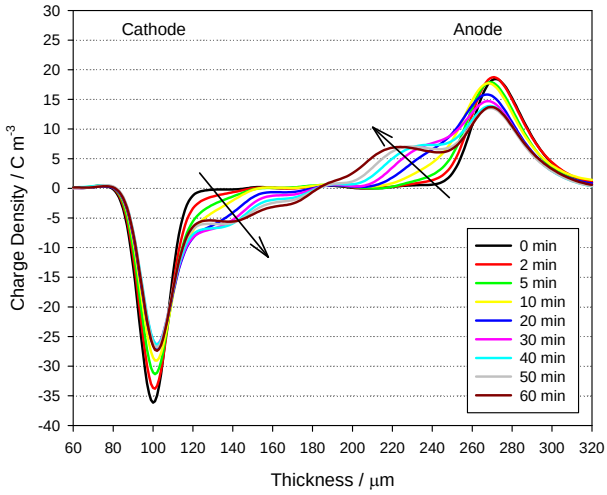

(a)

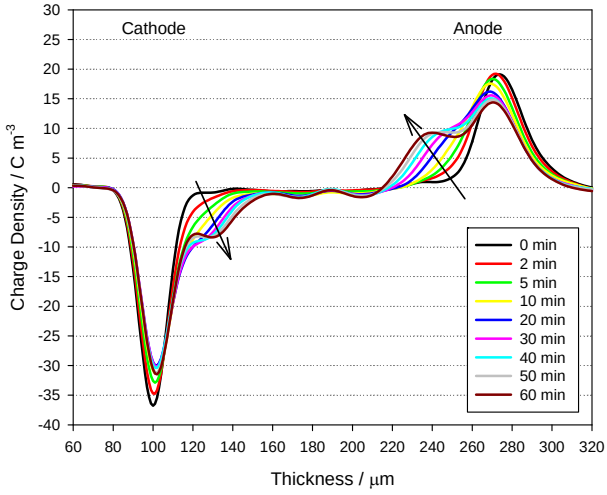

(b)

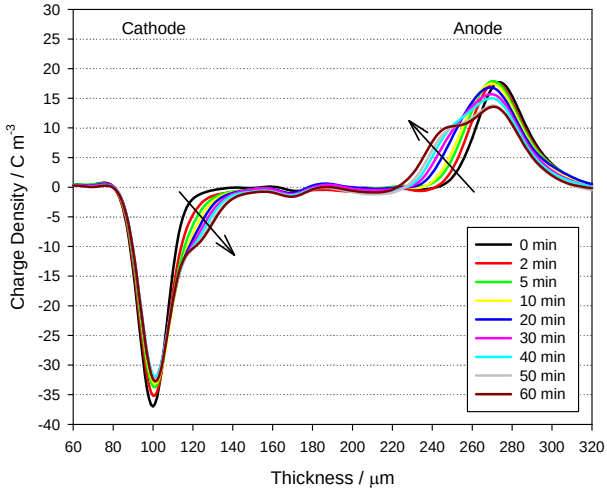

(c)

Figure 7.11: Space charge behaviour of nanocomposites crystallised isothermally at 115 ºC containing (a) 2 wt%, (b) 5 wt%, (c) 10 wt% of C3-treated nanosilica stressed at 40 kV mm^{-1} (arrow indicates increasing time)

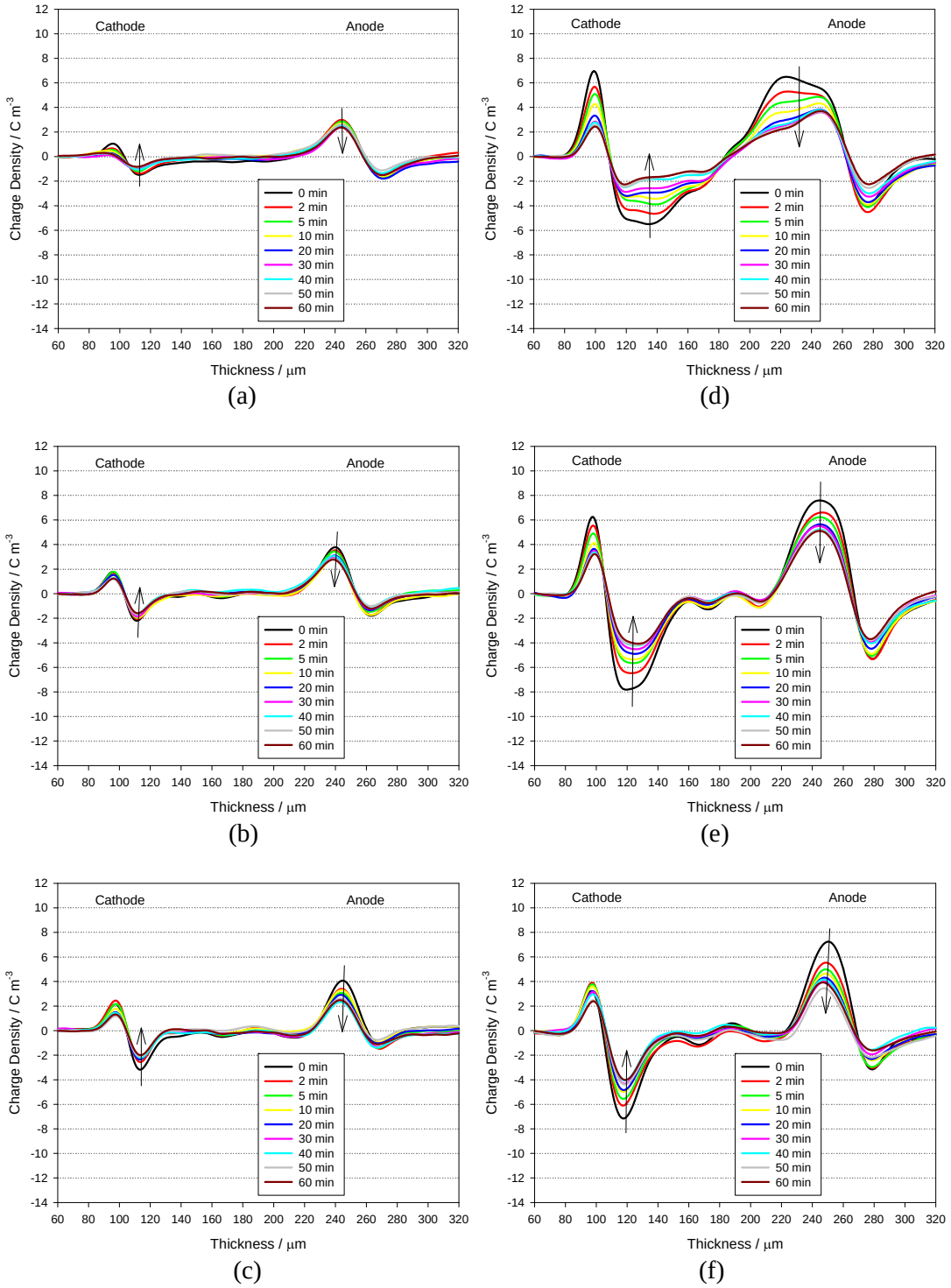

Figure 7.12: Charge decay of nanocomposites crystallised isothermally at 115 ºC containing (a) 2 wt%, (b) 5 wt%, (c) 10 wt% of C3-treated nanosilica upon the removal of 25 kV mm^{-1} electric field and (d) 2 wt%, (e) 5 wt%, (f) 10 wt% of C3-treated nanosilica upon the removal of 40 kV mm^{-1} electric field (arrow indicates increasing time)

7.2.4 Morphological Effects

The results presented above and in the previous chapters indicate that the addition of nanosilica has a distinct effect on the morphology, breakdown and space charge behaviour of the various systems. Since charge transport can be affected by both the morphology of the polymer (Ieda, 1984) and the added nanofiller (Montanari et al., 2006; Nelson et al., 2002; Smith et al., 2008; Tanaka., 2005), the effect of the former was examined by producing additional samples that were compositionally identical to those described above but which differed in terms of their morphology. Figure 7.13 shows representative space charge behaviour of samples produced by quenching directly into water, where the formation of a well-developed lamellar structure is suppressed and the morphology is similar in both unfilled and nanofilled samples. Again, the inclusion of untreated nanosilica results in increased homocharge development near both electrodes (see Figure 7.13b) and the use of C3-treated nanosilica reduces such effects (see Figure 7.13c). That is, the effects described above are directly attributable to the presence of the nanosilica and are not greatly influenced by morphological changes.

7.2.5 Discussion

The quantity of homocharge developed near both electrodes in unfilled polyethylene at 25 kV mm^{-1} and 40 kV mm^{-1} DC field is considered insignificant. In contrast, all systems containing nanosilica exhibited significant homocharge development near both electrodes; the quantity of homocharge increased with nanosilica loading level and tended to move towards the interior of each specimen, particularly at lower nanofiller loading levels. Evidently, the inclusion of the nanofiller and the resulting changes to the matrix material lead to the accumulation of increased amounts of space charge (Zha et al., 2010).

In the unfilled polyethylene, the development of homocharge may be associated with the semicrystalline nature of the material and/or impurity moieties, but comparison of the space charge characteristics of materials where the matrix is morphologically very different (quenched or isothermally crystallised at 115 ºC) implies that space

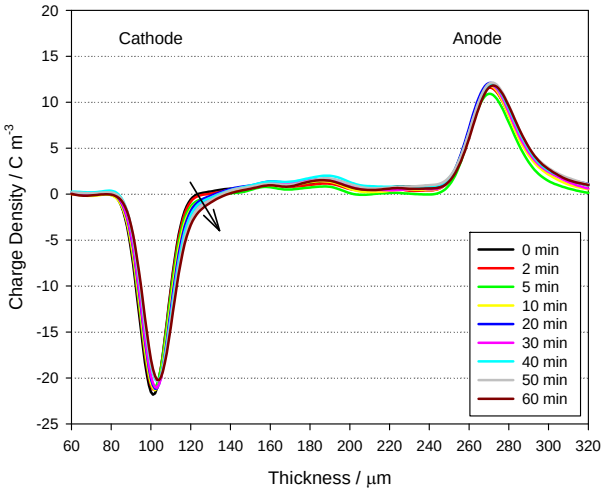

(a)

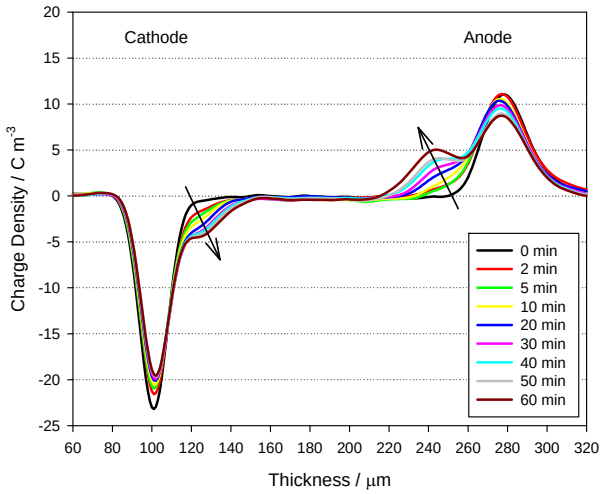

(b)

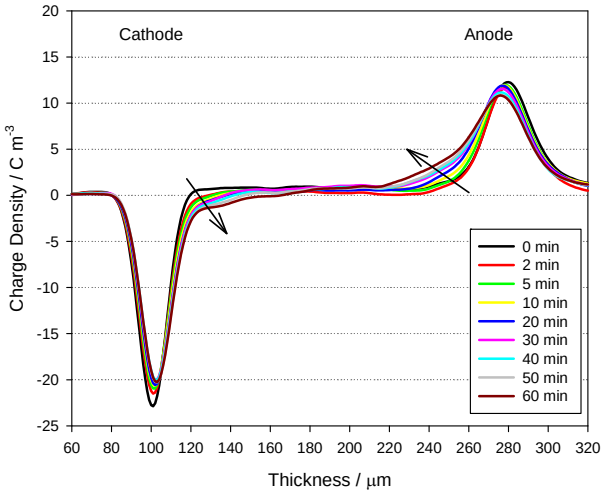

(c)

Figure 7.13: Space charge behaviour of quenched samples of (a) unfilled polyethylene and nanocomposites containing 5 wt% of (b) untreated nanosilica, (c) C3-treated nanosilica stressed at 25 kV mm^{-1} (arrow indicates increasing time)

charge is not greatly affected by even major changes in the lamellar texture of the polymer. Thus, although the inclusion of the nanofiller does clearly affect the morphology of the polyethylene, it is believed that such changes do not have a significant effect on the variations in space charge behaviour observed in the range of nanocomposites considered here. Rather, the fact that changes in both nanofiller loading level and nanofiller surface chemistry so markedly affect the observed space charge profiles clearly indicates that these effects are a direct consequence of the presence of the nanofiller particles themselves. The influence of the matrix microstructure on space charge development is considered to be a secondary effect; this conclusion is consistent with data presented elsewhere (Tanaka et al., 2003).

From the above discussion, it is reasonable to deduce that the introduction of nanosilica into the polyethylene blend results in the creation of a new trap band, in addition to the original trap band relevant to the base polymer, and that the latter is not able to support significant quantities of space charge. The introduction of additional traps is not atypical and has been anticipated elsewhere (Tanaka, 2005). The new trap band is therefore considered to be related to the presence of the nanofiller/polymer interfaces and its nature is determined by moieties carried on the nanoparticle surfaces. The space charge results from the nanocomposites containing C3-treated nanosilica show that homocharge development has been reduced compared with nanocomposites containing an equivalent amount of untreated nanosilica. In this study, no attempt was sought to manipulate such effects to achieve any specific material characteristics, but it is evident that by “tagging” the nanoparticles with different chemical species, a range of different electrical effects could be produced.

In the systems considered here, it is suggested that the enhanced migration of space charge towards the bulk seen in the various nanocomposites may be due to the presence of additional localised states that are shallower in energy than the trap band intrinsic to the polyethylene matrix. Then, the increase in space charge density may be indicative of a sequential process in which the charges initially fill the shallow traps, before entering deeper traps, as discussed elsewhere (Chen and Xu, 2009). As the amount of nanosilica increases, more nanofiller/polymer interfacial regions exist, so introducing more trapping sites that consequently lead to increased homocharge

development near both electrodes. The tendency for charges to be confined to the vicinity of the electrodes at higher nanofiller loading levels, which is evident at an applied field of 40 kV mm^{-1} in the systems based upon both the untreated and C3-treated nanosilica, suggests that these new electron states serve both to promote charge migration into the bulk and local trapping near the electrode. The balance between these two processes may be a direct result of the nanofiller loading level or, more likely, the fact that increasing the nanofiller loading level results in increased trap densities.

The differences seen in nanocomposite samples containing C3-treated nanosilica at different voltage levels indicate that surface treatment of nanosilica could have successfully increased the space charge threshold level of the C3-treated systems. At the lower field of 25 kV mm^{-1}, nanocomposites containing the C3-treated nanosilica did not experience significant charge injection from the electrodes, which is in sharp contrast to the nanocomposites containing the untreated nanosilica, where homocharge development could be seen at both electrodes on the inclusion of as little as 2 wt% of untreated nanosilica. At the higher field of 40 kV mm^{-1}, more charge injection occurred in the nanocomposites containing the C3-treated nanosilica, thus overcoming the space charge threshold level, resulting in notable homocharge development near both electrodes even for sample containing just 2 wt% of C3-treated nanosilica. However, the amount of homocharge that developed was still less than in the sample containing an equivalent amount of untreated nanosilica.

In Chapter 6, the DC breakdown strength of nanocomposites containing both the untreated and C3-treated nanosilica fell monotonically with increasing nanofiller loading level. The drop in strength was more pronounced for the former set of systems, where the space charge studies revealed increased space charge accumulation. Two explanations can be proposed for this. First, the space charge will inevitably perturb the local field distribution within the dielectric and lead to local enhancement. Under such conditions, the applied field calculated from the voltage at breakdown and the sample thickness will clearly not provide a measure of the local field at which breakdown was initiated. The effect of space charge on breakdown strength has been discussed elsewhere (Chen et al., 2012). Alternatively, the introduction of nanoparticles may affect the DC breakdown strength through

increased charge mobility which, at high fields, would result in damaging current flows at lower voltages. Evidently, nanoparticles and their surface chemistry are both critical in connection with the use of nanocomposites in DC applications and, while adding nanoparticles may well enhance charge mobility, where this is accompanied by increased charge trapping the result can be markedly different space charge characteristics and significantly inferior breakdown performance.

Moreover, the migration of space charge observed in the investigated nanocomposite systems indicates that, if the polarity of the applied field is reversed, the accumulated charge would be able to dissipate, thus resulting in insignificant overall space charge accumulation. This may additionally explain the similar AC breakdown strength values seen in both sets of materials in comparison with the unfilled polyethylene, as reported in Chapter 6.

7.3 Summary

From the space charge measurements presented above, it is apparent that significant quantities of homocharge develop near both electrodes in all nanocomposite systems, and that this effect is more pronounced with increasing nanofiller loading level. It is noteworthy that these homocharges are not apparent in the unfilled polyethylene system and, at lower DC field, they are less apparent for samples containing C3-treated nanosilica. At higher DC fields, charge injection appears to be greatly enhanced, but charge accumulation in samples containing C3-treated nanosilica is less than that in samples containing an equivalent amount of untreated nanosilica. These space charge effects correspond to the DC breakdown results; the drop in strength is less pronounced for samples containing C3-treated nanosilica in comparison with samples containing an equivalent amount of untreated nanosilica. The following inference is therefore made: the inclusion of the nanofiller results in the introduction of localised surface states and that these are related to the observed homocharge accumulation. The nature and number of these surface states will be dependent upon the nanosilica interface chemistry and, consequently, are modified by chemical functionalisation. As a result of the existence of these localised states,

charge transport dynamics through the nanofilled systems become modified, as will be shown in Chapter 8.

Chapter 8

Absorption Current Measurements

"Research cannot be forced very much. There is always danger of too much foliage and too little fruit."

- Theobald Smith -

8.1 Introduction

When an electric field is applied to a non-ideal dielectric material between two plane parallel electrodes, the applied field interacts with charges, causing their motion that manifests itself as a current flow in the external circuit (Adamec and Calderwood, 1978). The current flow can mainly be categorised into three types, as follows: the initial current that flows through the material is the capacitive charging current which causes a dramatic rise at the very beginning of the voltage application. This is followed by a gradual decrease of current, known as the absorption current or the anomalous current. Conventionally, the absorption current decreases slowly until it reaches a quasi-steady state, providing a conduction current that is often used to compare the conductivity of different dielectric materials. Upon discharging (voltage removed and the electrodes short-circuited), the behaviour of the change in current with time will be identical to the charging cycle and their numerical analysis will also be similar, provided the principle of superposition holds (Das Gupta and Brockley, 1978).

The slowly decaying current, i.e., the absorption current, is considered to be an important characteristic of polymers with regard to their time-domain response to a DC poling field. This is because the results of absorption current measurements can be related to space charge measurements to gain a better understanding of the relationship between space charge accumulation and movement, as well as the resulting effects in the external circuit (Smith, 2009). In general, factors affecting the absorption current include electrode polarisation, dipole orientation, charge accumulation and trapping, tunnelling of charge carriers from the electrodes to empty

traps and hopping of charge carriers through localised states (Das Gupta and Joyner, 1976).

The current-time characteristic of the absorption current is often found to follow the power law relationship:

$$I = At^{-b_n} \tag{8.1}$$

where I is the current, t is the time after the application or removal of the external voltage, A is a temperature dependent factor and b_n is a constant representing the slope of the log-log current-time plot. It should be noted that simple interpretation of the exponent b_n is complicated by the fact that polymers exhibit a distribution of relaxation times and that these times may not be easily determined in polyethylene at normal temperatures (Das Gupta and Joyner, 1976).

According to the work of Many and Rakavi (1962), who studied the effect of space charge limited current in solids in the presence of trapping, the charge carrier mobility can be estimated using the following formula:

$$\mu = \frac{0.787d^2}{t_p V} \tag{8.2}$$

where μ is the mobility of charge carriers, d is the sample thickness, t_p is the time at which a slope change occurs (i.e., when a charge front arrives at the electrode) and V is the applied voltage. In generating the above equation, several assumptions have been made, for example, the effect of diffusion current is omitted and the investigated sample contains only a single trap depth. Although the assumptions may not apply to all materials, the equation has been commonly used to estimate the charge carrier mobility (Roy, 2005; Smith et al., 2008) and is therefore used in this work.

The determination of the charge transport mechanism in polymeric insulation is, however, complicated in comparison with many conducting and semiconducting materials. In semicrystalline polyethylene, for example, the crystalline regions are

surrounded by the amorphous regions, and there is likely to be a high concentration of traps relevant to these structural features. With the addition of a nanofiller, the charge transport mechanism is likely to become more complicated than in the unfilled polymer. For example, the inclusion of nanoparticles will introduce additional interfaces between the nanofiller and the polymer, as has been emphasised by many researchers (Nelson, 2007; Lewis, 2004; Tanaka et al., 2005; Raetzke and Kindersberger, 2010), and the presence of such interfaces will affect the current flow due to the introduction of additional nanofiller/polymer trapping sites and/or through modification of the original trapping sites of the polymer. Therefore, investigations into absorption current behaviour could contribute to a better understanding of filler/polymer interactions in nanocomposites, in particular, in relation to charge transport mechanisms.

8.2 Results and Discussion

8.2.1 Absorption Current Measurements at 40 kV mm^{-1} DC Field

Figure 8.1 shows plots of the time dependence of absorption current for all investigated samples at a constant DC field of 40 kV mm^{-1} over 3 h at room temperature. It is obvious that all the nanocomposites showed a current-time characteristic that is different from that of the unfilled polyethylene. From this, the current behaviour of the nanocomposites can be interpreted based on three phases: the region corresponding to the initial decrease of current (Phase I), the region immediately following the initial reduction in slope (Phase II) and the region where the current rises (Phase III).

It is noteworthy that, although the absolute absorption current values differ for each sample at the beginning of the test, these variations fall within experimental uncertainties; repeated experimental runs showed that data variations within a factor of 3 are typical, and can occasionally be up to a factor of 5, which causes the quantitative analysis of such behaviour to become questionable. The poor reproducibility of test data is, however, a common issue with absorption current

measurements (Adamec and Calderwood, 1978). Quantitative analysis of this facet of the data is therefore not the primary interest of this study.

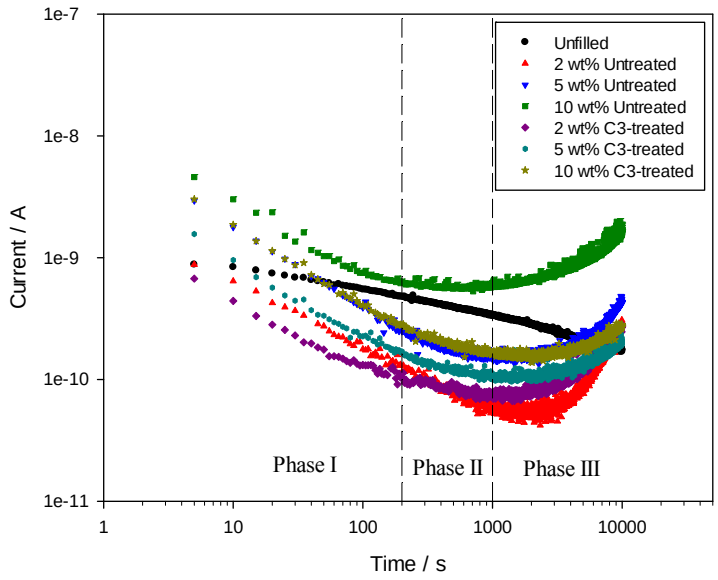

Figure 8.1: Plot of absorption current against time up to 10^4 s for all investigated samples crystallised isothermally at 115 ºC at an applied field of 40 kV mm^{-1}. The data were divided into three phases for the ease of interpretation

First consider Phase I, the rate of decrease of current for all the nanocomposites is significantly greater than for the unfilled polyethylene; although the absolute magnitude of the absorption current was found to vary from sample to sample, repeated experimental runs showed the rate of decrease of current with time to be reproducible in all the investigated nanocomposites. For a clearer interpretation, the current-time characteristic is re-plotted in Figure 8.2 for data up to 200 s, and the variation of current with poling time is summarised in Table 8.1.

Generally, all the nanocomposites possess a higher value of the exponent b_1 that characterises Phase I, when compared with the unfilled polyethylene. Also, this parameter increases with increasing amount of nanosilica present in the system, although any influence of nanosilica surface treatment appears to be comparable to experimental uncertainties. Figure 8.3 shows a plot of exponent b_1 against nanosilica content; the indicated b_1 values of the nanocomposites were obtained from the average values of the untreated and C3-treated systems and the error bars represent the standard deviation from both systems.

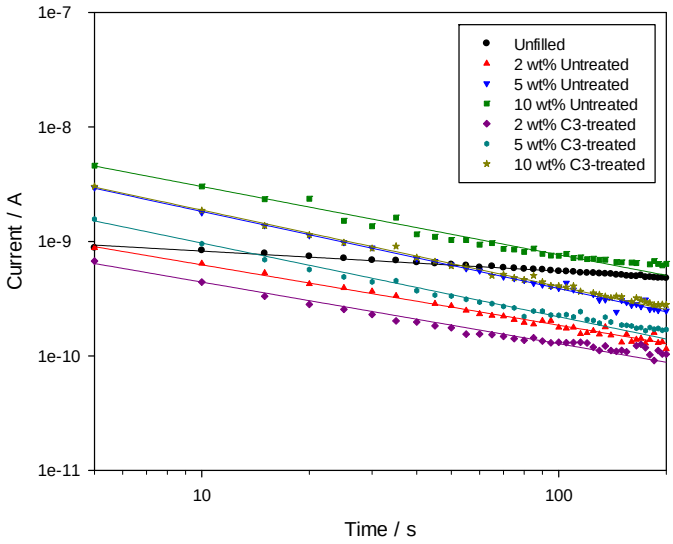

Figure 8.2: Comparison of experimental data and a power law line fitting for absorption current data up to 200 s. The slopes of all nanocomposites are steeper than that of the unfilled polyethylene

Table 8.1: Exponent calculated from the absorption current data at the beginning of the test (0 s to 200 s) at an applied field of 40 kV mm^{-1}

Sample	$b_1 \times 10^{-2}$
Unfilled	17.5 ± 0.3
2 wt% Untreated	52.7 ± 0.6
5 wt% Untreated	67.3 ± 0.4
10 wt% Untreated	59.6 ± 1.3
2 wt% C3-treated	53.9 ± 1.0
5 wt% C3-treated	64.4 ± 0.9
10 wt% C3-treated	66.7 ± 0.6

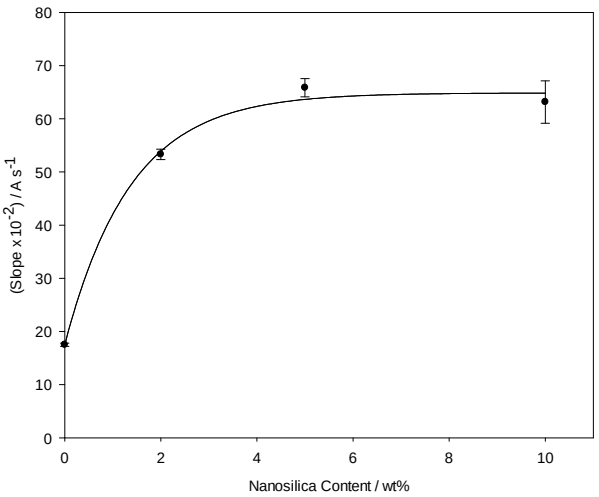

Figure 8.3: Plot showing the variation of the exponent b_1 as a function of nanosilica content. The b_1 values of the nanocomposites were obtained from the average values of the untreated and C3-treated systems and the error bars represent the standard deviation from both systems

In Phase II, the exact quantitative determination of the exponent b_2 was complicated somewhat by the difficulty in establishing the appropriate time range (see the fitted lines in Figure 8.4). The precise time at which the characteristic reduction in slope occurs varies from sample to sample, even if the same type of sample were used; no comparable change of slope occurs in the unfilled polyethylene. Despite this, the same fitting procedure described above was, nevertheless, employed and the resulting estimated b_2 values are shown in Table 8.2.

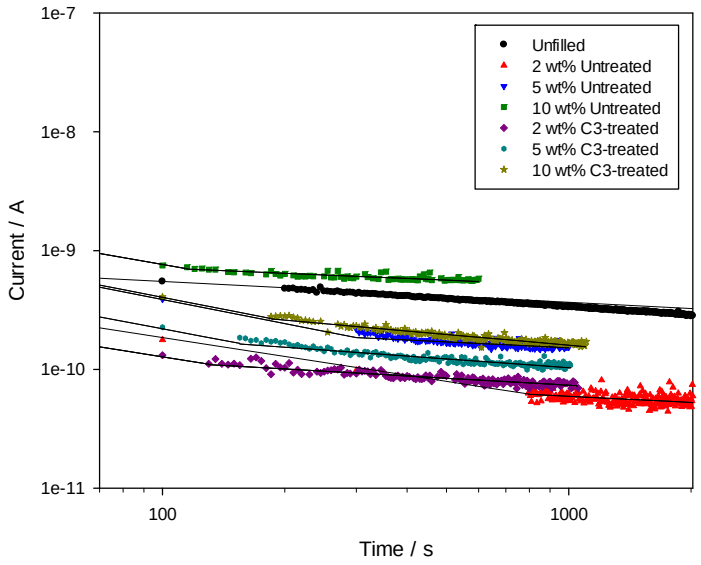

Figure 8.4: Comparison of experimental data and power law line fitting for absorption current data for Phase II at an applied field of 40 kV mm^{-1}. Line fitting for Phase I are also shown to indicate the point at which a change of slope occurs in nanocomposites

Table 8.2: Exponent calculated from the absorption current data in Phase II at an applied field of 40 kV mm^{-1}

Sample	$b_2 \times 10^{-2}$
Unfilled	17.5 ± 0.3
2 wt% Untreated	17.3 ± 2.0
5 wt% Untreated	16.5 ± 2.4
10 wt% Untreated	14.6 ± 1.3
2 wt% C3-treated	19.6 ± 0.9
5 wt% C3-treated	24.7 ± 0.8
10 wt% C3-treated	30.2 ± 0.8

Comparing the data presented in Table 8.1 and Table 8.2, it is evident that the rate at which the current decreases for all the nanocomposites in Phase II is much lower than in Phase I; this does not apply to the unfilled polyethylene. While the quantitative value of the exponent b_2 is not crucial for the argument here, it is

important to note that the values become comparable to that which characterises the unfilled polyethylene.

Using the slope change data in Figure 8.4, the charge carrier mobility was estimated in each system using Equation 8.2. The resulting charge carrier mobility is shown in Figure 8.5; the characteristic reduction in slope for the unfilled polyethylene was assumed to occur at 10^4 s. It can be noticed that all the nanocomposites are characterised by a higher charge carrier mobility than the unfilled polyethylene; the charge carrier mobility estimated for the unfilled polyethylene falls within the measurement range of a series of polyethylenes reported by Montanari et al. (2001), suggesting that the analysis is reasonable.

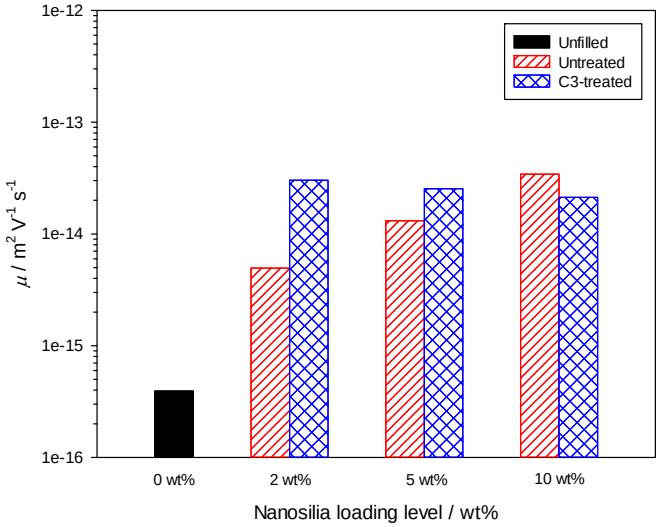

Figure 8.5: Charge carrier mobility of unfilled polyethylene and nanocomposites containing different types and amounts of nanosilica, obtained from an applied field of 40 kV mm^{-1}

In Phase III, the current flowing through the nanocomposites begins to rise and, due to the restrictions inherent in Equation 8.1, no data analysis comparable to that described above was attempted. No comparable behaviour was found in the unfilled polyethylene.

8.2.2 Absorption Current Measurements at 25 kV mm^{-1} DC Field

To confirm the absorption current behaviour of the nanocomposites, a reduced DC field of 25 kV mm^{-1} was applied, and the resulting plots of the time dependence of

absorption current for all investigated samples is shown in Figure 8.6. Again, all the nanocomposites showed a current-time characteristic that is different from that of the unfilled polyethylene, and the current behaviour of the nanocomposites can again be interpreted based on three phases: Phase I (for data up to 300 s), Phase II (for data from 300 s to 3600 s) and Phase III (for data from 3600 s onwards).

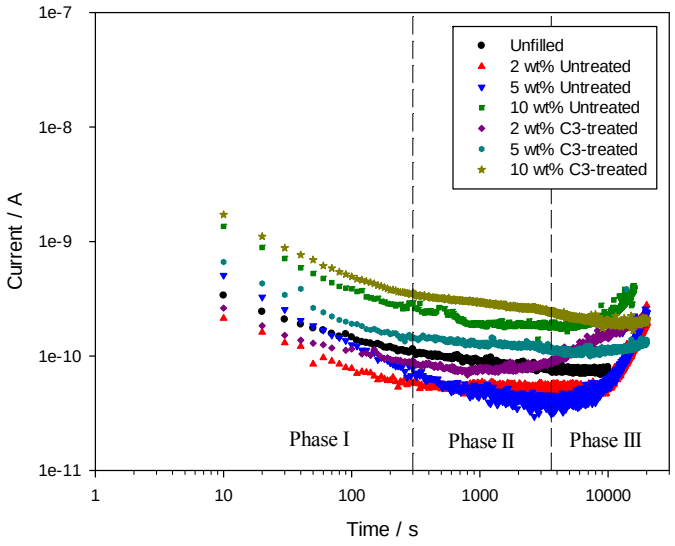

Figure 8.6: Plot of absorption current against time for all samples crystallised isothermally at 115 ºC at an applied field of 25 kV mm^{-1} up to (2×10^4) s

In Phase I, all the nanocomposites, again, possess a higher value of the exponent b_1 when compared with the unfilled polyethylene. The current-time characteristic is re-plotted in Figure 8.7 for data up to 300 s, and the variation of current with poling time is summarised in Table 8.3. Also, the exponent b_1 increases with increasing loading level of nanosilica (see Figure 8.8), but any influence of nanosilica surface treatment remains difficult to justify; the percentage uncertainties are, however, larger at 25 kV mm^{-1} than 40 kV mm^{-1}, due to the lower DC field and the resultant reduced current values.

The determination of the exponent b_2 in Phase II is shown in Figure 8.9; no comparable change of slope occurs in the unfilled polyethylene. The resulting estimated b_2 values are shown in Table 8.4. An investigation into the mobility of charge carriers in this case (see Figure 8.10) indicates that the charge mobility of nanocomposites falls in the range of 10^{-14} m^2 V^{-1} s^{-1} and, is again, about an order of magnitude higher than that of the unfilled polyethylene. This is similar to previous observation of charge mobility of nanocomposites at an applied field of 40 kV mm^{-1}.

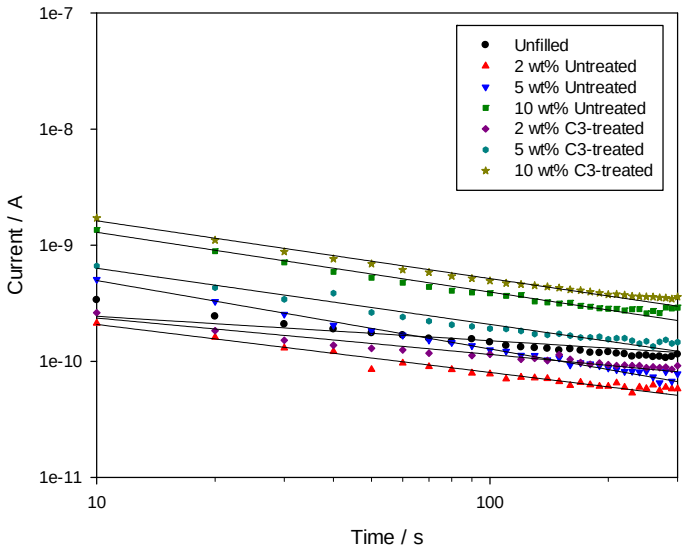

Figure 8.7: Comparison of experimental data and a power law line fitting for absorption current data up to 300 s (assumed as Phase I) at an applied field of 25 kV mm^{-1}. The slopes of all nanocomposites are steeper than that of the unfilled polyethylene

Table 8.3: Exponent calculated from the absorption current data at the beginning of the test (0 s to 300 s) at an applied field of 25 kV mm^{-1}

Sample	$b_1 \times 10^{-2}$
Unfilled	21.0 ± 0.4
2 wt% Untreated	41.3 ± 1.1
5 wt% Untreated	59.0 ± 0.6
10 wt% Untreated	51.5 ± 1.1
2 wt% C3-treated	31.4 ± 1.3
5 wt% C3-treated	48.3 ± 1.5
10 wt% C3-treated	49.8 ± 1.0

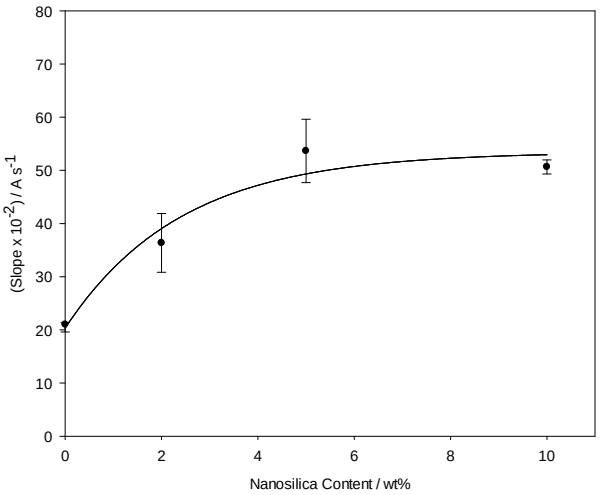

Figure 8.8: Plot showing the variation of the exponent b_1 as a function of nanosilica content. The b_1 values of the nanocomposites were obtained from the average values of the untreated and C3-treated systems and the error bars represent the standard deviation from both systems

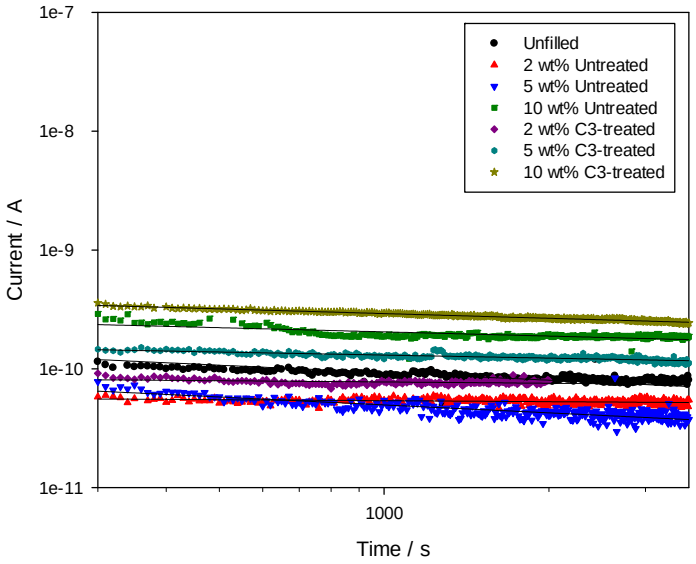

Figure 8.9: Comparison of experimental data and a power law line fitting for absorption current data from 300 s to 3600 s (assumed as Phase II) at an applied field of 25 kV mm^{-1}

Table 8.4: Exponent calculated from the absorption current data in Phase II at an applied field of 25 kV mm^{-1}

Sample	$b_2 \times 10^{-2}$
Unfilled	21.0 ± 0.4
2 wt% Untreated	2.8 ± 0.4
5 wt% Untreated	22.2 ± 0.9
10 wt% Untreated	11.7 ± 0.6
2 wt% C3-treated	3.5 ± 0.7
5 wt% C3-treated	8.5 ± 0.3
10 wt% C3-treated	13.2 ± 0.1

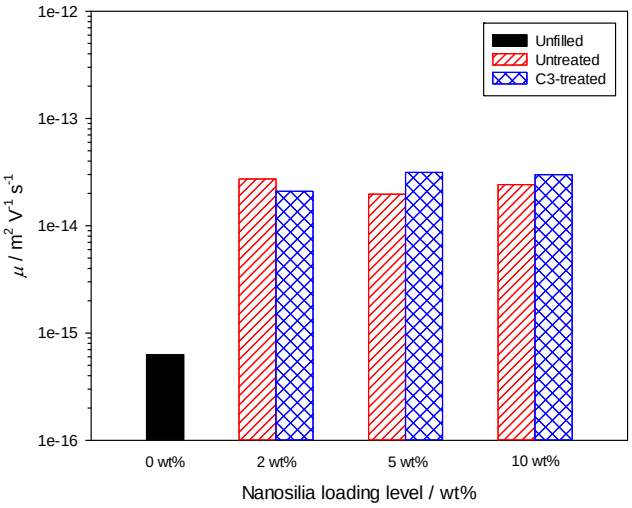

Figure 8.10: Charge carrier mobility of unfilled polyethylene and nanocomposites containing different types and amounts of nanosilica, obtained from an applied field of 25 kV mm^{-1}

In Phase III, the current rise is still noticeable for the case of nanocomposites containing untreated nanosilica, but is delayed for the case of nanocomposites containing higher amounts of C3-treated nanosilica (5 wt% and 10 wt%); such current rise behaviour is, again, not found in the unfilled polyethylene. Also, the characteristic reduction of slope (from Phase I to Phase II) and the increase of current in Phase III happened at later times as the applied field is reduced to 25 kV mm^{-1} (compare Figure 8.5 with Figure 8.1).

8.2.3 Discussion

In Phase I, the current decreases more rapidly in the nanocomposites than in the unfilled polyethylene. This implies that the incorporation of nanosilica into polyethylene has increased the mobility of charge carriers in the nanocomposites, so leading to faster decay of the current as the carriers take a shorter time to transit the specimen. It is noteworthy that $0 \leq b \leq 2$ is consistent with dipole orientation, carrier tunnelling and carrier hopping, while $0 \leq b \leq 1$ is consistent with charge injection forming trapped space charge (Wintle, 1983). While nanoparticles with their large surface areas may act as additional electron traps, they may also reduce the average hopping distance relative to that of the polymer matrix and thus increase the mobility (Fleming, 2010). As the nanofiller content increases, charge mobility may increase due to increased nanofiller/polymer interfaces. This is consistent with the analysis of b_1 in Phase I, where this parameter increases with the nanofiller content.

From previously reported space charge results, homocharge was found to develop near both electrodes and the charge moves towards the sample bulk. The transport of charge towards the bulk appears to be suppressed as the nanofiller loading level increases. In the case here, charge mobility appears to increase with increasing nanofiller content. While these results contradict with each other with regard to the movement of charge at different nanofiller loading level, it should be noted that the presence of new localised states upon nano-inclusions may serve both to promote charge migration into the bulk and to cause local trapping near the electrode with increased trap densities, and the balance between these two processes may have a different effect in these measurements. Nevertheless, both these measurement

techniques indicate that the inclusion of nanoparticles has a marked effect on charge transport dynamics.

The change in the b exponent seen in all the nanocomposites, on entering Phase II, could indicate a change in the dominant absorption current mechanism. This could be attributed to interfacial polarisation, as explained elsewhere in the literature (Roy et al., 2007; Roy, 2005). The change of slope could also be interpreted in the following way: electronic transport is effectively controlled by trapping, i.e., an electron may travel rapidly through the system for a short time, but its effective or average mobility is greatly reduced as a result of being immobilised for much longer period in localised states (traps) (Wintle, 1983). Alternatively, the change in slope could indicate that the absorption current in Phase II is dominated by the matrix rather than the nanofiller (which is believed to dominate in Phase I), since the decay in absorption current within this phase occurs at a rate that is: i) very different from Phase I and ii) appears comparable to that seen in the unfilled polyethylene, albeit that the b_2 data obtained at the applied field of 25 kV mm^{-1} causes such assertion to be questionable.

The mobility of charge carriers is highly dependent upon the release of charges from deep traps in addition to the underlying current caused by the large number of shallower traps introduced by the nanoparticles (Smith, 2009). Analysis of charge carrier mobility shows that all the nanocomposites initially possess higher charge mobility in comparison with the unfilled polyethylene. Although it remains difficult to judge the effect of nanofiller type and amount on the charge carrier mobility, it is reasonable to deduce that the incorporation of nanosilica into polyethylene results in the presence of shallower traps that are related to the nanofiller/polymer interfaces in addition to the original trap distribution that characterises the polymer's structure; the former serves to assist in charge transport.

Although the increasing absorption current with poling time seen in Phase III is highly unusual, such observations are not without precedent. A comparable increase of current was also discovered by Smith (2009) for microcomposites and was thought to be caused by interfacial polarisation related to the interfaces between the filler and the matrix. However, no convincing explanation has been proposed in

relation to this phenomenon. Nevertheless, at a lower DC field (i.e., 25 kV mm^{-1}), measurements showed that the increase of current in Phase III could be delayed, especially for samples containing C3-treated nanosilica. This shows that the absorption current characteristics at 25 kV mm^{-1} applied field is different for the case of nanocomposites containing C3-treated nanosilica and nanocomposites containing untreated nanosilica. This may be related to the observed space charge characteristics between the nanocomposites containing C3-treated nanosilica and nanocomposites containing untreated nanosilica; the nanocomposites containing C3-treated nanosilica showed less significant homocharge development near both electrodes in comparison with nanocomposites containing an equivalent amount of untreated nanosilica at an applied field of 25 kV mm^{-1}.

8.3 Summary

While the current behaviour through the unfilled polyethylene decreases with time in a conventional manner, all nanocomposites reveal an initial decrease followed by a period in which the current increases with increasing time of DC field application. In addition, the inclusion of nanosilica into polyethylene causes the decay of the absorption current initially to occur more rapidly than in the unfilled polyethylene, highlighting the possibility of increased charge mobility in the nanocomposites. In the current work, quantitative analysis for a specific nanofiller/polymer combination is very limited through these absorption current measurements and more work is necessary fully to explain the underlying charge transport mechanisms in nanocomposites.

Chapter 9

The Effect of Silane Chain Length

"Unless you believe, you will not understand."

- Saint Augustine -

9.1 Introduction

In the previous chapters, detailed discussions on the structure and electrical properties of nanocomposites containing untreated and C3-treated nanosilica have been provided. Clearly, the electrical properties, in particular in connection with DC applications of the nanocomposites, are influenced by the surface chemistries of the nanosilica, i.e., the interfaces. To date, there have been a few models proposed with regard to the interfacial properties of nanodielectrics. The interface models are presented hereafter for the purpose of a more in-depth understanding of the concept of interfaces.

As early as the mid-1990s, Lewis (1994) proposed a model concerning nanodielectrics via a diffuse electrical double layer; this was then refined in a later publication (Lewis, 2004; 2005), with the interface represented as in Figure 9.1. In the model, the theory related to electrical and electrochemical features of the interfaces was clarified based on the presence of a Stern layer and a Gouy-Chapman diffuse double layer surrounding a nanoparticle; the Stern layer is an ion layer of molecular dimensions bound to the surface of the nanoparticle by forces which are stronger than the electrostatic forces attracting the diffuse layer, while the diffuse layer contains a distribution of co-ions that are repelled and counter-ions that are attracted towards the nanoparticle. The formation of interfaces with nanometric dimensions via the Stern and diffuse layers between the particle and the matrix changes the internal charge activity and the resulting electrical potential distribution at the interfaces, which will then influence the dielectric properties of the resulting nanocomposites.

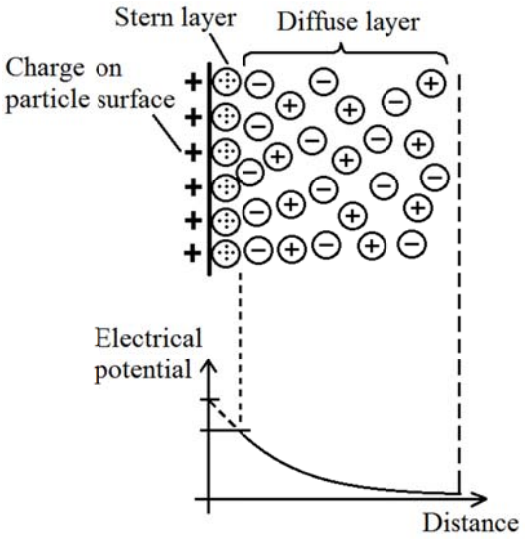

Figure 9.1: The diffuse electrical double layer and the resulting electrical potential distribution (Lewis, 2004)

A multi-core model was proposed by Tanaka et al. (2005) in an attempt to clarify the chemical and electrical properties of the interfaces, as shown in Figure 9.2. The model consists of four layers: the first layer (the bonded layer) corresponds to a transition layer tightly bonded to both filler and matrix by coupling agents such as silane; the second layer (the bound layer) is an interfacial region consists of a layer of polymer chains strongly bound and interacting with the first layer and the surface of the particle; the third layer (the loose layer) is a region loosely coupled and interacting with the second layer, and is considered to have different chain conformations, chain mobility, and even free volume or crystallinity from the matrix; the fourth layer (the Gouy-Chapman diffuse layer) superimposed on the first, the second and the third layers, with charge decays exponentially with distance and may extend beyond those three layers. This leads to the idea that the interface of the nanoparticle may overlap with that of its neighbouring nanoparticle, thus causing a far-field effect which results in a cooperative effect between the nanoparticles.

Meanwhile, a multi-region structure (see Figure 9.3) was proposed by Li et al. (2010b) by considering the effect of surface treatment of nanoparticles on the interfacial structures. The bonded region has the strongest bonding strength at the interface. This is due to the presence of abundant unsaturated bonds, e.g. hydrogen and organic groups (silane couplings) on the surface of the nanoparticle. The bonded region is speculated to contain deep traps with the highest density and determines the

short-term breakdown properties of the nanocomposites. The transitional region contains ordered polymer molecular chain with characteristics affected mainly by the cohesive energy density of the polymer and is considered as the crystalline structure region. It is noteworthy that the cohesive energy density is a parameter used to characterise the intermolecular force between polymer molecules and the flexibility of molecular chains. The higher the cohesive energy density, the better the flexibility of molecular chain and therefore the more energy is required to break up the chain, resulting in material having extended service life. The bonded region and the transition region collaboratively determine the long-term failure properties of the nanocomposites. The normal region is the region of the polymer unaffected by the interface, having random molecular chain structures around the nanoparticle.

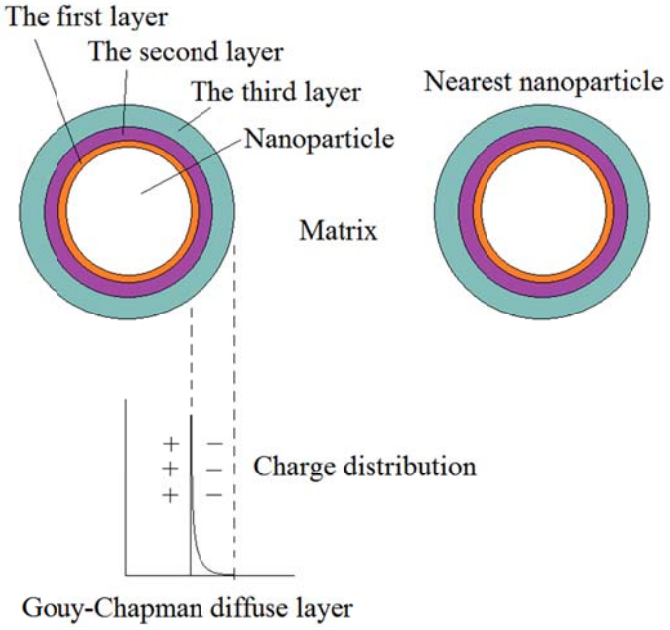

Figure 9.2: The multi-core model (Tanaka et al., 2005)

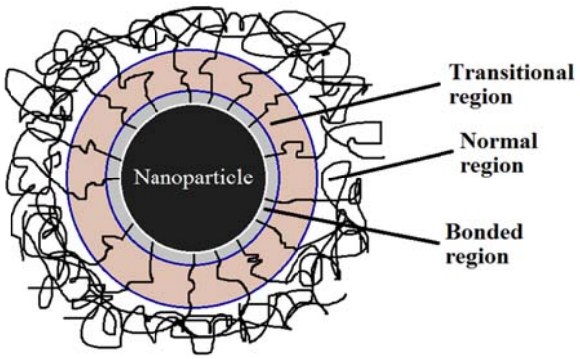

Figure 9.3: Multi-region structure around a spherical nanoparticle (Li et al., 2010b)

An interface model similar to the above models was also proposed by Andritsch (2010) in an attempt to clarify the interaction between untreated and treated nanofillers with polymer chains. It is known as the polymer chain alignment model, and is illustrated in Figure 9.4. In this model, an untreated particle is considered to have a weak interaction with the polymer (see Figure 9.4a) while a surface treated particle is considered to result in an aligned polymer chain region surrounding the particle, causing a restructuring of the surrounding polymer (see Figure 9.4b). The use of treated nanofiller therefore results in regions with different polymer chain alignment, which results in changes in electrical properties.

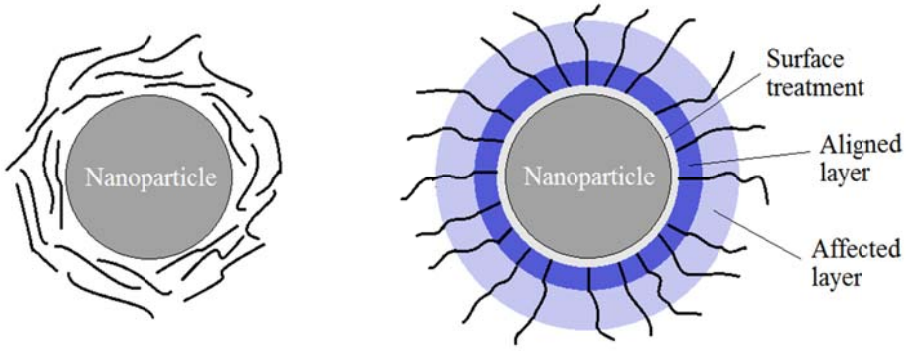

(a) (b)

Figure 9.4: (a) An unmodified particle having a weak interaction with the polymer, (b) surface treatment of the particle results in a layer of aligned polymer chains, which also affects the surrounding area (the affected layer), thus restructuring the polymer (Andritsch, 2010)

In the dual layer model (see Figure 9.5) suggested by Singha and Thomas (2008), based on the dual nanolayer theory proposed by Tsagaropoulos and Eisenberg (1995), it was suggested that the nanoparticle/polymer interactions lead to the formation of two nanolayers around the nanoparticle. The first nanolayer (innermost layer) is tightly bound to the surface of the nanoparticle, resulting in highly immobile polymer chains, while the second nanolayer (outer layer) contains loosely bound polymer chains with restricted mobility. If the loosely bound nanolayer dominates, a reduced glass transition temperature will be observed, and since the transfer of charge carriers is easy through this layer, increased conductivity and lower breakdown strength will be expected. Conversely, if the first nanolayer dominates, the glass transition temperature will increase, while the permittivity and conductivity will decrease due to the highly immobile polymer chain.

Meanwhile, a higher breakdown strength was attributed to the nanoparticles themselves acting as barriers to the flow of current between the electrodes (Preetha and Thomas, 2011; Singha and Thomas, 2008). Similar explanations have also been given with regard to electrical tree growth phenomena (Danikas and Tanaka, 2009) and surface discharge phenomena (Maity et al., 2008) in nanocomposites. Since the improvement of the degradation resistance at high nanoparticle loading is attributed to the reduction of the loose polymer region and the increase of the immobile polymer region with respect to the loose polymer region, it was assumed that the innermost layer is more resistant to degradation when compared with the outer layer (Pitsa and Danikas, 2011).

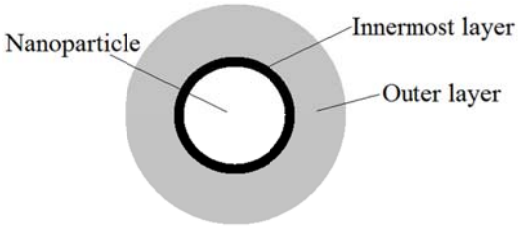

Figure 9.5: The dual layer model (Singha and Thomas, 2008)

In Chapter 6, comparisons of systems containing untreated and C3-treated nanosilica were reported, and it was demonstrated that the DC breakdown strength of the nanocomposites containing C3-treated nanosilica was higher than that of the nanocomposites containing an equivalent amount of untreated nanosilica. However, the DC breakdown strength of the C3-treated systems was still lower than that of the unfilled polyethylene. Meanwhile, from the above discussion, it can be concluded that the proposed interface models exhibit a common element: the interface layer most adjacent to the nanofiller, which is characterised by silane coupling agents, is the key to controlling the behaviour at the interface, thus affecting the electrical properties of the resulting nanocomposites. Therefore, a systematic study with a view to understanding the mechanisms underpinning the concept of filler functionalisation in nanodielectrics has been undertaken in this chapter, via the use of different aliphatic chain length silane coupling agents. This is thought to be capable of altering the interface layer most adjacent to the nanofiller, thus affecting the other interface layers and the resulting electrical properties, with the aim of improving the DC breakdown performance of the nanocomposites in particular.

9.2 Different Aliphatic Chain Length Silanes

A series of silane coupling agents, which differ with respect to their aliphatic chain length, was considered in this study with a view to improve the DC breakdown performance of the nanocomposites. This involves the use of trimethoxy(octyl)silane and trimethoxy(octadecyl)silane coupling agents, which carries octyl (C_8H_{17}) and octadecyl ($C_{18}H_{37}$) functional groups, respectively. In these, the octadecyl chain is the longest, followed by the octyl chain, in comparison with the propyl chain of the trimethoxy(propyl)silane.

To minimise experimental parameter changes, the surface functionalisation process and the nanocomposite sample preparation methods were kept the same as previously reported for the C3-treated system. In all cases, the same volume of silane was used and, therefore, although the length of the chains differs among the differently functionalised nanosilica, the number of CH_2 repeat units per unit area of interface is comparable in all. Moreover, the silane was based upon trimethoxysilane to ensure that, during the surface functionalisation process, the nature of silane interactions with the nanosilica would be comparable to those in the C3-treated nanosilica.

For notation purposes, nanosilicas subject to surface functionalisation using trimethoxy(octyl)silane and trimethoxy(octadecyl)silane are referred to as C8-treated nanosilica and C18-treated nanosilica, respectively; this reflects the length of the silane attached to the surface of the nanosilica.

9.3 Results and Discussion

9.3.1 Thermal Analysis

Figure 9.6 compares the crystallisation rate constant, K_3 values obtained from nanocomposites containing untreated, C3-treated, C8-treated and C18-treated nanosilica at a representative crystallisation temperature of 115 ºC. The behaviour of the untreated and C3-treated systems has been discussed in Chapter 3 and is therefore not repeated here. For the case of C8-treated system, the K_3 values are the highest

among all nanocomposites at all nanofiller loading levels. Meanwhile, the K_3 values for the C18-treated system are intermediate between the C3-treated and the C8-treated systems.

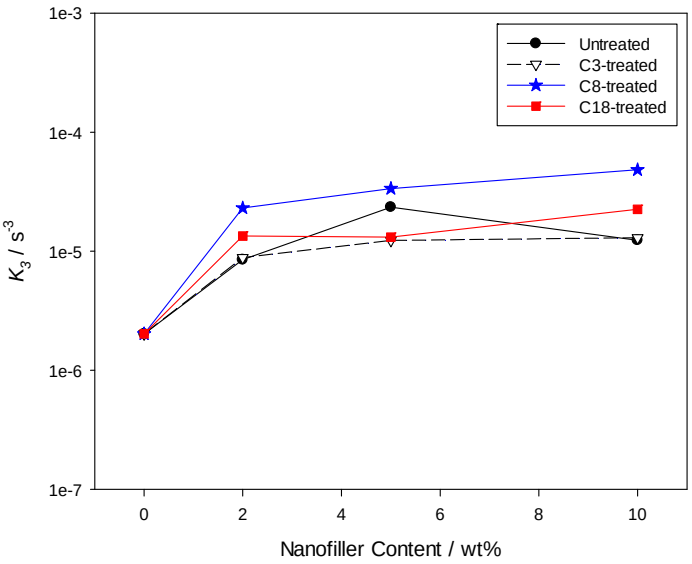

Figure 9.6: Plot showing the effect of nanosilica surface chemistry and nanosilica content on K_3 at a representative crystallisation temperature of 115 ºC. The fitted lines represent the K_3 variation of each system

9.3.2 Fourier Transform Infrared Spectroscopy

Figure 9.7 shows the FTIR spectra of the C8-treated and the C18-treated silica nanopowder. There is, however, no appreciable reduction of the intensity at 3400 cm^{-1} in comparison with the untreated silica nanopowder (see Figure 4.3).

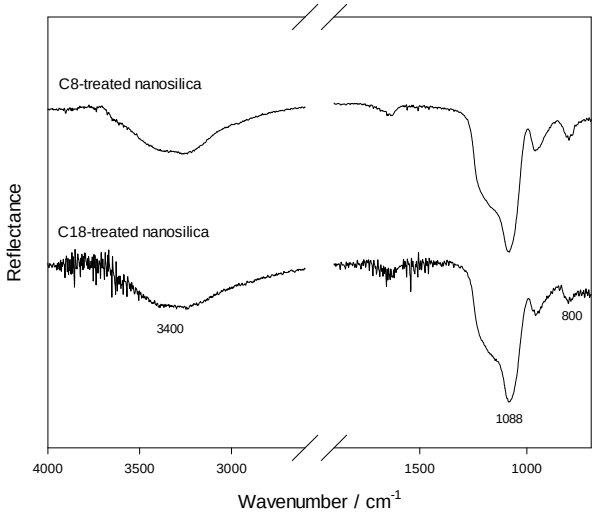

Figure 9.7: FTIR spectra for C8-treated and C18-treated silica nanopowder

9.3.3 Morphological Characterisation

Figure 9.8 shows SEM micrographs of nanocomposites containing 2 wt%, 5 wt% and 10 wt% of C8-treated and C18-treated nanosilica. Again, perturbed spherulitic development can be observed in these nanocomposite systems (i.e., C8-treated and C18-treated systems), and this effect becomes more dramatic as the nanofiller

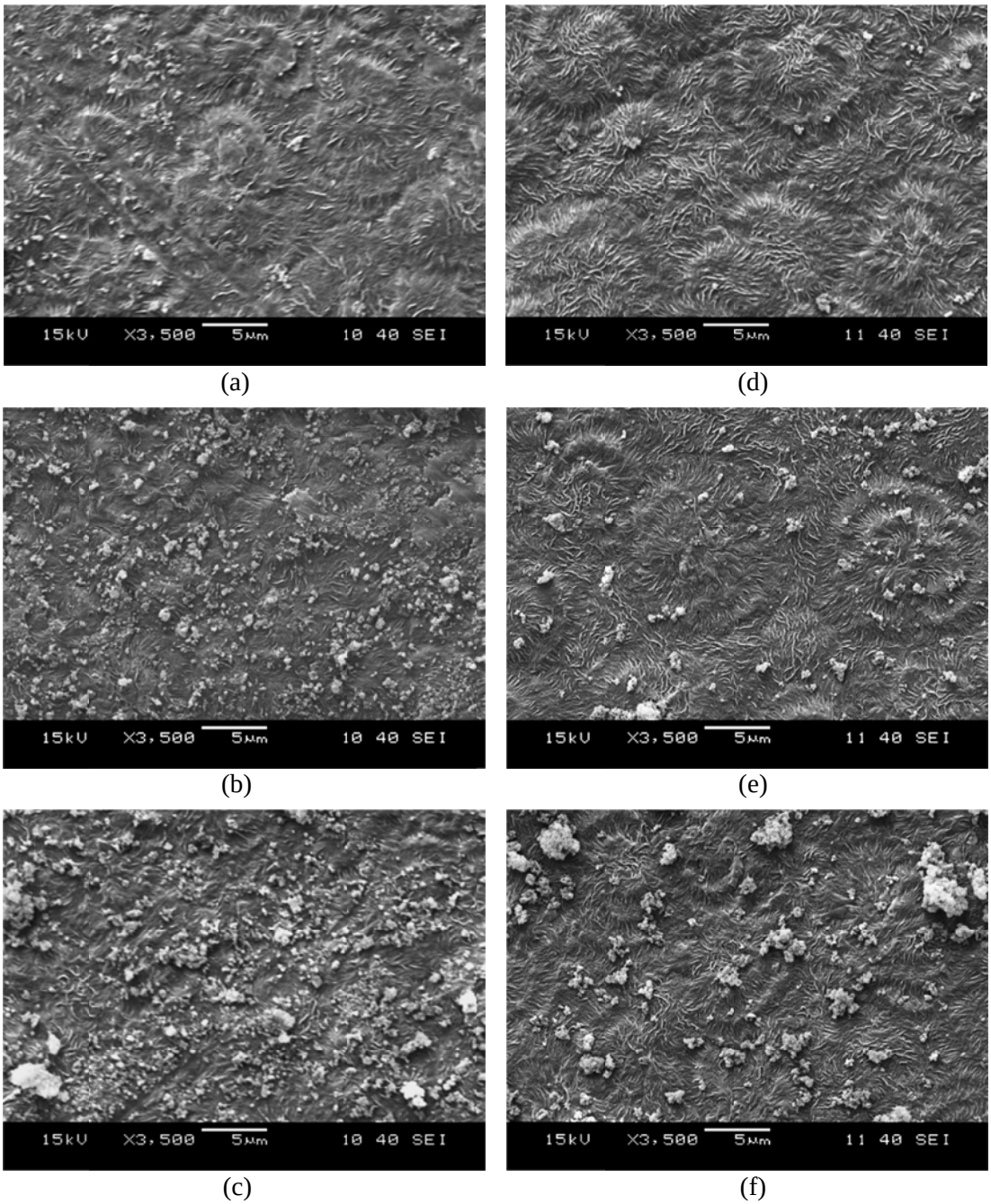

Figure 9.8: Dispersion state of (a) 2 wt%, (b) 5 wt%, (c) 10 wt% of C8-treated nanosilica and (d) 2 wt%, (e) 5 wt%, (f) 10 wt% of C18-treated nanosilica in polyethylene crystallised at 115 ºC

content increases. In terms of nanoparticle dispersion, more fine-sized particles can be observed in the nanocomposites containing C8-treated nanosilica; the dispersion of nanoparticles appears to be the best in the C8-treated system in comparison with all the other nanocomposite systems considered in this study (i.e., untreated, C3-treated and C18-treated systems). Meanwhile, the dispersion state of the C18-treated nanosilica appear slightly better than samples containing an equivalent amount of untreated and C3-treated nanosilica (compare Figure 9.8 with Figure 4.8).

Figure 9.9 shows higher magnification SEM micrographs of nanocomposites containing 5 wt% of C8-treated and C18-treated nanosilica. Although nanometre-sized distributions remained difficult to image due to the presence of the underlying lamellar texture, it can be observed that there are indeed more fine-sized nanoparticles present in the C8-treated system in comparison with the C18-treated system. Also, the size of nanoparticles in these systems (i.e., C8-treated and C18-treated systems) appears to be less than that found in the AFM images of the untreated and C3-treated systems (see Figure 4.12).

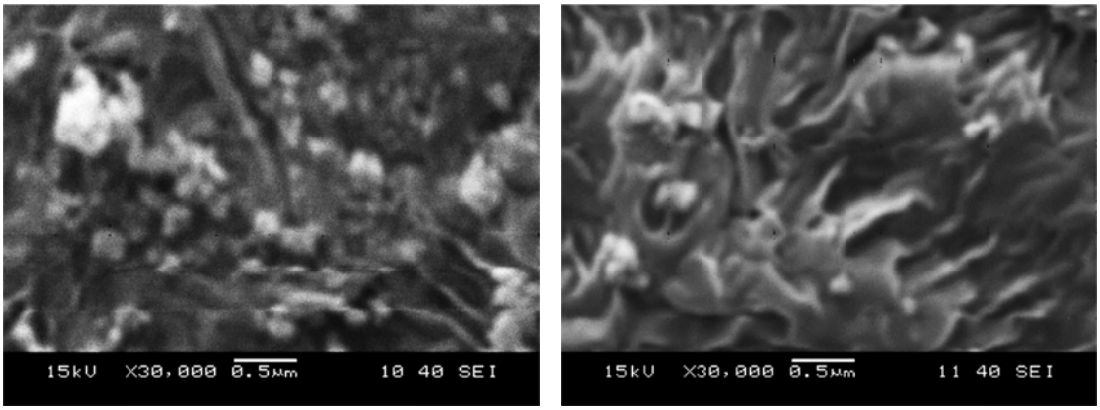

(a) (b)

Figure 9.9: Dispersion state of 5 wt% of (a) C8-treated, (b) C18-treated nanosilica in polyethylene crystallised at 115 ºC

9.3.4 DC Breakdown Strength

Figure 9.10 compares the DC breakdown strength of unfilled polyethylene and nanocomposites containing varying amounts of untreated, C3-treated, C8-treated and C18-treated nanosilica, with the derived Weibull parameter values being listed in Table 9.1. Repeated breakdown measurements from unfilled polyethylene samples

showed that data variation was within an acceptable range of uncertainties. For nanocomposite samples, the DC breakdown strength is markedly affected by both the nanofiller loading level and nanofiller surface chemistry. Indeed, at all filler loading levels, it is evident that by increasing the chain length, the breakdown strength can be increased and, at higher loading levels, the effect appears to be quite dramatic.

First, consider the case of the C8-treated system, although the DC breakdown strength is lower than that of the unfilled polyethylene, the values are the highest among all the nanocomposite samples. The DC breakdown strength reduces for the case of the C18-treated system as compared with the C8-treated system, but the values are still higher than that of the untreated and the C3-treated systems. In both the C8-treated and C18-treated systems, the DC breakdown strength remains comparable at 2 wt% and 5 wt% of nanofiller loading before reducing at 10 wt% of nanofiller loading. It should be noted that the shape parameter reduces in the C8-treated and C18-treated systems in comparison with the untreated and C3-treated systems (see Table 9.1).

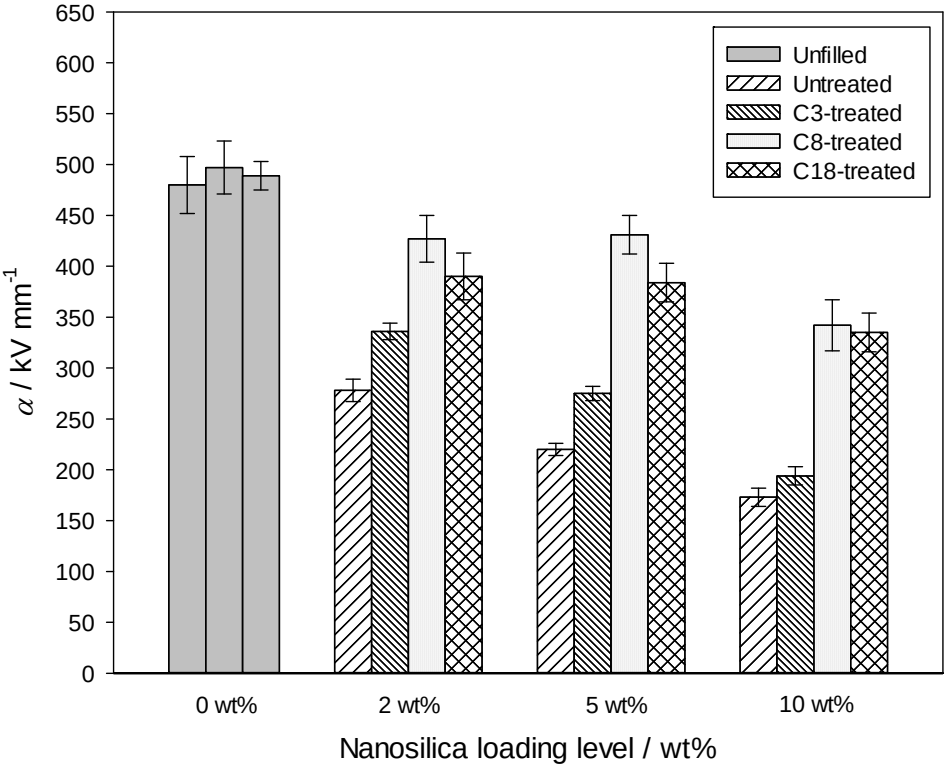

Figure 9.10: Plots comparing the DC breakdown strength of the unfilled polyethylene and nanocomposites containing the untreated, the C3-treated, the C8-treated and the C18-treated nanosilica crystallised at 115 ºC, obtained from Weibull analysis. The uncertainties correspond to 90 % confidence bounds

Table 9.1: DC breakdown data from Weibull analysis

Sample	α / kV mm^{-1}	β
Unfilled	480 ± 28	7 ± 2
Unfilled	497 ± 26	8 ± 2
Unfilled	489 ± 14	14 ± 4
2 wt% C18-treated	390 ± 23	7 ± 2
2 wt% C8-treated	427 ± 23	8 ± 2
2 wt% C3-treated	336 ± 8	18 ± 5
2 wt% Untreated	278 ± 11	11 ± 3
5 wt% C18-treated	384 ± 19	8 ± 2
5 wt% C8-treated	431 ± 19	9 ± 3
5 wt% C3-treated	275 ± 7	16 ± 5
5 wt% Untreated	220 ± 6	15 ± 4
10 wt% C18-treated	335 ± 19	7 ± 2
10 wt% C8-treated	342 ± 25	6 ± 2
10 wt% C3-treated	194 ± 9	19 ± 6
10 wt% Untreated	173 ± 9	8 ± 2

9.3.5 Space Charge Dynamics

Figure 9.11 shows representative space charge profiles obtained from nanocomposites containing 5 wt% of C8-treated nanosilica and the nanocomposites containing 5 wt% of C18-treated nanosilica. In the case of the C8-treated system (see Figure 9.11a), the space charge profile is comparable with those exhibited by the nanocomposites containing the untreated and C3-treated nanosilica, albeit that the

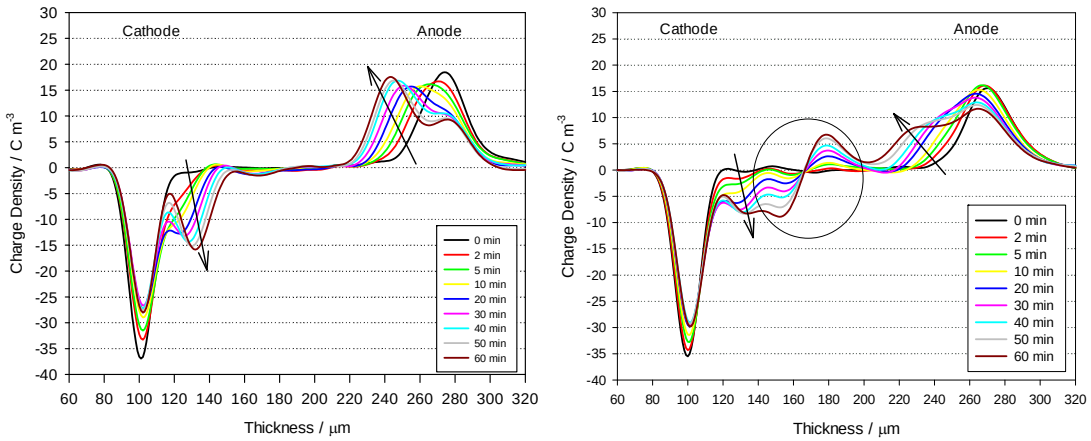

(a) (b)

Figure 9.11: Space charge behaviour of nanocomposite samples crystallised isothermally at 115 ºC containing (a) 5 wt% of C8-treated nanosilica, (b) 5 wt% of C18-treated nanosilica stressed at 40 kV mm^{-1} (the arrows indicate increasing time while the circle indicates charge accumulation in the sample bulk)

magnitude of the homocharge is greater. In the case of the C18-treated system (see Figure 9.11b), a distinct feature can immediately be identified – charge accumulation was found in the bulk of the C18-treated system in addition to homocharge development near both electrodes. This is very different from the space charge profiles of the untreated, C3-treated and C8-treated systems.

9.3.6 Discussion

In characterising the surface state of the untreated and C3-treated nanopowder, it was suggested in Chapter 4 that reduced FTIR intensity at 3400 cm^{-1} is attributed to the replacement of surface hydroxyl groups by propyl groups from silane. From the FTIR spectra of the C8-treated and the C18-treated nanopowder (see Figure 9.7), there is no appreciable reduction of the intensity at 3400 cm^{-1} in comparison with the untreated silica nanopowder (see Figure 4.3). This is, however, not surprising since surface functionalisation process of the C8-treated nanosilica and the C18-treated nanosilica involves the same volume of silane used as in the case of the C3-treated nanosilica. This would subsequently reduce the degree of filler functionalisation, thus resulting in a less number of silane functional groups in exchange with the surface hydroxyl groups, albeit increasing the chain length per attached unit.

From DC breakdown testing, the DC breakdown strength of the nanocomposites containing C8-treated and C18-treated nanosilica has been improved in comparison with the DC breakdown strength of the nanocomposites containing an equivalent amount of untreated and C3-treated nanosilica. The increase in DC breakdown strength can be attributed to the use of long chain silanes for nanosilica surface functionalisation purposes. However, the DC breakdown strength reduces for the case of C18-treated system (which has been functionalised using longer aliphatic chain silane) in comparison with the C8-treated system.

It is noteworthy that the melting behaviour and the crystallinity level of the C8-treated and C18-treated systems were not significantly different from those of the untreated and C3-treated systems. As explained in the previous chapters, these properties are considered to be secondary in determining the DC breakdown

behaviour, and are therefore not discussed in this chapter. However, these properties are discussed in Appendix A, for the case of the C18-treated system.

In Chapter 7, it was suggested that reduced space charge development could be linked to increased DC breakdown strength. Although such an effect was not seen in the C8-treated system, a higher DC breakdown strength could still be achieved. Moreover, in the case of the C18-treated system, while the magnitude of homocharge accumulation near both electrodes is comparable to that of the C3-treated system, and accompanied by charge accumulation in the bulk of the sample, the DC breakdown strength is yet higher than that of the C3-treated system.

The improved DC breakdown performance of the C8-treated system can, however, be correlated with the analysis of crystallisation rate constant, K_3. At all nanofiller loading levels, K_3 values for the C8-treated system are the highest. This indicates that chemical treatment of nanosilica using trimethoxy(octyl)silane has modified the surface interactions between the polymer and the silica in such a way as to increase its effectiveness as a nucleating agent, so that the polymer and the filler can interact more strongly. This will subsequently have an effect on the interface region, and it is convenient to assume that the interface has been controlled in a way as to increase the DC breakdown performance. Also, as deduced from the SEM micrographs, steric hindrance between approaching nanoparticles may be a credible explanation of the breakdown effects that are seen, where improved nanoparticle dispersion are observed.

While increasing the silane chain length using trimethoxy(octadecyl)silane is expected further to improve the interactions between the filler and the polymer, this effect is not seen in the C18-treated system. The K_3 values of the C18-treated system were found to reduce in comparison with the C8-treated system – the K_3 values for the C18-treated system are intermediate between the C3-treated and C8-treated systems. In addition, enhanced steric hindrance effect between approaching nanoparticles was also not seen in the C18-treated system in comparison with the C8-treated system, as evinced from the SEM micrographs. Nevertheless, these effects are in line with the observed DC breakdown performance of the C18-treated system.

The above observations on K_3 parameter variations and steric hindrance effects suggest that the enhanced crystal nucleation effect found in the C8-treated system with respect to the C3-treated system could not be reliably attributed to the increase of silane chain length. It is noteworthy that, while K_3 values can be used to assess the interactions between the nanofiller and the polymer, nanofiller/nanofiller interactions also exist, and this may lead to various aggregation states of the nanofiller which would subsequently affect the nucleation process. Consequently, it is rather difficult to justify the nature of interactions between the nanofiller and the polymer based the interpretation of the K_3 values.

Meanwhile, the above observations on the DC breakdown strength of the C18-treated system lead to the following inference: while using long aliphatic chain silane coupling agent may improve the DC breakdown performance of the resulting nanocomposites, additional subtle and, thus far, unidentified factors may also need to be considered. For example, examination of the relevant chemical data sheets indicates that the longer chain silane comes with the compromise of having lower purity – the purity of the trimethoxy(propyl)silane, trimethoxy(octyl)silane and trimethoxy(octadecyl)silane was 97 %, 96 % and 90 %, respectively. Therefore, the increase of silane chain length, especially in the case of trimethoxy(octadecyl)silane, will probably introduce more impurities into the system. In this regard, it is reasonable to expect a reduced DC breakdown strength of the C18-treated system in comparison with the C8-treated system. This may also explain the additional space charge formation found in the sample bulk of the C18-treated system.

Also, longer chain silanes may result in interfacial structures and properties becoming more variable. In an investigation by Kim and White (2002), the authors highlighted the possibility of long aliphatic silane chains forming “mushroom-like” conformations, as opposed to the brush-like shape of the short aliphatic silane chains (see Figure 9.12). The more random chain conformations on the nanosilica surface may then lead to irregularities at the interfaces of the resulting nanocomposites. In this regard, it is therefore reasonable to expect an optimal chain conformation that leads to the optimum DC breakdown strength; the C8-treated system exhibits the highest DC breakdown strength among all the nanocomposites. Beyond this optimal

point, a reduced DC breakdown strength is expected; the C18-treated system has a lower DC breakdown strength than that of the C8-treated system.

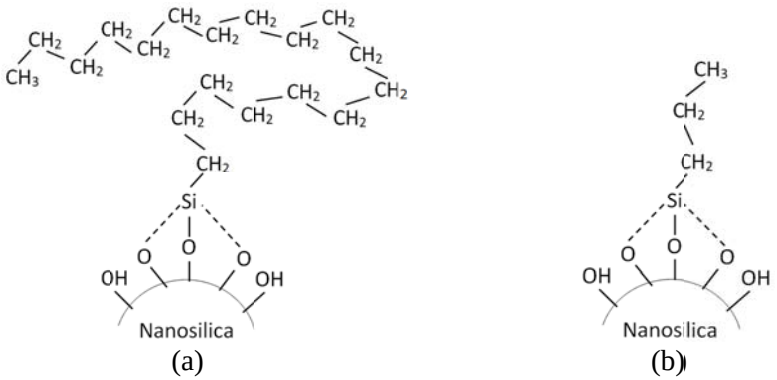

Figure 9.12: Schematic representation of different chain length silane bonded on nanosilica surface having (a) mushroom-like shape for long chain octadecyl group, (b) brush-like shape for short chain propyl group, as depicted by Kim and White (2002). Drawings are not to scale

Recently, Yeung and Vaughan (2012) demonstrated that varying the degrees of functionalisation on a nanofiller has a dramatic effect on the breakdown strength of nanocomposites, and there is an optimum degree of filler functionalisation which produces the highest breakdown strength. Correlating the FTIR spectra with the experimental DC breakdown strength, a third inference arises: what would happen if the surface functionalisation process of the C8-treated nanosilica and the C18-treated nanosilica involves a different volume of silane so that the degree of filler functionalisation is kept similar with the C3-treated system? This will be addressed in the following paragraph.

Chemical data sheets of the silanes show that the molecular weights of the trimethoxy(propyl)silane, trimethoxy(octyl)silane and trimethoxy(octadecyl)silane are 164.27 g mol^{-1}, 234.41 g mol^{-1} and 374.67 g mol^{-1}, respectively. Assuming that the degree of filler functionalisation in C3-treated nanosilica is optimal and unity, the degrees of filler functionalisation for the case of C8-treated nanosilica and C18-treated nanosilica would subsequently be reduced to 0.701 and 0.438, respectively, as shown in Figure 9.13a. From these degrees of filler functionalisation, the experimental DC breakdown strength of the resulting nanocomposite sample containing C8-treated nanosilica and C18-treated nanosilica were found to be 431 kV mm^{-1} and 384 kV mm^{-1}, respectively, as shown in Figure 9.13b (only samples containing 5 wt% of nanofillers were shown for representative purposes). So

if the degrees of filler functionalisation for the case of C8-treated nanosilica and C18-treated nanosilica are kept similar with the C3-treated nanosilica (which is equal to 1), the subsequent DC breakdown strength is likely to improve, as highlighted by the plots in red in Figure 9.13. More importantly, the DC breakdown strength of the nanocomposites containing C8-treated nanosilica and C18-treated nanosilica could even be higher than that of the unfilled polyethylene. Nevertheless, the suggested effects do not take into account factors such as purity and silane chain conformations, which would inevitably affect the DC breakdown strength, as previously discussed.

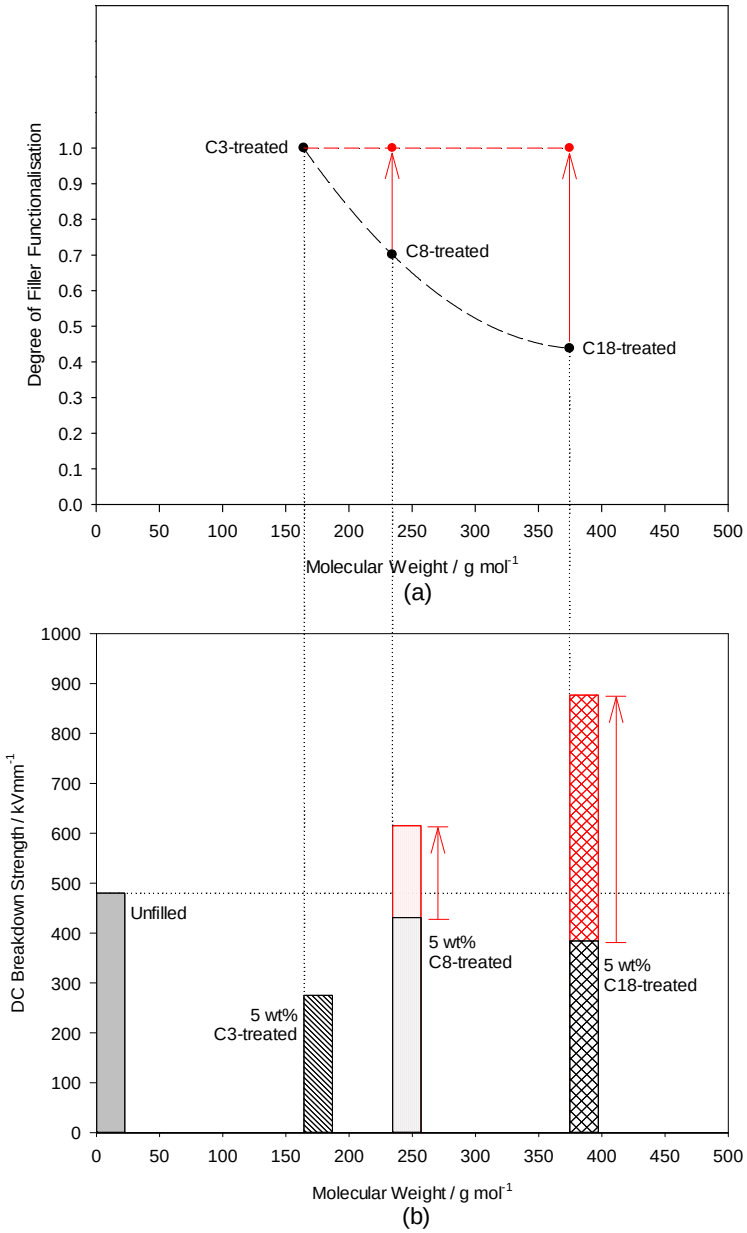

Figure 9.13: Plots correlating (a) the degree of filler functionalisation with (b) the experimental DC breakdown strength (the unfilled polyethylene serves as a reference in DC breakdown). The plots in red highlight the possible increase in the degree of filler functionalisation and its subsequent impact on the DC breakdown strength

9.4 Summary

Surface functionalisation of nanofillers using different aliphatic chain length silane coupling agents does have an impact on the DC breakdown strength of the resulting nanocomposites, in which the use of long silane chains enhances the DC breakdown strength. However, to optimise the DC breakdown strength, factors such as purity, silane chain conformation and degree of filler functionalisation need to be carefully considered. For example, increasing the silane chain length will necessary involves reducing the degree of filler functionalisation, if the amount of silane is kept the same. So if the amount of silane is varied to ensure that the degree of filler functionalisation is kept optimal, the enhancement in DC breakdown strength is expected to be much more impactful.

Chapter 10

Conclusions and Future Work

"Believe those who are seeking the truth. Doubt those who find it."

- Andre Gide -

10.1 Summary of Findings

In the current work, the formulation of nanocomposites was conducted based on the use of a polyethylene blend (with the ratio LDPE: HDPE of 4: 1) as the polymer matrix and nanosilica as the nanofiller. The amount of the nanofiller used was 2 wt%, 5 wt% and 10 wt%, and the surface chemistry was varied by the use of a trimethoxy(propyl)silane coupling agent. This resulted in two main different types of nanocomposites, i.e., nanocomposites containing untreated nanosilica and nanocomposites containing C3-treated nanosilica.

For characterisation purposes, thermal analysis was performed as reported in Chapter 3. Based on non-linear Avrami analysis, the addition of nanosilica into polyethylene enhances the nucleation density, and this is true for both the untreated and C3-treated nanosilica, as evinced by the faster crystallisation process and higher values of crystallisation rate constant, K_3, for both types of nanofilled polyethylene when compared with the unfilled polyethylene. However, nucleation effects were found to be stronger in the case of nanocomposites based upon the untreated nanofiller, despite the fact that simplistic concepts might suggest that surfaces containing propyl moieties would be more compatible with polyethylene than polar surfaces dominated by hydroxyl groups. Nevertheless, the inclusion of nanosilica, either untreated or C3-treated, did not lead to notable effects in the DSC melting traces of polyethylene; the peak melting temperatures are equivalent when subjected to the same isothermal crystallisation conditions. An investigation into the thermodynamics of crystallisation and melting indicates that both types of nanosilica used did not exert a significant effect on the final crystallinity of the polyethylene.

To validate the results obtained from thermal analysis further, morphological analysis was performed through the use of POM and SEM and was reported in Chapter 4. Both microscopy techniques confirmed that isothermal crystallisation of the polyethylene resulted in the development of spherulites. However, the incorporation of both types of nanosilica into polyethylene suppressed spherulitic development and thus perturbed the morphological structure of the isothermally crystallised material. Such effects become more pronounced with increasing amount of nanosilica.

In terms of nanoparticle dispersion, SEM micrographs show that nanosilica is generally well distributed in polyethylene, but the effect of nanoparticle agglomeration cannot be completely avoided. As the amount of nanosilica increases, agglomeration becomes more and more apparent. The aggregation effect, however, could be reduced somewhat through the use of the trimethoxy(propyl)silane coupling agent. This is particularly evident on inclusion of 10 wt% of nanosilica, where the severe aggregation effects seen in the nanocomposite containing 10 wt% of untreated nanosilica were not seen in the nanocomposite containing 10 wt% of C3-treated nanosilica. The topological images obtained from AFM provide good morphological agreement with the SEM micrographs.

From the dielectric spectroscopy testing reported in Chapter 5, the incorporation of nanosilica into polyethylene increases both the real relative permittivity and the dielectric loss tangent of the resulting nanocomposites when compared with the unfilled polyethylene, and such an effect is notable especially in the low frequency region. As the nanosilica content increases, the permittivity becomes higher. In the low frequency region, the higher dielectric loss of the nanocomposites is possibly associated with Maxwell-Wagner-Sillars interfacial polarisation. With surface treatment of nanosilica, the increase of permittivity and loss is less than that observed in the nanocomposites containing an equivalent amount of untreated nanosilica. This is attributed to the change of functional groups on the surface of the nanosilica.

The subsequent study of water absorption showed that, for nanocomposites containing either untreated or C3-treated nanosilica, the amount of absorbed water increased with increasing nanosilica content. The permittivity and loss also increased

with water immersion duration. However, surface treatment of nanosilica reduced the water absorption effect and modified the subsequent dielectric response when compared with nanocomposites containing an equivalent amount of untreated nanosilica. From dielectric spectroscopy analysis, three frequency dispersion regions (low-frequency, intermediate-frequency and high-frequency) were considered for the nanocomposites containing untreated nanosilica, with broad loss peaks indicating various relaxation processes. In contrast, the nanocomposites containing C3-treated nanosilica only showed dispersion effects confined to the low frequency range. Since the influence of water appears quite different in the nanocomposites following nanosilica surface treatment, it is reasonable to deduce that the interfacial structure of nanocomposites containing untreated nanosilica is different from that of the nanocomposites containing C3-treated nanosilica.

AC and DC breakdown testing were carried out and the results were reported in Chapter 6. It was found that the addition of nanosilica into polyethylene did not have a notable effect on the AC breakdown strength. This applies to both the untreated and C3-treated nanosilica, where the AC breakdown strength is commensurate with that of the unfilled polyethylene. However, severe clustering can cause the AC breakdown strength to be reduced significantly, as shown by nanocomposites containing 10 wt% of untreated nanosilica. Although the addition of nanosilica only shows a modest effect on AC breakdown strength of the final nanocomposites, the results are encouraging.

Meanwhile, DC breakdown testing showed that increasing the amount of untreated nanosilica further reduced the DC breakdown strength of the system significantly. Surface treatment of nanosilica improved the DC breakdown strength in comparison with samples containing an equivalent amount of untreated nanosilica. While there could be several explanations (the particle size distribution, the morphology and the existence of electrical defects that promote space charge development) for the observed DC breakdown behaviour, the exact mechanisms that govern the DC breakdown behaviour are complex and difficult to justify. Although the incorporation of nanosilica into polyethylene reduced the DC breakdown strength, the improvement of DC breakdown strength brought about by nanosilica surface

treatment (C3-treated nanosilica) underlined the potential of engineering such dielectric materials to give good DC breakdown properties.

In Chapter 7, the space charge behaviour of the nanocomposites was analysed based on the pulsed electro-acoustic technique. The investigated nanocomposites showed homocharge development near both electrodes, not apparent in the unfilled polyethylene. The space charge behaviour correlated with the DC breakdown behaviour of the nanocomposites; nanocomposites containing C3-treated nanosilica showed less homocharge development near both electrodes in comparison with nanocomposites containing untreated nanosilica, where the DC breakdown strength of the nanocomposites containing C3-treated nanosilica was higher than that of the nanocomposites containing untreated nanosilica. Meanwhile, the migration of charge observed from the space charge behaviour of the nanocomposites indicates that the application of an AC field may not be harmful to the investigated nanocomposite systems due to the polarity reversal of the AC field which may cause insignificant overall space charge accumulation.

The absorption current measurements reported in Chapter 8 were performed to help analysing the breakdown data as well as the space charge behaviour of the nanocomposites. It was found that, at the beginning of the absorption current test, the rate of decrease of current for all the nanocomposites was significantly greater than for the unfilled polyethylene, highlighting the possibility of increased charge mobility in the nanocomposites. While it is certain that the absorption current will be affected by the nanofiller/polymer interfaces, quantitative analysis for a specific nanofiller/polymer combination is very limited through these absorption current measurements. No clear distinction can be made on the effect of nanosilica surface treatment as well as nanosilica loading level. Nevertheless, the observed absorption current characteristics did help in the analysis of the mechanisms of charge transport.

Finally in Chapter 9, a systematic study with a view to understanding the mechanisms underpinning the concept of filler functionalisation in nanodielectrics was undertaken. It was demonstrated that long silane chains improved the DC breakdown strength of the resulting nanocomposites, and possible factors such as purity, silane chain conformation and degree of filler functionalisation that lead to

the observed breakdown performance were considered. The possible further enhancement of the DC breakdown strength was also highlighted, in particular in relation to the degree of filler functionalisation.

10.2 Conclusions

Before concluding the current work, it is worthwhile to revisit the objectives set out in this research:

i) To formulate and characterise reproducible polymer nanocomposites for dielectric applications.
ii) To investigate the effect of nanoparticles on electrical breakdown and space charge characteristics of polymer nanocomposites.
iii) To investigate the role of the interface in determining the unique dielectric properties of polymer nanocomposites.

The first objective answers the common question raised in materials research: how will a nanofiller affect a polymer? In this work, the use of a polyethylene blend as a matrix material allows the control of the underlying matrix morphology and enables structural changes to be readily detected. Structurally, neither nanofiller (untreated and C3-treated nanosilica) was found to affect the growth of lamellar crystals, although both promoted crystal nucleation. This observation can be linked to the statistically indistinguishable AC breakdown strength of the investigated materials. While less organised structures would be expected to lead to a lower breakdown strength, this does not appear to be the case for the polyethylene blends considered here under AC fields. The use of this blend system, however, comes with the compromise of having a complex lamellar texture which prevents nanometre-sized filler particles from being imaged.

The second objective mainly addresses industrial interests: what about the use of nanocomposites in DC applications? In short, the DC breakdown strength of both the nanocomposites containing untreated and C3-treated nanosilica fell monotonically with increasing nanofiller loading level. The drop in strength was more pronounced

for the former set of systems. Meanwhile, space charge studies revealed increased space charge accumulation in the presence of the untreated nanofiller, suggesting that space charge accumulation and DC failure are related in these systems. Thus, it would seem that control of surface chemistry is particularly critical in connection with the use of nanocomposites in DC applications, since the introduction of localised interfacial electronic states can result in markedly inferior performance. Nevertheless, appropriate surface treatment of the nanosilica, as shown in this work, highlights the potential use of the silane coupling agent in improving the electrical properties of nanocomposites.

In the third objective, the role of the nanocomposites' interface was emphasised. This was inspired from a critical question concerning nanodielectrics research: how do interfaces lead to changes in dielectric properties? In this work, the use of nanosilica with different surface chemistries (untreated and C3-treated nanosilica) has demonstrated how the electrical properties of the final nanocomposite systems can be modified through the use of silane coupling agents. Specifically, the dielectric response of nanocomposites containing nanosilica with different surface chemistries showed how the surface treatment of nanosilica can alter the water absorption behaviours of the nanocomposites, especially at the interfaces. While water absorption may not be a technologically desirable characteristic, the results indicate that water molecules can act as effective dielectric probes of interfacial factors.

Following a comprehensive characterisation and testing between two nanocomposite systems (untreated and C3-treated systems), it was found that the behaviours of the nanocomposites, even after surface treatment, were not comparable with that of the unfilled polyethylene, especially in terms of DC breakdown strength. So what is the promise of nanocomposites as electrical insulation materials, and how would interfaces, as emphasised in the third objective, play a role in this? The answer can be deduced from the work on surface functionalisation of nanosilica using different aliphatic chain length silanes. Results show that surface functionalisation of nanosilica using long silane chains enhances the nanocomposites' (C8-treated and C18-treated systems) DC breakdown strength, albeit that factors such as purity, silane chain conformation and degree of filler functionalisation need to be carefully considered. The possible further enhancement in DC breakdown strength was also

highlighted. At present, few systematic studies of this area have been undertaken with a view to understanding the mechanisms underpinning the concept of filler functionalisation in nanodielectrics, and this work demonstrates a promising way to tailoring the properties of nanodielectrics via different silane chain lengths and through optimising the degree of functionalisation.

10.3 Future Work

The degree of filler functionalisation is worth studying further to understand its effect on nanoparticle/nanoparticle interactions and consequent agglomeration, nanoparticle/matrix interactions, matrix morphology and the electrical properties of the resulting nanocomposites. In this study, the volume of silane used was kept constant to ensure that the number of CH_2 repeat units per unit area of interface is comparable in each type of nanocomposite. This strategy is, however, likely to lead to a reduced degree of filler functionalisation with increasing chain length. Therefore, varying the amount of silane to reflect changes in the molecular weight of the silane might be preferable in optimising the degree of filler functionalisation, which is expected to subsequently optimise the electrical properties.

The study of space charge dynamics reported in this work considers stressing the sample for the typical period, i.e., 1 hour. It is recommended that space charge studies be performed for a much longer duration to determine the possible mechanism changes that may occur, which may help to explain the current rise behaviour in the absorption current measurements. Also, space charge dynamics of nanocomposites containing nanofiller with different degrees of functionalisation are worth investigating to determine the effect of varying the density of alkyl functional groups in the resulting nanocomposites.

Meanwhile, the current work considers the use of nanosilica and polyethylene as the respective filler and matrix. It should be noted that different nanofiller/polymer combinations may result in different interfacial properties of the final nanocomposites. Under these circumstances, the underlying mechanisms determining the property changes may change entirely. Therefore, investigations into various

types of nanofiller/polymer combinations would provide invaluable knowledge concerning the characteristics of nanocomposites.

To date, dispersion of nanoparticles in polymers is still an issue to be highlighted. Due to their small size, nanoparticles tend to agglomerate rather than appear as isolated particles when incorporated into polymers. This happens even though the polymers should be relatively compatible with nanoparticles. Therefore, alternative nanoparticle preparation techniques, such as the use of sol-gel process, are worth exploring with a view to minimising agglomeration effects.

Finally, the current work demonstrates that a significant mass fraction of the nanofiller appears in the form of agglomerates in the nanocomposites and that these are not easily broken up even after surface functionalisation. Nevertheless, with the use of a different alkyl silane, significant improvements in DC breakdown performance can be achieved. This raises an interesting question: provided the interface can be appropriately managed, how small do nano-inclusions have to be to lead to property enhancement? This question is worth exploring since, the larger the particle, the less of an issue of agglomeration is likely to be.

Appendix A

Nanocomposites Containing C18-treated Nanosilica

A.1 Introduction

In Chapter 9, several important aspects of the effect of silane chain length have been highlighted. In this appendix, a detailed characterisation of nanocomposites containing C18-treated nanosilica is presented. It should be noted that these properties are similar with the untreated, C3-treated and C8-treated systems and are therefore not discussed in length in Chapter 9.

A.2 Results and Discussion

A.2.1 Thermal Analysis

From thermal analysis, C18-treated nanosilica does not exert any appreciable effect on the melting behaviour of the polymer. This is illustrated as in Figure A.1, where the melting traces are similar to those shown in Figure 3.10 at an equivalent isothermal crystallisation temperature. Determination of the crystallinity of the nanocomposites containing C18-treated nanosilica also indicates that these samples do not have significant difference when compared with the crystallinity of the samples previously reported in Table 3.5.

The crystallisation rate constant, K_3 values of the nanocomposites containing C18-treated nanosilica under different isothermal crystallisation temperatures are shown in Figure A.2. Briefly, the addition of C18-treated nanosilica in polyethylene causes an increase in K_3 of about 1 order of magnitude compared with the unfilled polyethylene. This clearly indicates the nucleation effect of nanosilica in polyethylene. The precise effect of the interaction between the C18-treated nanosilica and the polyethylene has been discussed in Chapter 9.

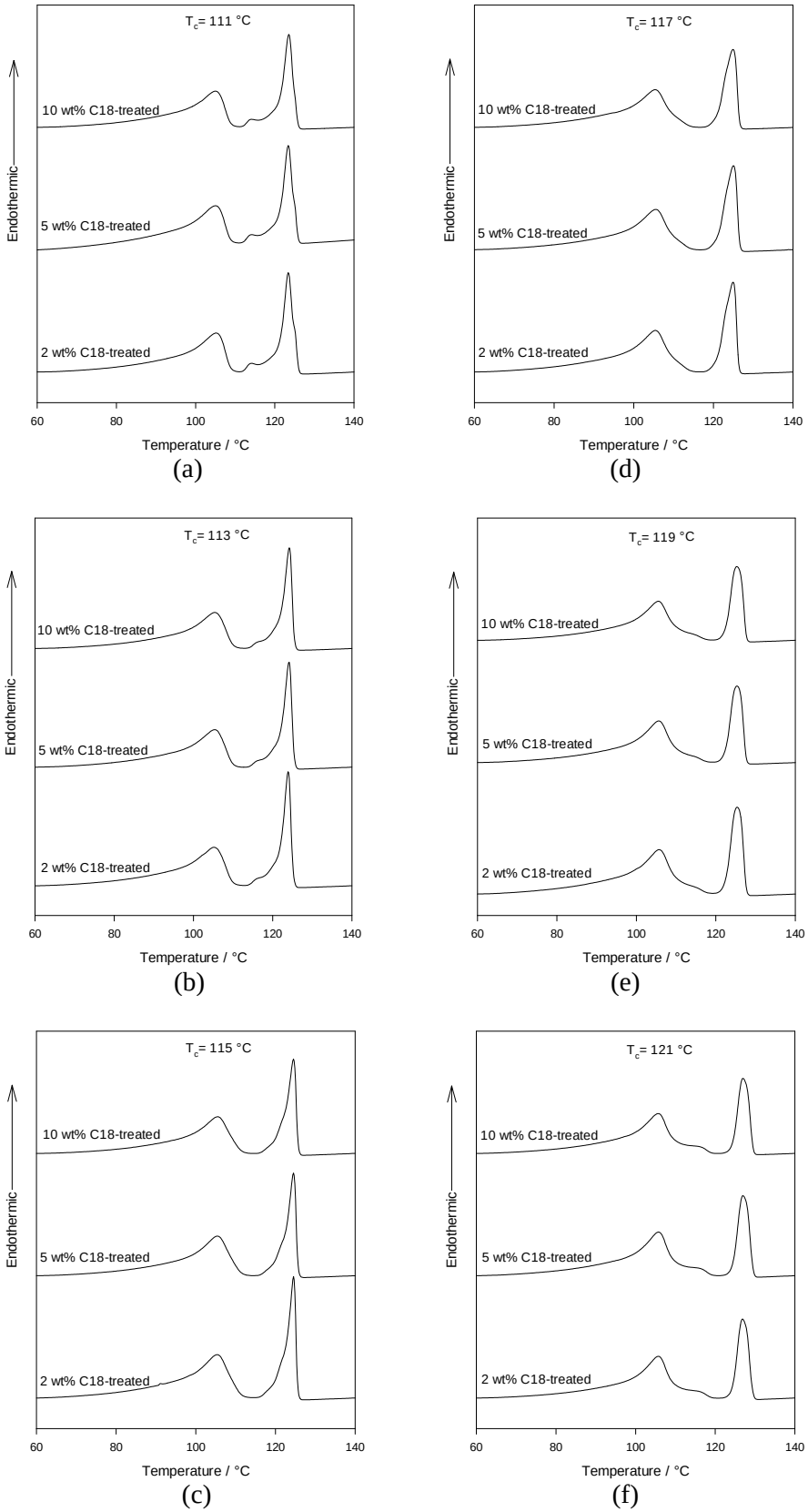

Figure A.1: DSC melting traces for nanocomposites containing C18-treated nanosilica upon isothermal crystallisation at (a) 111 ºC, (b) 113 ºC, (c) 115 ºC, (d) 117 ºC, (e) 119 ºC, (f) 121 ºC

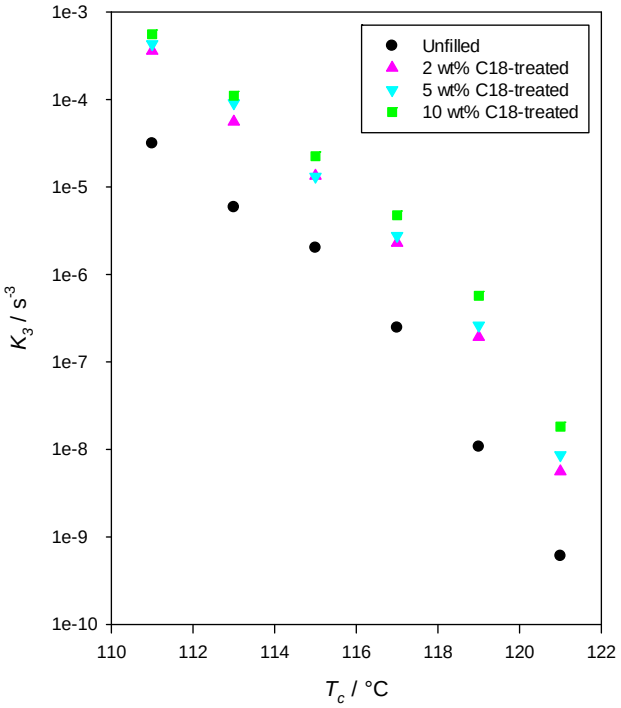

Figure A.2: Plots showing the content of C18-treated nanosilica on K_3 parameter of polyethylene

A.2.2 AC Breakdown Testing

Figure A.3 shows the AC breakdown strength of nanocomposites containing C18-treated nanosilica. The introduction of 2 wt% and 5 wt% of C18-treated nanosilica did not significantly affect the AC breakdown strength. This observation, again, is in line with the AC breakdown behaviour of nanocomposites containing untreated and C3-treated nanosilica as reported in Chapter 6. However, at 10 wt% of C18-treated nanosilica loading, the AC breakdown strength is reduced slightly. This is probably associated with the agglomeration of C18-treated nanosilica in the final nanocomposites that formed.

A.2.3 Absorption Current Measurements

The plot of absorption current data shown in Figure A.4 indicates that there is no obvious difference when comparing this type of nanocomposite system with the previously investigated nanocomposite systems. Nevertheless, there is an obvious

trend among all the investigated nanocomposite systems – the current behaviour of all the nanocomposites can be interpreted based on three phases: the region corresponding to the initial decrease of current (Phase I), the region immediately following the initial reduction in slope (Phase II) and the region where the current rises (Phase III), not found in the case of the unfilled polyethylene.

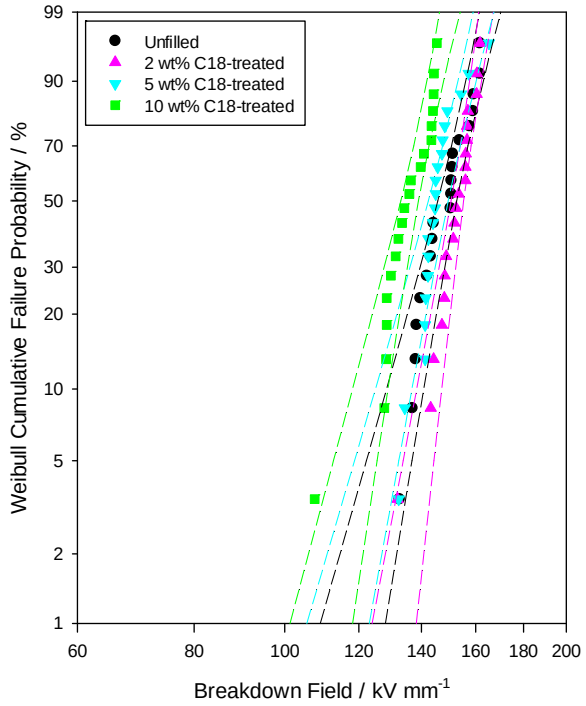

Sample	α / kV mm^{-1}	β
Unfilled	152 ± 3	19 ± 6
2 wt% C18-treated	155 ± 2	29 ± 9
5 wt% C18-treated	149 ± 3	18 ± 5
10 wt% C18-treated	139 ± 3	21 ± 6

Figure A.3: Weibull plots comparing the AC breakdown strength of unfilled polyethylene and nanocomposites containing 2 wt%, 5 wt% and 10 wt% of C18-treated nanosilica, crystallised isothermally at 115 ºC

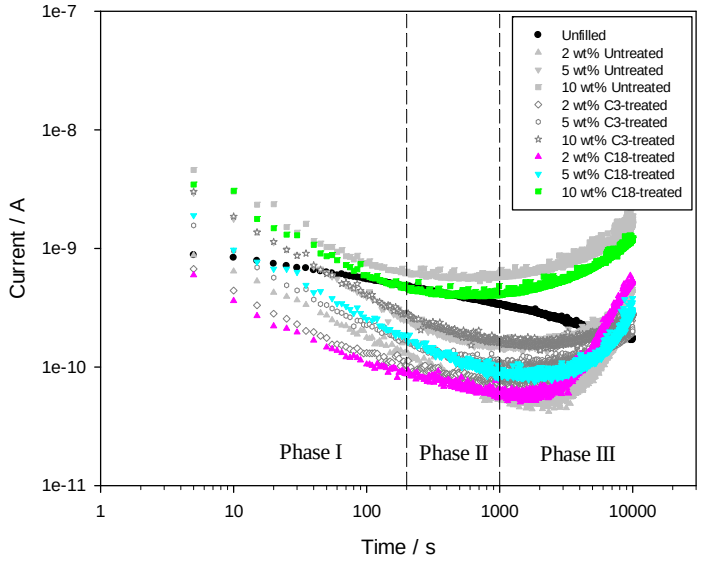

Figure A.4: Plot of absorption current against time up to 10^4 s for nanocomposites containing C18-treated nanosilica crystallised isothermally at 115 ºC at an applied field of 40 kV mm^{-1}. The effect of untreated and C3-treated nanosilica are re-shown as grey coloured background

A.3 Summary

While successful dielectric improvement may not have been fully achieved by using nanocomposites containing C18-treated nanosilica, it is worthwhile to mention that the use of this type of nanocomposite has, at least, served to further confirm the thermal, morphological and electrical behaviours of the previous nanocomposite systems and outlined the possible future work associated with nanodielectrics, in particular, in relation to the nanofiller/polymer interfaces. Since no appreciable effect was found on the properties reported here, no similar measurements were attempted for the case of nanocomposites containing C8-treated nanosilica.

References

Adamec, V., and Calderwood, J. H. (1978). Electrical conduction and polarisation phenomena in polymeric dielectrics at low fields. *Journal of Physics D: Applied Physics*, 11(6), 781-800.

Alfrey, T., Gurnee, E. F., and Lloyd, W. G. (1966). Diffusion in glassy polymers. *Journal of Polymer Science C*, 12(1), 249-261.

Ambid, M., Mary, D., Teyssedre, G., Laurent, C., and Montanari, G. C. (2006). Optical properties and luminescence behaviour of PP/clay nanocomposites. *IEEJ Transactions on Fundamentals and Materials*, 126(11), 1097-1104.

Andritsch, T. (2010). Epoxy based nanodielectrics for high voltage DC applications – synthesis, dielectric properties and space charge dynamics. Ph.D. Thesis, Delft University of Technology.

Aoyama, H., Tanaka, Y., Takada, T., and Murata, Y. (2006). Space charge formation in LDPE/MgO nano-composite thin film under ultra-high DC electric stress. *Proceedings of the International Conference on Properties and Applications of Dielectric Materials*, June, Bali: IEEE, 159-162.

Avrami, M. (1939). Kinetics of phase change. I General theory. *Journal of Chemical Physics*, 7(12), 1103-1112.

Avrami, M. (1940). Kinetics of phase change. II Transformation-time relations for random distribution of nuclei. *Journal of Chemical Physics*, 8(2), 212-224.

Avrami, M. (1941). Kinetics of phase change. III Granulation, phase change, and microstructure kinetics of phase change. *Journal of Chemical Physics*, 9(2), 177-184.

Bamji, S. S., Abou-Dakka, M., Bulinski, A. T., Utracki, L., and Cole, K. (2005). Dielectric properties of polypropylene containing nano-particles. *Annual Report Conference on Electrical Insulation and Dielectric Phenomena*, 16-19 October. Nashville, Tennessee: IEEE, 166-170.

Bernstein, B. S. (2003). Electrical Properties of Insulating Materials. In Thue, W. A. (Ed.) *Electrical Power Cable Engineering* (101-115). New York: Marcel Dekker.

Bernstein, B. S., and Tarpey, J. W. (2003). Electrical Insulation Materials. In Thue, W. A. (Ed.) *Electrical Power Cable Engineering* (58-100). New York: Marcel Dekker.

Bhattarcharya S. N., Gupta, R. K., and Kamal, M. R. (2008). *Polymeric Nanocomposites: Theory and Practice*. (1st ed.) Munich: Hanser.

Blythe, A. R., and Bloor, D. (2005). *Electrical Properties of Polymers*. (2nd ed.). New York: Cambridge University Press.

Calebrese, C., Hui, L., Schadler, L. S., and Nelson, J. K. (2011). A review on the importance of nanocomposite processing to enhance electrical insulation. *IEEE Transactions on Dielectrics and Electrical Insulation*, 18(4), 938-945.

Callister, W. D., (2007). *Materials Science and Engineering: An Introduction*. (7th ed.). New York: John Wiley and Sons.

Cao, Y., Irwin, P. C., and Younsi, K. (2004). The future of nanodielectrics in the electrical power industry. *IEEE Transactions on Dielectrics and Electrical Insulation*, 11(5), 797-807.

Chen, G., and Xu, Z. (2009). Charge trapping and detrapping in polymeric materials. *Journal of Applied Physics*, 106(12), 123707.

Chen, G., Zhao, J., Li, S., Zhoing, L. (2012). Origin of thickness dependent dc electrical breakdown in dielectrics. Applied Physics Letters, 100(22), 222904.

Chen, G., Zhang, C., and Stevens, G. (2007). Space charge in LLDPE loaded with nanoparticles. *Annual Report Conference on Electrical Insulation and Dielectric Phenomena*, 14-17 October. Vancouver, British Columbia: IEEE, 275-278.

Chen, H., Zhou, S., Gu, G., and Wu, L. (2004). Modification and dispersion of nanosilica. *Journal of Dispersion Science and Technology*, 25(6), 837-848.

Cheng, W., Miao, W., Zhang, L., and Peng, J. (2011). Covalently bonded PE/SiO_2 nanocomposites synthesised by reactive extrusion. *Iranian Polymer Journal*, 20(8), 681-687.

Christ, B. (2007). Yet another visit to the melting of polyethylene crystals. *Journal of Polymer Science B*, 45(24), 3231-3236.

Dakin, T. W. (1983). Composite Insulating Materials and Systems. In Bartnikas, R., and Eichhorn, R. M. (Eds.) *Engineering Dielectrics* (663-696). (vol. IIA) Philadelphia: ASTM.

Danikas, M. G., and Tanaka, T. (2009). Nanocomposites - A review of electrical treeing and breakdown. *IEEE Electrical Insulation Magazine*, 25(4), 19-25.

Daoud, W. A., Xin, J. H., and Tao, X. (2006). Synthesis and characterisation of hydrophobic silica nanocomposites. *Applied Surface Science*, 252(15), 5368-5371.

Das Gupta, D. K., and Brockley, R. S. (1978). A study of 'absorption currents' in low-density polyethylene. *Journal of Physics D: Applied Physics*, 11(6), 955-962.

Das Gupta, D. K., and Joyner, K. (1976). On the nature of absorption currents in polyethylene terephthalate (PET). *Journal of Physics D: Applied Physics*, 9(5), 829-840.

Dissado, L. A., and Fothergill, J. C. (1992). *Electrical Degradation and Breakdown in Polymers*. Stevens, G. C. (Ed.). London: Peter Peregrinus.

Dissado, L. A., Fothergill, J. C., Wolfe, S. V., and Hill, R. M. (1984). Weibull statistics in dielectric breakdown: theoretical basis, applications and implications. *IEEE Transactions on Electrical Insulation*, 19(3), 227-233.

Eaton, P., and West, P. (2010). *Atomic Force Microscopy*. Oxford: Oxford University Press.

Fabiani, D., Montanari, G. C., and Testa, L. (2010). Effect of aspect ratio and water contaminant on the electric properties of nanostructured insulating materials. *IEEE Transactions on Dielectrics and Electrical Insulation*, 17(1), 221-230.

Fenwick, D., Smith, P., and Wittman, J. C. (1996). Epitaxial and graphoepitaxial growth of materials on highly orientated PTFE substrates. *Journal of Materials Science*, 31(1), 128-131.

Flory, P. J. (1953). *Principles of Polymer Chemistry*. New York: Cornell University Press.

Fothergill, J. C. (1990). Estimating the cumulative probability of failure data points to be plotted on Weibull and other probability paper. *IEEE Transactions on Electrical Insulation*, 25(3), 489-492.

Fournier, D., and Lamarre, L. (1992). Effect of pressure and length on interfacial breakdown between two dielectric surfaces. *Conference Record of International Symposium on Electrical Insulation*, 7-10 June. Baltimore, Maryland: IEEE, 270-272.

Frechétte, M. F., Trudeau, M. L., Alamdari, H. D., and Boily, S. (2004). Introductory remarks on nanodielectrics. *IEEE Transactions on Dielectrics and Electrical Insulation*, 11(5), 808-818.

Fréchette, M. F., Vijh, A., Utracki, L., Trudeau, M. L., Sami, A., Laurent, C., Morshuis, P., Vaughan, A. S., David, E., Castellon, J., Fabiani, D., Gubanski, S., Kindersberger, J., Reed, C., Krivda, A., Fothergill, J., Guastavino, F., and Alamdari, H. (2010) Nanodielectrics: a panacea for solving all electrical insulation problems? *Proceedings of the International Conference on Solid Dielectrics*, 4-9 July. Potsdam: IEEE, 130-158.

Fuse, N., Tanaka, T., and Ohki, Y. (2009). Evaluation of dielectric properties in polypropylene/clay nanocomposites. *Annual Report Conference on Electrical Insulation and Dielectric Phenomena*, 18-21 October. Virginia Beach, Virginia: IEEE, 507-510.

Gedde, U. W. (1995). *Polymer Physics*. Norwell: Kluwer Academic Publishers.

Gherbaz, G. (2008). *Nanostructured Polymers: Morphology and Properties*. Ph.D. Thesis, University of Southampton.

Goshowaki, M., Reddy, C. C., Sekiguchi, Y., Hishinuma, N., Hayase, Y., Tanaka, Y., and Takada, T. (2008). Investigation of space charge distribution and volume resistivity of XLPE/MgO nanocomposite material under DC voltage application. *Proceedings of the International Symposium on Electrical Insulating Materials*, 7-11 September, Mie: IEEE, 502-505.

Green, C. D. (2008). *Polyethylene-Monomorillonite Nanocomposites*. Ph.D. Thesis, University of Southampton.

Green, C., and Vaughan, A. (2008). Nanodielectrics - How much do we really understand? *IEEE Electrical Insulation Magazine*, 24(4), 6-16.

Green, C. D., Vaughan, A. S., Mitchell, G. R., and Liu, T. (2008). Structure property relationships in polyethylene/montmorillonite nanodielectrics. *IEEE Transactions on Dielectrics and Electrical Insulation*, 15(1), 134-143.

Greso, A. J., and Phillips, P. J. (1994). The role of epitaxy in the development of morphology in carbon fiber composites. *Journal of Advanced Materials*, 25(4), 51-60.

Groeninckx, G., Vanneste, M., and Everaert, V. (2002). Crystallisation, morphological structure, and melting of polymer blends. In Utracki, L. A. (Ed.) *Polymer Blends Handbook* (203-294). (vol. 2) Dordrecht: Kluwer Academic Publishers.

Gulmine, J. V., Janissek, P. R., Heise, H. M., and Akcelrud, L. (2002). Polyethylene characterisation by FTIR. *Polymer Testing*, 21(5), 557-563.

Henk, P. O., Kortsen, T. W., and Kvarts, T. (1999). Increasing the electrical discharge endurance of acid anhydride cured DGEBA epoxy resin by dispersion of nanoparticle silica. *High Performance Polymers*, 11(3), 281-296.

Henk, P. O., Kortsen, T. W., and Saeidi, A. (2001). Increasing the PD-endurance of epoxy and XLPE insulation by nanoparticle silica dispersion in the polymer. *Proceedings of the Nordic Insulation Symposium*. 11-13 June. Stockholm: IEEE, 1-8.

Hoffman, J. D., Davis, G. T., and Lauritzen, J. I. (1976). The Rate of Crystallisation of Linear Polymers with Chain Folding. In Hannay, N. B. (Ed.) *Treatise on Solid State Chemistry* (497-614). (vol. III) New York: Plenum Press.

Hoffman, J. D., and Miller, R. L. (1997). Kinetic of crystallisation from the melt and chain folding in polyethylene fractions revisited: theory and experiment. *Polymer*, 38(13), 3151-3212.

Hoffman, J. D., and Weeks, J. J. (1962). Melting process and the equilibrium melting temperature of polychlorotrifluoroethylene. *Journal of Research of the National Bureau of Standards A*, 66(1), 13-28.

Holt, A. F., Brown, L. J., and Brown, R. C. D. (2011). Personal Communication.

Hosier, I. L. (1996). *Morphology and Electrical Properties of Polyethylene Blend*. Ph.D. Thesis, University of Reading.

Hosier, I. L., Vaughan, A. S., and Swingler, S. G. (2010). An investigation of the potential of ethylene vinyl acetate/ polyethylene blends for use in recyclable high voltage cable insulation systems. *Journal of Materials Science*, 45(10), 2747-2759.

Hosier, I. L., Vaughan, A. S., and Swingler, S. G. (1997). Structure-property relationships in polyethylene blends: the effect of morphology on electrical breakdown strength. *Journal of Materials Science*, 32(17), 4523-4531.

Hosier, I. L., Vaughan, A. S., and Swingler, S. G. (2000). On the effects of morphology and molecular composition on the electrical strength of polyethylene blend. *Journal of Polymer Science B*, 38(17), 2309-2322.

Huang, X. Y., Jiang, P. K., and Kim, C. U. (2007). Electrical properties of polyethylene/aluminium nanocomposites. *Journal of Applied Physics*, 102(12), 124103.

Huang, X., Jiang, P., Kim, C., Ke, Q., and Wang, G. (2008). Preparation, microstructure and properties of polyethylene aluminium nanocomposite dielectric. *Composites Science and Technology*, 68(9), 2134-2140.

Huang, X., Liu, F., and Jiang P. (2010). Effect of nanoparticle surface treatment on morphology, electrical, and water treeing behaviour of LLDPE composites. *IEEE Transactions on Dielectrics and Electrical Insulation*, 17(6),1697-1704.

Huang, X., Ma, Z., Wang, Y., Jiang, P., Yin, Y., and Li, Z. (2009). Polyethylene/aluminium nanocomposites: improvement of dielectric strength by nanoparticle surface modification. *Journal of Applied Polymer Science*, 113(6), 3577-3584.

Hui, L., Nelson, J. K., and Schadler, L. S. (2010). The influence of moisture on the electrical performance of XLPE/silica nanocomposites. *Proceedings of the International Conference on Solid Dielectrics*, 4-9 July. Potsdam: IEEE, 1-4.

Hussain, F., Hojjati, M., Okamoto, M., and Gorga, R. E. (2006). Review article: polymer-matrix nanocomposites, processing, manufacturing, and application: an overview. *Journal of Composite Materials*, 40(17), 1511-1575.

Ieda, M. (1977). Carrier injection, space charge and electrical breakdown in insulating polymers. *IEEE Transactions on Electrical Insulation*, 22(3), 261-267.

Ieda, M. (1980). Dielectric breakdown process of polymers. *IEEE Transactions on Electrical Insulation*, 15(3), 206-224.

Ieda, M. (1984). Electrical conduction and carrier traps in polymeric materials. *IEEE Transactions on Electrical Insulation*, 19(3), 162-178.

Imai, T., Sawa, F., Yoshimitsu, T., Ozaki, T., and Shimizu, T. (2004). Preparation and insulation properties of epoxy-layered silicate nanocomposite. *Annual Report Conference on Electrical Insulation and Dielectric Phenomena*, 17-20 October. Boulder, Colorado: IEEE, 402-405.

Iyer, G., Gorur, R. S., and Richert, R. (2011). Dielectric properties of epoxy based nanocomposites for high voltage insulation. *IEEE Transactions on Dielectrics and Electrical Insulation*, 18(3), 659-666.

Khalil, M. S., Henk, P. O., and Henriksen, M. (1990). The influence of titanium dioxide additive on the short-term DC breakdown strength of polyethylene. *Conference Record of International Symposium on Electrical Insulation*, 3-6 June. Toronto: IEEE, 268-271.

Kim, K., and White, J. L. (2002). Silica surface modification using different aliphatic chain length coupling agents and their effects on silica agglomerate size and processability. *Composite Interfaces*, 9(6), 541-556.

Kinloch, A. J., Little, M. S. G., and Watts, J. F. (2000). The role of the interphase in the environmental failure of adhesive joints. *Acta Materialia*, 48(18-19), 4543-4553.

Kolesov, S. N. (1980). The influence of morphology on the electrical strength of polymer insulation. *IEEE Transactions on Electrical Insulation*, 15(5), 382-388.

Kontou, E., and Niaounakis, M. (2006). Thermo-mechanical properties of LLDPE/SiO_2 nanocomposites. *Polymer*, 47(4), 1267-1280.

Kopp, S., Wittman, J. C., and Lotz, B. (1994). Epitaxial crystallisation and crystalline polymorphism of poly(1-butene): Form I'. *Polymer*, 35(5), 916-924.

Kowalewski, T., and Galeski, A. (1986). Influence of chalk and its surface-treatment on crystallisation of filled polypropylene. *Journal of Applied Polymer Science*, 32(1), 2919-2934.

Kozako, M., Fuse, N., Ohki, Y., Okamoto, T., and Tanaka, T. (2004). Surface degradation of polyamide nanocomposites caused by partial discharges using IEC (b) electrodes. *IEEE Transactions on Dielectrics and Electrical Insulation*, 11(5), 833-839.

Ku, C. C., and Liepins, R. (1987). *Electrical Properties of Polymers*. Munich: Hanser.

Kuffel, E., Zaengl, W. S., and Kuffel, J. (2000). Breakdown in solid and liquid dielectrics. In *High Voltage Engineering: Fundamentals* (367-385). (2nd ed.) Oxford: Newnes.

Lai, S., Huang, C., Li, S., Chen, Y., Hsu, H., Yu, Y., and Hsiou, Y. (2011). Preparation and properties of melt-mixed metallocene polyethylene/silica nanocomposites. *Polymer Engineering and Science*, 51(3), 434-444.

Lewiner, J. (1986). Evolution of experimental techniques for the study of the electrical properties of insulating materials. *IEEE Transactions on Electrical Insulation*, 21(3), 351-360.

Lewis, T. J. (1994). Nanometric dielectrics. *IEEE Transactions on Dielectrics and Electrical Insulation*, 1(5), 812-825.

Lewis, T. J. (2004). Interfaces are the dominant feature of dielectrics at the nanometric level. *IEEE Transactions on Dielectrics and Electrical Insulation*, 11(5), 739-753.

Lewis, T. J. (2005). Interfaces: nanometric dielectrics. *Journal of Physics D: Applied Physics*, 38(2), 202-212.

Li, D., Lin, M. M., Toprak, M. S., Kim, D. K., and Muhammed, M. (2010a). Nanocomposites of polymer and inorganic nanoparticles for optical and magnetic applications. *Nano Reviews*, 1, 5214.

Li, S., Yin, G., Chen, G., Li, J., Bai, S., Zhong, L., Zhang, Y., and Lei, Q. (2010b). Short-term breakdown and long-term failure in nanodielectrics: a review. *IEEE Transactions on Dielectrics and Electrical Insulation*, 17(5), 1523-1535.

Lopez, J. F., Perez, L. D., and Lopez, B. L. (2011). Effect of silica modification on the chemical interactions in NBR-based composites. *Journal of Applied Polymer Science*, 122(3), 2130-2138.

Lorenzo, A. T., Arnal, M. L., Albuerne, J., and Müller, J. (2007). DSC isothermal polymer crystallisation kinetics measurements and the use of the Avrami equation to fit the data: guidelines to avoid common problems. *Polymer Testing*, 26(2), 222-231.

Ma, D., Akpalu, Y. A., Li, Y., Siegel, R. W., and Schadler, L. S. (2005a). Effect of titania nanoparticles on the morphology of low density polyethylene. *Journal of Polymer Science B*, 43(5), 488-497.

Ma, D., Hugener, T. A., Siegel, R. W., Christerson, A., Mårtensson, E., and Önneby, C, and Schadler, L. S. (2005b). Influence of nanoparticle surface modification on the electrical behaviour of polyethylene nanocomposites. *Nanotechnology*, 16(6), 724-731.

Ma, D., Siegel, R. W., Hong, J-I., Schadler, L. S., Mårtensson, E., and Önneby, C. (2003). Influence of nanoparticle surfaces on the electrical breakdown strength of nanoparticle-filled low-density polyethylene. *Journal of Materials Research*, 19(3), 857-863.

Maity, P., Basu, S., Parameswaran, V., and Gupta, N. (2008). Degradation of polymer dielectrics with nanometric metal-oxide fillers due to surface discharges. *IEEE Transactions on Dielectrics and Electrical Insulation*, 15(1), 52-61.

Mandelkern, L. (1992). Crystallisation and Melting. In Booth, C. and Price, C. (Eds.) *Comprehensive Polymer Science: Vol.2, Polymer Properties* (363-414). Oxford: Pergamon Press.

Marand, H., Xu, J., and Srinivas, S. (1998). Determination of the equilibrium melting temperature of polymer crystals: linear and nonlinear Hoffman-Weeks extrapolations. *Macromolecules*, 31(23), 8219-8229.

Mayoux, C. (2000). Whitehead Memorial Lecture: degradation of insulating materials under electrical stress. *IEEE Transactions on Dielectrics and Electrical Insulation*, 7(5), 590-601.

MEDAC Ltd. (2011). Analytical and chemical consultancy services. Available at http://www.medacltd.com/

Miller, H. C. (1993). Flashover of insulators in vacuum: review of the phenomena and techniques to improve holdoff voltage. *IEEE Transactions on Electrical Insulation*, 28(4), 512-527.

Mizutani, T. (1994). Space charge measurement techniques and space charge in polyethylene. *IEEE Transactions on Dielectrics and Electrical Insulation*, 1(5), 923-933.

Montanari, G. C., Fabiani, D., Palmieri, F., Kaempfer, D., Thomann, R., and Mulhaupt, R. (2004). Modification of electrical properties and performance of EVA and PP insulation through nanostructure by organophilic silicates. *IEEE Transactions on Dielectrics and Electrical Insulation*, 11(5), 754-762.

Montanari, G. C., Palmieri, F., Testa, L., Motori, A., Saccani, A., and Patuelli, F. (2006). Polarization processes of nanocomposite silicate-EVA and PP materials. *IEEJ Transactions on Fundamentals and Materials*, 126(11), 1090-1096.

Muchová M., and Lednický, F. (1995). Induction time as a measure for heterogeneous spherulite nucleation: quantitative evaluation of early-stage growth kinetics. *Journal of Macromolecular Science B: Physics*, 34(1-2), 55-73.

Muchová M., and Lednický, F. (1996). Investigation of heterogeneous nucleation using the induction time of crystallisation: 1. Theory of induction time. *Polymer*, 37(14), 3031-3036.

Nelson, J. K. (2007). Overview of nanodielectrics: insulating materials of the future. Proceedings of the Electrical Insulation Conference and Electrical Manufacturing Expo. 22-24 October. Nashville, Tennessee: IEEE, 229-235.

Nelson, J. K. (2010). Background, principles and promise of nanodielectrics. In Nelson, J. K. (Ed.) *Dielectric Polymer Nanocomposites* (1-30). New York: Springer.

Nelson, J. K., and Fothergill, J. C. (2004). Internal charge behaviour of nanocomposites. *Nanotechnology*, 15(5), 586-595.

Nelson, J. K., Fothergill, J. C., Dissado, L. A., and Peasgood, W. (2002). Towards an understanding of nanometric dielectrics. *Annual Report Conference on Electrical Insulation and Dielectric Phenomena*. 20-24 October. Cancun: IEEE, 295-298.

Nishi, T., and Wang, T. T. (1975). Melting point depression and kinetic effects of cooling on crystallisation in poly(vinylidene fluoride)-poly(methyl methacrylate) mixtures. Macromolecules, 8(6), 909-915.

Olley, R. H., and Bassett, D. C. (1982). An improved permanganic etchant for polyolefins. *Polymer*, 23(12), 1707-1710.

Panaitescu, D., Ciuprina, F., Iorga, M., Frone, A., Radovici, C., Ghiurea, M., Sever, S., and Plesa, I. (2011). Effects of SiO_2 and Al_2O_3 nanofillers on polyethylene properties. *Journal of Applied Polymer Science*, 122(3), 1921-1935.

Parvinzadeh, M., Moradian, S., Rashidi, A., and Yazdanshenas, M. (2010). Surface characterisation of polyethylene terephthalate/silica nanocomposites. *Applied Surface Science*, 256(9), 2792-2802.

Pitsa, D., and Danikas, M. G. (2011). Interfaces features in polymer nanocomposites: a review of proposed models. *NANO*, 6(6), 497-508.

Preetha, P., and Thomas, M. J. (2011). AC breakdown characteristics of epoxy nanocomposites. *IEEE Transactions on Dielectrics and Electrical Insulation*, 18(5), 1526-1534.

Psarras, G. C. (2008). Nanodielectrics: an emerging sector of polymer nanocomposites. *Express Polymer Letters*, 2(7), 460.

Raetzke, S., and Kindersberger, J. (2010). Role of interphase on the resistance to high-voltage arcing, on tracking and erosion of silicone/SiO_2 nanocomposites. *IEEE Transactions on Dielectrics and Electrical Insulation*, 17(2), 607-614.

Reed, C. W. (2010). The chemistry and physics of the interface region and functionalization. In Nelson, J. K. (Ed.) *Dielectric Polymer Nanocomposites* (117-122). New York: Springer.

Roy, M. (2005). *An Examination of the Potential for Nano-composites in the Formulation of HV Cable Insulation*. Ph.D. Thesis, Rensselaer Polytechnic Institute.

Roy, M., Reed, C. W., MacCrone, R. K., Schadler, L. S., Nelson, J. K., Keefe, R., and Zenger, W. (2005a). Evidence for the role of the interface in polyolefin nanocomposites. *Proceedings of the International Symposium on Electrical Insulating Materials*. 5-9 June. Kitakyushu: IEEE, 223-226.

Roy, M., Nelson, J. K., MacCrone, R. K., Schadler, L. S., Reed, C. W., Keefe, R., and Zenger, W. (2005b). Polymer nanocomposite dielectrics - The role of the interface. *IEEE Transactions on Dielectrics and Electrical Insulation*, 12(4), 629-642.

Roy, M., Nelson, J. K., MacCrone, R. K., and Schadler, L. S. (2007). Candidate mechanisms controlling the electrical characteristics of silica/XLPE nanodielectrics. *Journal of Materials Science*, 42(11), 3789-3799.

Singha, S., and Thomas, M. J. (2008). Dielectric properties of epoxy nanocomposites. *IEEE Transactions on Dielectrics and Electrical Insulation*, 15(1), 12-23.

Smith, R. C. (2009). *Mechanistic Electrical Behaviour of Crosslinked Polyethylene / Silica Nanocomposites*. Ph.D. Thesis, Rensselaer Polytechnic Institute.

Smith, R. C., Liang, C., Landry, M., Nelson, J. K., and Schadler, L. S. (2008). The mechanisms leading to the useful electrical properties of polymer nanodielectrics. *IEEE Transactions on Dielectrics and Electrical Insulation*, 15(1), 187-196.

Steeman, P. A. M., and Maurer, F. H. J. (1990). An interlayer model for complex dielectric constant of composites. *Colloid and Polymer Science*, 268(4), 315-325.

Steeman, P. A. M., Maurer, F. H. J., and van Es, M. A. (1991). Dielectric monitoring of water absorption in glass-bead-filled high-density polyethylene. *Polymer*, 32(3), 523-530.

Stefanescu, M., Stoia, M., Stefanescu, O., Davidescu, C., Vlase, G., and Sfirloaga, P. (2010). Synthesis and characterisation of poly(vinyl alcohol)/ethylene glycol/silica hybrids. Thermal analysis and FT-IR study. *Romanian Journal of Chemistry*, 55(1), 17-23.

Stone, G. C., and Lawless, J. F. (1979). The application of Weibull statistics to insulation aging tests. *IEEE Transactions on Electrical Insulation*, 14(5), 233-239.

Takada, T., and Sakai, T. (1983). Measurement of electric fields at a dielectric/electrode interface using an acoustic transducer technique. *IEEE Transactions on Electrical Insulation*, 18(6), 619-628.

Tanaka, T. (2005). Dielectric nanocomposites with insulating properties. *IEEE Transactions on Dielectrics and Electrical Insulation*, 12(5), 914-928.

Tanaka, Y., Chen, G., Zhao, Y., Davies, A. E., Vaughan, A. S., and Takada, T. (2003). Effect of additives on morphology and space charge accumulation in low density polyethylene. *IEEE Transactions on Dielectrics and Electrical Insulation*, 10(1), 148-154.

Tanaka, T., Kozako, M., Fuse, N., and Ohki, Y. (2005). Proposal of a multi-core model for polymer nanocomposite dielectrics. *IEEE Transactions on Dielectrics and Electrical Insulation*, 12(4), 669-681.

Tanaka, T., Fréchette, M., Montanari, G. C., Tanaka, Y., Ohki, Y., Bulinski, A., Gubanski, S., Nagao, M., Pélissou, S., Reed, C. W., Castellon, J., Kindersberger, J., Morshuis, P. Vaughan, A., Sutton, S., and Han, S. J. (2011). Dielectric properties of XLPE/SiO_2 nanocomposites based on CIGRE WG D1.24 cooperative test results. *IEEE Transactions on Dielectrics and Electrical Insulation*, 18(5), 1484-1517.

Tanaka, T., Montanari, G. C., and Mülhaupt, R. (2004). Polymer nanocomposites as dielectrics and electrical insulation- perspectives for processing technologies, material characterisation and future applications. *IEEE Transactions on Dielectrics and Electrical Insulation*, 11(5), 763-784.

The Institute of Electrical and Electronics Engineers (1987). *ANSI/IEEE Std. 930-1987: IEEE Guide for the Statistical Analysis of Electrical Insulation Voltage Endurance Data*. New York: The Institute of Electrical and Electronics Engineers.

Tian, X., Ruan, C., Cui, P., Liu, W., Zheng, J., Zhang, X., Yao, X., Zheng, K., and Li, Y. (2006). Isothermal crystallisation and subsequent melting behaviour of poly(ethylene terephthalate)/silica nanocomposites. *Journal of Macromolecular Science B*, 45(5), 835-848.

Todd, M. G., and Shi, F. G. (2003). Characterising the interphase dielectric constant of polymer composite materials: effect of chemical coupling agents. *Journal of Applied Physics*, 94(7), 4551-4557.

Tsagaropoulos, G., and Eisenberg, A. (1995). Dynamic mechanical study of the factors affecting the two glass transition behaviour of filled polymers. Similarities and Differences with random ionomers. *Macromolecules*, 28(18), 6067-6077.

Usuki, A., Kawasumi, M., Kojima, Y., Okada, A., Kurauchi, T., and Kamigaito, O.J. (1993a). Swelling behaviour of montmorillonite cation exchanged forω-amino acids by ε-caprolactam. *Journal of Materials Research*, 8(5), 1174-1188.

Usuki, A., Kojima, Y., Kawasumi, M., Okada, A., Fukusima, Y., Kurauchi, T., and Kamigaito, O (1993b). Synthesis of nylon 6-clay hybrid. *Journal of Materials Research*, 8(5), 1179-1184.

Vaughan, A. S., Swingler, S. G., and Zhang, Y. (2006). Polyethylene nanodielectrics: the influence of nanoclays on structure formation and dielectric breakdown. *IEEJ Transactions on Fundamentals and Materials*, 126(11), 1057-1063.

Wei, L., Tang, T., and Huang, B. (2004). Synthesis and characterisation of polyethylene/clay-silica nanocomposites: a montmorillonite/silica-hybrid-supported catalyst and in situ polymerisation. *Journal of Polymer Science A*, 42(4), 941-949.

Weibull, W. (1951). A statistical distribution function of wide applicability. *Journal of Applied Mechanics*, 18(3), 293-297.

Wintle, H. J. (1983). Conduction processes in polymers. In Bartnikas, R. , and Eichhorn, R. M. (Eds.) *Engineering Dielectrics* (239-354). (vol. IIA) Philadelphia: ASTM.

Wu, C., and Liao, H. (2003). In situ polymerisation of silicic acid in polyethylene-octene elastomer: properties and characterisation of the hybrid nanocomposites. *Journal of Polymer Science B*, 41(4), 351-359.

Wunderlich, B., and Czornyj, G. (1977). A study of equilibrium melting of polyethylene. *Macromolecules*, 10(5), 906-913.

Xu, Z. (2009). *Space Charge Measurement and Analysis in Low Density Polyethylene Film*. Ph.D. Thesis, University of Southampton.

Yeung, C., and Vaughan, A. S. (2012). A study of how varying degrees of functionalised nanofiller have an effect on nanodielectrics. *Annual Report Conference on Electrical Insulation and Dielectric Phenomena*. 14-17 October. Montreal: IEEE, 319-322.

Yin, Y., Chen, J., Yang, J., Xiao, D., Tu, D., Yin, R., and Qian, H. (2003). Effect of space charge in nanocomposite of LDPE/TiO_2. *Proceedings of the International Conference on Properties and Applications of Dielectric Materials*. 1-5 June. Nagoya: IEEE, 913-916.

Zha, J., Dang, Z., Song, H., Yin, Y., and Chen, G. (2010). Dielectric properties and effect of electrical ageing on space charge accumulation in polyimide/TiO_2 nanocomposite films. *Journal of Applied Physics*, 108(9), 094113.

Zhang, C., and Stevens, G. C. (2008). The dielectric response of polar and non-polar nanodielectrics. *IEEE Transactions on Dielectrics and Electrical Insulation*, 15(2), 606-617.

Zilg, C., Kaempfer, D., Thomann, R., Mülhaupt, R., and Montanari, G. C. (2003). Electrical properties of polymer nanocomposites based upon organophilic layered silicates. *Annual Report Conference on Electrical Insulation and Dielectric Phenomena*. 19-22 October. Albuquerque, New Mexico: IEEE, 546-550.

Zou, C., Fothergill, J. C., and Rowe, S. W. (2008). The effect of water absorption on the dielectric properties of epoxy nanocomposites. *IEEE Transactions on Dielectrics and Electrical Insulation*, 15(1), 106-117.